ФОТОЭЛЕКТРОНИКА

PHOTOELECTRONICS
INTER-UNIVERSITIES SCIENTIFIC ARTICLES

Founded in 1986

Number 30

UDC 621.315.592:621.383.51:537.221

The results of theoretical and experimental studies in problems of the semiconductor and micro-electronic devices physics, optoand qantum electronics, quantum optics, spectroscopy and photophysics of nucleus, atoms, molecules and solids are presented in the issue. New directions in the photoelectronics, stimulated by problems of the super intense laser radiation interaction with nuclei, atomic systems and substance, are considered.

Scientific articles «Photoelectronics» collection abstracted in: Index Copernicus, Scientific Periodicals in National Library of Ukraine Vernadsky, Ukrainian Abstract Journal, Україніка наукова, Джерело, Українські наукові журнали: The issue is introduced to the List of special editions of the Ukrainian Higher Certification Com¬mission in physics-mathematics and technical sciences.

For lecturers, scientists, post-graduates and students.

У збірнику наведено результати теоретичних і експериментальних досліджень з питань фізики напівпровідників та мікроелектронних приладів, опто- та квантової електроніки, квантової оптики, спектроскопії та фотофізики ядра, атомів, молекул та твердих тіл. Розглянуто нові напрямки розвитку фотоелектроніки, пов'язані із задачами взаємодії надінтенсивного лазерного випромінювання з ядром, атомними системами, речовиною.

Збірник включено до Переліку спеціальних видань ВАК України з фізико-математичних та технічних наук. Збірник реферується: Index Copernicus, Scientific Periodicals in National Library of Ukraine Vernadsky, Ukrainian Abstract Journal, Україніка наукова, ВИНИТИ, Джерело, Українські наукові журнали.

Для викладачів, наукових працівників, аспіранітв, студентів.

В сборнике приведены результаты теоретических и экспериментальных исследований по вопросам физики полупроводников и микроэлектронных приборов, опто- и квантовой электроники, квантовой оптики, спектроскопии и фотофизики ядра, атомов, молекул и твердых тел. Рассмотрены новые направления развития фотоэлектроники, связанные с задачами взаимодействия сверхинтенсивного лазерного излучения с ядром, атомными системами, веществом.

Сборник включен в Список специальных изданий ВАК Украины по физико-математическим и техническим наукам. Сборник «Photoelectronics» реферируется в Index Copernicus, Scientific Periodicals in National Library of Ukraine Vernadsky, Ukrainian Abstract Journal, Україніка наукова, ВИНИТИ, Джерело, Українські наукові журнали.

Для преподавателей, научных работников, аспирантов, студентов.

Table of contents:

UDC 621.315.592

A. Tereshchenko, V. Smyntyna

Odesa National I.I. Mechnikov University, Odesa, Ukraine

INTERACTION OF TIO$_2$ NANOPARTICLES AND PROTEINS OF AN IMMUNE COMPLEX IN PHOTOLUMINESCENCE BASED BIOSENSOR

Interaction between nanostructured semiconductor thin layers and immune complex based proteins is a fundamental issue of the formation of nanobiointerface in the various biosensors, in particular, optical biosensors. In this work, the main aspects of the interaction between photoluminescent TiO$_2$ nanoparticles and Bovine leucosis virus (BLV) protein *gp51*, used as a model protein, during the formation of photoluminescence based immunosensor have been discussed. The antigens of *gp51* were immobilized on the surface of a nanostructured TiO$_2$ thin film formed on the glass substrates. As a result, an increase of the photoluminescence (PL) signal intensity and PL peak shift from 517 nm to 499 nm were observed. An incubation of TiO$_2$/*gp51* structure in a solution containing anti-*gp51* antibodies resulted in the backward PL peak shift from 499 nm to 516 nm and decrease of the PL intensity. The main reason of the changes in the PL spectra (i.e. PL maxima shifts and PL intensity variations) as a result of BLV protein *gp51* adsorption on the surface TiO$_2$ thin film is an electrostatic interaction between negatively charged surface of TiO$_2$ and positively charged atoms and groups provided by the adsorbed *gp51* protein due to the presence of partial uncompensated charges within the proteins.

Introduction

Nanostructured Titanium dioxide (TiO$_2$) is a well-known material for biosensors application due to its good bio-compatibility and high chemical stability [1-4]. As a wide band gap semiconductor that has an intense photoluminescence (PL) at room temperature, TiO$_2$ is broadly applied in optical biosensors and immunosensors due to its affinity towards proteins [5,6]. Optical transduction is an attractive technique for biosensing due to its high sensitivity and specificity, applicability in real-time monitoring, capability for high throughput and simple sample pre-treatment. Both label-free and labelled determination of the target analyte are possible by TiO$_2$ based optical transducers [7]. Recently, immunosensors based on optical transducers e.g. photo-luminescence, absorbance, reflectance etc, are of great interest since they demonstrate simple, fast and accurate determination of the target analytes [6,7]. Among various optical immunosensors, the photo-luminescence-based sensors seem to be the most promising for the improvement in the diagnosis of virus induced diseases, such as Bovine leucosis that is a lethal cancerous disease caused by Bovine leukemia virus (BLV)

[5,8]. Immunosensors are the class of biosensors that based on the reaction between antibody and antigen by formation of an immune complex (Fig. 1) [7]. Interaction between antigen-antibody couple is highly specific and selective one. The main advantage of the optical systems is that optical signal can detect the bio-molecular interaction contactless, *i.e.* without contamination or significant damage of the bio-samples. Besides, no additional labels (such as quantum dots or dyes) for the target analytes and no electrical contacts for measurements are required. However, despite of many reports on photoluminescence-based immunosensors, the interaction of biomolecules with semiconducting materials, which are used as analytical signal transducers in the most promising PL-based immunosensors, is poorly discussed [4-8]. In this research an optical immunosensor based on TiO$_2$ thin film which consisted of TiO$_2$ nanoparticles for the determination of Bovine Leucosis antibodies has been developed and the origin of the changes in the photoluminescent properties of TiO$_2$ nanoparticles as a result of the adsorption of Bovine leucosis proteins have been determined.

Experimental

The TiO$_2$ thin film consisted of TiO$_2$ nanoparticles (anatase, d~32 nm, purchased from Sigma Aldrich) was formed by sol-gel synthesis on the glass substrates. The details of the deposition procedure and structural characterization of TiO$_2$ thin film are described in some previous authors' works [2,8].
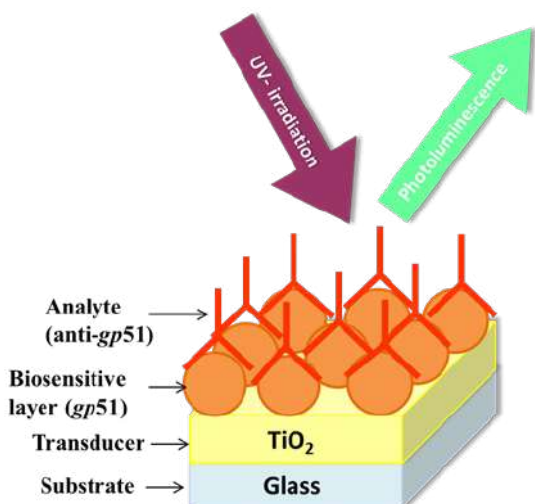
Figure 1. The scheme of photoluminescence immunosensor based on TiO2 nanoparticles.

The PL spectrum of TiO$_2$ nanoparticles, shown in figure 1a, is characterized by broad non-symmetric maximum around 500 nm, which can be splinted (using Origin 8.0 Pro) in two peaks, related to self-trapped exciton (STE) emission and luminescence caused by oxygen vacancies (V$_{[O]}$) [9]. Bovine leucosis antigens gp51 were immobilized on the surface of a nanostructured TiO$_2$ thin film by direct adsorption similarly using the process described in [5,6,8,10]. In brief: a solution of PBS containing gp51 antigens at a high concentration was directly immobilized on the TiO$_2$ surface (Fig.1). Then the sample was placed into a Petri cup for the incubation in a medium saturated with water vapor at 25°C. After 10 minutes of incubation, the surface of the sample was washed with PBS solution in order to remove non-immobilized antigens on the TiO$_2$ surface. To prevent a nonspecific interaction (i.e., binding of anti-gp51 antibodies directly to unmodified TiO$_2$ surface), the surface of TiO$_2$ was further treated with a solution of bovine serum albumin (BSA) that filled possible adsorption sites that remained free after the modification of TiO$_2$ surface with gp51.

It was found that immobilization of gp51 leukemia antigens on the surface of TiO$_2$ is accompanied by an increase of photoluminescence signal of the sample as well as the shift of the photoluminescence peak from 517 nm to 499 nm was observed after modification of the TiO$_2$ by adsorbed gp51 antigens (Fig. 2). Further interaction of immobilized gp51 antigens with gp51 antibodies resulted in reversed changes in TiO2 photoluminescence spectra, i.e. a decrease in PL intensity and the backward PL peak shift from 499 nm to 516 nm. The sensitivity of the obtained immunosensor was in the range of 2-8 mg/ml (Fig. 2) [5,8].
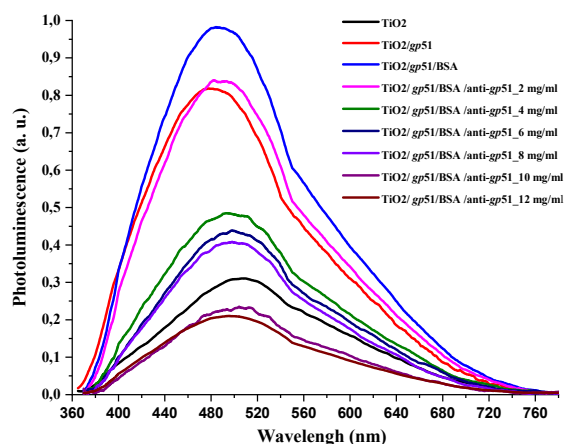
Figure 2. Photoluminescence spectra of TiO$_2$ nanoparticles before and after the immobilization of gp51 antigens on the TiO$_2$ surface, subsequent BSA deposition and after the interaction of TiO$_2$/gp51 based immunosensor after with analyte (anti-gp51 antibodies) of different concentrations.

Results and Discussion

Interaction of proteins and semiconductor nanostructures can take place in a few possible mechanisms of interaction: charge transfer, electrostatic interaction, resonance energy transfer and some others [1]. Since Bovine Leucosis protein gp51 is not a redox protein, i.e. it cannot be involved in reduction-oxidation reactions therefore the charge transfer between gp51 antigens and TiO$_2$ nanoparticles is not possible [11]. Meanwhile, the proteins consist of amino acids that might contain positively and/or negatively charged radicals that are determining the charge of the different protein domains [12]. A large quantity of negatively charged groups such as aldehyde (-CHO), hydroxyl (-OH), carboxyl (-COOH) and primary amine (-NH$_2$) and some other

groups, involved into the structure of amino acids, are responsible for the partial (δ+ and δ-) charges of particular protein domains. Therefore the proteins are characterized by electrostatic properties, and sometimes even significant electrostatic 'asymmetry of protein molecule' because the atoms and functional groups forming the protein molecules are charged differently both in their sign and in absolute charge value. Naturally, the charges at least partly are compensating each other, but since the ternary structure of proteins is relatively rigid and the charged groups have only limited degree of freedom to move within the protein globule, therefore in some parts of the protein some uncompensated charge on the surface and inside of the protein still remains. It should be taken into account that even if the structure of the most proteins is at some extent 'rigid' there is some degree of flexibility because both secondary and tertiary structures of the protein are supported by a large number of hydrogen bonds but many of them are not very strong. The electrostatic bonds, which are based on Coulomb forces, between the opposite charges, van der Waals forces and disulfide bonds also play an important role in the formation of both secondary and tertiary structures of protein [13,15].

TiO$_2$ (anatase) is known as a semiconductor of n-type conductivity, usually with an 'upward' band bending of the energy levels when closing the surface of TiO$_2$, which indicates the accumulation of a negative charge (bound at surface levels) on its surface [12]. The adsorption of the most of molecules is known to introduce an additional charge on the solid state surface and it can change the existing surface energy levels or form the additional ones that are involved in the exchange of charges with the volume of a solid material [14]. The presence of the mentioned above partial charges "δ-" and "δ +" suggests that the electrostatic influence on the surface charge of TiO$_2$ from the side of partially uncompensated charges in those parts of the gp51 protein that located on the surface of TiO$_2$ is responsible for the adsorption of this protein on the TiO$_2$ surface. The Coulomb interaction takes place between charged groups in the gp51 protein and the negatively charged surface of the TiO$_2$ because such electrostatic interactions are very

strong at small distances ranging from several Angstroms to few nanometers. Therefore, among the other interactions such as hydrogen bonds, disulfide bonds, Van der Waals interaction, etc, which also have significant role during the adsorption of proteins, the electrostatic interaction plays one of the most important role during the adsorption of proteins to electrically charged surfaces, such as TiO$_2$. In addition, the local electric fields of charged domains of adsorbed proteins are affecting the PL-centers of TiO$_2$ and it causes the shift in the photoluminescence spectra of TiO$_2$ nanoparticles (Fig. 3). Therefore, the photoluminescence maximum caused by STE shifts from 517 to 499 nm (i.e., to 18 nm), which corresponds to ~ 0.086 eV that is less than 0.1 eV, and it is one of the proofs of electrostatic interaction based physical adsorption of gp51 [10,13].
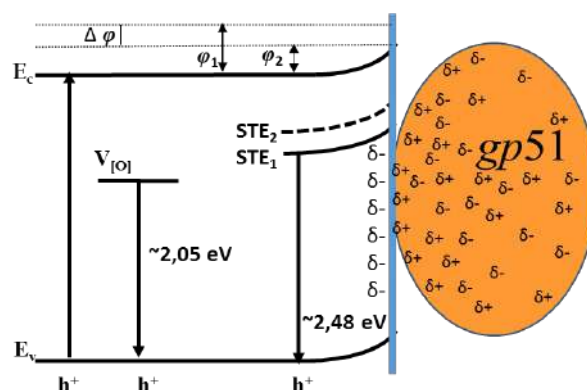
Figure 3. Energetic levels of TiO$_2$/gp51 immunosensing structure.

Further interaction of TiO$_2$/gp51 structure with anti-gp51, which is also a protein, led to the inverse changes in the photoluminescence spectra, i.e., to UV-shift of the spectrum and decrease the photoluminescence intensity to the value that corresponds to the pure TiO$_2$ (Fig.2). The latter effect is based on the formation an immune complex between immobilized antigens gp51 and anti-gp51 antibodies, which were present in aliquot. Formation of this immune complex, besides of the van der Waals interaction and other interactions, at a very high extent is based on the interaction between oppositely charged domains, functional groups and atoms in gp51 and anti-gp51 antibody molecules (including the formation of number of hydrogen bounds, which can be estimated as specific kind of electrostatic interaction). It

can be assumed that uncompensated charges ($\delta+$ and $\delta-$) of both proteins are involved in electrostatic interactions during the formation of immune complex (Fig. 3). As a result, some of the charged groups that were originally involved in the interaction between gp51 and TiO_2 are at least partially compensated by the opposite charge of the anti-gp51 protein groups, thereby reducing the direct electrostatic effect from immobilized gp51 proteins to the charged surface of TiO_2 and to light emitting centers. The effects described above have an effect on the shift of PL-maximum and on the decrease in the potential barrier on TiO_2/gp51 interface due to the charge-charge interaction between TiO_2 and gp51. The potential barrier at the interface between TiO_2 and gp51 has greater value in TiO_2/gp51 structure in comparison with that in TiO_2/gp51/anti-gp51 due to partial compensation (decrease in value) and/or delocalization of charges, which were initially involved into interaction between TiO_2 and gp51 after formation of TiO_2/gp51 structure [13,15].

The distribution of charges in TiO_2/gp51 structure can also be interpreted as a model based on an 'imaginary flat capacitor', formed as a result of the electrostatic interaction between oppositely charged protein gp51 layer and the TiO_2 surface (Fig. 4). The capacitor is formed as a result of protein gp51 adsorption on TiO_2 surface, after which the charges are distributed in energetically most favorable way, partially compensating each other. Consequently, the positive 'imaginary capacitor plate' is based on the positive charges, which are predominant in the protein gp51 area that after adsorption appears in close proximity to TiO_2/gp51 interface and/or due to the negative electrostatic effect of TiO_2 are induced/attracted closer to negatively charged surface. These charged atoms/groups/domains of gp51 that are localized in the close proximity to the TiO_2 surface and they electrostatically affect the TiO_2 emission centers and the energy value of the surface potential barrier. Hence, the position of the energy levels of the TiO_2 emission maximum depends on TiO_2 surface modification stage (TiO_2 or TiO_2/gp51) shifts from/backwards the initial position of the demarcation level. Figure 4a demonstrates an imaginary flat capacitor consisting of a negatively

charged plate on the surface of TiO_2 and an 'imaginary positively charged plate' formed in gp51 protein in close proximity to TiO_2/gp51 interphase. Hence, the interaction of TiO_2/gp51 with anti-gp51 antibodies and the formation of gp51/anti-gp51-based immune complex leads to a 'deformation' and the reduction of charge 'stored' on 'the positive imaginary capacitor plate' (Fig. 4b).
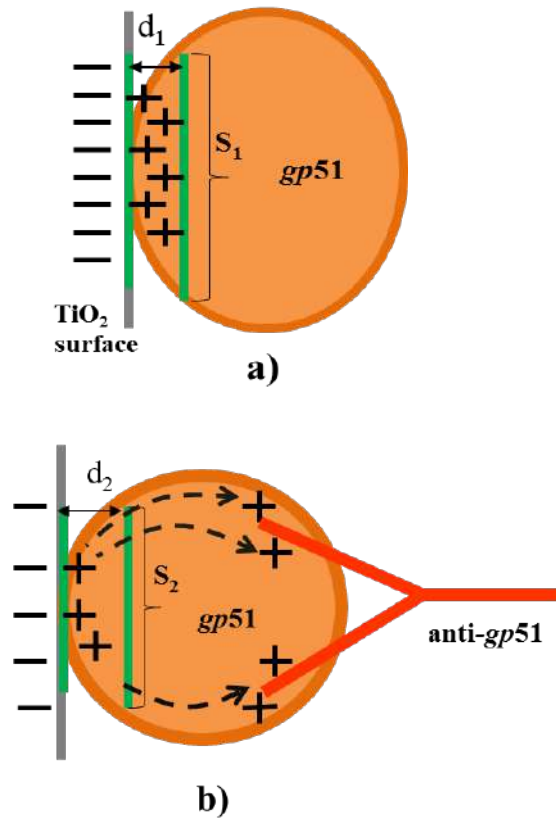
Figure 4. Flat capacitor based model of the charges interaction between TiO_2 surface and gp51 proteins: a) electrostatic interaction of partial uncompensated charges of immobilized gp51 antigens with negative charges located on the surface of TiO_2; b) model of interaction that takes into account the electrostatic interaction of charges within gp51 antigens and anti-gp51 antibodies of BLV immune complex.

This is mainly due to the redistribution and partial compensation of charges during the formation of the gp51/anti-gp51 immune complex, which in turn reduces the charge of 'the imaginary capacitor plate' based on gp51 ($q_2 < q_1$). Due to this reduced charge it can be interpreted as the reduction of the area of the same plate (S_2) and/or the increase of the distance (d_2) between the two imaginary capacitor plates based on gp51 and TiO_2 which leads to

the decrease of capacitance according to equation (1).

$$C = \varepsilon\varepsilon_0 S/d \qquad (1)$$

This effect is observed because some of the $gp51$ protein charges move from the TiO_2/$gp51$ interface towards interacting anti-$gp51$ protein and are partially compensated by the charge present in anti-$gp51$, whereby an imaginary positive $gp51$-based capacitor plate of the capacitor is reduced in imaginary surface area and/or correspondingly moving apart from the negative TiO_2 plate. This effect leads to a decrease in the capacitance of this imaginary capacitor and the electric field induced by $gp51$ becomes reduced. Therefore, after the interaction of TiO_2/$gp51$ with anti-$gp51$ antibodies and the formation of $gp51$/anti-$gp51$ complex, which is involved into TiO_2/$gp51$/anti-$gp51$ structure, the electrostatic effect of $gp51$ initially adsorbed on TiO_2 towards the TiO_2 surface significantly decreases. The PL shifts are attributed to the variations in the self-trapped exciton energy level, which were induced by the changes of electrostatic interaction between positively charged atoms and groups, provided by the adsorbed $gp51$ protein and negatively charged surface of TiO_2 [10,13,15].

Conclusions

The main aspects of the interaction mechanism between nanostructured TiO_2 layer and BLV proteins $gp51$ have been evaluated during the formation of photoluminescence-based immunosensor. Bovine leucosis protein $gp51$ was adsorbed on the surface of a nanostructured TiO_2 thin film, formed on glass substrates. A photoluminescence (PL) peak shift from 517 nm to 499 nm was observed after modification of the TiO_2 by adsorbed $gp51$ (i.e. formation of the biosensitive layer $gp51$/TiO_2). An incubation of $gp51$/TiO_2 in a solution containing anti-$gp51$ resulted in the formation of a new structure (anti-$gp51$/gp51/TiO_2) and the backward PL peak shift from 499 nm to 516 nm. The PL shifts are attributed to the variations in the self-trapped exciton energy level, which were induced by the changes of electrostatic interaction between positively charged atoms and groups, provided by the ad-

sorbed $gp51$ protein and negatively charged surface of TiO_2. The charge–charge-based interaction in the double charged layers $gp51$/TiO_2 can also be interpreted as a model based on 'imaginary capacitor', formed as a result of the electrostatic interaction between oppositely charged protein $gp51$ layer and the TiO_2 surface. Development of advanced bioanalytical systems based on photoluminescence immunosensors seems to be very promising direction in the development of new biosensors.

References:

1. J. Preclíková, P. Galář, F. Trojánek, S. Daniš, B. Rezek, I. Gregora, Y. Němcová, P. Malý, Nanocrystalline titanium dioxide films: Influuence of ambient conditions on surface- and volume-related photoluminescence, Journal of Applied Physics 108, 2010, 113502.
2. A. Tereshchenko, R. Viter, I. Konup, V. Ivanitsa, S.A. Geveliuk, Yu. Ishkov, V. Smyntyna, TiO_2 Optical Sensor for Amino Acid Detection, Proceedings of SPIE, The International Society for Optical Engineering 2013, 9032.
3. A. Tereschenko, A. Kusevitch, R. Viter, V. Smyntyna, J. Buk, J. M. Macak, A. Gurov, I. Konup, S. Gevuluk, Optical and structural properties of TiO_2 Nanofibers prepared by the electrospinning method, Photoelectronics, 2011, 8-11.
4. S. Ramanavicius, A. Tereshchenko, R. Karpicz et.al., TiO_{2-x}/TiO_2-Structure Based 'Self-Heated' Sensor for the Determination of Some Reducing Gases, Sensors, 20, 2020, 74.
5. R. Viter, A. Tereshchenko, V. Smyntyna, J. Ogorodniichuk, N. Starodub, R. Yakimova, V. Khranovskyy, A. Ramanavicius, Toward development of optical biosensors based on photoluminescence of TiO_2 nanoparticles for the detection of Salmonella, Sensors and Actuators B: Chemical, 252, 2017, 95.
6. A. Tereshchenko, M. Bechelany, R. Viter, V. Khranovskyy, V. Smyntyna, N. Starodub, R. Yakimova, Optical biosensors based on ZnO nanostructures: advantages and perspectives. A review, Sensors and Actuators B Chemical 229, 2016, 664.
7. A. Tereshchenko, V. Fedorenko, V. Smyntyna, I. Konup, A. Konup, M. Eriksson, R.

Yakimova, A. Ramanavicius, S. Balme, M. Bechelany, ZnO films formed by atomic layer deposition as an optical biosensor platform for the detection of Grapevine virus A-type proteins, Biosensors and Bioelectronics 92, 2017, 763.

8. R. Viter, V. Smyntyna, N. Starodub, A. Tereshchenko, A. Kusevitch, I. Doycho, S. Geveluk, N. Slishik, J. Buk, J. Duchoslav, J. Lubchuk, I. Konup, A. Ubelis and J. Spigulis, Novel Immune TiO$_2$ Photoluminescence Biosensors for Leucosis Detection, Procedia Engineering, 47, 2012, 338–341.

9. I. Sildos, A. Suisalu, V. Kiisk, M. Schuisky, H. Mandar, T. Uustare and J. Aarik, Effect of Structure Development on Self-Trapped Exciton Emission of TiO$_2$ Thin Films, Proc. SPIE, 4086, 2000, 427–430.

10. A. Tereshchenko, V. Smyntyna, A. Ramanavicius, Model of interaction between TiO2 nanostructures and Bovine Leucosis proteins in photoluminescence based Immunosensors, Advanced Nanomaterials for Detection of CBRN, Chapter 14. NATO Science for Peace and Security Series A: Chemistry and Biology, Springer Nature B.V., 2020.

11. T. Ogawa, Biochemistry, Genetics and Molecular Biology, Volume 'Protein Engineering-Technology and Application' (ISBN 978-953-51-1138-2).

12. S. M. Gupta, M. Tripathi, A review of TiO$_2$ nanoparticles, Chin. Sci. Bull., 56, 2011, 1639.

13. A. Tereshchenko, V. Smyntyna, A. Ramanavicius, "Interaction mechanism between TiO$_2$ nanostructures and bovine leukemia virus proteins in photoluminescence-based immunosensors", RSC Advances 8, 2018, pp. 37740.

14. V. Smyntyna, Electron and Molecular Phenomena on the Surface of Semiconductors, Nova Publishers, New York, 2013.

15. A. Tereshchenko, V. Smyntyna, U. Bubniene A. Ramanavicius, Optical immunosensor based on photoluminescent TiO2 nanostructures for determination of Bovine Leucosis proteins. Model of interaction mechanism, Chapter 25, Nanomaterials in Biomedical Application and Biosensors (NAP-2019), Springer Proceedings in Physics 244, Springer Nature Singapore Pte Ltd., 2020.

A. Tereshchenko, V. Smyntyna

INTERACTION OF TIO$_2$ NANOPARTICLES AND PROTEINS OF AN IMMUNE COMPLEX IN PHOTOLUMINESCENCE BASED BIOSENSOR

Summary.

It has been investigated an interaction between nanostructured semiconductor thin layers and immune complex based proteins that is a fundamental issue of the formation of nanobiointerface in the various biosensors, in particular, optical biosensors. In this work, the main aspects of the interaction between photoluminescent TiO$_2$ nanoparticles and Bovine leucosis virus (BLV) protein *gp51*, used as a model protein, during the formation of photoluminescence based immunosensor have been discussed. The antigens of *gp51* were immobilized on the surface of a nanostructured TiO$_2$ thin film formed on the glass substrates. As a result, an increase of the photoluminescence (PL) signal intensity and PL peak shift from 517 nm to 499 nm were observed. An incubation of TiO$_2$/*gp51* structure in a solution containing anti-*gp51* antibodies resulted in the backward PL peak shift from 499 nm to 516 nm and decrease of the PL intensity. The main reason of the changes in the PL spectra (i.e. PL maxima shifts and PL intensity variations) as a result of BLV protein *gp51* adsorption on the surface TiO$_2$ thin film is an electrostatic interaction between negatively charged surface of TiO$_2$ and positively charged

atoms and groups provided by the adsorbed *gp51* protein due to the presence of partial uncompensated charges within the proteins.

Key words: TiO$_2$ nanoparticles, photoluminescence, biosensor.

А. Терещенко, В. Сминтина

ВЗАЄМОДІЯ НАНОЧАСТИНОК ТІО$_2$ ТА БІЛКІВ ІМУННОГО КОМПЛЕКСУ У БІОСЕНСОРІ НА ОСНОВІ ФОТОЛЮМІНЕСЦЕНЦІЇ

Резюме.

Досліджена взаємодія між тонкими наноструктурованими напівпровідниковими шарами та білками на основі імунних комплексів, яка є фундаментальним питанням формування нанобіоінтерфейсу в різних біосенсорах, зокрема, в оптичних біосенсорах. В роботі обговорено основні аспекти взаємодії фотолюмінесцентних наночастинок TiO$_2$ з білком *gp*51 вірусу лейкозу великої рогатої худоби (BLV), який використовується як модельний білок, під час формування імуносенсора на основі фотолюмінесценції. Антигени *gp*51 були іммобілізовані на поверхні наноструктурованої тонкої плівки TiO$_2$, сформованої на скляних підкладках. В результаті спостерігалося збільшення інтенсивності сигналу фотолюмінесценції (ФЛ) та зсув піку ФЛ з 517 нм до 499 нм. Інкубація структури TiO$_2$/*gp*51 у розчині, що містить антитіла до *gp*51, призвела до зсуву піку ФЛ у зворотному напрямку від 499 нм до 516 нм та зниження інтенсивності ФЛ. Основною причиною змін у спектрах ФЛ (тобто зсувів максимумів ФЛ та зміни інтенсивності ФЛ) в результаті адсорбції білка BLV *gp*51 на поверхні тонкої плівки TiO$_2$ є електростатична взаємодія між негативно зарядженою поверхнею TiO$_2$ та позитивно зарядженими атомами та групами адсорбованого білка *gp*51 через наявність часткових нескомпенсованих зарядів всередині білків.

Ключові слова: TiO$_2$ наночастинки, фотолюмінесценція, біосенсор.

А. Терещенко, В. Смынтына

ВЗАИМОДЕЙСТВИЕ НАНОЧАСТИЦ ТІО$_2$ И БЕЛКОВ ИММУННОГО КОМПЛЕКСА В БИОСЕНСОРЕ НА ОСНОВЕ ФОТОЛЮМИНЕСЦЕНЦИИ

Резюме

. Исследовано взаимодействие между тонкими слоями наноструктурированных полупроводников и белками на основе иммунных комплексов, которое является фундаментальной проблемой формирования нанобиоинтерфейса в различных биосенсорах, в частности, оптических биосенсорах. В работе обсуждаются основные аспекты взаимодействия фотолюминесцентных наночастиц TiO$_2$ с белком *gp*51 вируса лейкоза крупного рогатого скота (BLV), используемым в качестве модельного белка, при формировании иммуносенсора на основе фотолюминесценции. Антигены *gp*51 были иммобилизованы на поверхности наноструктурированной тонкой пленки TiO$_2$, сформированной на стеклянных подложках. В результате наблюдалось увеличение интенсивности сигнала фотолюминесценции (ФЛ) и сдвиг пика ФЛ с 517 нм до 499 нм. Инкубация структуры TiO$_2$/*gp*51 в растворе, содержащем антитела против *gp*51, приводила к обратному сдвигу пика ФЛ с 499 нм до 516 нм и снижению интенсивности ФЛ. Основной причиной изменений спектров ФЛ (т.е. сдвигов максимумов и вариаций интенсивности ФЛ) в результате адсорбции белка *gp*51 BLV на поверхностной тонкой

пленке TiO_2 является электростатическое взаимодействие между отрицательно заряженной поверхностью TiO_2 и положительно заряженными атомами и группами адсорбированного белка *gp*51 из-за наличия частичных нескомпенсированных зарядов внутри белков.

Fedosov SN, Sergeeva AE

Odessa National University of Technology, vul. Kanatna 112, Odessa, 65039, Ukraine,
e-mail <snfedosov@ukr.net>

USING THE PYROELECTRIC RESPONSE TO STUDY THE POLARIZED STATE IN A TYPICAL FERROELECTRIC POLYMERS

This article examines the correlation between the pyroelectric response in typical films of ferroelectric polymers and the value of the residual ferroelectric polarization. The pyroelectric response was obtained by the thermal pulse method proposed by Collins. The magnitude of the residual polarization was measured depending on the magnitude of the applied electric field during primary electrification (poling) and during its switching. It is shown that the used method has the high sensitivity. It was found that the magnitude of the pyroelectric response depends significantly on the polarized state, which is determined by the values of the electric field during electrification and polarization switching and on the duration of exposure to this field. The identity of the graphs of the dependence of the residual polarization on the field and time and the corresponding graphs of the magnitude of the pyroelectric response led to the final conclusion about the proportionality of the magnitude of the response to the residual polarization. Thus, it is concluded that the pyroelectric response method can be used to estimate the magnitude of polarization in ferroelectric polymers.

Introduction

Ferroelectric polymers, in particular polyvinylidene fluoride (PVDF) and its copolymers with tetrafluoroethylene P(VDF-TFE) and trifluoroethylene P(VDF-TrFE), have been considered for a number of years as an alternative material for replacing ceramic ferroelectrics in production of various types of sensors and electromechanical converters [1].

The most important parameter of such materials is the magnitude and stability of the residual ferroelectric polarization P. Such polarization is created in original materials, usually thin films, by electrifying (poling) them in a strong DC electric field, which is carried out either by the sandwich method (a polymer film is located between two metal electrodes [2]), or under the action of corona discharge [3].

Performance characteristics of the finite elements, such as the piezoelectric and pyroelectric coefficients, depend on the magnitude of the residual polarization.

At the same time, it is known that the magnitude of the residual polarization in ferroelectric polymers depends on the value of the applied electric field during poling, as well as on the duration of poling, and on temperature [4].

It is also known that a part of the formed residual polarization can be switched back, if the conditions for neutralizing the depolarizing field, which inevitably arises during electrification, are not provided [5].

Given the above, it is clear how important to know the magnitude of the polarization. Unfortunately, the known methods for determining the value of the residual polarization are rather complicated and cumbersome. The most commonly used method is to construct a hysteresis curve in the coordinates of the dependence of polarization on the changing electric field [6]. The Sawyer-Tower method [7] often used in the study of ceramic ferroelectrics for obtaining dielectric hysteresis loops at frequency of 1 kHz is not suitable for ferroelectric polymers because of the long relaxation time in such polymers [8]. To obtain the correct polarization values, measurements must be carried out at infra-low frequencies during long time.

The purpose of this article is to prove that the dependences of the polarization value on the field strength and the poling time in ferroelectric polymers correlate with similar dependences of the pyroresponse obtained by the heat pulse method.

The carried out experimental studies confirm this position, which allows us to recommend the pyroresponse method for the rapid

determination of the value of ferroelectric polarization in ferroelectric polymers.

Pyroelectricity in ferroelectric polymers

Pyroelectric effect in PVDF films was discovered more than 40 years ago. However, despite the large number of works, the nature of pyroelectricity in PVDF still remains unclear. A series of papers were devoted to the pyroelectric properties of the ferroelectric polymers, the results of which are summarized in reviews [10-13] that describe the main proposed models of pyroelectricity in PVDF. It is stipulated in all models that electrostriction, fluctuation of dipoles and change in the dimensions contribute to the pyroelectricity.

Under the pyroelectric effect, one means the range of phenomena associated with reversible changes in the electric displacement D vector (induction) when the temperature changes. Since induction depends on the internal polarization P, then for the case of a flat short-circuited sample with homogeneous polarization P we obtain

$$p_o = \frac{\partial D}{\partial T} = \frac{\partial P}{\partial T} = \frac{\partial \sigma}{\partial T} = \frac{\partial (q/S)}{\partial T}, \qquad (1)$$

where p_o is the pyroelectric coefficient, q and σ are magnitude and density of the bound surface charge; S is the surface area.

In the experimental conditions, the current $I(T) = \frac{dq}{dt}$ is measured occurring when the temperature change (dT/dt), and the pyrocoefficient p is considered to have the following value

$$p = \frac{1}{S}\frac{dq}{dT} = \frac{1}{S}\frac{I(T)}{dT/dt}. \qquad (2)$$

Investigating the pyroelectric effect in PVDF, Lines and Glass [8] came to the conclusion that this is a real pyroelectricity, but not a depolarization effect observed in many polar electrets, because the crystalline phase of PVDF completely corresponds to the definition of a ferroelectric, as a pyroelectric with reversible spontaneous polarization under application of the electric field.

Fedosov and von Seggern [4,14,15] proved that compensating charges localized on the surface of crystallites are very important in two-component ferroelectric polymers of the PVDF type for obtaining high and stable polarization. It is generally accepted that the pyrocoefficient in PVDF is directly proportional to the value of the residual polarization.

Material and methods

We studied thin films of ferroelectric polymers, such as PVDF and its copolymer with tetrafluoroethylene P(VDF-TFE). Samples of PVDF and P(VDF-TFE) films having thickness of 20-30 μm were obtained from the experimental batches of "Plastpolymer", St. Petersburg, produced by the method of extrusion, followed by uniaxial orientation (stretching) in the ratio 1:4 at the temperature of 100 °C followed by annealing at 120 °C for 1 hour. The degree of crystallinity of PVDF and P(VDF-TFE) films according to the manufacturer was (47 ± 3) %. The crystallites sizes according to the results of X-ray analysis have the following values: $L_\alpha = 96\pm6$ Å, $L_\beta = 70\pm8$ Å. The percentage of tetrafluorethylene in P(VDF-TFE) was 5-10%.

Biauxally oriented PVDF films of the Kureha Co. had a thickness of 12.5 μm. In order to determine the relation between non-polar α-phase and ferroelectric β-phase, transmission and reflection spectra of all types of films in the range of 400-650 cm^{-1} were studied using the IR spectrometer FT-IR Perkin-Elmer 1750 with Fourier transform. Judging by the magnitude of 535 and 510 cm^{-1} peaks, it was found that the ratio 43:57 was between α and β in PVDF (Plastpolymer) films, 30:70 in Kureha Co. films, and 5: 95 in P(VDF-TFE) films.

The pyroelectric effect is usually investigated in quasi-static or dynamic mode. In the first case, the pyroelectric current is measured during the slow heating of the short-circuited sample, while in the second case, the variable component of the current is studied during a rapid change of temperature. The main difficulties of the quasi-static method are the separation of the pyroelectric (reversible) component of the thermal shock from the relaxation (irreversible) component in the Thermally Stimulated Depolarization (TSD) current.

We measured the pyroelectric dynamic coefficient by the thermal pulse method developed by Collins [16] and used in a number of other studies.

The light pulse of 50 μs duration was generated using the Metz 45 CT-3 flashlight and was used as a reproduced heat source that penetrates the surface of the poled films. The pyroelectric signal was recorded using a broadband Tektronix TDS 510A. oscilloscope. This method is the dynamic one.

With the help of a highly sensitive pyroelectric sensor it was established that light pulses are characterized by a rather high reproducibility. The average energy scatter in measuring of 200 consecutive pulses was 2.4%. The magnitude of the pyroelectric coefficient was judged by the maximum value of the electric signal. Thus the results were obtained in relative units.

Dependence of the residual spontaneous polarization on electric field and poling time was studied on samples of PVDF by the method of poling and switching of polarization described in details in works of Fedosov and von Seggern [4,14,15]

Results and discussion

Pyroelectric studies of PVDF films have an independent value, since PVDF is widely used in pyroelectric sensors. However, it is interesting to study pyroactivity in conjunction with the residual ferroelectric polarization, because it will allow on one side to clarify the nature of the pyroelectricity in PVDF, and on the other to ensure its stability.
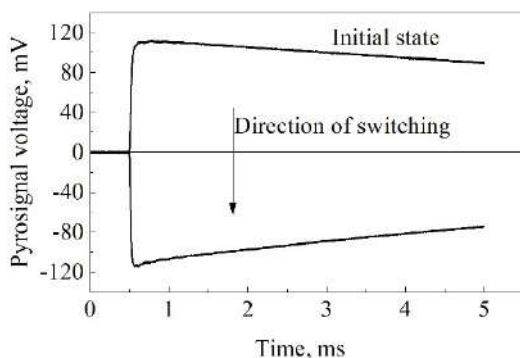
Fig. 1. The pyroelectric signal after the polarization switching of PVDF film by applying 2 kV voltage for 50 seconds. Pyroelectricity was measured after 1.5 min after the voltage switching off.

Measurement of the pyroactivity by the Collins method was carried out immediately after poling or polarization switching. Fig. 1 shows how the pyroelectric signal changes when the polarization is fully switched from a fully polarized state. Although the value of the pyrocoefficient can only be judged in relative units, it is evident that the sensitivity of the method is rather high and the signal is completely symmetric after the full switching. In Fig. 2 it is shown that full switching occurs only if the voltage pulse duration exceeds 100 s. At a shorter duration of the voltage pulse, there is only a partial switching of polarization judging from the data of Fig. 2.
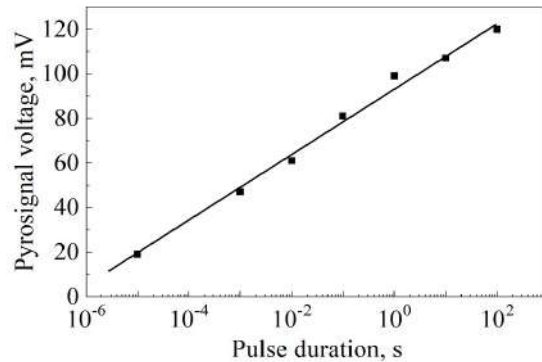
Fig. 2. Dependence of the pyroelectric signal on the duration of the polarizing pulse in the range from 10 μs to 100 s during initial poling of the PVDF film by 2.5 kV voltage.

Fig. 3 shows the results of four series of experiments, in which the polarization switching was performed at different durations of the voltage pulse, but with the same magnitude in each series. At a voltage of 0.5 kV (Fig. 3) that provides a field strength of about 40 MV/m, being in the same order as the coercive field, even with a pulse duration of 50 s, only 6.4% of the polarization is switched, which in principle can be switched, and if the pulse duration is shorter than 50 ms, no switching is practically happening.
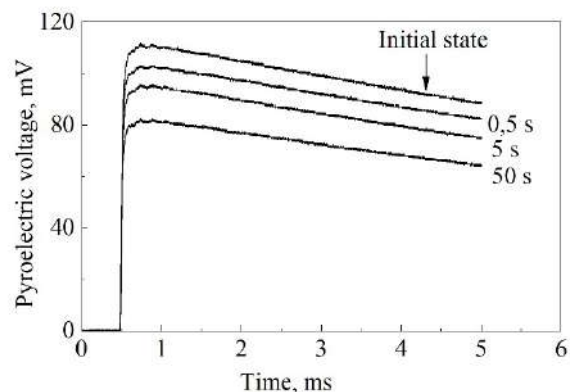
Fig. 3. Pyrosignal at sequential polarization switching in PVDF films by pulses of 0.5 kV voltage with duration from 5 ms to 50 s. The duration of the voltage pulse is indicated near the curves.

At the voltage of 1 kV applied for 50 s, 44.4% of the residual polarization is switched, that is, the sample is almost converted to the state with zero mean polarization. At this voltage, the 2.2% polarization is switched even within 50 μs of the switching voltage application. Increasing the voltage to 1.5 kV leads to the switching of 79.4% of the residual polarization by 50 s application of voltage.

At a voltage of 2 kV for 50 s, the polarization is completely switched. It is interesting to note that the specific shape of the pyroelectric signal when switched polarization is more than 50%, that is, when the direction of the average predominant orientation of the dipoles changes to the opposite direction.
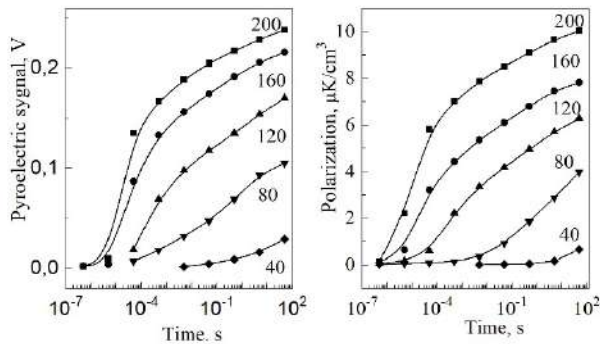
Fig. 4. Evolution of pyroelectric activity and stable ferroelectric part of polarization obtained by sequential application of switching voltage pulses with increasing duration from 0.5 μs to 50 s and at different field strength.

In the electrode zone, which the thermal pulse passes during $t_o = 0.2$ ms, when the polarity direction changes to the opposite, a non-symmetric in shape pyroelectric signal is formed in relation to the initial one. In the vicinity of the electrode, the direction of the pyroelectric signal change is maintained during the switching of polarization indicating the existence of a near-to-electrode layer of thickness about $x = \sqrt{\lambda t_o}$ where λ is the thermal conductivity of PVDF. According to the literature data, the coefficient of thermal conductivity of PVDF is $\lambda = 6 \cdot 10^{-8}$ m^2/s, thus the thickness of the electrode layer is of the order of 3 μm. We believe that the feature revealed by us is due to the fact that the originally formed polarization in this layer does not switch even in high fields [17].

It is natural to assume that polarization near the electrode does not increase sharply, but there is some transition layer in which the polarization grows from zero at the electrode to a maximum uniform value in the volume of the film.

According to the Poisson equation, inhomogeneous polarization in any layer can be stable only with the presence of a compensating charge in this layer [15]. Apparently, this charge was trapped by deep traps and not released during the polarization switching. The revealed phenomenon is similar to the established by us feature about impossibility of improving the polarization uniformity if its initial formation took place in weak or medium fields [17].

It was found that polarization switched under the action of several successive short voltage pulses is much smaller than the polarization switched by one pulse of the duration equal to the total time of several short pulses. This indicates that there is some distribution of switching times, i.e. some dipoles are easily switched, while others require more time to be switched. Under the influence of short voltage pulses, only "fast" dipoles are switched, while during the continuous voltage application both "fast" and "slow" dipoles are switched, so the total switched polarization significantly increases.

All described experiments were carries out on PVDF and P(VDF-TFE). It was found that obtained results were identical for both kinds of samples.

Conclusion

In this paper, polarization switching at different times and field strength is compared with the values of the pyroelectric signal under the same poling and switching conditions. The absolute similarity of the above experimental graphs indicates that there is a direct proportional relationship between the residual ferroelectric polarization and the value of the pyroelectric coefficient in the studied ferroelectric polymer. This provision makes it possible to use the technically simple pyrocoefficient measurement to evaluate the polarized state of poled ferroelectric polymer films, that is, to estimate the magnitude and the direction of the residual polarization.

References

1. Sessler G. M. Electrets: Recent Developments // J. Electrostatics – 2001, - v.51, No. 2 – p. 137-145.
2. von Seggern H, Fedosov S. N. Conductivity induced polarization in a semicrystalline ferroelectric polymer // IEEE Trans. Diel. Elect. Insul. – 2004. – v. 11, No. 2. – p. 232– 241.
3. Fedosov S. N., Sergeeva A. E. Corona poling of ferroelectric and nonlinear optical polymers // Moldavian Journal of the Physical Sciences, 2002, No.2, p.28-31.
4. Fedosov S. N., von Seggern H. Pyroelectricity in polyvinylidene fluoride: influence of polarization and charge // J. Appl. Phys. – 2008. – v. 103, No.1. – p. 014105–014109.
5. Fedosov S. N., von Seggern H., Backswitching of ferroelectric polarization in two-component systems // J. Appl. Phys. – 2004. – v. 96, No. 4. – p. 2173–2180.
6. Furukawa T., Nakajima T., Yoshiyuki T., Factors Governing Ferroelectric Switching Characteristics of Thin VDF/TrFE Copolymer Films // IEEE Transactions on Dielectrics and Electrical Insulation – 2006, v. 13, No. 5 - p.1120-1131.
7. Stewart M., Cain M. G., Weaver P. Electrical Measurement of Ferroelectric Propertie // in Characterisation of Ferroelectric Bulk Materials and Thin Films (ed. Cain M. G.), Springer, 2014, 280 p.
8. Lines M. E. and Glass A. M., Principles and Applications of Ferroelectrics and Related Materials (Oxford University Press, Oxford, Science - 2001), 680 p.
9. Mort J. Polymers, Electronic Properties // in Encyclopedia of Physical Science and Technology (Third Edition), 2003.
10. Stewart M., Cain M. G., Weaver P. Electrical Measurement of Ferroelectric Propertie // in Characterisation of Ferroelectric Bulk Materials and Thin Films (ed. Cain M. G.), Springer, 2014, 280 p.
11. Fukada E. History and Recent Progress in Pyroelectric Polymer // IEEE Trans. Ultrason. Ferroelectrics and Freq. Control. – 2000. – v.47, No. 6. –p.1277–1290.
12. Bauer S., Bauer-Gogonea S., Lindner M., Schrattbauer K. Piezo-, Pyro- and Ferroelectric Polymers. In: Galassi C. (eds) Advances in Science, Technology and Applications. NATO Science Series, Springer, Dordrecht, 2000, vol 76.
13. Lang S. B., Muensit S. Review of some lesser-known applications of piezoelectric and pyroelectric polymers // Appl. Phys. 2006, - v. A 85, p. 125–134.
14. von Seggern H., Fedosov S. N. Conductivity-induced polarization buildup in PVDF // Appl. Phys. Lett. 2002, v. 81, No. 15. – p. 2830–2832.
15. von Seggern H., Fedosov S. N. Importance of screening charge dynamics on polarization switching in polyvinylidene fluoride // Appl. Phys. Lett. – 2007. – v. 91, No. 6. – p. 62914–62918.
16. Raju G. G. The Thermal Pulse Method of Collins // in Dielectrics in Electric Fields, CRC Press, 2003, p. 520-525
17. Fedosov S. N., Sergeeva A. E. Distribution of the Ferroelectric Polarization in PVDF During Initial Poling and Polarization Reversal // J. Nano- Electron. Phys. – 2019, v. 11, No 1, 01012 (7pp).

Fedosov S. N., Sergeeva A. E.

USING THE PYROELECTRIC RESPONSE TO STUDY THE POLARIZED STATE IN A TYPICAL FERROELECTRIC POLYMERS

Summary

In the presented paper, the correlation between the pyroelectric response in typical films of ferroelectric polymers PVDF and P(VDF-TFE) and the value of the residual ferroelectric polarization was investigated. The pyroelectric response was measured by the thermal pulse

Collins method. Dependence of the residual polarization on the value of the applied electric field during primary electrification (poling) and during its switching was also measured. It has been found that the used methods have high sensitivity and reproducibility. It was shown that the magnitude of the pyroelectric response depended significantly on the polarized state, which was determined by the values of the electric field during electrification and polarization switching and on the duration of exposure to this field. The identity and absolute similarity of the residual polarization dependence graphs on the field and time and corresponding graphs of the pyroelectric response magnitude led to the conclusion that the magnitude of the pyroelectric was proportional to the residual polarization. Thus, the pyroelectric response method can be used to estimate the value of the residual polarization in ferroelectric polymers.

Key words: ferroelectric polymers, pyroelectricity, residual polarization

Федосов С.Н., Сергєєва О.Є.

ВИКОРИСТАННЯ ПІРОЕЛЕКТРИЧНОГО ВІДГУКУ ДЛЯ ДОСЛІДЖЕННЯ ПОЛЯРИЗОВАННОГО СТАНУ У ТИПОВИХ СЕГНЕТОЕЛЕКТРИЧНИХ ПОЛІМЕРАХ

Резюме

У представленій роботі досліджено кореляцію між піроелектричним відгуком у типових плівках сегнетоелектричних полімерів ПВДФ та П(ВДФ-ТФЕ) та величиною залишкової поляризації. Піроелектричну реакцію вимірювали методом Коллінза теплового імпульсу. Виміряно також залежність залишкової поляризації від величини електричного поля під час первинної електризації та під час її перемикання. Встановлено, що використані методи мають високу чутливість. Показано, що величина піроелектричного відгуку залежить від поляризованого стану, який визначався величинами електричного поля при електризації та перемиканні поляризації та від тривалості впливу поля. Тотожність та абсолютна подібність графіків залежності залишкової поляризації від поля та часу та відповідних графіків величини піроелектричної реакції дозволили зробити висновок, що величина піроелектричного відгуку була пропорційна залишковій поляризації. Таким чином, метод піроелектричного відгуку може бути використаний для оцінки величини залишкової поляризації в сегнетоелектричних полімерах.

Ключові слова: сегнетоелектричні полімери, піроелектрика, залишкова поляризація

Федосов С.Н., Сергеева А.Е.

ИСПОЛЬЗОВАНИЕ ПИРОЭЛЕКТРИЧЕСКОГО ОТКЛИКА ДЛЯ ИССЛЕДОВАНИЯ ПОЛЯРИЗИРОВАННОГО СОСТОЯНИЯ В ТИПИЧНЫХ СЕГНЕТОЭЛЕКТРИЧЕСКИХ ПОЛИМЕРАХ

Резюме

В представленной работе исследована корреляция между пироэлектрическим откликом в типичных пленках сегнетоэлектрических полимеров ПВДФ и П(ВДФ-ТФЭ) и величиной остаточной сегнетоэлектрической поляризации. Пироэлектрическую реакцию измеряли методом теплового импульса, предложенного Коллинзом. Измерена также зависимость

остаточной поляризации от величины приложенного электрического поля при первичной электризации и при ее переключении. Установлено, что использованные методы обладают высокой чувствительностью и воспроизводимостью. Показано, что величина пироэлектрического отклика существенно зависит от поляризованного состояния, определяемого значениями электрического поля при электризации и переключении поляризации и продолжительности воздействия этого поля. Тождество и абсолютное сходство графиков зависимости остаточной поляризации от поля и времени и соответствующих графиков величины пироэлектрической реакции позволили заключить, что величина пироэлектрического отклика была пропорциональна остаточной поляризации. Таким образом, метод пироэлектрического отклика может быть использован для оценки величины остаточной поляризации в сегнетоэлектрических полимерах.

V.M. Skobeeva[2], V.A. Smyntyna[1], M. I.Kiose[1], N.V. Malushin[2]

[1] Odessa I.I. Mechnikov National University, Dvoryanskaya St. 2, 65082 Odessa, Ukraine,
[2]Odessa I. I. Mechnikov National University, Research Institute of Physics, 65082, Odessa.
Pastera, 27, Ukraine
e-mail: v_skobeeva@ukr.net

EVOLUTION OF LUMINESCENT PROPERTIES DURING STORAGE CdS QDs IN AIR

This paper presents the results of a study the CdS QDs and nanostructures of CdS / ZnS QDs obtained by the sol - gel technology in an aqueous solution of gelatin and the effect of storage on their luminescence. An increase in the luminescence intensity was found after storage the samples in air. It is revealed that the highest growth factor of the luminescence intensity is observed in CdS QDs without a shell. A mechanism has been formulated that affects the luminescent properties of CdS QDs and nanostructures of CdS / ZnS QDs during storage.

Introduction

One of the most unique properties semiconductor nanomaterials in terms of their practical application is luminescence. In this case, nanocrystals (NC) or quantum dots (QDs) must have an effective emissivity, controlled by the emission spectrum, and stable physical and optical characteristics. Studies of physico-chemical and optical phenomena in QDs are relevant for their practical application. [1 – 5].

First of all, interest is the question of how these phenomena depend on the conditions for the synthesis of NCs. In the colloid – chemical method, the physicochemical properties of the obtained NCs are influenced by many factors, including such as: the ratio of the concentrations of the initial components of the chemical reaction, the temperature and speed of the process, the type and concentration of stabilizers limiting the growth of nanocrystals, alloying and introduction of inorganic and organic substances forming shells covering the surface of nanocrystals [6 – 8]. From the point of view of the practical application nanocrystals and nanostructures based on them, the question of the stability the optical, electrophysical, and chemical properties of quantum dots during their storage in air is the interest. Semiconductor NCs are gaining increasing attention for using in light-emitting devices and biological markers. For these applications, important fac-tors are high luminescence efficiency, which is very sensitive to the nature of the particle surface. However, the effect of the surface on radiation hasn't been completely studied. The issue of improving the efficiency of the emitting properties of nanocrystals by technological methods is gaining relevance.

Materials and methods

Cadmium nitrate $Cd(NO_3)_2$ and sodium sulfide Na_2S, as well as zinc salt $ZnCl2$, which was used to create a CdS NC shell (manufactured by the company "Simestavaal", Odessa), were used as precursors in the synthesis of NC CdS. An aqueous solution of gelatin was used to stabilize the size of the NC.

To measure the optical density spectra, an SF-26 spectrophotometer with a spectral range from 186 to 1100 nm was used. The luminescence spectra were measured using an LCS-DTL- 374QT solid – state laser with pumping, semiconductor diodes operating in the optoacoustic modulation mode.

Synthesis of CdS QDs without and with a shell

In this work, the objects of study were CdS QDs without a shell and CdS QDs covered with a ZnS shell. The synthesis of NCs CdS was carried out by the colloidal - chemical method as a result of the exchange reaction be-

tween the cadmium salt Cd (NO$_3$)$_2$ and the sulfur salt and Na$_2$S. 5 ml. is added to an aqueous solution of 1% gelatin an aqueous solution of Cd(NO$_3$)$_2$ (0.25 mol / L), followed by stirring for 10 min, after which 5 ml. was added dropwise. an aqueous solution of Na$_2$S (0.25 mol / L).The synthesis reaction took place for 20 minutes at a temperature of 40° C with continuous stirring. As the reaction proceeded, the color of the solution changed from clear to orange.

Our previous studies [7] showed that the build-up of the zinc sulfide shell occurs when an aqueous solution of ZnCl$_2$ and Na$_2$S is added to the solution in which NCs CdS are synthesized. In this work, the growth of the shell on the CdS NC was carried out at such concentration parameters. In a colloidal solution of 1% gelatin containing CdS nanoparticles, 5 ml. of an aqueous solution of ZnCl$_2$ (0.25 mol/L) was added with the addition of an aqueous solution of sodium sulfide (0.25 mol / L) to the growth reactor. In order to increase the shell thickness, the volume of the added sodium sulfide solution was varied from 1 to 5 ml. With continuous stirring of the solution for 10 minutes, the color of the solution changed from orange to light yellow. The synthesis reaction is as follows (1):

$$CdS + ZnCl_2 + Na_2S \rightarrow CdS/ZnS + 2NaCl \quad (1)$$
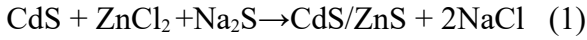
The average radius of nanoparticles was estimated by formula (2), in accordance with the theoretical concepts of the theory of absorption in spherical nanoobjects [9].

$$R = \frac{h}{\sqrt{8\mu\Delta Eg}} \quad (2)$$

Here h – Planck's constant; $\mu = ((m_{e*})^{-1} + (m_{h*})^{-1})^{-1}$, where $m_{e*} = 0.19m_e$, $m_{h*} = 0.8m_e$ are the effective masses of an electron and a hole in cadmium sulfide, respectively, me is the mass of a free electron; ΔE_g is the difference between the band gap in a nanoparticle and a bulk CdS crystal (2.4 eV). The average radius of CdS QDs, according to calculated estimates, was 2.2 nm.

Results and discussion

To study the effect of storage of quantum dots in air on luminescence, the following samples were selected, namely, CdS QDs without a shell, CdS QDs with a shell: CdS / ZnS + Na$_2$S (1 mL.); CdS / ZnS + Na$_2$S (2 mL.); CdS / ZnS + Na$_2$S (4 mL.). It was found that storage of CdS QD samples in uncoated air led to an increase in the luminescence intensity (Fig. 1).
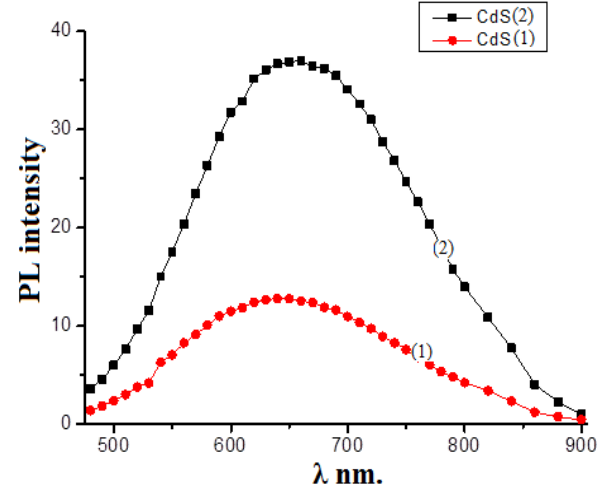
Fig. 1. CdS QD photoluminescence spectra: freshly grown (1), after 5 months of storage (2).

A similar fact of the effect of storage on the luminescence intensity was found in samples of CdS/ZnS QDs prepared with different concentrations of added Na$_2$S (Figs. 2–4).
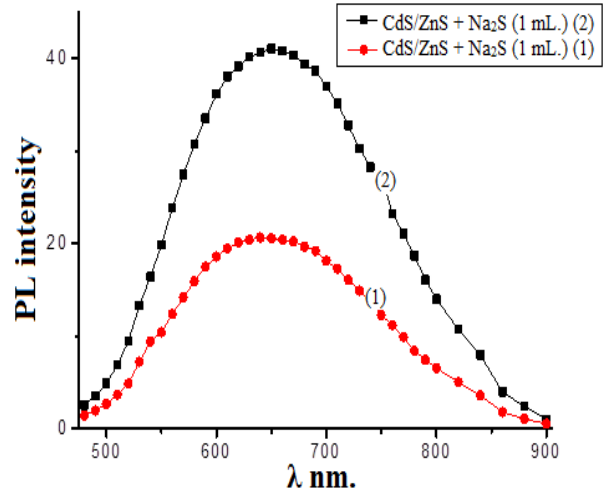
Fig. 2. Photoluminescence spectra of CdS / ZnS + Na$_2$S (1 mL): freshly grown (1), after 5 months of storage (2).

The data on the change in the intensity of the luminescence bands of CdS QDs, CdS / ZnS nanostructures and the luminescence enhancement factor during storage in air are summarized in Table 1.
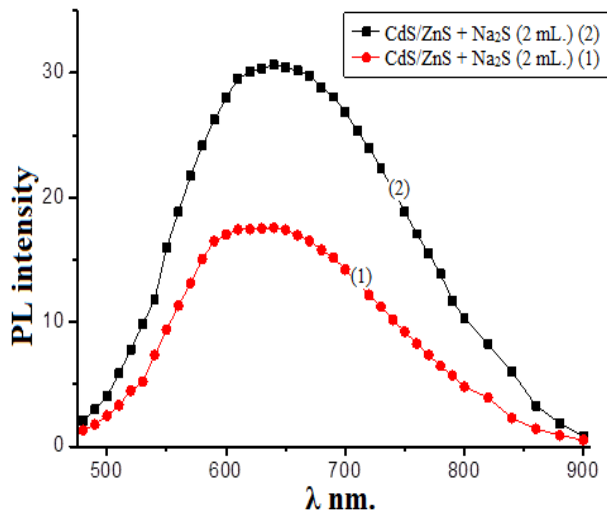
Fig. 3. Photoluminescence spectra of CdS / ZnS + Na$_2$S (2 mL): freshly grown (1), after 5 months of storage (2).
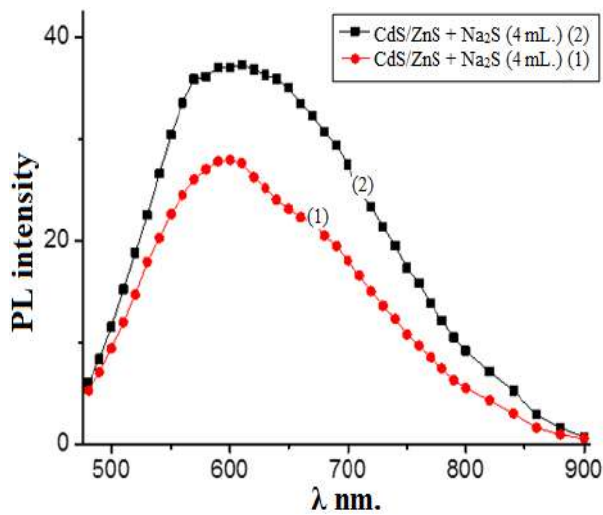
Fig. 4. Photoluminescence spectra of CdS / ZnS + Na$_2$S (4 mL): freshly grown (1), after 5 months of storage (2).

It is noteworthy that the highest luminescence enhancement factor is observed for the CdS QD sample without a shell and decreases with increasing shell thickness.

Table 1. Data on changes in the intensity of the luminescence bands of CdS and CdS / ZnS QDs during storage in air

Freshly grown samples			After air storage		Gain factor
Sample types	λ, nm.	I, a.u.	λ, nm.	I, a.u.	
CdS	640	12.7	654	37	2.9
CdS / ZnS + Na$_2$S (1 mL.)	645	21	650	41	1.95
CdS / ZnS + Na$_2$S (2 mL.)	625	18	640	31	1.7
CdS / ZnS + Na$_2$S (4 mL.)	596	27	589	37	1.3

To explain the changes in the luminescent properties of the samples under study during long-term storage in air, the mechanisms associated with the features of their structure are considered. Nanocrystals dispersed in matrices are structures containing organic (polymer molecules, organic media, DNA) or inorganic environment (shells of semiconductor compounds). In the case of the complexity of the formation of nanostructures synthesized in colloidal solutions, it is necessary to take into account the influence of the specific conditions of their synthesis, the influence of external factors on the state of the surface of nanocrystals.

For example, in [10], the results of observing an increase in the luminescence intensity of NCs CdSe as a result of their irradiation with UV light are described. The authors explain this phenomenon by the action of the oxidative mechanism: water, penetrating through the gelatinous shell, which is surrounded by CdS NCs, leads to the replacement of gelatin chains attached by amino groups to the surface cadmium atoms by hydroxyl groups. The NCs themselves practically lose the surface layer of cadmium atoms, which are now associated with hydroxyl groups. As a result, conditions are created for the formation of a cadmium hydroxide compound, which can play a coating role for cadmium sulfide nanocrystals. At the same time, a decrease in the size of nanocrystals was observed, which manifests itself in a shift of the absorption spectrum to shorter wavelengths.

The effect of oxygen on the luminescence of CdSe nanocrystals was discovered in the work. [11]. The authors observed an increase in the luminescence intensity of nanocrystals after exposing the samples to air without changing the position of the emission band maximum and the band half-width. The photoelectric effect was not taken into account, since all solutions were in darkness, except for photoluminescence measurements. The authors explain the fact that luminescence is enhanced by the reaction of nanocrystals with dissolved oxygen, which leads to surface passivation. As described in [12], oxygen reacts with NCs CdSe with the possible formation of surface CdO and SeO$_2$. In addition, CdSe NCs in a growth solution with substances (TOP /

TOPO) did not show an increase in photoluminescence, which confirms the interaction of oxygen with the "bare" surface of nanocrystals.

In our experiment, CdS QDs were synthesized in air without fulfilling the conditions for degassing the growth solution. In this process, similar to [11, 12], the solution will be saturated with oxygen. The NCs CdS were synthesized in a gelatin solution in the open air, which facilitates the saturation of the solution with oxygen. Cadmium ions on the surface of nanocrystals form complexes in the metal associate of several gelatinous molecules surrounding the nanocrystal. Oxygen in a gelatinous medium can interact with cadmium to form cadmium oxide.

Thus, the mechanism for increasing luminescence is the diffusion of oxygen to the surface of cadmium sulfide nanocrystals and the formation of cadmium oxide - CdO. The resulting cadmium oxide will act as the outer coating layer. The luminescence of cadmium sulfide nanocrystals, as a result of this alleged process, will be enhanced. Although thermodynamic reasoning suggests that adsorbed oxygen molecules react with CdS to form surface oxides, the adsorbed oxygen molecules in our samples do not create a macroscopic oxide layer, which can lead to a decrease in the NC size, as well as a loss of photoluminescence efficiency.

Our results show that when the proposed mechanism is implemented, the luminescence enhancement factor for CdS / ZnS samples relative to CdS QDs without a shell should decrease, which is observed in our experiment (see Table 1).

Thus, the results obtained on the evolution of the properties of colloidal CdS nanocrystals indicate the complexity of physicochemical processes occurring during synthesis in open air and the need to take into account the interaction between the nanocrystal surface and the environment, namely, with oxygen.

Conclusion

This work describes the results of studies of changes in the optical properties of CdS nanocrystals and nanostructures of the core-shell CdS / ZnS type during storage in air. Experimental data are demonstrated that indicate an increase in the QD luminescence intensity during storage in air. It was revealed that the highest growth rate of photoluminescence during storage is observed for CdS nanocrystals without a shell. A mechanism is proposed for improving the luminescence intensity associated with the adsorption of oxygen and the passivation of the surface of CdSnanocrystals through the formation of cadmium oxide on their surface.

References

1. Fábio Pereira Ramanery, Alexandra Ancelmo Piscitelli Mansur, Herman Sander Mansur. Synthesis and Characterization of Water-dispersed CdSe/CdS Core-shell Quantum Dots Prepared via Layer-by-layer Method Capped with Carboxylic-functionalized Poly(Vinyl Alcohol). Materials Research. 2014; 17 (Suppl. 1): 133-140. DOI: httpI://dx.doi.org/10.1590/S1516-14392014005000060

2. Adolfas K. Gaigalas, Paul DeRose, Lili Wang, and Yu-Zhong Zhang. Optical Properties of CdSe/ZnS Nanocrystals. Journal of Research of the National Institute of Standards and Technology. Volume 119 (2014). P. 609-628. http://dx.doi.org/10.6028/jres.119.026

3. Bonghwan Chon, Sung Jun Lim, Wonjung Kim, JongcheolSeo, Hyeonggon Kang, TaihaJoo, Jeeseong Hwang and Seung Koo Shin. Shell and ligand-dependent blinking of CdSe-based core/shell nanocrystals. Phys. Chem. Chem. Phys.,2010,12, 9312-9319 DOI: 10.1039/b924917f

4. Synthesis and Characterization of Zinc-Blende CdSe-Based Core/Shell Nanocrystals and Their Luminescence in Water. J. Phys. Chem. C, Vol. 112, No. 6, 2008 Sung Jun Lim, Bonghwan Chon, TaihaJoo, and Seung Koo Shin. 2008, 112, 1744-1747 10.1021/jp710648g

5. James Cassidy, Mikhail Zamkov. Nanoshell quantum dots: Quantum confinement beyond the exciton Bohr radius. J. Chem. Phys. 152, 110902 (2020); https://doi.org/10.1063/1.5126423

6. Yu.A.Nitsuk, M.I. Kiose, Yu.F.Vaksman, V.A. Smyntyna, I.R. Yatsunskyi.: Optical

properties of CdS nanocrystals, doped with zinc and copper. Physics and technology of semiconductors, 2019, volume 53, no. 3, 381 – 387.

7. V. M. Skobeeva, V. A. Smyntyna, M. I. Kiose, N. V. Malushin.: Increasing the photoluminescence efficiency of cdsnc grown in a gelatinous environment. Sensor Electronics and Microsystem Technologies 2021 – T. 18, № 1, 10 – 19.

8. V.A. Smyntyna, V.M.Skobeeva, V.M., N.V. Malushin, Lyuminescentnye svojstva nanokristallov sulfide kadmiya, legirovannyh atomami litiya i alyuminiya. Sensor Electronics and Microsystem Technologies. T. 2 (8) 1/2011. C..55-58.

9. A.I. Gusev, A.A. Rempel'. Nanokristallicheskie materialy (M., Fizmatlit, 2000), c. 224.

10. S.R. Cordero. P.J. Carson, R.A. Estabrook, G.F. Strouse, S.K. Buratto. PhotoActivated Luminescence of CdSe Quantum Dot Monolayers // J. Phys. Chem. B 2000, 104, 12137-12142.

11. Noseung Myung,Yoonjung Bae, and Allen J. Bard. Enhancement of the Photoluminescence of CdSe Nanocrystals Dispersed in $CHCl_3$ by Oxygen Passivation of Surface States. NANOLETTERS 2003 Vol. 3, No. 6 747-74910.1021/nl034165s

12. Liping Liu, Qing Peng, and Yadong Li. An Effective Oxidation Routeto Blue Emission CdSe QuantumDots. Inorg. Chem. 2008, 47, 8, 3182–3187. https://doi.org/10.1021/ic702203c

V.M. Skobeeva[2], V.A. Smyntyna[1], M. I.Kiose[1], N.V. Malushin[2]

EVOLUTION OF LUMINESCENT PROPERTIES DURING STORAGE OF CdS QDs IN AIR.

Summary This paper presents the results of a study of the of CdS QDs and nanostructures of CdS / ZnS QDs obtained by the sol - gel technology in an aqueous solution of gelatin and the effect of storage on their luminescence. An increase in the luminescence intensity was found after storage of the samples in air. It is revealed that the highest growth factor of the luminescence intensity is observed in CdS QDs without a shell. A mechanism has been formulated that affects the luminescent properties of CdS QDs and nanostructures of CdS / ZnS QDs during storage.

Key words: Luminescence, cadmium sulfide, zinc sulfide, core-shell nanostructure, storage in air.

В.М.Скобєєва, В.А.Сминтина, М.І. Кіосе, Н.В.Малушин

ЕВОЛЮЦІЯ ЛЮМІНЕСЦЕНТНИХ ВЛАСТИВОСТЕЙ ПРИ ЗБЕРІГАННІ КТ CdS У ПОВІТРІ.

Резюме В роботі представлені результати дослідження КТ CdS та наностуктур КТ CdS / ZnS, отриманих методом золь - гель технології в водному розчині желатини і впливу зберігання на їх люмінесценцію. Виявлено зростання інтенсивності світіння після зберігання зразків на повітрі. Виявлено, що найбільший коефіцієнт зростання інтенсивності люмінесценції спостерігається в КТ CdS без оболонки. Сформульовано механізм, що впливає на люмінесцентні властивості КТ CdS та наностуктур КТ CdS / ZnS при їх зберіганні.

Ключові слова: Люмінесценція, сульфід кадмію, сульфід цинку, наноструктура ядро-оболонка, зберігання на повітрі.

В.М.Скобеева, В.А.Смынтына, М.И. Киосе, Н.В.Малушин

ЭВОЛЮЦИЯ ЛЮМИНЕСЦЕНТНЫХ СВОЙСТВ ПРИ ХРАНЕНИИ КТ CdS НА ВОЗДУХЕ.

Резюме В работе представлены результаты исследования КТ CdS и наностуктур КТ CdS / ZnS, полученных методом золь - гель технологии в водном растворе желатины и влияния хранения на их люминесценцию. Обнаружен рост интенсивности свечения после хранения образцов на воздухе. Выявлено, что наибольший коэффициент роста интенсивности люминесценции наблюдается в КТ CdS без оболочки.Сформулировано механизм, влияющий на люминесцентные свойства КТ CdS и наностуктур КТ CdS / ZnS при их хранении.

Ключевые слова: Люминесценция, сульфид кадмия, сульфид цинка, наноструктура ядро - оболочка, хранение на воздухе.

L.M. Filevska, A.P. Chebanenko, V.S. Grinevych, V.A. Smyntyna, and V.I. Irkha*

Odessa I.I. Mechnikov National University, str. Dvoryanska, 2, Odesa, Ukraine,
e-mail: lfilevska@gmail.com
* Odessa State University of Intellectual Technologies and Communications

SnO$_2$ AND ZnO FILMS STRUCTURED USING POLYMERS FOR AMMONIA DETECTION

The electrophysical properties in air and in the atmosphere with ammonia vapor content of nanosized films of ZnO and SnO$_2$ structured in the process of production using polymers were studied. The investigated electrophysical properties of those films in air and in an atmosphere containing ammonia vapors showed the presence of significant changes in the conductivity of both types of films. The nature of these changes is somewhat different. In ammonia vapors, the current in a zinc oxide film is many times greater than in air. And the tin oxide film in ammonia vapor becomes more high-resistant in comparison with its resistance in air. It was found that the conductivity of both types of films is controlled by intercrystalline potential barriers. However, upon contact with ammonia vapors, these barriers decrease in the zinc oxide films, while the opposite process is observed in the tin dioxide film. The reversible nature of the processes of ammonia molecules interaction with oxide films is observed in both cases. Both for ZnO and for SnO$_2$ the sensitivity to ammonia is recorded already at room temperature. It was also established that the initial characteristics of both types of films were quickly restored without additional measures. These facts make the studied nanostructured films of ZnO and SnO$_2$ using polymers to be promising material for sensitive elements for ammonia gas sensors.

Introduction

Nanosized oxide materials, in particular tin and zinc oxides are actively used as ones for gas analysis [1-3]. Due to their electronic characteristics (large band gap), chemical resistance in the active medium, as well as a large active surface area, they provide a significant response in their conductivity and long-term operation. To increase the efficiency of these materials as sensitive elements of gas sensors, various technological methods are used to increase their active surface, for the main physical and chemical processes responsible for this parameter occur mainly at the interface, being the surface of the sensitive element. Among the production technologies are both physical (atomic layer-by-layer deposition, magnetron sputtering, etc.) [4] and chemical (vapor-phase deposition on a heated substrate, methods of decomposition of organometallic compounds, sol-gel methods [5,6], hydrothermal method [7]). The latter are the most popular due to their relative simplicity and low cost. By such methods with various modifications it is possible to receive various nanostructures - from

film to micellar-like [8].

The ammonia content control, like of many other pollutants, is essential to ensure the safety of the environment. This applies to public places, ambient air and the air of production areas. This makes the need for constant monitoring of the gaseous environment composition and the improvement of devices for it as a priority for environmental protection. Therefore, the creation of efficient, high-speed and renewable gas sensors elements sensitive to ammonia becomes a necessary solution to this problem. Oxide nanomaterials, namely, tin and zinc oxides, exhibit high sensitivity to ammonia vapors and are used as materials for sensitive elements of ammonia sensors. [9]. For the operation of sensors based on them, as a rule, additional heating and a sufficiently long recovery time of the active element after interaction with the detected gas are required. Therefore, lowering the operating temperature and rapid recovery after interaction with the detected gas is necessary to save energy and materials when creating and operating sensors.

In the work, the electrophysical properties in air and in the atmosphere with ammonia va-

por content of nanosized films of zinc and tin oxides structured in the process of production using polymers were studied in order to evaluate their application as effective and renewable sensitive elements for ammonia sensors.

Methods for films production and research

The precursor's solutions (organometallic compounds of zinc and tin) were mixed with polymer solutions during their preparation and applied by drop coating method onto prepared glass substrates. Zinc acetate was used as a precursor for zinc oxide, and bis(acetylacetonato)dichlorotin(IV) was used for tin oxide.

The latter was obtained by the technology described in [10]. The workpieces dried in a drying oven were annealed in air in a muffle furnace. After the removal of the products of polymer thermal decomposition during annealing, the transparent nanostructured metal oxides remain on the substrate. Figure 1 shows an electronic microscope image of the obtained zinc oxide films (a), as well as a three-dimensional AFM image of the surface of tin oxide films. The images confirm the presence of nanostructuring in the films under study.

The study of the electrophysical properties in air and their changes in the presence of ammonia vapors were carried out according to standard methods in the equipment described in [11].

a)   b)
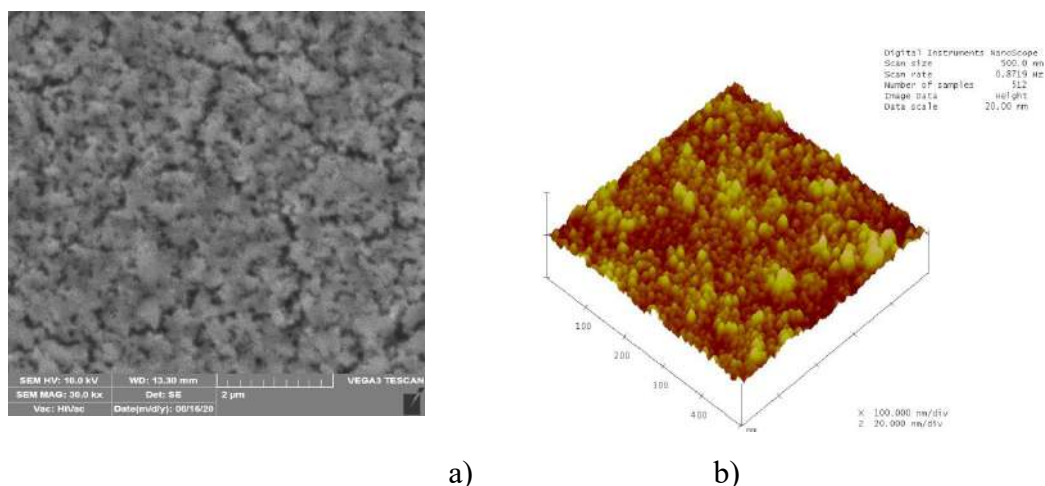
Fig. 1. SEM image of the studied zinc oxide film (a) and three dimensional tin dioxide film's surface view (b).

Results and discussion

The band gap of the obtained oxide films established from its optical density vs energy study was from 2.9 to 3.15 eV for both types of films. The resistance of both types of oxide films calculated from the current-voltage characteristics was $(0.2-3) \times 10^9$ Ohm, what is expected for wide gap materials.

The electrical conductivity of polymer-structured nanosized zinc and tin oxide films was found to be sensitive to the ammonia content in the surrounding atmosphere. It is interesting that the character of the conductivity change of the films is not similar.

Figure 2 shows the current-voltage characteristics of the studied films of zinc oxide (a)

and tin dioxide (b) in air (curves 1 in both figures) and in an atmosphere with an ammonia vapor content (curves 2). It can be seen in both figures that current-voltage characteristics measured in the atmosphere with an ammonia vapor content, differs from I–V characteristics measured in air .

Curve 1 in Figure 2a shows the current-voltage characteristic of the ZnO film measured in air. The exponential nature of the dependence of the current on the applied voltage is confirmed by the straightining of the CVC in lnI-V ^ coordinates (1/4). This means that the current flow in the ZnO film in air at room temperature is conditioned by over-barrier Schottky emission over thin intercrystalline barriers [12]. The presence of these barriers is

also confirmed by the nanocrystalline grain sizes of the film in SEM images.
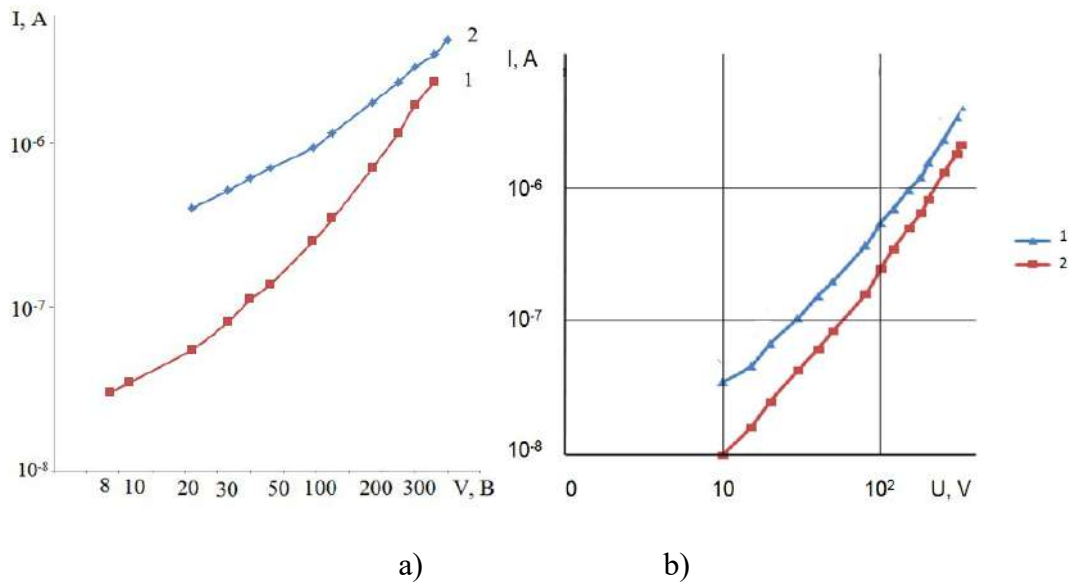
Fig. 2. CVC of ZnO film (a) and SnO$_2$ film (b) in air (curves 1 in both figures) and with ammonia vapor (curves 2 in both figures) at 290 K.

The CV characteristic of SnO2 films in a dry air atmosphere (curve 1, Fig. 2b) is superlinear and shows a weak an exponential dependency of the current on the applied voltage. This dependence is also due to the barrier mechanisms of current flow. Thus, the intercrystalline potential barriers in the tin dioxide film, as in the zinc oxide film, noticeably influence the current flow.

Curve 2 in Fig. 2a shows the I-V characteristic of the ZnO film in an atmosphere with ammonia vapor. It is noteworthy that in ammonia vapor, the current in the film (especially in the region of low voltages) is several times higher than in air. As shown in [13], during the adsorption of ammonia on the surface of ZnO, the nitrogen atom (N) is mainly bound with the surface zinc atom (Zn). This configuration is stable when NH3 is adsorbed on the zinc oxide surface. NH3 molecules are molecular chemisorbed on the ZnO surface and become charged donors. With this character of adsorption, the equilibrius surface energy bands bending decreases, which leads to the conductivity growth of thin zinc oxide films under the influence of NH3 vapors. This is the nature of the current flow change in zinc oxide films in an atmosphere with ammonia vapor in Fig. 2a.

In ammonia vapor, the studied SnO2 film, unlike to the ZnO film, on the contrary, becomes more resistive than that in air. The superlinearity of its CV characteristic also increases (Fig. 2b, curve 2). Thus, it may be supposed, that the adsorption of ammonia molecules promotes the intercrystalline potential barriers growth in the tin dioxide film and an increase of the blocking bend of the surface energy bands. It is known [14] that ammonia molecules can form complexes SnO$_2$ [NH3] on the surface of tin dioxide. The formation of such complexes on intergranular barriers increases the surface bending of the zones. The consequence of this is a decrease in the conductivity of the film.

The conductivity decrease upon contact of a tin dioxide film with ammonia is possible in the processes of physical adsorption of oxygen and ammonia, besides the creation of ammonia complexes with surface atoms of tin or its oxides. These processes can take place at room temperature. But in the case of physical adsorption, there is no exchange of carriers (charges) between the adsorbate and the adsorbent. However, the nanostructuring of the film grains leads to a slight decrease of the chemisorption reactions temperature. In addition, it is also possible to influence the current

transfer due to a decrease in the carrier mobility of the near-surface region and an increase in barriers to current flow due to physical adsorption, which can also lead to a decrease in conductivity.

Figure 3 shows the current temperature dependences in the ZnO (a) and SnO2 (b) films.

The zinc oxide film current temperature dependence measured in air and in ammonia vapor has an activation character. The activation energy of conductivity in ammonia vapor calculated from its slope is Ea≈0.32 eV. The obtained value of Ea is close to the activation energies obtained with the CTD of the ZnO film in an air atmosphere (0.35-0.37) eV (in the inset in Fig. 3a). The established values indicate that the electrical conductivity is controlled by intercrystalline potential barriers and the current flow mechanism in both cases can be described by a semiconductor model with large-scale fluctuations of the potential relief [15].

a)   b)
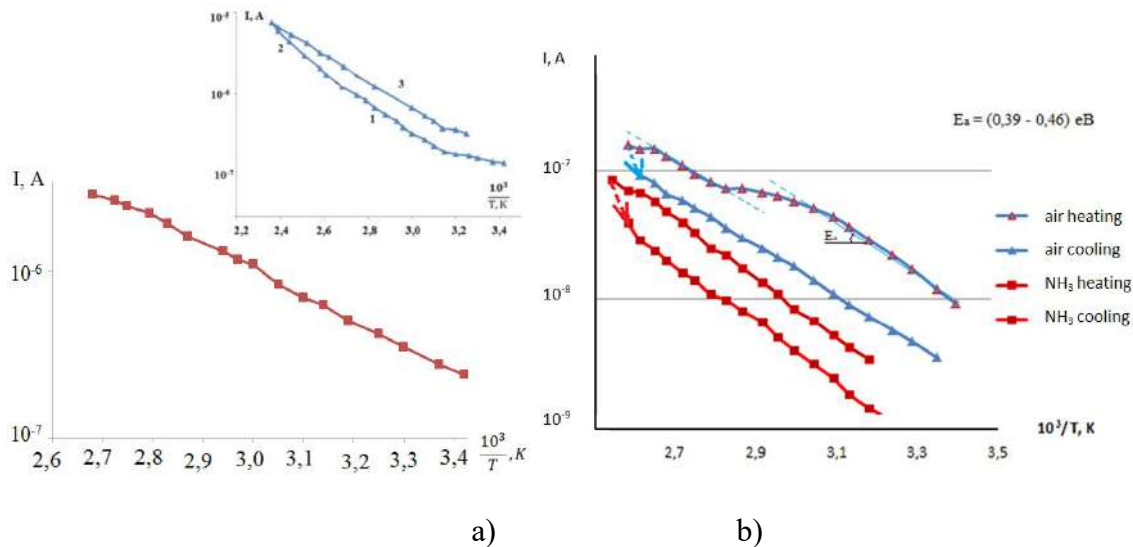
Fig.3.The current temperature dependence in ZnO film in dry air and in ammonia vapor (V = 100 B) (a) and SnO$_2$ film in dry air and in ammonia vapor (U = 150 V) (b).

The same picture is observed in the current temperature dependence of tin dioxide films (Fig. 3b). The only difference is in a decrease in conductivity in ammonia vapors. The slope of all curves is almost the same and corresponds to the activation energy Ea = 0.39-0.45 eV. This slope shows that the conductivity is also controlled by defects and the activation energy approaching the depth of the levels corresponding most likely to ionized molecularly adsorbed oxygen [16]. A decrease in the conductivity in this case is possible due to the surface oxygen molecules influence in the presence of ammonia molecules when complexes are formed on the SNO2 [NH3] surface. The curves' slope retention may indicate both the localization of ammonia molecules on the same surface defects where oxygen has already been preliminarily adsorbed, and binding with oxygen itself.

The current kinetic changes during periodic inflow of ammonia vapors or dry air into the measuring chamber are shown in Figure 4a. It can be seen that the presence of ammonia leads to an almost double current growth in the ZnO film. The response time (the time of reaching 90% of the steady-state current value) is about 48 s, which indicates to low inertia of the ammonia absorption process. The current strength decrease to its initial value (that is, the process of ammonia desorption) after admitting dry air into the chamber is more inertial than the adsorption process. The recovery time (the time necessary to reach 90% of the current from its stationary value) is about 180 s. It can be seen that the decrease in the first seconds is quite sharp. This behavior indicates to a weak bond of the most of the adsorbed molecules with the zinc oxide surface.
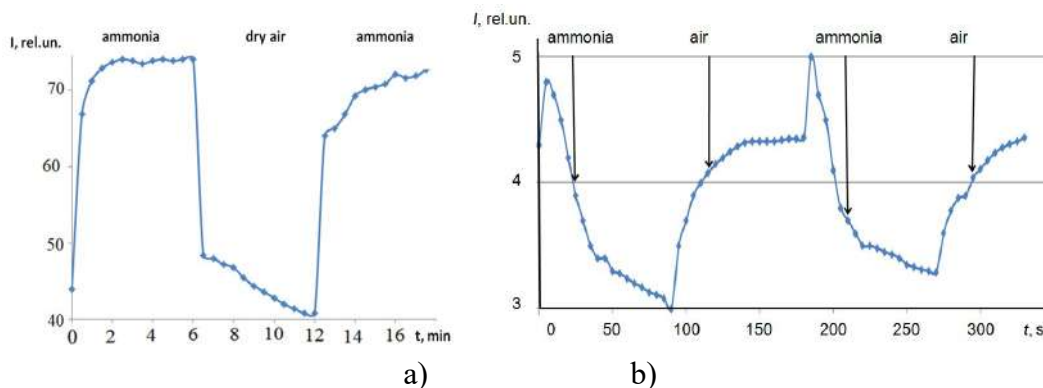
Fig. 4. Kinetics of the current in the ZnO film measured at periodic inflow of ammonia vapor or dry air into the chamber (V = 175 B) at T = 293 K(a) and for the SnO2 film (V = 300 V) (b).

A slightly different picture of nanosized SnO$_2$ films sensitivity to ammonia is shown in Fig. 4b. The current strength decreases when ammonia is let into the test chamber. The response time in this case is slightly higher and amounts to about 70-75 s. The recovery time is close to the response time. The short desorption time shows a weak bond of adsorbed molecules with the surface of the tin dioxide film, which can be supposed at room temperature. The said also confirms the physical nature of the adsorption of ammonia on tin dioxide films at room temperature. Desorption of chemisorbed molecules even on nanosized crystallites would require more energy, which means that during desorption (with the admission of dry air) such a sharp change in conductivity would not be registered.

Despite all the differences in the mechanisms of sensitivity of zinc oxide and tin dioxide, their behavior when interacting with ammonia has common features. Both types of films show a fairly rapid recovery of the original characteristics without additional actions - an increase in temperature or field action. Besides that, the observed processes of both oxides films' interaction with ammonia occur at room temperature. These properties are extremely important in gas analysis applications as sensitive elements.

Conclusions

The investigated electrophysical properties of nanosized films of zinc and tin oxides, structured using polymers in the process of production, in air and in an atmosphere containing ammonia vapors showed the presence of significant changes in the conductivity of both types of films. The nature of these changes is somewhat different.

In particular, in ammonia vapors, the current in a zinc oxide film (especially in the region of low voltages) is many times greater than in air. And the tin oxide film in ammonia vapor becomes more high-resistant in comparison with its resistance in air, that is, its electrical conductivity decreases. These facts indicate to different mechanisms of chemisorption processes on different oxides, since ammonia acts as a donor for zinc oxide, and exhibits acceptor properties for tin dioxide.

It was found that the conductivity of both types of films is controlled by intercrystalline potential barriers. However, upon contact with ammonia vapors, these barriers decrease in the zinc oxide films, while the opposite process is observed in the tin dioxide film.

The reversible nature of the processes of ammonia molecules interaction with oxide films is observed in both cases. At the same time, both for zinc oxide and for tin oxide, the sensitivity to ammonia is recorded already at room temperature. It was also established that the initial characteristics of both types of films were quickly restored without additional measures. These facts make the studied nanostructured films of tin and zinc oxides using polymers to be promising material for sensitive elements for ammonia gas sensors.

References

1. X. Wang, F. Sun, Y. Duan, Z. Yin, W. Luo, Y. Huang, J. Chen Highly sensitive, temperature-dependent gas sensor based on hierarchical ZnO

nanorod arrays J. Mater. Chem. C., 3 (2015), pp. 11397-11405, 10.1039 / C5TC02187A.

2. Nguyen Xuan Thai, Nguyen Van Duy, Nguyen Van Toan, Chu Manh Hung, Nguyen Van Hieu and Nguyen Duc Hoa Effective monitoring and classification of hydrogen and ammonia gases with a bilayer Pt/SnO2 thin film sensor, International Journal of Hydrogen Energy, 2020, 45, 2418, DOI: 10.1016/j.ijhydene.2019.11.072

3. Moos R. Solid State Gas Sensor Research in Germany – a Status Report, Sensors, 2009, Vol. 9, P. 4323—4365.

4. O. V. Anisimov, N. K. Maksimova, E. V. Chernikov, E. Y. Sevastyanov and N. V. Sergeychenko, "Sensitivity to NH3 of SnO2 thin films prepared by magnetron sputtering," *2009 International Siberian Conference on Control and Communications*, 2009, pp. 189-193, doi: 10.1109/SIBCON.2009.5044854.

5. Znaidi, L. Sol–gel–deposited ZnO thin films: A review – Materials Science and Engineering: B, 2010, vol. 174, Issues 1—3, p. 18–30.

6. Foo K.L. Fabrication and Characterization of ZnO Thin Films by Sol–Gel Spin Coating Method for the Determination of Phosphate Buffer Saline Concentration – Current Nanoscience, 2013, №9, p. 1—5.

7. Dasari Sunil Gavaskar, P. Nagaraju, Yelsani Vijayakumar, P. S. Reddy & M. V. Ramana Reddy (2020) Low-cost ultra-sensitive SnO2-based ammonia sensor synthesized by hydrothermal method, Journal of Asian Ceramic Societies, 8:3, 605-614, DOI: 10.1080/21870764.2020.1769820.

8. R. Sankar Ganesh, E. Durgadevi, M. Navaneethan, V.L. Patil, S. Ponnusamy, C. Muthamizhchelvan, S. Kawasaki, P.S. Patil and Y. Hayakawa Low temperature ammonia gas sensor based on Mn-doped ZnO nanoparticle decorated microspheres, Journal of Alloys and Compounds, 2017, 721, 182, DOI: 10.1016/j.jallcom.2017.05.315

9. Xu Liu, Nan Chen, Bingqian Han, Xuechun Xiao, Gang Chen, Igor Djerdj and Yude Wang, Nanoparticle cluster gas sensor: Pt activated SnO2 nanoparticles for NH3 detection with ultrahigh sensitivity, **Nanoscale**, 2015,**7**, 14872-14880, https://doi.org/10.1039/C5NR03585F/

10. B. Ulug, H.M. Türkdemir, A. Ulug, O. Büyükgüngör, M. B. Yücel, V. S. Grinevich*, L. N. Filevskaya and V.A. Smyntyna. Structure, spectroscopic and thermal characterization of bis(acetylacetonato)dichlorotin(IV) synthesized in aqueous solution. Ukranian chemical journal. 2010, N 7. – P. 12-17.

11. Chebanenko A.P., Filevska L.M., Grinevych V.S., Smyntyna V.A. (2021) The Sensitivity to Moisture Peculiarities of Nanoscale Tin Dioxide Films Obtained by Means of Polymers. In: Fesenko O., Yatsenko L. (eds) Nanomaterials and Nanocomposites, Nanostructure Surfaces, and Their Applications. Springer Proceedings in Physics, vol 246. Springer, Cham. https://doi.org/10.1007/978-3-030-51905-6_25/

12. Pikus G.E. Fundamentals of the theory of semiconductor devices, M., Nauka, 1972, 340S.

13. Kovalenko M.V. Electronic energy structure, optical-spectral and sensory properties of ZnO-based nanostructures. -Kand.dis., Lvov, 2017, 198 pp.

14. Gevelyuk, S.A., Grinevych, V.S., Doycho, I.K. *et al.* The active environment influence on the luminescence of SnO$_2$ nanoparticles' ensembles in a porous matrix. *Appl. Phys. A* **126,** 919 (2020). https://doi.org/10.1007/s00339-020-04101-4

15. Шейкмвн М.К., Шик А. Я. Долговременныерелаксации и остаточнаяпроводимость в полупроводниках (обзор). – ФТП, 1976, т.10(2), с. 209-233.

16. Kostiantyn V. Sopiha, Oleksandr I. Malyi, Clas Persson, and Ping Wu, Chemistry of Oxygen Ionosorption on SnO2 Surfaces, ACS Applied Materials & Interfaces 2021 13 (28), 33664-33676, DOI: 10.1021/acsami.1c08236.

L.M. Filevska, A.P. Chebanenko, V.S. Grinevych, V.A. Smyntyna, and V.I. Irkha

SnO₂ AND ZnO FILMS STRUCTURED USING POLYMERS FOR AMMONIA DETECTION

Summary The electrophysical properties in air and in the atmosphere with ammonia vapor content of nanosized films of ZnO and SnO$_2$ structured in the process of production using poly-

mers were studied. The investigated electrophysical properties of those films in air and in an atmosphere with ammonia vapors showed the presence of significant changes in the conductivity of both types of films. The nature of these changes is somewhat different. In ammonia vapors, the current in a zinc oxide film is many times greater than in air. And the tin oxide film in ammonia vapor becomes more high-resistant in comparison with its resistance in air. It was found that the conductivity of both types of films is controlled by intercrystalline potential barriers. However, upon contact with ammonia vapors, these barriers decrease in the zinc oxide films, while the opposite process is observed in the tin dioxide film. The reversible nature of the processes of ammonia molecules interaction with oxide films is observed in both cases. Both for ZnO and for SnO$_2$ the sensitivity to ammonia is recorded already at room temperature. It was also established that the initial characteristics of both types of films were quickly restored without additional measures. These facts make the studied nanostructured films of ZnO and SnO$_2$ using polymers to be promising material for sensitive elements for ammonia gas sensors.

Key word: tin oxide, zinc oxide, nanosized thin films, sensitivity, ammonia detection.

Л.М. Филевская, А.П. Чебаненко, В.С. Гриневич, В.А. Смынтына, В.И. Ирха

ПЛЕНКИ SnO$_2$ И ZnO, СТРУКТУРИРОВАННЫЕ С ИСПОЛЬЗОВАНИЕМ ПОЛИМЕРОВ ДЛЯ ОБНАРУЖЕНИЯ АММИАКА

Резюме

Изучены электрофизические свойства на воздухе и в атмосфере с содержанием паров аммиака наноразмерных пленок ZnO и SnO$_2$, структурированных в процессе получения с использованием полимеров. Исследованные электрофизические свойства этих пленок на воздухе и в атмосфере с парами аммиака показали наличие значительных изменений проводимости обоих типов пленок. Природа этих изменений различна. В парах аммиака ток в пленке оксида цинка во много раз больше, чем в воздухе. А пленка оксида олова в парах аммиака становится более высокоомной по сравнению с ее сопротивлением на воздухе. Было обнаружено, что проводимость обоих типов пленок контролируется межкристаллическими потенциальными барьерами. Однако при контакте с парами аммиака эти барьеры уменьшаются в пленках оксида цинка, тогда как в пленке диоксида олова наблюдается обратный процесс. В обоих случаях наблюдается обратимый характер процессов взаимодействия молекул аммиака с оксидными пленками. И для ZnO, и для SnO2 чувствительность к аммиаку регистрируется уже при комнатной температуре. Также было установлено, что исходные характеристики обоих типов пленок быстро восстанавливались без дополнительных мер. Эти факты делают исследованные наноструктурированные с использованием полимеров пленки ZnO и SnO$_2$ перспективным материалом для чувствительных элементов газовых сенсоров аммиака.

Ключевые слова: оксид цинк, диоксид олова, наноразмерные тонкие пленки, чувствительность, детектирование аммиака.

Л.М. Філевська, А.П. Чебаненко, В.С. Гриневич, В.А. Сминтина, В.І. Ірха

ПЛІВКИ SnO$_2$ І ZnO, СТРУКТУРОВАНІ З ВИКОРИСТАННЯМ ПОЛІМЕРІВ, ДЛЯ ВИЯВЛЕННЯ АМІАКУ

Резюме

Вивчено електрофізичні властивості на повітрі та в атмосфері з вмістом парів аміаку нанорозмірних плівок ZnO та SnO_2, структурованих у процесі одержання з використанням полімерів. Досліджені електрофізичні властивості цих плівок на повітрі та в атмосфері з парами аміаку показали наявність значних змін провідності обох типів плівок. Природа цих змін різна. У парах аміаку струм у плівці оксиду цинку в багато разів більший, ніж у повітрі. А плівка оксиду олова в парах аміаку стає більш високоомною порівняно з її опором на повітрі. Виявлено, що провідність обох типів плівок контролюється міжкристалічними потенційними бар'єрами. Однак при контакті з парами аміаку ці бар'єри зменшуються в плівках оксиду цинку, тоді як плівці діоксиду олова спостерігається зворотний процес. В обох випадках спостерігається оборотний характер взаємодії молекул аміаку з оксидними плівками. І для ZnO, і для SnO2 чутливість до аміаку реєструється вже за кімнатної температури. Також було встановлено, що вихідні характеристики обох типів плівок швидко відновлювалися без додаткових заходів. Ці факти роблять досліджені наноструктуровані з використанням полімерів плівки ZnO та SnO2 перспективним матеріалом для чутливих елементів газових сенсорів аміаку.

Ключові слова: оксид цинку, діоксид олова, нанорозмірні тонкі плівки, чутливість, детектування аміаку.

UDC 621.315.592

Kulikov S.S., Brytavskyi Ye.V., Borshchak V.A.,
Zatovskaya N.P., Kutalova M.I., Karakis Y.N.

Odesa I. I. Mechnikov National University, 2, Dvoryanskaya str.
phone: 723-34-61 e-mail: photoelectronics@onu.edu.ua

THE STUDY OF HOMOGENEOUS AND HETEROGENEOUS SENSITIZED CRYSTALS OF CADMIUM SULFIDE. PART V. HETEROGENEOUS DOPPING

.

A technology for processing semiconductor crystals in a corona discharge has been developed. It w2as found that as a result of this exposure, the samples acquire alternating spectral sensitivity. The observed phenomena are explained by the appearance of a two-pitched potential barrier in the near-surface region of the element, the unusual properties of which may allow the creation of a new type of device.

Introduction

This publication is a continuation of the reviews [1-4]. In order to preserve the generality of the work, the numbering of sections is selected general. Numbers of formulas and figures are presented by sections. References to the literature in each review are given individually.

Cadmium sulfide crystals are used in our research as a convenient model material. The results obtained on them and the constructed models also apply to other semiconductor substances.

In the previous parts of the review, it is considered how the photovoltaic properties of a semiconductor changes, in which, under the influence of external factors (light, electric field, temperature), the redistribution of a sensitive impurity occurs. Samples in which the conductivity is controlled by the Bube-Rose model are selected as systems that are particularly sensitive to these influences. That is, crystals initially already contain R – and S-centers.

It is of interest to investigate how the properties of the elements will change if the alloying additive itself is an external factor. That is, a change in the photoelectric properties of initially uniformly alloyed samples, in the contact layers of which, from the surface, an alloying impurity appears.

It should be noted that the heterogeneous distribution of the impurity in this case is a typical situation that one has to face in practice.

It is known that the properties of semiconductor crystals can vary widely depending on the quantity and quality of the defects formed. This should also affect the contacting part of the semiconductor sample.

In this paper, we consider the problem of the behavior of ohmic contact to a semiconductor in the initial state when unevenly distributed charged electron traps appear in its spatial charge region. Despite the urgency of this problem, it is practically not covered in the literature.

The introduction of trap centers into the contact layer of the crystal can radically change the energy structure of this area. In particular, in the case of electronic traps, the formation of a locking barrier is possible. At the same time, the conditions of current transfer change significantly and specific effects occur that are close in nature to negative photoconductivity.

To analyze this situation, it is necessary to derive dependencies describing the type of barrier that occurs in the conduction band, both in the dark and in the light. As well as determining the relationship of the parameters of this barrier – its width, height, coordinates of the maximum, the steepness of the walls - from the properties of the traps – their energy

depth, initial concentration and distribution over the depth of the sample.

The goal of this work is to show that unevenly distributed charged electron traps are able to form a locking barrier in the area of the spatial charge of the ohmic contact. Its parameters are uniquely related to the parameters of traps and, therefore, are controlled technologically. At the same time, due to the barrier that has arisen, the sensor based on a semiconductor crystal acquires new properties, including anomalous ones.

Changes in photoconductivity caused by the treatment of single-crystal samples of cadmium chalcogenides in a gas discharge were investigated by the authors [5-7]. The technology of such processing is as follows. The element was placed in a vacuum ″ $10^{-2} \oplus 10^{-3}$ mmHg. between the electrodes, to which a voltage of the order of several kilovolts was applied. Variable fields of industrial frequency were used. In the resulting discharge streamer, charged particles bombard the sample surface. It has been established that gas discharge treatment of the surface of cadmium chalcogenide crystals leads to the creation of a large concentration of electron traps in the near-surface layer.

In the case of crystal excitation by strongly absorbed light, nonequilibrium carriers are created in a thin near-surface layer. At the same time, it should be borne in mind that the treatment of a single crystal with a gas discharge, it is in this layer that causes an increase in the concentration of traps. Therefore, the change in photoconductivity in this case depends on the ratio of the depth of penetration of exciting light into the sample and the depth of propagation of the trap centers. The most favorable condition for changing the photoconductivity can be considered the coincidence of the depth of light penetration with the depth of propagation of traps.

In a pure semiconductor for ohmic contact, the energy distribution changes according to the logarithmic law

$$E = 2kT \ln\left(1 + \frac{x}{a}\right)$$

(8.1)

where, a there is some characteristic length.

The distribution of the electron concentration in this case is expressed by the ratio

$$n = n_k \exp\frac{E}{2kT} = n_k\left(\frac{a}{a+x}\right)^2$$

(8.2)

Thus, the semiconductor layers bordering to the metal electrodes, the thickness of which ~ a, they can be "filled" with charge carriers. At the same time, the concentration of carriers near the contacts n_k, as formula (8.1) shows, it does not depend on their concentration in the depth of the semiconductor, which may be small (insulator). Therefore, the electrical conductivity of such a contact can be high, even if the specific electrical conductivity of the semiconductor (in the absence of contact) is negligible, for example, in the case of a wide-band CdS.

8.1. The effect of traps on the barrier structure

If the contact is formed for a high-resistance semiconductor, then due to the significant difference in conductivities, almost the entire area of the spatial charge (ASC) is located in its contact layer.

Let electronic traps be introduced into such a semiconductor N_t, the concentration of which decreases from the surface deep into the volume according to the law

$$N_t = N_{t0}e^{-\frac{x}{\ell_0}},$$

(8.3)

where N_{t0} – this is their concentration on a geometric surface, and l_0 – a characteristic length showing at what distance the number of traps decreases in e times.

The activation energy of these traps (E_c–E_t). Then, directly at the contact (area I fig. 8.1), the traps end up under the Fermi level. Such traps are filled with electrons regardless of the concentration of free charge. On the surface itself, their distance from the Fermi energy and, consequently, filling, will be maximal. Therefore, at the point $x=0$ the appearance of such traps will not change the concentration of free electrons and the distribution of energy. They are still described by formulas (8.1) and (8.2).

As can be seen from Figure 8.1, the greater the depth of the traps (E_c–E_t), the wider the

electron-enriched region I, since up to large x coordinates the traps are located below the Fermi level or in the Fermi level region.

At the same time, as will be shown in more detail below, the greater the initial concentration of traps N_{t0}, the steeper the dependence goes up $\dfrac{dE}{dx}$. Both of these factors, acting together, should ensure a greater height of the barrier formed.

On the contrary, in the depth of the volume at $x > L_1$ the appearance of electronic traps will change the conditions significantly. The traps are partially filled and are able to capture an additional charge. In this case, the concentration of the free charge, initially constituting n_0 (curve 1 Figure 8.1), it should decrease, which is accompanied by an increase in the distance from the bottom of the conduction band to the Fermi level.

Consider the far edge of the impurity propagation front N_t (area III of Figure 8.1). The concentration of traps in the area $x = L_1$ it is small, so in general it remains electroneutral. Part of the free charge goes to the traps. The equation of electroneutrality in this case looks like this:

$$N_d^+ = n_0 e^{-\frac{E(x)}{kT}} + N_{t0} e^{-\frac{x}{\ell_0}} . \quad (8.4)$$

Taking into account that numerically the concentration of ionized donors N_d^+ equal to n_0 and using the exponential expansion in a series, from (8.4) we obtain

$$n_0 \frac{E(x)}{kT} = N_{t0} e^{-\frac{x}{\ell_0}} .$$

Where from

$$E_3(x)\big|_{x \to L_2} = \frac{N_{t0}}{n_0} kT e^{-\frac{x}{\ell_0}} . \quad (8.5)$$

As the x coordinate decreases towards the surface, the energy value of the edge of the conduction band increases, although slightly. If the whole free charge n_0 will switch to traps, then $(E–E_c) \sim kT$ (on the border of regions II and III).
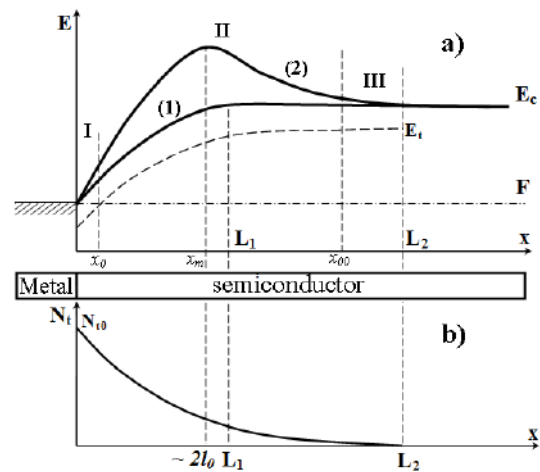
Fig. 8.1. (a) – the structure of the ASC ohmic contact to a high-resistance semiconductor: (1) - initial state; (2) - after the introduction of traps; (b) - distribution of the concentration of electronic traps by depth

The processes considered at the edges of the ASC are sufficient to predict changes in the energy distribution. If there is an energy curve in the depth of the volume $E_c(x)$ rushes upwards, and at the very contact with the metal comes to the same point where it was without taking into account traps, then in general the ASC profile should have the form of a bell-shaped maximum (curve 2 Fig. 8.1a). Moreover, its width is controlled only by the penetration depth of electronic traps, determined by the technological factors of crystal processing.

8.2. Energy distribution in the contact layers of a crystal with electron traps

The barrier profile in area I of Figure 8.1 a can be determined using the Poisson equation

$$\frac{d^2 E_1}{dx^2} = \frac{4\pi e^2}{\varepsilon} \rho(x) = \frac{4\pi e^2}{\varepsilon} \left[N_d^+ - N_t(x) - n(x) \right], \quad (8.6)$$

where E – energy, and N_d^+ = $n_0 \ll n_k$. Using expressions (8.2) and (8.3) formula (8.6) acquires the form:

$$\frac{d^2 E_1}{dx^2} = \frac{4\pi e^2}{\varepsilon} \left[-N_{t0} e^{-\frac{x}{\ell_0}} - n_k \left(\frac{a}{a+x} \right)^2 \right]. \quad (8.7)$$

Note that negative values of the second derivative indicate the convexity of the function E_1 within area I. After integration

$$E_1(x) = \frac{4\pi e^2}{\varepsilon}\left[-\ell_0^2 N_{t0}e^{-\frac{x}{\ell_0}} + n_k a^2 \ln|a+x| + C_1 x + C_2\right]$$

$$(8.8)$$

values of constants C_1 and C_2 can be determined from a comparison with the distribution (8.1) for a pure semiconductor.

When used for metal contacts with possibly small output operation, the value of the jump at the boundary $\Delta E (0) \rightarrow 0$. In this case, when $x=0$ $(E_c–F) = 0$ and $n_k \approx N_c = 10^{19}\text{sm}^{-3}$. According to [8], the value of the cadmium concentration on the surface ~ 10^{21}sm^{-3}. Taking this amount as 0.1-1% of the total value, we get that on the surface it is true $N_{t0} \le n_k$.

Taking into account also the calculations given in clause 8.1, regarding the filling of traps without changing the concentration of free charge, it will be fair:

$$\frac{dE}{dx}\bigg|_{x=0} = \frac{dE_1}{dx}\bigg|_{x=0}$$

or from (8.7) and (8.1):

$$\frac{2kT}{a+x} = \frac{4\pi e^2}{\varepsilon}\left[\ell_0 N_{t0}e^{-\frac{x}{\ell_0}} + \frac{n_k a^2}{a+x} + C_1\right],$$

when x = 0:

$$C_1 = \frac{2kT}{a}\frac{\varepsilon}{4\pi e^2} - \ell_0 N_{t0} - n_k a$$

$$. \quad (8.9)$$

The value of the constant C_2 in (8.8) can be found from the condition $E_1(0) = 0$. It follows from it

$$C_2 = \ell_0^2 N_{t0} - n_k a^2 \ln a$$

$$. \quad (8.10)$$

Finally (8.8), taking into account (8.9) and (8.10), takes the form:

$$E_1(x) = \frac{4\pi e^2}{\varepsilon}\left[\ell_0^2 N_{t0}\left(1 - e^{-\frac{x}{\ell_0}}\right) + n_k a^2 \ln\frac{a+x}{a} + \left(\frac{2kT}{a}\frac{\varepsilon}{4\pi e^2} - \ell_0 N_{t0} - n_k a\right)x\right]$$

$$(8.11)$$

The resulting expression is too cumbersome for further analysis. Therefore, we assume that the value of l_0 in the distribution of traps is large enough, and the stitching point with the function $E_2 (x)$ (i.e., the width of the area I)

lies at a coordinate smaller than the radius of the shielding a. Then putting the exponent and the logarithm in a row, from (8.11) the expression is obtained:

$$E_1(x) = \frac{2kT}{a}x,\qquad (8.12)$$

which, as expected, is not affected by trap parameters l_0 and N_{t0}. In the near-surface layer, the energy distribution in the barrier is represented by an almost straight line with a slope $2kT/a$. At the same time, the graph $E_1(x)$ lies above the curve 1fig. 8.1a. That is, from the very beginning, with the growth of the coordinate, the concentration of the free charge drops faster than the concentration of traps.

8.3. Barrier structure in the depleted layer

In the central part of the barrier (region II of Figure 8.1), there is practically no free charge and the concentration of electrons on the traps significantly exceeds the number of ionized donors, since for these distances x the number of traps themselves is still quite large. Then $n_t(x) \gg N_d^+$; $n(x)$. In this case, the charge density:

$$\rho(x) = -en_t(x) = -eN_t(x)f(x),$$

where $f(x)$ - Fermi-Dirac probability for filling traps:

$$f(x) = e^{-\frac{(Ec-E_t)-(Ec-F)}{kT}} = e^{\frac{Ec-E_t}{kT}} \cdot e^{-\frac{Ec-F}{kT}}.$$

In this expression, the first exponent associated with the activation energy of the traps does not change with the coordinate, and the exponent of the second exponent depends on x.

Finally, the Poisson equation has the form

$$\frac{d^2 E_2(x)}{dx^2} = -Ae^{-\frac{x}{\ell_0}}e^{\frac{E_2}{kT}},\qquad (8.13)$$

where

$$A = \frac{4\pi e^2}{\varepsilon}N_{t0}e^{\frac{E_c-E_t}{kT}}.\qquad (8.14)$$

It can be seen that in this whole area the second derivative is negative. The curve is concave. Using substitution

$$Z = -\left(\frac{x}{\ell_0} + \frac{E_2}{kT}\right), \quad (8.15)$$

we have

$$\frac{d^2z}{dx^2} = \frac{A}{kT}e^Z. \quad (8.16)$$

Or

$$\frac{1}{2}d\left(\frac{dz}{dx}\right)^2 = \frac{A}{kT}e^Z dz.$$

From where after integration

$$\left(\frac{dz}{dx}\right)^2 = 2\frac{A}{kT}e^Z + C_1. \quad (8.17)$$

The value of C_1 can be obtained at the maximum position, where $\frac{dE}{dx} = 0$. When

$$C_1 = \left(\frac{1}{\ell_0}\right)^2 - 2\frac{A}{kT}e^{-\frac{x_{max}}{\ell_0}} \cdot e^{-\frac{E_{max}}{kT}}. \quad (8.18)$$

On the ascending curve, where $x < x_{max}$ and $E < E_{max}$ rightfully (see 8.15)

$$C_1 << 2\frac{A}{kT}e^Z.$$

For sufficiently sharp barriers on the descending part of the magnitude x and x_{max} of the same order, and $E < E_{max}$. Therefore, this condition remains true here. In general, the formula (8.17) takes the form:

$$\left(\frac{dz}{dx}\right)^2 = 2\frac{A}{kT}e^Z.$$

Where

$$\frac{dz}{dx} = \pm\sqrt{\frac{2A}{kT}}e^{\frac{Z}{2}}. \quad (8.19)$$

In accordance with (8.11), the derivative is negative on the ascending part of the curve. On the falling part for everyone $\frac{dE}{dx} < \frac{kT}{\ell_0}$ (that is, a slow decline), this also remains in

force. Then the "–" sign should be left in (8.19). As a result, after integration, it is determined

$$-2e^{-\frac{Z}{2}} = -\sqrt{\frac{2A}{kT}}x - C_2. \quad (8.20)$$

Substituting (8.15) into (8.20) and simplifying the expression, we get

$$E_2(x) = -kT\frac{x}{\ell_0} + 2kT\ln\left(\sqrt{\frac{A}{2kT}}x + C_2\right). \quad (8.21)$$

8.4. Detailing of the energy distribution function explicit form

From the equality of derivatives at the crosslinking point x_0 is:

$$\frac{2kT}{a} = -\frac{kT}{\ell_0} + \frac{2kT\sqrt{\frac{A}{2kT}}}{x_0\sqrt{\frac{A}{2kT}} + C_2},$$

therefore for the big ones l_0, where $\frac{1}{2\ell_0} << \frac{1}{a}$, we get

$$x_0\sqrt{\frac{A}{2kT}} + C_2 = a\sqrt{\frac{A}{2kT}} \quad (8.22)$$

Then the value

$$x_0 = a - \frac{C_2}{\sqrt{\frac{A}{2kT}}}. \quad (8.23)$$

After substituting it into the expression $E_1(x_0) = E_2(x_0)$ we find:

$$\frac{2kT}{a}\left(a - \frac{C_2}{\sqrt{\frac{A}{2kT}}}\right) = -\frac{kT}{\ell_0}\left(a - \frac{C_2}{\sqrt{\frac{A}{2kT}}}\right) + 2kT\ln\left(a\sqrt{\frac{A}{2kT}}\right). \quad (8.24)$$

In the second term on the right in (8.24), the dependence (8.22) is taken into account. Re-

ducing by $2kT$ and giving similar ones, we get for $2\ell_0 \gg a$

$$\left[1 - \ln\left(a\sqrt{\frac{A}{2kT}}\right)\right] \cdot a \cdot \sqrt{\frac{A}{2kT}} = C_2 \quad (8.25)$$

If the increasing part of the barrier is sharp enough, then the value x_0 in (8.23) is not great compared to a. In this case, from equation (8.23) and (8.25) follows

$$\ln\left(a\sqrt{\frac{A}{2kT}}\right) \ll 1$$

and finally

$$C_2 = a\sqrt{\frac{A}{2kT}},$$

$$E_2(x) = -\frac{kT}{\ell_0}x + 2kT\ln\left[\sqrt{\frac{A}{2kT}}(x+a)\right]. \quad (8.26)$$

As can be seen from (8.26) at the maximum when

$$\frac{dE_2}{dx} = -\frac{kT}{\ell_0} + \frac{2kT}{x_m + a} = 0,$$

meaning $x_m = 2\ell_0 - a \approx 2\ell_0.$ (8.27)

The width of the increasing part of the barrier and, consequently, the field strength here is controlled by the parameters of the trap distribution $2l_0$. Substituting (8.27) into (8.26) determines the value of the function E_2 at the maximum:

$$E_{2\max} \cong -2kT + 2kT\ln\sqrt{\frac{A}{2kT}}(2\ell_0). \quad (8.28)$$

More than $2l_0$, the higher the barrier.

Dependence on the initial concentration of traps N_{t0} and their activation energies $(E_c - E_t)$ is set by the value

$$A = \frac{4\pi e^2}{\varepsilon} N_{t0} e^{\frac{E_c - E_t}{kT}}.$$

It follows from (8.28) that with an increase in these parameters, the height of the barrier

also increases linearly proportionally $(E_c - E_t)$ and logarithmically proportional N_{t0}.

The total width of the ASC can be determined when $E_2(x)=0$:

$$\frac{L_2}{2\ell_0} = \ln\left(\sqrt{\frac{A}{2kT}}L_2\right). \quad (8.29)$$

It is taken into account here that, according to the conditions of the problem, the traps diffuse further L_1 and already at the maximum coordinate $x_{max}>a$. Equation (8.29) does not explicitly allow to obtain the dependence $L_2(l_0, A)$, but it allows us to identify the trends of this dependence using methods borrowed from number theory.

Imagine (8.29) as

$$\frac{L_2}{2\ell_0} - \ln L_2 = \ln\sqrt{\frac{A}{2kT}}. \quad (8.30)$$

Let the type of traps not change (i.e. "A" is fixed), but due to technological techniques it increases l_0. In this case, since the right part does not change, and the denominator of the first term increases, the value L_2 it should increase, although not proportionally. If only L_2 it did not change, the left part (8.30) also decreased. This follows from

$$\frac{d\left(\dfrac{L_2}{2\ell_0} - \ln L_2\right)}{dL_2} = \frac{1}{2\ell_0}\downarrow - \frac{1}{L_2}\uparrow < 0.$$

On the contrary, let l_0=const, and the value of "A" increases. Then the left part at (8.30) should increase. Since the logarithmic function y=lnL_2 changes slower than linear $y = \dfrac{L_2}{2\ell_0}$, generally L_2 increases. With the increasing concentration of traps on the surface N_{t0} and their activation energies $(E_c–E_t)$ the width of the ASC increases.

Note at the same time that for such a conclusion, it is important to simultaneously increase both parameters. In principle, a situation is possible when deeper traps [$exp\left(\frac{E_c - E_t}{kT}\right)$ more] on a geometric surface is not enough (N_{t0} less). Since the value of N_{t0} managed technologically, this competition can be avoided.

8.5. Energy profile of the barrier in the semiconductor volume

After stitching at the point x_0 type of function $E_2(x)$ the depth of the volume also turned out to be related to the state of the surface (see 8.6). The standard procedure for stitching in depth volume functions $E_2(x)$ and $E(x)$ leads to an overly complex system of equations that can be solved only by numerical methods.

Therefore, an artificial technique was used [9]. Function value $\dfrac{dE_2}{dx}$ at the maximum when $x=x_m$ is equal

$$\frac{dE_2(x_m)}{dx} = -\frac{kT}{\ell_0} + \frac{2kT\sqrt{\dfrac{A}{2kT}}}{\sqrt{\dfrac{A}{2kT}}x_m + C_2} = 0$$

when $\sqrt{\dfrac{A}{2kT}}x_m + C_2 = 2\ell_0\sqrt{\dfrac{A}{2kT}}$

and $C_2 = \sqrt{\dfrac{A}{2kT}}(2\ell_0 - x_m)$.

This after substituting in $E_2(x)$ gives

$$E_2(x) = -\frac{kT}{\ell_0}x + 2kT\ln\left[\sqrt{\frac{A}{2kT}}(x + 2\ell_0 - x_m)\right]$$

and at the maximum $(x=x_m)$

$$E_{2\max} = -\frac{kT}{\ell_0}x_m + 2kT\ln\left(\frac{A}{2kT}4\ell_0^2\right)$$

(8.31)

It can be seen that the closer to the interface the barrier is formed (x_m decreasing), the higher it is. With the increasing concentration of traps N_{t0} and their depths ($E_c - E_t$) (i.e. "A" increases) the barrier is also increasing. This is the same as the one received earlier.

At the stitching point of the barrier function $E_2(x)$ with a function in the quasi-neutral domain, the value $E \approx kT$. Therefore, we can assume that x_m determines the overall width of the ASC: $x_m=L_2$. Obtain:

$$2\ln\left[\sqrt{\frac{A}{2kT}}(L_2 + 2\ell_0 - x_m)\right] = \frac{L_2}{\ell_0} + 1$$,

when $L_2>>l_0$ and therefore, $\dfrac{L_2}{\ell_0} >> 1$.

When $L_2 + 2\ell_0 - x_m = \dfrac{e^{\frac{L_2}{2\ell_0}}}{\sqrt{\dfrac{A}{kT}}}$,

or

$$L_2 \approx 2\ell_0 \ln\left(2\ell_0\sqrt{\frac{A}{2kT}}\right)$$. (8.32)

The width of the spatial charge area increases with growth $2l_0$, which also coincides with what was received earlier.

8.6. Sample doping technology

The article [6] describes a method for creating electronic traps on the surface of a semiconductor by treating it with a gas discharge. The advantages of this technique are associated with the presence of an electric field during technological operations. By varying the magnitude and direction of this field, it is possible to control the process of introducing defects and the profile of their distribution.

At [10] indicates a significant migration of impurity ions in wide-band semiconductors in fields of the order 10^5 V/m.

In addition to creating electronic traps and a controlled process of their introduction into the volume of a semiconductor sensor, the proposed corona discharge processing method promotes the formation of donors on the sample surface [7]. The same electric field that promotes the outflow of electronic traps accumulates donors at the surface, increasing the conductivity in the subsurface layers. In this case, it becomes possible to process crystals with already applied contacts and in the same cycle to make measurements without the presence of air in the chamber.

The sample under study was a rectangular plate of monocrystalline cadmium sulfide with a thickness of 1.5 mm and a frontal surface area of about one square centimeter. The crystal was placed in a vacuum chamber, where a vacuum of the order of $10^{-2} \oplus 10^{-3}$ mmHg was created.

A stable symmetrical discharge (Fig. 8.2.b) was created [11] when the end of the cathode was given a conical shape. With an insufficient

degree of discharge in the chamber, the discharge turned into an avalanche and was laced, and in the working area of high voltages, the moment of lacing practically did not depend on the field. All the results given below were obtained after processing in the glow discharge mode.

<div align="center">(A)   (B)</div>
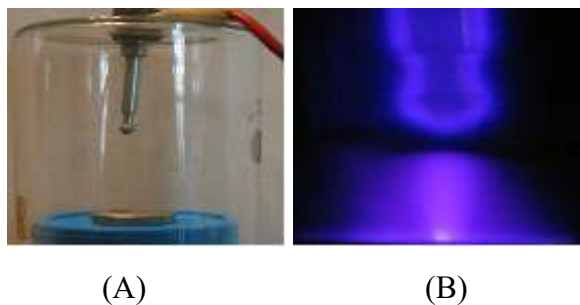
Fig. 8.2. The design of the spark gap (A) and the processing of samples in vacuum in a gas discharge (B)

The best results were obtained with a gap of 8-12 mm. We attribute this to the fact that when the gap was insufficient, the expiring electrons did not gain enough energy to create defects in the structure of the crystal under study.

A high voltage of the order of 4-5 kV was created using a high-voltage rectifier. In this case, the difference from the one described earlier (see [5-7]) is the use of constant voltage for processing.

For processing in a gas discharge, samples were selected that had symmetrical linear CVC graphs both in the dark and in the light. Sufficiently photosensitive crystals were used. In both cases – both in the dark and under illumination – after the technological process, the total resistance of the crystal increased. After the appearance of electronic traps, the initially low-resistance area of the spatial charge of the ohmic contact significantly increases its resistance as a result of the formation of a barrier. The resistance of the base in the dark was ” $5 \triangleleft 10^4$ Om, in the light $(2 \odot 3)10^4$ Om. A slight difference in the obtained values allows us to conclude that the width of the formed barrier is determined only by the depth of penetration of traps. There are very few traps in the layers far from the crystal surface, and therefore all of them are already filled in the dark. The light does not change their filling and, therefore, the width of the ASC, and with it the resistance.

When illuminated by strongly absorbed light, carriers are created in the near-surface layers of the sensor and are forced to move along the surface by the applied field. Gas discharge treatment promotes, according to [5,6], the formation of additional donor centers on the surface. At the same time, the surface conductivity increases, and the effect of recombination weakens.

8.7. Photoelectric properties of the obtained samples

In the spectral range 540–600 nm for samples pretreated in a gas discharge, we observed a slight increase in photocurrent. This indicates the predicted appearance of deep trap levels as a result of crystal processing.

The conditions for the formation of a barrier in our structures are also manifested in the dependence of the shape of the spectral distribution curve of the photocurrent on the polarity of the applied voltage. For conventional barriers, as the applied forward displacement increases, the height of the barrier and its width decrease. At the same time, the field strength in the ASC of the barrier, as the ratio of these values, changes little. When the polarity of the applied field is reversed, both these parameters – height and width – simultaneously increase, but their ratio again does not undergo significant changes.

In our case, this is not the case. The width of the formed barrier is determined only by the depth of penetration of traps and does not depend on the applied voltage. In this case, the external electric field lowers the height of the barrier and distorts its symmetry (see Figure 8.1). The side of the potential barrier in which the field strength is opposite to the external one decreases to a greater extent. Since one-way illumination is produced at the same time, the short-wave and long-wave part of the spectral distribution curve of the photocurrent with a change in the polarity of the offset are distorted in different ways.

If, under the action of the applied field, the increasing – from the lighting side – half of the barrier is modified more (see Figure 8.1), then the short-wave (with strong light absorption) part of the spectral dependence changes significantly.

On the contrary, if the direction of the field is such that it mainly changes the back, falling side of the barrier, then basically changes should be expected for photocurrents excited by long-wave, deeply penetrating light.

Experimentally, it turned out to be more correct to investigate the spectral distribution of the emerging photo-EMF. This approach makes it possible not to take into account the nuances of photocurrent formation – recombination in the inner regions of the crystal, the influence of the resistances of its parts, etc. And instead, the main thing to identify is the influence of emerging traps in the near-surface layers of the sample due to processing in a gas discharge and donor levels on its geometric surface.

Without the participation of an external field on samples treated in a gas discharge, for longitudinal conductivity, we observed the occurrence and unusual distribution of EMF when excited by light of different wavelengths. The curve is shown in Figure 8.3.

In our case, we found that the value of the photo-EMF in white light up to 100 lk it turned out to be smaller than with monochromatic lighting. This is due to the unusual appearance of the graph Fig. 8.3. The short-wave and long-wave contributions do not add up, as usual, in white light, but are subtracted.

This happens because of the non-trivial type of barrier. As a rule, the ASC is represented either by an increasing part from the surface deep into the crystal (ohmic contact), or by a falling part (shut-off contact). In our case, both slopes of the barrier are represented (Fig. 8.1). It is all displaced in the volume of the crystal from the surface. In this regard, when illuminated from the contact side on the sample surface, absorption first occurs in the increasing part of the barrier for short wavelengths of light with strong absorption. Photoexcited electrons by the barrier field return to the contact on the illuminated surface, where they increase the negative potential relative to the lower contact to the sample. In Figure 8.3, we took this value for the positive part of the curve (the area of 440-540 nm).

As can be seen from the figure, as the excitation wavelength increases, the contribution of this component decreases. This happens because the light absorption coefficient decreases

for longer wavelengths, and some of the photons reach deeper layers of the crystal, where the falling part of the barrier is located.
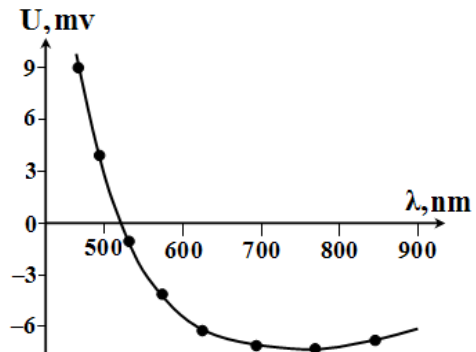
Fig. 8.3. Spectral distribution of photo-EMF. For crystals treated in a gas discharge

In this case, the field strength causes the nonequilibrium electrons to move in the opposite direction. Obviously, for a wavelength of 540 nm, when Fig. 8.3 there is an intersection of the graph and the abscissa axis, both of these processes balance each other and the resulting potential difference turns out to be zero.

With a further increase in the wavelength, more and more photons are absorbed from the side of the declining part of the barrier (Fig. 8.1). The barrier field mainly directs electrons deep into the sample, the negative potential of the lower contact increases.

At sufficiently large wavelengths of ~800 nm or more, the signal stabilizes (Fig. 8.3), remaining negative. This indicates the predominant absorption of light in the right side of the barrier (Fig. 8.1). In addition, part of the photons can penetrate deep enough into the crystal and be absorbed outside the contact ASC zone, without making any contribution to the formation of the graph Fig. 8.3.

The technological techniques used cause changes in this graph with a certain ratio of temperature, lighting, the intensity of the field used and the duration of processing. In our case, we got the best results when 15 min processing with a distance of 8 mm to the needle on which it was 4000 V. Then the graph takes on an anomalous appearance with the largest possible area of negative values.

The limit of changes in the curve of Figure 8.3 is the usual spectral distribution of the pho-

toresponse. If there is too much saturation of traps during processing in a gas discharge, the gradient of their concentration turns out to be insignificant, and the spectral distribution returns to its initial state. This is the same crystal in which the resistance has simply increased due to the presence of traps.

Thus, the proposed technology for creating sensors, in full accordance with the developed model, makes it possible to obtain sensors with abnormal spectral sensitivity. The type of dependence of Fig. 8.3 makes it possible to use them as receptors for a certain wavelength of radiation, predetermined in advance during processing. Moreover, since the signal value is zero at this point, such a sensor will be completely insensitive to any noise and interference, including artificially supplied.

In addition, when illuminated from different regions of the spectrum, the EMF sign, and hence the current, changes to the opposite. This property can be used to create a new generation of optical devices.

References

1. Simanovych N.S., Brytavskyi Ye.V., Kutalova M.I., Borshchak V.A., Karakis Y.N. "The study of heterogeneous sensitized crystals of cadmium sulfide. Part I. About charge state of the centers recombination" // "Photoelectronics", n. 26. Odesa, 2017. P. 124 – 138 .

2. S.S.Kulikov, Ye.V. Brytavskyi, M.I., Kutalova, N.P. Zatovskaya, V.A. Borshchak, N.V. Konopel'skaya, Y.N. Karakis "The study of cadmium sulfide heterogeneously sensitized crystals. Part II. Relaxation characteristics" // "Photoelectronics", №. 27. Odesa, 2018. P. 79 – 93 .

3. Kulikov S.S., Brytavskyi Ye.V., Kutalova M.I., Zatovskaya N.P., Borshchak V.A., Karakis Y.N. "The study of cadmium sulfide heterogeneously sensitized crystals. Part III. Oscillations of excited carriers", // "Photoelectronics", №. 28. Odesa, 2019. P. 133 – 144.

4. Kulikov S.S., Brytavskyi Ye.V., Kutalova M.I., Zatovskaya N.P., Borshchak V.A., Karakis Y.N. "The study of cadmium sulfide heterogeneously sensitized crystals. Part IV. Oscillations of excited carriers", // "Photoelectronics", №. 29. Odesa, 2019. P. 21-37.

5. Чемересюк Г.Г., Сердюк В.В. Явления, обусловленные захватом носителей, инжектированных в освещенные монокристаллы селенида кадмия // Известия высших учебных заведений. Физика.– 1968.– №12.– С.7 – 12.

6. Чемересюк Г.Г. Отрицательная фотопроводимость в селениде кадмия, обусловленная уменьшением подвижности свободных носителей // Studia Universitatis babes-bolyai: Series Physica Fasciculus 1.–1972. С. 21.

7. Чемересюк Г.Г., Сердюк В.В. Коротковолновое гашение продольной фотопроводимости монокристаллов селенида кадмия // Физика и техника полупроводников.-1969.-Т.3, в.3. С. 396-399.

8. Физика и химия соединений $A_{II}B_{VI}$.// Под ред. проф. С.А. Медведева.- М.: Мир, 1970. С. 103 – 104.

9. Драгоев А.А., Каракис Ю.Н., Балабан А.П., Чемересюк Г.Г. Расчёт профиля ОПЗ датчиков со знакопеременной спектральной чувствительностью // 4nd International Scientific and Technical Conference "Sensors Electronics and Microsystems Technology" SEMST-4). Україна, Одеса, 28 червня – 2 липня 2010 р. "Астропринт". 2010. С. 192.

10. A.A. Dragoev, A.V. Muntjanu, Yu. N. Karakis, M. I. Kutalova Calculation for migration-dependent changes in near-contact space-charge regions of sensitized crystals // "Photoelectronics", №. 19. Odesa "Astroprint" 2010. P. 74 – 78.

11. Минаева О.П. Влияние газового разряда на формирование энергетического барьера в приповерхностной области кристаллов сульфида кадмия // Материалы 63-й отчетной студенческой научной конференции. Секция физики полупроводников и диэлектриков.– Одесса, 2007, С. 3 – 4.

UDC621.315.592

Kulikov S.S., Brytavskyi Ye.V., Borshchak V.A., Zatovskaya N.P.,

Vikulin I. M.[1], Vikulina L. F.[2], Gorbachev V. E.[1], Litvinenko V. M.[3], Markolenko P. Y.[1]

[1] State University of Intellectual Technologies and Communications
Ukraine, 65029. Odessa, Kuznechna st., 1, e-mail: physonat@gmail.com
[2] Odessa State Agrarian University
Ukraine, 65012. Odessa, Panteleimonovska st., 13, e-mail: lepole1@gmail.com
[3] Kherson National Technical University
Ukraine, 73008. Kherson, Berislavske road, 24, e-mail: hersonlvn@gmail.com

DETECTORS BASED ON FIELD EFFECT TRANSISTORS

The possibility of using the method of combining several sensor elements with opposite sensitivity to various external influences to obtain new designs of sensors for light, temperature and magnetic field has been experimentally investigated. Standard industrial samples of FEJT and a MOSFET in saturation mode with two-pole connection, when the gate is closed with the source, were used as sensor elements in the work. It is shown that the FEJT has a negative temperature coefficient of current change, while the MOSFET has a positive one. At the same time, the sign of the radiative action factor of the MOSFET is determined by the initial value of the drain current before irradiation. It has been experimentally confirmed that the use of four transistors in a bridge measurement circuit increases the sensitivity of the sensor tenfold compared to one transistor due to the internal mechanism of increasing the sensitivity for series-connected pairs of transistors.

1. Introduction

The employment of the IoT concept in industry, transport and everyday life has led to a rapid growth in research on new designs of various sensors that fill intelligent control and control systems with numerical information.

Light sensors occupy a special place among sensors of physical quantities, since in our life photodetectors are used everywhere from devices for automatic switching of street lighting to cameras and optical signal detectors in fiber-optic communication lines. More and more sophisticated technologies are being used to improve the performance of photodetectors.

Thus, in paper [1], a modern design of a high-speed contact photodiode with a Ge-on-Si structure with surface illumination and increased efficiency is presented. High external quantum efficiency is achieved due to the peculiarities of capturing photons by a surface with micro-holes.

In [2], a new architecture of a photodiode detector with resonant cells is proposed, in which the mirrors are replaced by lattice-patterned metasurfaces. It has been shown that structured mid-IR photodetectors less than 10 μm thick with a 75 nm HgCdTe photoabsorber can provide maximum efficiency.

Photodiodes based on mixed one-dimensional (1D) and three-dimensional (3D) p-n-heterostructures with synergistic properties of various dimensions have shown unique optical properties due to their large transition areas and high absorption cross-section, which provides excellent optoelectronic characteristics [3]. However, due to the complexity of designing and constructing a proper 1D-3D p-n-junction, their electronic properties are still unclear. As a photo detector, it covers the range from ultraviolet to visible light.

The work [4] presents the development of germanium vertical p-i-n-photodiodes with a matrix of holes in the shape of a pumpkin. Photodiodes were fabricated on a germanium substrate with a sensitivity of 0.74 A/W. It is estimated that the design of the pumpkin-shaped hole provides higher optical absorption compared to the cylinder-shaped hole.

In paper [5] microstructures for capturing photons were introduced into photodetectors based on GeSn and achieved highly efficient photodetection at 2 μm with a sensitivity of 0.11 A/W. The demonstration samples were implemented on the basis of a GeSn/Ge p-i-n-photodiode with quantum wells on the GeOI architecture.

In paper [6], designs of organic phototransistors are considered and it is argued that the practical application of inorganic photodetectors is significantly limited due to many disadvantages, including complex manufacturing processes and poor mechanical flexibility. In this scenario, organic phototransistors emerge as potential competitors with impressive performance characteristics such as high flexibility and ease of manufacture and low cost, making them suitable for next generation wearable electronic devices.

Investigations of new designs of temperature sensors are of great interest, since all industries and research without exception require temperature control of technological processes. Temperature sensors are needed to control the parameters of all electronic systems, environmental parameters, in medicine, in everyday life. They are used in most hard-to-reach places, even where other parameters cannot be measured. Often, according to their readings, other physical parameters are also evaluated (pressure, density, ignition intensity, rate of nuclear decay or chemical reaction, etc.). Therefore, in recent years, new designs of temperature sensors based on FET have been developed for narrow applications: in the aviation industry [7], for measurements in biomedicine [8], for implantation devices [9], for fire extinguishing systems [10], for monitoring the energy efficiency of buildings [11].

At the same time, magnetic field sensors are among the most common sensors. In every car, the sensor device for position and crankshaft speed sensors are magnetic field sensors; in every modern mobile phone there is an electronic compass based on a $Ni_{80}Fe_{20}$ thin-film sensor [12] a motion tracking device based on a fluxgate sensor [13], in any a computer and a processor device have magnetic storage devices based on magnetic tunnel junctions [14], systems based on Hall sensors are used for the finest research in biomedicine and neurosurgery [15], and based on magnetoelectric sensors in magnetic resonance imaging [16]. Therefore, the study of new designs of highly sensitive and low-energy magnetic field sensors is urgent.

With the development of the IoT concept, a new class of intelligent temperature sensors that built directly into the object, began to appear. Such smart sensors are found in abundance in any IoT network from computers and cars to smart homes and smart cities. It often turns out that their power consumption limits the further development of the sensor network. Therefore, new designs of ultra-low power sensors are being developed [7, 9], special energy-saving technologies are used [17, 18].

However, the use of special designs and innovative technologies requires significant costs for research and manufacture of devices, and also significantly increases the cost of finished products. In this work, we studied the possibility of using the existing element base to create cost-effective temperature and light sensors that would meet modern requirements.

In addition, sensors are often used in extreme conditions of increased level of ionized radiation, near nuclear reactors [19], in elementary particle accelerators [20], in the upper layers of atmosphere [7] and in outer space [21]. It is well known that ionizing radiation fundamentally changes the electrical properties of any sensitive structures [22, 23], and for sensors that are exposed to radiation, special methods are needed to compensate for such effects [21]. However, neither new designs of sensors, nor the latest materials and components of sensors are practically studied from the point of view of the influence of ionizing radiation.

FETs are more sensitive to external influences and consume less power than bipolar transistors. In addition, advanced CMOS technologies have allowed the development and implementation of fully integrated with digital systems, low-power intelligent sensors based on sensitive MOS elements. Therefore, in recent years, it is FETs that are increasingly used as sensing elements of various sensors.

To obtain the required properties, various designs of field-effect transistors (FETs) are used: an organic field-effect transistor (OFET) [24], a floating gate field-effect transistor (FGFET) [8], an FET based on a polymer ferroelectric [25], as well as state-of-the-art manufacturing technologies FET such as inkjet volumetric printing and chemical vapor deposition [17].

However, the use of FET-based sensors requires a special approach, since the electrical parameters of the FET are highly dependent on

unwanted external influences such as ionizing radiation.

The aim of this work is to study the possibility of using standard industrial FETs as sensing elements in cost-effective temperature, magnetic field and light sensors at objects with an increased background radiation.

To fulfill the set goals, we used the method of combining several sensory elements with opposite sensitivity to various external influences.

Until now, the most preferred sensor circuit is a measuring bridge of four resistors, one of which is sensitive to the measured effect, for example, a thermoresistor [26]. The advantage of this scheme is the simplicity of establishing the zero value of the output signal at $T = 0$ °C, its further calibration and correction.

The sensitivity of the sensor is doubled if, instead of a constant resistance, a second sensor of the same type is connected to the diagonally opposite shoulder of the bridge.

However, it is also possible to further increase the sensitivity of the sensor if there will be elements sensitive to external influences in all four branches of the bridge. A feature of this combination of sensitive elements is that two pairs of sensors must have opposite resistance coefficients. Sensor elements with the same resistance coefficients should be located in diagonally opposite branches of the bridge.

In this work, it is shown that if, instead of bridge resistors, FET pairs with opposite sensitivity to the measured effect are used, then it is possible to obtain sensors with a sensitivity that is an order of magnitude higher than that of a single sensor.

2. Temperature detector

FETs can be used as temperature sensors; however, the spread of the temperature-sensitive parameter values causes certain difficulties in calibrating such sensors. The most convenient sensitive parameter for recording external influences is the saturation current of the FET at two-pole switching, when the gate of the transistor is closed with the source.

In our work [27], it was experimentally established that the temperature coefficient of the current change is negative for FEJT, and positive for MOSFETs. This difference in the properties of the two types of FETs can be used for temperature stabilization of reference current generators, as in [27], and also in our case to increase the sensitivity of the combined bridge temperature sensor.

In this way, the advantage of the bridge measurement can be maximized by connecting temperature-sensitive FETs to all four of its branches (Fig. 1).
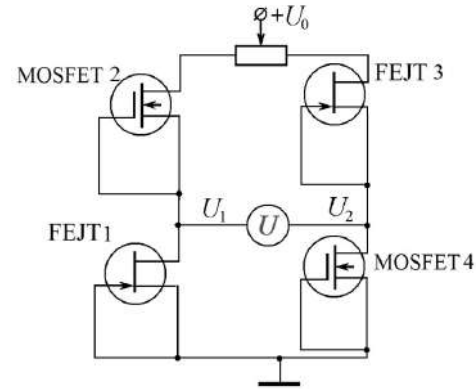
Figure 1. Schematic diagram of the bridge temperature detector

In the first pair of elements FEJT1 and FEJT3, connected in opposite branches of the bridge, the current decreases with increasing temperature, and in the other pair of MOSFET2 and MOSFET4 in other branches, it increases. The voltage of the output signal in the measuring diagonal of the bridge for such a circuit for switching on the primary converters has the form:

$$U = 2\frac{U_0 \cdot \Delta R}{R} \qquad (1)$$

where U_0 – bridge supply voltage; R – is the resistance of the transistor channel in the "source-drain" circuit; ΔR – is the change in this resistance with a change in temperature. The trimmer resistor is used to accurately set the zero value of the output signal.

As the first pair, we used FEJT type KP202 (analogs: C681 or 2N3958) with a p-n-junction as a gate. The experimental value of the temperature coefficient of the current of such transistors is $\beta = -3281$ ppm/°C, and the saturation current decreases with increasing temperature due to a decrease in the mobility of charge carriers in the channel [27]. A KP305 type MOSFET (analogs: MFE3002 or 2N4224) was con-

nected as the second pair. The experimental value of the temperature coefficient of the current of such transistors is $\beta = +14285$ ppm/°C, and the saturation current increases with increasing temperature. This happens due to an increase in the gate cutoff voltage when the charge changes on the surface states under the gate [27].

It was experimentally established that the sensitivity of a sensor with four FETs $\alpha = 1$ V/°C at a power supply voltage $U_0 = 20$ V in the temperature range from 0 °C to +30 °C, which is 10 times higher than the sensitivity of bridge sensors based on one FET. However, the linear range of the output characteristic is limited to 30 °C.

The linear range of the output characteristics of such a temperature sensor can be expanded by connecting a stabilizing resistor into the source circuit of each FET [28].

At Fig. 2 shows the experimental dependence of the output voltage of a bridge temperature sensor with four FETs and four stabilizing resistors. Sensor sensitivity $\alpha = 0.28$ V/°C at power supply voltage $U_0 = 20$ V in the temperature range from –20 °C to +190 °C. Outside this range, the sensitivity decreases and the nonlinearity of the sensor output characteristic increases.
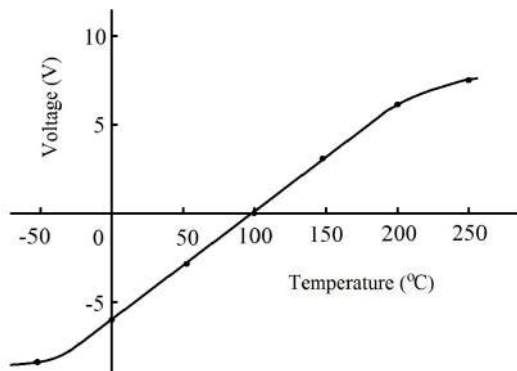
Figure 2. Temperature detector output characteristic with four FETs and four stabilizing resistors

Balancing resistors can be used instead of a trimmer to balance the bridge at any given temperature.

In our previous work [29], experimental studies of the effects of radiation on the FET were carried out. To study the effect of radiation on transistors, a batch of FEJT samples of the KP202 type and MOSFET of the KP305 type were irradiated with gamma quanta with

an exposure dose of 10^4, 10^5, 10^6, 10^7 and 10^8 R. The work on irradiation was carried out within the framework of the state budget research work "Radiation effects in semiconductor sensors", which was carried out by order of the Ministry of Education and Science of Ukraine, state registration number 0115U000855. It was found that the electrical properties of different types of FETs react differently on the received dose of ionizing radiation.

Experiments have shown that the saturation current of the drain for all FEJT samples after irradiation decreases, while according to the radiation sensitivity, MOSFETs are divided into two groups depending on the initial value of the saturation current before irradiation. For all samples of the group with low saturation currents before irradiation (low concentration of electrons in the channel), the saturation current continues to increase, and for all samples from the group with high saturation currents before irradiation (high electron concentration in the channel), the saturation current decreases. Thus, it was found that all MOSFETs selected for the second group due to high saturation currents have a radiation sensitivity the same as that of a JFET. However, their temperature sensitivity remains the opposite. For the manufacture of samples of radiation-stable temperature sensors, just such MOSFET were used.

It was experimentally established that the imbalance of the bridge with four FETs at doses of 10^4 R and 10^5 R is disturbed by only 4% and 6%, respectively. Subsequent irradiation stabilized the operation of the bridge and after a dose of $5 \cdot 10^5$ R the imbalance was only 3%, but after a dose of 10^6 R it was 40 %, and after a dose of 10^7 R it was already 80 %. The sensitivity of the detector samples remained within 250-60 mV/°C up to 10^6 R.

Thus, by combination in the opposite branches of the bridge specially selected FEJT and MOSFET pairs with opposite signs of temperature sensitivity, but with the same sign of sensitivity to ionizing radiation, it is possible to obtain a temperature sensor with high sensitivity and with a minimum number of constituent elements. It was experimentally confirmed that the temperature sensor obtained in this way consumes 49 mW of energy, with a

linear output characteristic and sensitivity α = 0.28 V/ºC in the temperature range from –20 ºC to +190 ºC, with readings deviations of no more than 6% before doses irradiation $5 \cdot 10^5$ R.

3. Magnetic field detector

When the FET operates as a primary converter of any external influence, in order to reduce the dependence of the output signal on the supply voltage, it is convenient to connect it as a two-pole, when the gate is closed with the source, and the gate voltage is absent $U_G = 0$. In this case, the saturation current of the FET is defined as

$$I_s = An^2 \, \mu, \qquad (2)$$

where n, μ – concentration and mobility of charge carriers in the channel; A – constant, which is determined by the geometric and electrical parameters of the channel, which depend on the supply voltage.

If the FET through which the electric current flows is situated in a magnetic field transverse to the direction of the current, then the charge carriers begin to move along spiral trajectories, a magnetoresistive effect arises, consisting in a decrease in the effective free path of the majority charge carriers in the direction of the electric field. A decrease in the mean free path of charge carriers along the direction of the electric field is equivalent to a decrease in their mobility, and hence, according to (2), the saturation current FET. The relative change in the mobility of charge carriers in weak magnetic fields, with sufficient dimensions of the sample transverse to the electric field, is described by the formula [30]:

$$\frac{\Delta\mu}{\mu} = -c\mu^2 B^2 \qquad (3)$$

where c – coefficient depending on the scattering mechanism and the geometric dimensions of the sample. When the semiconductor is limited in the direction transverse to the electric field, then the Lorentz force can be compensated by the force of the Hall electric field, and the flow of charge carriers will cease to be deflected by the magnetic field. What was said above fully applies to the FET channel, placed in a transverse magnetic field [30], while, for the magnetoresistive effect to appear, the transverse dimensions of the channel must be greater than its length. This condition is satisfied, for example, by an FEJT of the KP303 type (analogue of 2N5556) with an n-type channel and a p-n junction as a gate, therefore it can be used as a magnetically sensitive field-effect transistor (MFET).

After substituting expression (3) into equation (2), we obtain the dependence of the saturation current MFET Is on the transverse component of the magnetic field induction B:

$$I_s = An^2 \, (1 - c\mu^3 B^2). \qquad (4)$$

It can be seen from relation (4) that the saturation current of the MFET in a magnetic field will decrease. However, as experiments have shown, the change in the saturation current of FEJT type KP303 in a magnetic field up to 0.5 T is only about 3%. This is due to the fact that in the serial KP303 transistor the transverse dimensions of the channel are not large enough for the complete absence of the Hall effect in weak magnetic fields. Only in magnetic fields greater than 0.5 T the radius of the spiral trajectory of the charge carriers in the channel decreases so much that the Hall effect is absent for the standard transverse dimensions of the KP303 channel. Therefore, the use of an individual KP303 as an independent magnetic field sensor for detecting weak fields is ineffective. It is possible to use separate FETs as an independent weak magnetic field sensor if special MFET designs are made in which the transverse dimensions of the channel are much larger than its length.

However, standard industrial transistors of the KP303 type can be used to detect weak magnetic fields as sensor elements in a combined bridge sensor based on four FEJTs, because in this case, an internal mechanism of increasing the sensitivity arises in both legs of the bridge in each pair of series-connected FEJTs [30]. Fig. 3 shows a schematic diagram of a bridge magnetic field sensor with four FEJTs. Two transistors of the first pair MFEJT1 and MFEJT3 are located in opposite arms of the bridge and must be oriented so that the current in the channel flows across the magnetic field, then they play the role of sensitive elements. And two transistors of the second pair FEJT2 and FEJT3 are located in the other arms

of the bridge and must be oriented so that the current in the channel flows along the magnetic field, then there is no magnetoresistive effect in them, therefore they play the role of load elements for the first pair.

With this inclusion of FEJT, an internal mechanism for increasing the sensitivity operates in each arm of the bridge for a pair of transistors [30]: a decrease in the mobility of charge carriers in a magnetic field in any of the MFEJT transistors leads to an increase in the voltage drop across it and a decrease in the voltage drop across the paired FEJT, which causes an additional an increase in the resistance of the MFEJT channel and an additional decrease in the resistance of the FEJT channel, and, hence, an additional increase in the voltage U.

iments have shown that, unlike magnetoresistors, the magnetic sensitivity of sensors based on FEJT is maximum in the region of weak magnetic fields due to the internal mechanism of increasing the sensitivity associated with an increase in the resistance of the FEJT channel with increasing voltage at the I-V-characteristic saturation region and a corresponding increase in bridge misbalance.

In addition, such a bridge circuit eliminates the temperature drift of the output voltage zero, since all four FEJTs have the same saturation current temperature coefficient. According to the experimental data, in the temperature range from 0 to 120 °C, the relative change in the magnetic sensitivity does not exceed 0.2%.

Figure 3. Magnetic field detector bridge with four FEJTs
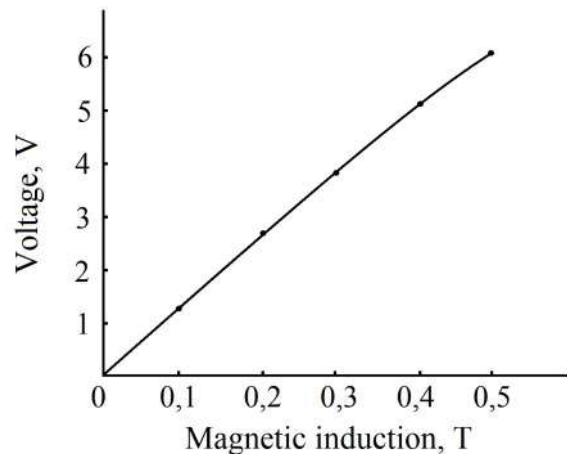
Figure 4. Output characteristic of a bridge sensor with four FEJTs

Resistor trimmer serves for precise zero setting (bridge balancing) in the absence of a magnetic field. As with all magnetic field sensors, a prerequisite for using such a scheme is strict adherence to the orientation of all elements.

For experimental studies of the characteristics of a bridge magnetic field sensor on four FEJTs, standard industrial FEJTs of the KP303B type were used. The experimental dependences of the bridge misbalance voltage U on the magnetic induction B of the external field are shown in Fig. 4 for supply voltage U_0 = 25 V.

Fig. 4 it is clearly seen that the output characteristic of the sensor is linear. The magnetic sensitivity of such a bridge sensor is $\beta = 10160$ V/A/T, which is two orders of magnitude higher than that of silicon Hall sensors. Exper-

Experimental studies of the effect of ionizing radiation on the characteristics of FEJT-based sensor elements have shown that after gamma irradiation of FEJT samples doses of the order of 10^5 R, the saturation current decreases by more than 10% [29]. This fact imposes restrictions on the use of FEJT-based sensor elements in conditions of increased background radiation. However, the use of a bridge measurement circuit eliminates this drawback: since the same FEJTs are used in the bridge sensor, ionizing radiation equally affects all four bridge elements, and the balance of the bridge does not change. It was experimentally established that after irradiation of the bridge sensor elements with Co^{60} gamma quanta on a K100000 cobalt irradiator, the output signal changed by no more than

0.6% up to doses of 10^5 R.

If two sensitive elements of the bridge sensor MFEJT1 and MFEJT3 (Fig. 4) are situated at spaced points of an inhomogeneous magnetic field, then the output signal will be proportional to the difference in magnetic field induction at these points where the MFEJT channels are located. Such a sensor can be used to measure the gradient of an inhomogeneous magnetic field.

Thus, using the method of combination of several sensor elements with characteristics insufficient for use in modern sensor networks in a bridge measurement circuit, it is possible to obtain a sufficiently sensitive, thermostable, radiation-resistant magnetic field sensor, which at the same time consumes a minimum of energy. The use of four transistors in the bridge measurement circuit increases the sensitivity of the sensor tenfold due to the internal mechanism of increasing the sensitivity for series-connected pairs of transistors.

4. Photodetector

It is obvious that the method of combination several sensor elements using the advantages of the bridge measurement circuit can be applied to the creation of a photodetector (PD). To do this, it is necessary to select pairs of FETs for which the saturation current flowing through one pair increases when exposed to light, and decreases through the other.

A typical industrial MOSFET (Fig. 5, a) with a built-in channel (CH) based on an n-type semiconductor has a very thin oxide film (O) between the channel and a thin film of the metal gate (G). When the MOS structure is illuminated from the side of the semitransparent metal gate (G), the light passes through a thin oxide film (O) and is absorbed in the (CH) channel, the concentration of charge carriers in it increases, and the current through the MOSFET increases.

MOSFETs of the second type (Fig. 5, b) differ in that an n-type semiconductor layer (S) is located between the metal layer of the gate (G) and the oxide film (O). The metal-semiconductor contact is a Schottky diode (SD). Such SMOSFETs with a Schottky barrier are used in optical frequency converters [31]. When this structure is illuminated from the side of a semitransparent metal, a photo-emf

appears in SD: "plus" – on the metal, "minus" – on the semiconductor. This photo-emf acts as a negative input for the SMOSFET and reduces the carrier concentration in the channel. As a consequence, the current through the SMOSFET is reduced when exposed by light. In this case, all light is absorbed in the n-layer of the gate and does not reach the channel.
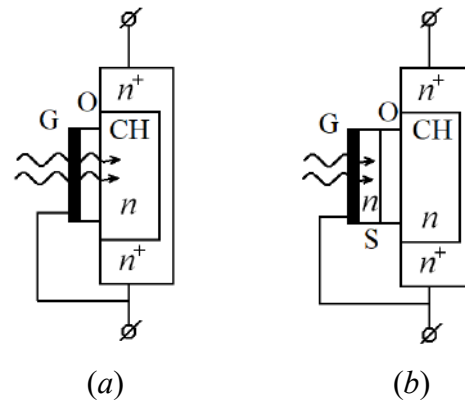
Figure 5. MOSFET with built-in channel (*a*), SMOSFET with Schottky barrier (*b*)ю
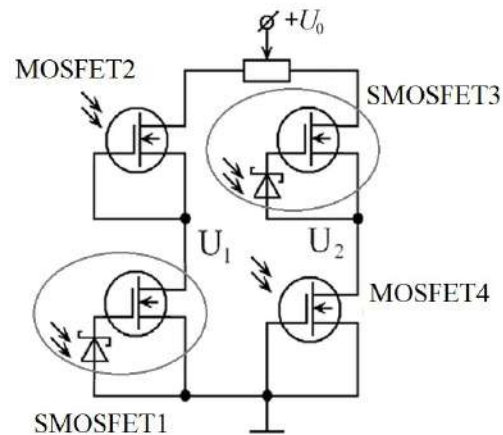
Figure 6. Equivalent bridge photodetector circuit

The operation of the bridge light sensor is explained using an equivalent circuit (Fig. 6). The first pair of sensing elements SMOSFET1 and SMOSFET3 are connected in opposite legs of the bridge, and the other pair of MOSFET2 and MOSFET4 are connected in the other legs. When there is no illumination, the resistance of all MOSFETs in the bridge legs is the same. The supply voltage U_0 is distributed equally between SMOSFET1 and MOSFET2, the potentials U_1 and U_2 in the measuring diagonal of the bridge are equal to each other and the output signal $U = U_1 - U_2 = 0$, i.e. the bridge is balanced. In reality, MOS-

FETs have some variation in parameters, therefore, using a trimming resistor, the initial balancing of the bridge is performed. Lighting causes the resistance of channels of MOSFET2 and MOSFET4 to decrease and the resistance of channels of SMOSFET1 and SMOSFET3 to increase. This leads to an imbalance in the bridge, the potential U_1 increases, the potential U_2 decreases, i.e. the output signal $U = U_1 - U_2$ increases with increasing luminous flux. In this case, the internal amplification mechanism appears in both branches of the photodetector bridge for each pair of MOSFETs, as in the bridge magnetic field sensor.

For experimental studies, we used MOSFET samples made on the basis of a standard industrial KP305 (analogs – MFE3002 or 2N4224). With a source-drain voltage U_{SD} = 10 V and a closed MOSFET gate, the channel resistance was ~ 10 kΩ. To illuminate the phototransistors, a "green" LED of the AL102DM type was used (maximum radiation at a wavelength of $\lambda = 0.56$ µm). The maximum illumination power was 0.6 mW with a 100 mA LED current. It was found that the sensitivity of the experimental samples of the photodetector at $U_0 = 20$ V was an order of magnitude higher than that of a bridge photodetector based on one MOSFET.

The use of a bridge measurement circuit makes it possible to stabilize the photodetector readings during temperature fluctuations, since the bridge sensor uses a MOSFET of the same type, the temperature change affects all four bridge elements equally, and the voltage on the bridge measuring diagonal does not change. According to the experimental data, in the temperature range from 0 to 120 °C, the relative change in the sensitivity of the photodetector does not exceed 0.4%.

To stabilize the readings of the photodetector when exposed to ionizing radiation, it is necessary to select the MOSFET pairs according to the initial value of the drain saturation current before the radiation exposure. As noted above, it was experimentally determined [29] that, according to the radiation sensitivity, MOSFETs are divided into two groups, depending on the initial value of the saturation current before irradiation: for all samples of the group with low saturation current values before irradiation (I_{S0} <0.1 mA), the saturation current increases upon exposure to ionizing radiation and for all samples from the group with large saturation currents before irradiation (I_{S0}> 3 mA), the saturation current decreases upon exposure to ionizing radiation. To obtain a radiation-stable photodetector, it is necessary to use in one circuit MOSFETs, either all with low or all with high saturation current values. It was experimentally determined that after irradiation of the photodetector sensor elements with Co^{60} gamma quanta on a cobalt irradiator, the output signal changed by no more than 1.8% up to doses of 10^5 R.

Thus, by combination various photosensitive elements using the advantages of a bridge measurement circuit, it is possible to obtain a sufficiently sensitive, thermostable, radiation-resistant light sensor based on existing industrial transistors with a minimum number of parts.

5. Results and conclusions

It is shown in the work that by combination specially selected FEJT and MOSFET pairs with opposite signs of temperature sensitivity, but with the same sign of sensitivity to ionizing radiation, in the opposite branches of the bridge, it is possible to obtain a high sensitivity temperature sensor with a minimum number of constituent elements. It has been experimentally confirmed that the temperature sensor obtained in this way, when exposed to radiation, retains high sensitivity and linearity of the output characteristic in the temperature range from –20 ºC to +190 ºC with deviations of readings of no more than 6% up to radiation doses of $5·10^5$ R.

It has been experimentally confirmed that when used in a bridge measurement circuit, the method of combination of several sensor FET elements with characteristics insufficient for their use in modern sensor networks, it is possible to obtain a sufficiently sensitive, thermostable, radiation-resistant magnetic field sensor, which at the same time consumes a minimum of energy due to the minimum the number of items.

The use of four transistors in the bridge measurement circuit increases the sensitivity of the sensor tenfold compared to one transistor due to the internal mechanism of increasing

the sensitivity for series-connected pairs of transistors.

It has been experimentally confirmed that by using four photosensitive MOSFETs in the bridge circuit instead of one, it is possible to obtain a photodetector with a sensitivity ten times higher than that of a single transistor. Moreover, such a photodetector has increased temperature stability, as well as radiation resistance with preliminary selection of transistors.

The described sensors can be widely used since only a standard element base is used in their design, they are very energy efficient due to the minimum number of constituent elements, they have increased thermal stability and radiation resistance.

References

1. Dushaq G., Dushaq G., Rasras M. Thin Film GaAs Photodetector Integrated on Silicon using Ultra-Thin Ge Buffer Layer for Visible Photonics Applications. *Asia Communications and Photonics Conference - International Conference on Information Photonics and Optical Communications (ACP-IPOC)*. **2020**, *FTu2E*, 5-12. DOI: https://doi.org/10.1364/FIO.2020.FTu2E.5.

2. Avrahamy R., Zohar M., Auslender M., Hava S., et al. Upmost Efficiency Mid IR Thin HgCdTe Photodetectors. *Asia Communications and Photonics Conference – Intern. Conference on Information Photonics and Optical Communications (ACP-IPOC)*. **2020**, 21-29. DOI: https://doi.org/10.1364/CLEO_AT.2020.JTu2D.21

3. Liu J., Liu J., Liu F., Liu H., et al. Mixed-dimensional $CsPbBr_3$-ZnO heterostructures for high-performance *p-n* diodes and photodetectors. *Nano Today*. **2021**, *36*, 101055-101069.

4. Son B., Zhou H., Lin Y., Hong Lee K., et al, Gourd-shaped hole array germanium (Ge)-on-insulator photodiodes with improved responsivity and specific detectivity at 1,550 nm, *Optical Express*. **2021**, *29*, 16520-16533.

5. Zhou H., Xu S., Lin Y., Huang Y. C., et al. High-efficiency GeSn/Ge multiple-quantum-well photodetectors with photon-trapping microstructures operating at 2 μm. *Optical Express*. **2020**, *28*(7), 10280-10293.

6. Zhao C., Ali M. U., Ning J., et al. Organic single crystal phototransistors: Recent approaches and achievements. *Frontiers of Physics*. **2021**, *16*, 43202-43219.

7. Prasad D., Nath V. An ultra-low power high-performance CMOS temperature sensor with an inaccuracy of 2 at 0.3 ºC/ + 0.1 ºC for aerospace applications. *Microsystem Technologies*. **2017**, *25*(5), 1553-1563.

8. Lai S., Viola F. A., Cosseddu P., Bonfiglio A. Floating Gate, Organic Field-Effect Transistor-Based Sensors towards Biomedical Applications Fabricated with Large-Area Processes over Flexible Substrates. *Sensors*. **2018**, *18*, 688–699.

9. Hedayatipour A., Shanta A. S., McFarlane N. A sub-μW CMOS temperature to frequency sensor for implantable devices. *IEEE 60th International Midwest Symposium on Circuits and Systems (MWSCAS), Boston*. **2017**, 253-256.

10. Li J., Ali M. U., Ning J., et al. Long-range Raman Distributed Fiber Temperature Sensor with Early Warning Model for Fire Detection and Prevention. *IEEE Sensors Journal*. **2019**, *19*(10), 3711-3717.

11. Moreira Mota L.T., Viola F. A., Cosseddu P., et al. Development of a Surface Temperature Sensor to Enhance Energy Efficiency Actions in Buildings. *Sensors*. **2018**, *18*(9), 3046-3062.

12. Quynh, L.K., Hien N.T., Binh N.H., Dung T.T., et. al. Simple planar Hall effect based sensors for low-magnetic field detection. *Advances in Natural Sciences: Nanoscience and Nanotechnology*. **2019**, *10*(2), 1072-1074.

13. Jeng J., Lu C., Ku H., Huang B., et. al. Three-Axis Micofluxgate With a Fluxguide. *IEEE Transactions on Magnetics*. **2019**, *55*(7), 1-4.

14. Yamamoto T., Nozaki T., Imamura H., Tamaru S., et. al. Voltage-Driven Magnetization Switching Using Inverse-Bias Schemes. *Phys. Rev. Applied*. **2020**, *13*(1), 014045:26-39.

15. Manzin A., Nabaei V., Ferrero R. Quantification of Magnetic Nanobeads with Micrometer Hall Sensors. *IEEE Sensors Journal*. **2018**, *18*(24), 10058-10065.

16. Lukat N., Ron-Marco F., Spetzler B., Kirchhof C. Mapping of magnetic

nanoparticles and cells using thin film magnetoelectric sensors based on the delta-E effect. *Sensors and Actuators A: Physical*. **2020**, *309*(1), 112023:1-6.

17. Zhang G., Wu D., et al. Multifunctional sensor based on organic field-effect transistor and ferroelectric poly (vinylidene fluoride trifluoroethylene). *Organic Electronics*. **2018**, *56*, 170-176.

18. Chen Z., Deng F., Fu Z., Wu X. Design of an Ultra-low Power Wireless Temperature Sensor Based on Backscattering Mechanism. *Sensing and Imaging An International Journal*. **2018**, *19*(1), 19-24.

19. Fernandez A.F., Nabaei V., Ferrero R., et al. Radiation-tolerant Raman distributed temperature monitoring system for large nuclear infrastructures. *IEEE Transactions on Nuclear Science*. **2005**, *52*(6), 2689-2694.

20. Courts S. High level gamma radiation effects on Cernox™ cryogenic temperature sensors. *IOP Conference Series: Materials Science and Engineering, Madison, Wisconsin, USA*. **2017**, *278*, 1-8.

21. Xu Z.M., Liu P., Chang X.Y. Space Measurement System Design and Space Environment Adaptation Experiment of Commercial Sensor DS18B20. *Applied Mechanics and Materials*. **2014**, *635/637*, 760-767.

22. Hofman J., Sharp R. A total ionising dose, in-situ test campaign of DS18B20 temperature sensors. *12th European Conference on Radiation and Its Effects on Components and Systems, Sevilla*. **2011**, 871-876.

23. Álvarez M., Jiménez J. J., González-Guerrero M., Hernando C., et al. Total Ionizing Dose Radiation Test on the Temperature Sensor TMP36 from Analog Devices. *IEEE Radiation Effects Data Workshop, Tucson*, **2012**, 1-7.

24. Hannah S., Davidson A., et al. Multifunctional sensor based on organic field-effect transistor and ferroelectric poly (vinyli-

dene fluoride trifluoroethylene). *Organic Electronics*. **2018**, *56*, 170-176.

25. Lai S., Cosseddu P., et al., Combining inkjet printing and chemical vapor deposition for fabricating low voltage, organic field-effect transistors on flexible substrates. *Sensors*. **2017**, *631*, 124–131.

26. Pan S., Makinwa K. A. 0.25 mm^2-Resistor-Based Temperature Sensor with an Inaccuracy of 0.12 °C (3 σ) From −55 °C to 125 °C. *IEEE Journal of Solid-State Circuits*. **2018**, *53*(12), 3347-3355.

27. Vikulin I. M., Vikulina L. F., Gorbachev V. E., Mykhailov N. S. Temperature stable radiation-resistant current reference generator based on field-effect transistors. *Radioelectronics and Communications Systems*. **2021**, *64*(6), 310-318.

28. Vikulin I., Gorbachev V., Gorbacheva A., Krasova V., Litvinenko V. Radiation resistant FET-based Temperature Sensor for End Devices of IoT. *Proceedings of 3rd IEEE International Conference on Advanced Information and Communication Technologies (AICT-2019). Lviv, Ukraine, 2-6 July*. **2019**, 272-277. DOI:10.1109/AIACT.2019.8847905.

29. Vikulin I. M., Gorbachev V. E., Nazarenko A. A. Radiation Sensitive Detector Based on Field-Effect Transistors. *Radioelectronics and Communications Systems*, **2017**, *60* (9), 401-404.

30. Викулин И.М.; Викулина Л.Ф.; Горбачев В.Э. Магниточувствительные приборы для сенсорных и исполнительных сетей «интернета вещей. *М.: РУСАЙНС*. **2019**. 156.

31. Osadchuk O. V., Osadchuk V. S., Osadchuk I. O., Kolimoldayev M., et. al. Optical transducers with frequency output. *Proc. SPIE 10445, Photonics Applications in Astronomy, Communications, Industry, and High Energy Physics Experiments*. **2017**, 10445, 3467-3482.

Vikulin I. M.[1], Vikulina L. F.[2], Gorbachev V. E.[1], Litvinenko V. M.[3], Markolrnko P. Y.[1]

DETECTORS BASED ON FIELD EFFECT TRANSISTORS

Summary. The possibility of using the method of combining several sensor elements with opposite sensitivity to various external influences to obtain new designs of sensors for light, temperature and magnetic field has been experimentally investigated. Standard industrial samples of FEJT and a MOSFET in saturation mode with two-pole connection, when the gate is closed with the source, were used as sensor elements in the work. It is shown that the FEJT has a negative temperature coefficient of current change, while the MOSFET has a positive one. At the same time, the sign of the radiative action factor of the MOSFET is determined by the initial value of the drain current before irradiation. It has been experimentally confirmed that the use of four transistors in a bridge measurement circuit increases the sensitivity of the sensor tenfold compared to one transistor due to the internal mechanism of increasing the sensitivity for series-connected pairs of transistors.

Key words: FEJT, MOSFET, temperature detector, magnetic field detector, photodetector, temperature stability, radiation resistance

Вікулин І. М.[1], Вікулина Л. Ф.[2], Горбачов В. Е.[1], Литвиненко В. М.[3], Марколенко П. Ю.[1]

ДАТЧИКИ НА ОСНОВІ ПОЛЬОВИХ ТРАНЗИСТОРІВ

Резюме. Експериментально досліджено можливість використання методу комбінації кількох сенсорних елементів із протилежною чутливістю до різних зовнішніх впливів для отримання нових конструкцій датчиків світла, температури та магнітного поля. В якості сенсорних елементів в роботі були використані промислові зразки польових транзисторів з *p-n*-переходом в якості затвору (FEJT) і МОН ПТ (MOSFET) в режимі насичення при двополюсному включенні, коли затвор є замкнутим з витоком. Показано, що у FEJT температурний коефіцієнт зміни струму негативний, а у MOSFET – позитивний. У той же час знак коефіцієнта радіаційного впливу MOSFET визначається початковою величиною струму стоку до опромінення. Експериментально підтверджено, що використання чотирьох транзисторів у мостової схемі вимірів підвищує чутливість датчика в десятки разів у порівнянні з одним транзистором за рахунок внутрішнього механізму збільшення чутливості для послідовно з'єднаних пар транзисторів.

Ключові слова: польовий транзистор, МОП-транзистор, датчик температури, датчик магнітного поля, фотодетектор, температурна стабільність, радіаційна стійкість

Викулин И. М.[1], Викулина Л. Ф.[2], Горбачев В. Э.[1], Литвиненко В. М.[3], Марколенко П. Ю.[1]

ДАТЧИКИ НА ОСНОВЕ ПОЛЕВЫХ ТРАНЗИСТОРОВ

Резюме. Экспериментально исследована возможность использования метода комбинации нескольких сенсорных элементов с противоположной чувствительностью к различным внешним воздействиям для получения новых конструкций датчиков света, температуры и магнитного поля. В качестве сенсорных элементов в работе были использовались промышленные образцы полевых транзисторов с *p-n*-переходом в качестве затвора (FEJT) и МОП ПТ (MOSFET) в режиме насыщения при двухполюсном включении, когда затвор замкнут с истоком. Показано, что у FEJT температурный коэффициент изменения тока отрицательный, а у MOSFET – положительный. В то же время, знак коэффициента радиаци-

онного воздействия MOSFET определяется начальной величиной тока стока до облучения. Экспериментально подтверждено, что использование четырех транзисторов в мостовой схеме измерений повышает чувствительность датчика в десятки раз по сравнению с одним транзистором за счет внутреннего механизма увеличения чувствительности для последовательно соединенных пар транзисторов.

Ключевые слова: полевой транзистор, МОП-транзистор, датчик температуры, датчик магнитного поля, фотодетектор, температурная стабильность, радиационная стойкостью

V. T. Shvets

Odesa National Academy of Food Technologies
ONAFT, str. Kanatna, 112, Odesa, Ukraine, 65039
E-mail: valtarmax@ukr.net

ENTROPY AND ELECTIONS. SOCIAL SYSTEMS ANALYSIS BY STATISTICAL PHYSICS METHODS

The article proposed a formula for assessing the level of freedom of choice of a person during elections, similar to the formula is used to compare the freedom of elections in the presidential and parliamentary elections in Ukraine.

Introduction

Statistical physics confidently gains new positions in the areas, which seemingly have nothing to do with it. One of the fundamental concepts of statistical physics is the concept of entropy. In 1877, the brilliant Austrian physicist Ludwig Edward Bolzman was the first to understand the connection between the entropy of the physical system and the probability of its stay in one or another macroscopic state associated with the number of microscopic states that implement this macroscopic state [1-4]. In 1948, the famous American electrical engineer and mathematician Claude Elwood Shannon proposed to use the concept of entropy to assess the uncertainty of information about a particular event [5-7]. Thus, he launched a new mathematical discipline - the theory of information, where entropy was called information entropy. The connection of information entropy with the probability of the onset of a particular event, he proposed in the same form as the connection of the system's stay in one or another macroscopic state, that is, actually used the Bolzman formula for information entropy. Consider the formula for information entropy.

Entropy, intormation entropy and election entropy

Let us conduct a random experiment with the consequences E_1, E_2, …, E_n, that can be implemented with probabilities of p_1, p_2, …, p_n. Then the information we received in the afterbirth of this experiment is a random value that takes the value $I(E_i)$ when the experiment is a consequence E_i. At the same time

$$I(E_i) = -\log_2(p_i).$$

The mathematical expectation of this information (information entropy), that is, the average amount of information that accounts for one consequence of the experiment, is determined in a standard way [8]

$$M(I) = \sum_{i=1}^{n} p_i I(E_i).$$

The last result can be recorded in a form adopted for statistical physics and information theory

$$S = -\sum_{i=1}^{m} p_i \log_2(p_i).$$

Many political processes resemble a random experiment. In particular, in our opinion, this process is elections of different levels. If the possible consequences of this political process are considered to be the victory of a particular candidate, i.e. the events of E_1, E_2, …, E_n with probabilities p_1, p_2, …, p_n, you can use the previous formula to assess the election results. Now it would be expedient to use instead the term information entropy of the term election entropy. First of all, it characterizes the level of uncertainty of the election results. The more candidates for an elected posi-

tion and the more evenly the probabilities of victory of different candidates are distributed, the greater is the entropy of elections, the greater is the information entropy. This universal property of entropy was also warned by Ludwig Edward Bolzman.

In the case of two candidate who have equal chances to win, that is, in the simplest political random experiment of election entropy, as well as information entropy, we get the result 1. In theory of information, this amount of information is called a bit. In our case, it would be more appropriate to call it differently, for example, fried - from the first letters of the English word freedom. It is precisely in order for in the simplest political experiment that we get the answer unit, the logarithm in the formula for the entropy of elections is advisable to take on the basis of two.

It should be noted that in many countries, the level of democracy in which is considered high, in fact, elections take place between two candidates with approximately equal chances of winning. It is clear that in this case, the entropy of choice will be quite small, compared to, for example, with Ukraine.

In the Soviet Union, elections have always been held on a non-alternative basis. This means that one of the probabilities, for example, is $p_1 = 1$, and all others are zero. In this case, the formula for election entropy gives zero result.

Is the elections are held in two rounds, then for the second round you should use the same formula for election entropy, and the results, according to the universal properties of entropy of two independent subsystems of the same system, should be compiled

$$S = S_1 + S_2,$$

where

$$S_1 = -\sum_{i=1}^{m} p_i \log_2(p_i),$$

$$S_2 = -\sum_{i=1}^{2} P_i \log_2(P_i).$$

From our point of view, the uncertainty of the election results indicates the level of voter freedom in such elections, that is, the level of freedom of the elections themselves. Therefore, since there are no competing options for definition for obvious reasons, we propose to call the entropy of elections a level of freedom of elections. At the same time, if a voter votes for i-th candidate, he exercises his freedom of choice in quantitative terms as $-\log_2(p_i)$.

The question of the source of information about the probabilities of victory of individual candidates is important. In fact, the main source of information about these probabilities is the election results. Then these probabilities are simply equal to the fates of voters who voted for this candidate. Quite accurately, information can be obtained about these probabilities and based on the study of various sociological studies, but this is also an election with a rather limited sample size, that is, voters.

Such a political substance as power is inextricably linked with elections. Unrestricted power never relies on any elections. In 1917, the Bolsheviks came to power in the Russian Empire without receiving a mandate for power from voters. Their power was frightening. Then the Communist Party began to imitate elections in some secondary levels of public administration, conducting them on a non-alternative basis. The entire party hierarchy, which had absolute power in the country, never received the mandate of voters. It seems to us that such a concept as power is inextricably linked with such a well-defined characteristic as entropy, or rather the entropy of elections. As such a connection, we offer its simplest option. The government, the mandate for which elections are given, is the value inverted to the entropy of elections, that is,

$$V = 1/S.$$

In this case, the power gained in non-alternative elections, or without edict at all, is absolute. In our mathematical model is infinite. Such was the power of the Communist Party in the Soviet Union, as is the current power of the Communist Party in China.

Presidential and parliamentary elections in Ukraine

It is quite useful to test the proposed formulas based on the results of the elections in Ukraine. On the Internet, the relevant information is easily accessible, so in the future we will not use specific links to its sources. The following chart shows the results of the presi-

dential elections in Ukraine during the years of independence.
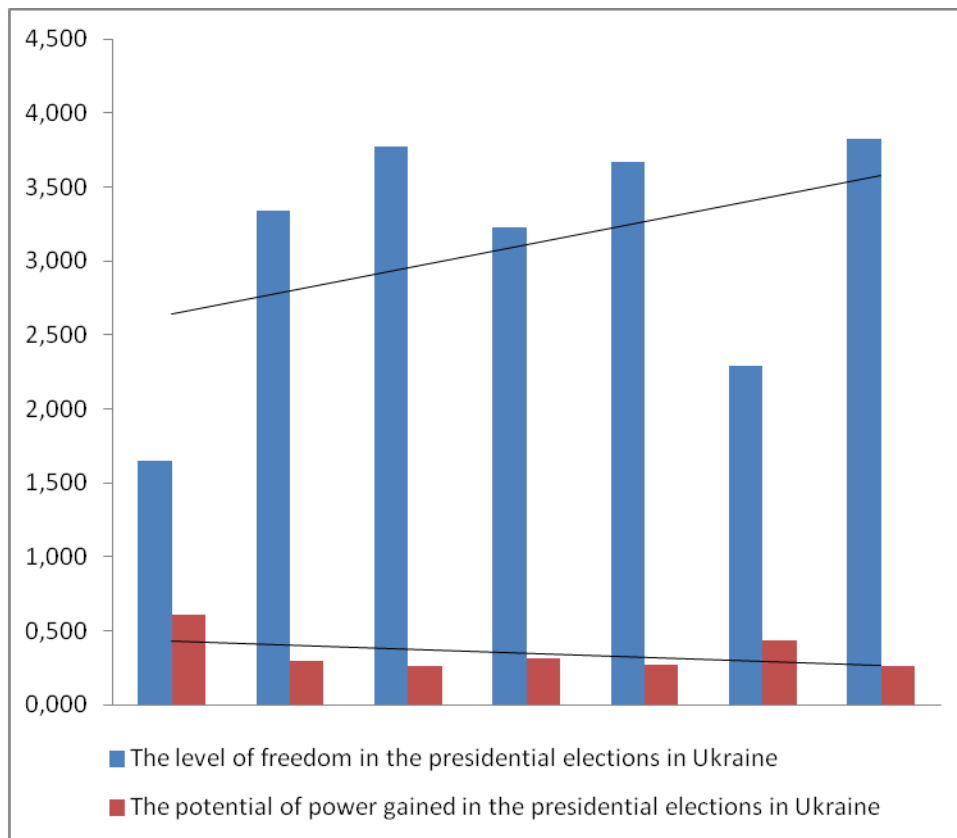
Fig 1.

The diagram shows that the level of freedom of elections in Ukraine is extremely high, possibly the highest in Europe. This level was the lowest at the first elections in the modern history of Ukraine. In our opinion, this was due to the inertia of thinking of voters, as well as candidates, as a result of the recent Soviet past. This level was relatively small in elections in 2014. Then Ukraine was imminent war with the Russian Federation. The wishing to lead the state at this tragic time for Ukraine was relatively small. Elections in two rounds would be too dangerous for the country. The responsibility of voters for the fate of the state determined just such a result. One of the candidates confidently won in the first round.

The highest level of freedom of elections was at the last elections in 2019. Here the elections were held in two rounds. The number of candidates was unprecedentedly high. The winner of the second round in the first received only a little more than thirty percent of the votes.

If we follow all the presidential elections in independent Ukraine, then there is a clear tendency to increase the level of freedom of elections.

The second significant result of the presidential election is that the potential of the government gained by the winner of the elections is quite small, perhaps the smallest in Europe, and this potential tends to decrease. That is, the freer the elections, the less power delegated by voters ends up in the hands of the winner. The level of freedom of elections is the level of real power of the people. The potential of power is, in fact, the real power of the winner. If the winner forgets about the limits of his power, then the rebellion of the people with tragic consequences for the usurper is inevitable. Such experience is already in recent Ukrainian history. The following charts show similar results of parliamentary elections in Ukraine during the years of independence
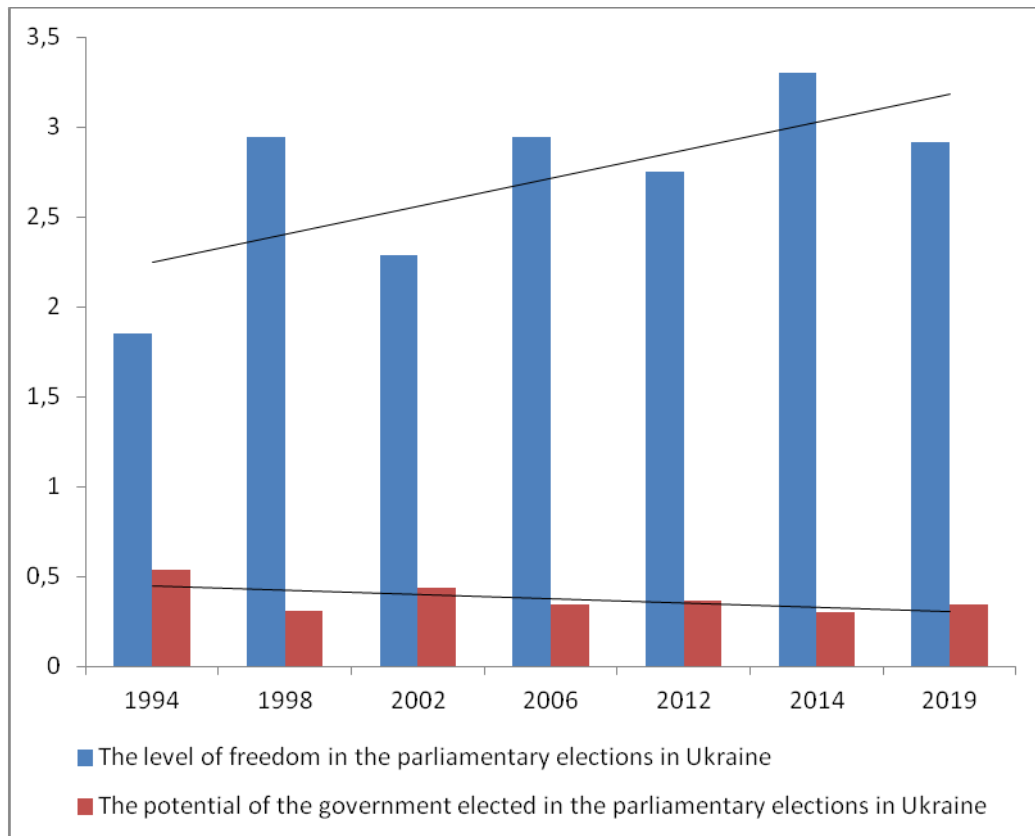
Fig. 2.

The level of freedom in parliamentary elections is also quite high and correlates well with the level of freedom of presidential elections. It also tends to grow. The lowest freedom of elections was in the first parliamentary elections in 1994, which is consistent with the lowest rate of presidential elections. However, it was the highest for Ukraine in 2014. The real chances of winning were given to more political parties, and the votes were more evenly distributed between them than in other parliamentary elections. Having elected in May the president, a Ukrainian voter on a patriotic wave brought a huge number of nationally conscious deputies to parliament. There were also parties that, under other conditions, did not have such a chance. The parliament did not have a large number of deputies from the regions of Ukraine occupied by the Russian Federation, traditionally orthogonal to Ukrainian values. Parliament has never worked as effectively as it did between 2014 and 2019.

Presidential and parliamentary elections in the Russian federation

Ukrainian elections are most useful compared with elections in countries that arose on the ruins of the Ukrainian elections are most useful compared with elections in countries that arose on the ruins of the Soviet Union. An important factor here is the commonality of the starting political and economic conditions. Also an important aligning factor is the mentality of the Soviet person, present in all, even the most remote corners of the former Soviet Union at the time of its collapse. If the election results in different countries revealed significant differences, then these differences, first of all, would be due to differences in ethnic origin.

61
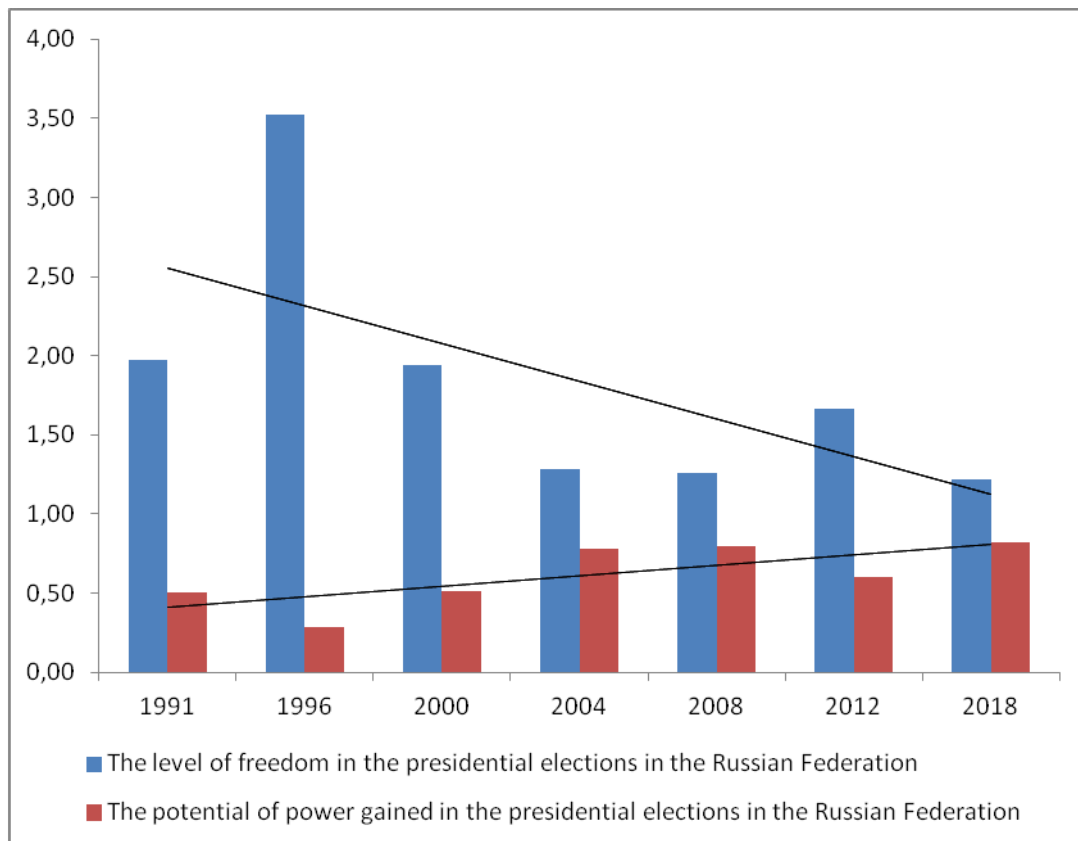
Fig. 3.

The choice of the Russian Federation as an object for comparison is quite understandable for various reasons. Of course, it would be extremely expedient to conduct a comparative analysis of all the countries formed on the territory of the former Soviet Union, but this is already material for many subsequent publications. The results of the elections in the Russian Federation are also easily accessible from the Internet and we will not make special links to these results.

The diagram shows that the level of freedom of the presidential elections in the Russian Federation immediately started from a fairly high level in 1991. In 1996, it peaked, and in the last almost twenty years it has shown an obvious tendency to decrease. The direct reasons for this behavior of the level of freedom of elections are both a decrease in the number of candidates and an increase in the uneven distribution of votes between them. That is, a large number of candidates receives a symbolically small number of votes, but one of the candidates receives an unprecedentedly high number of them.

An interesting trend is the tendency to significantly increase the potential of the president's power in the Russian Federation over the past twenty-eight years. Starting from a level typical of other democracies, it quickly increased to a level that can be called authoritarian.

The results of the parliamentary elections are given in the following chart. This chart also demonstrates the high level of freedom of parliamentary elections in the Russian Federation in 1994, 1996, 2000. However, it also demonstrates a powerful tendency to reduce this level over all the years analyzed. There is also a strong correlation between the results of the presidential and parliamentary elections. Such a correlation, as in the case of Ukraine, indicates, in our opinion, the objective nature of the election process for each people, no matter what the elections are called. That is, the nature of elections is an imprint of the mentality of one or another people, its fundamental ethnic values.
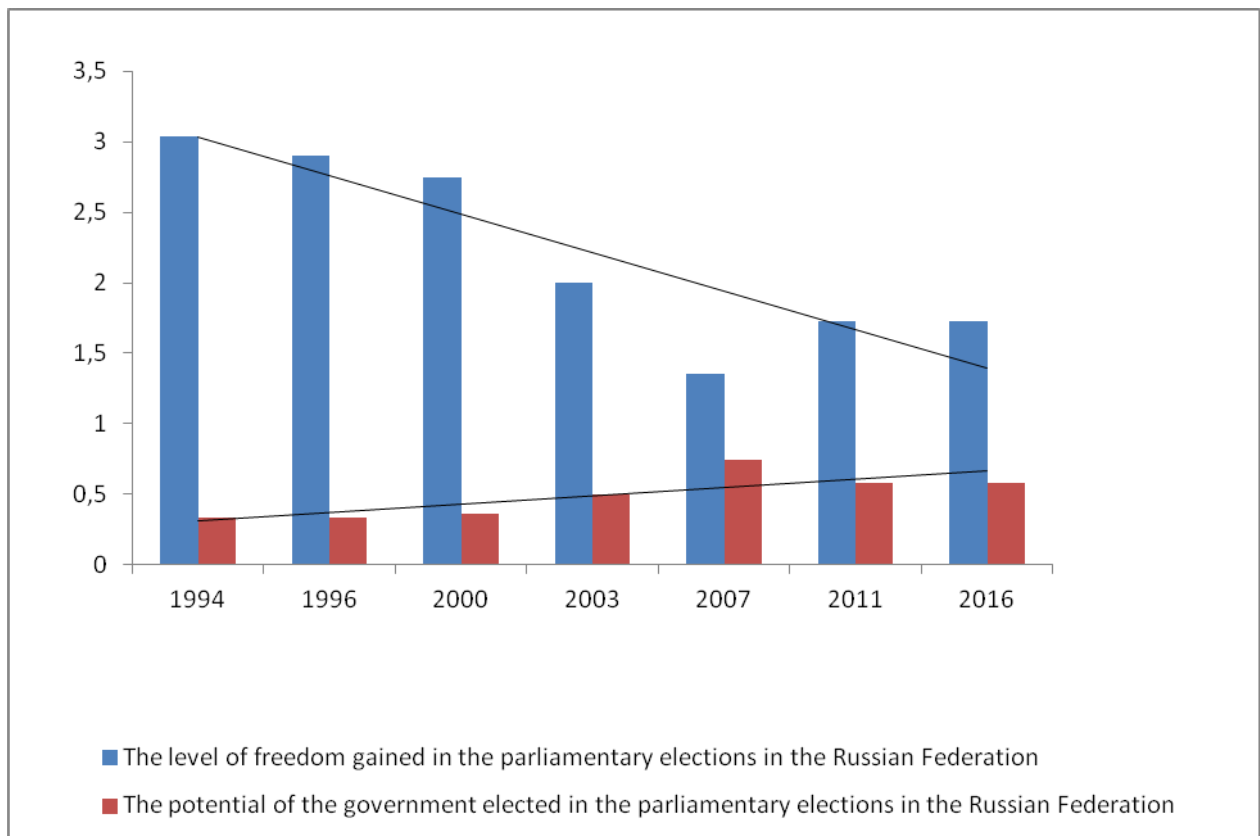
Fig. 4.

Comparison of elections in Ukraine and in the Russian federation

Only comparing the results of elections in different countries makes it possible to decide on our own place in the modern world political process. In the following chart, this comparison is given for the presidential elections in Ukraine and the Russian Federation.

The chart shows that the level of freedom of elections in 1991 started in both countries from almost the same level. This can be explained by the inertia of thinking of Ukrainians and residents of the Russian Federation. Generations of voters in both countries were fully formed in the conditions of the same political reality – the Soviet Union. But over time, disagreements began to increase. This happened as generations of politically formed or even born in an independent Ukrainian state began to come to the electoral urns in Ukraine. Accordingly, the number of voters whose outlook was formed in the Soviet Union began to decrease significantly for natural reasons. The same evolution began among voters of the Russian Federation, but in the exact opposite direction. It seems that Soviet education was a compromise for the various ethnic groups that inhabited the Soviet Union. The collapse of the Soviet Union was both the disappearance of this compromise.

Then began the evolution of each ethnic group to its own, characterized by it mentally worldview. In the result, we received the highest level of freedom of choice in the last presidential elections in Ukraine, and the lowest in the presidential elections in the Russian Federation, respectively. At the same time, these results differ significantly.

In the following chart, we have a comparative analysis of the presidential elections in both countries.

Freedom of parliamentary elections in Ukraine and the Russian Federation will also differ significantly in favor of greater freedom of elections in Ukraine compared to the Russian Federation. For Ukraine, there is a clear tendency to increase freedom of elections, for the Russian Federation there is a clear tendency to reduce it. However, there are certain differences.
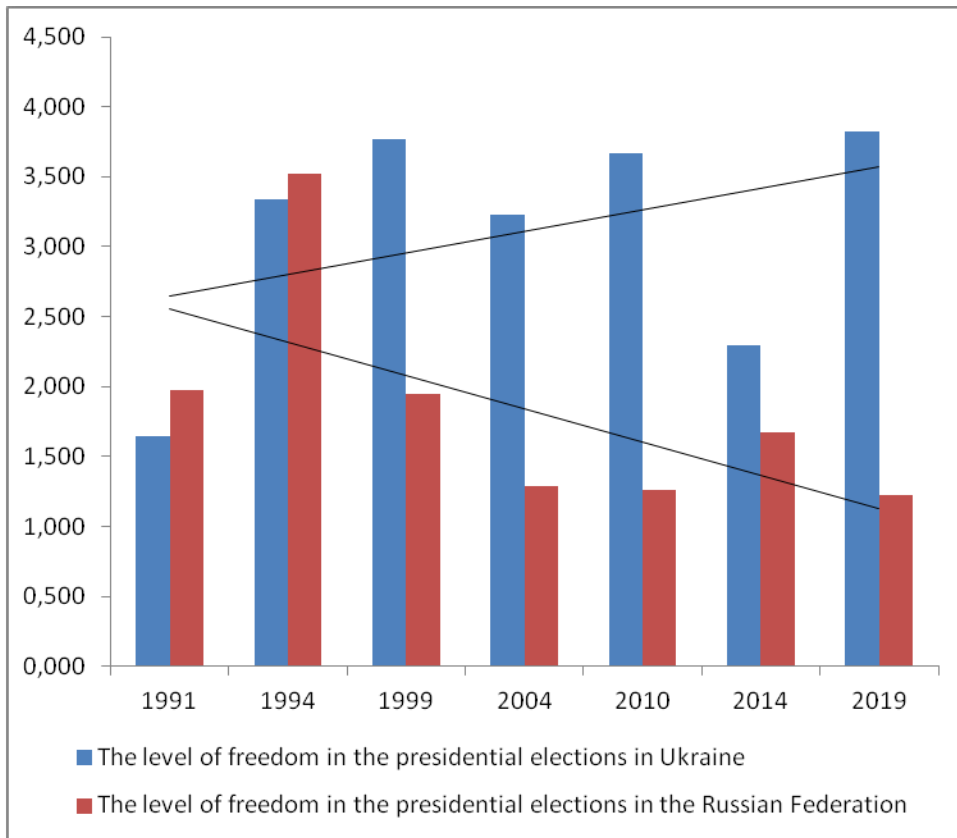
Fig 5.

Freedom of parliamentary elections in the Russian Federation started from higher values compared to Ukraine.

The tendency to significantly reduce the freedom of parliamentary elections in the Russian Federation has become clear over the past twenty years, when the concentration of power in the hands of the president has increased markedly.

As in the case of presidential elections, the results of all recent parliamentary elections in both countries differ significantly in favor of significantly greater freedom of elections in Ukraine.

From the above comparative analysis of the presidential and parliamentary elections in Ukraine and the Russian Federation, we be-

lieve that the significant difference in the results of elections in both countries for almost thirty years indicates a significant mental difference between Ukrainians and residents of the Russian Federation. Most likely, this distinction is programmed at the genetic level.

The very opportunity to notice and analyze the smallest details of both presidential and parliamentary elections in both countries at the number level indicates, in our opinion, that the formulas proposed by the author for quantitative analysis of elections are an effective tool for quantitative research of this political process. We are confident that this approach can be applied to quantitative analysis and other aspects of the political life of our country.
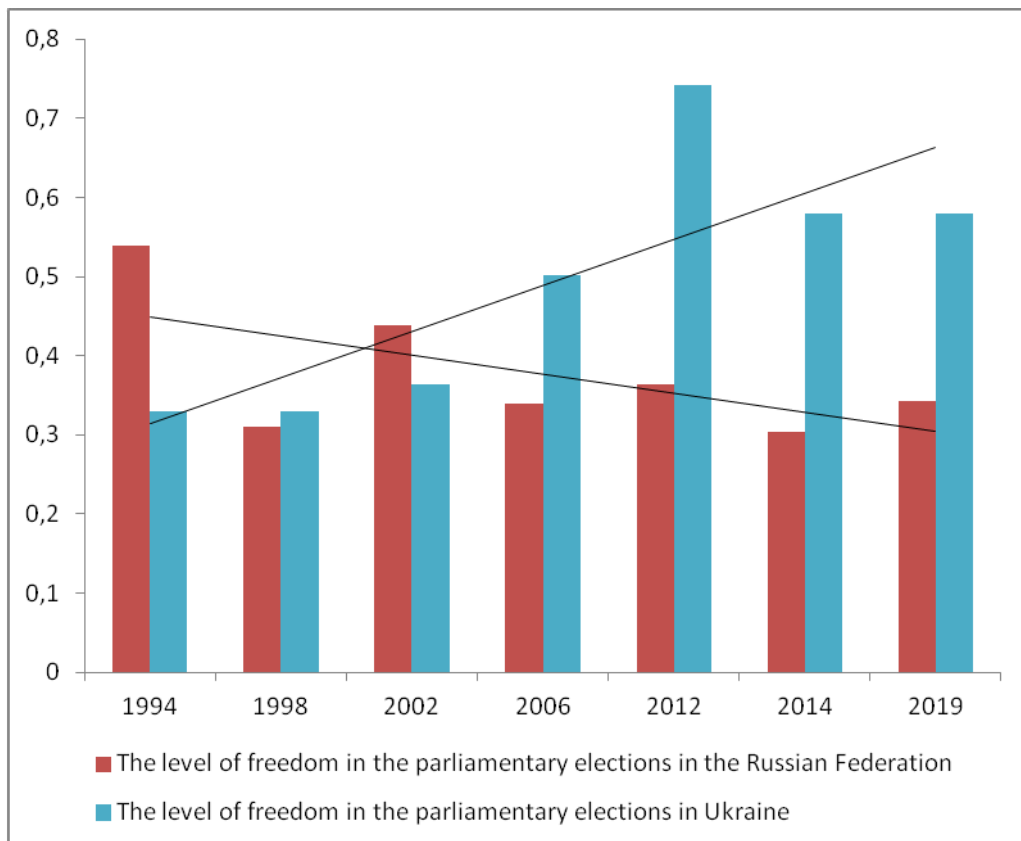
Fig. 6.

The author expresses sincere gratitude to his colleagues for the fruitful discussion of the results of the article [9], as well as Yuriy Ivanovich Radkovets not only for useful discussions, but also for the very idea of applying the mathematical apparatus to the analysis of political processes.

References:

1. Больцман Л. Избранные труды. Часть 1.- М.: Наука, 1994. - 446 с.
2. Больцман Л. Очерки по методологии физики. -М.: Гостехиздат, 1999.- 324 с.
3. Больцман Л. Кинетическая теория материи. - М.: Гостехиздат , 1969.-424 с.
4. Больцман Л. Лекции по теории газов. — М.: Гостехиздат, 1983.- 356 с.
5. Шеннон К. Работы по теории информации и кибернетике. - М. :Иностранная литература, 1983. - 830 с.
6. Shannon C.E. A Mathematical Theory of Communication // Bell System Technical Journal. - 1968. - V. 27. - P. 379-423.
7. Shannon C.E. Communication in the presence of noise// Proc. Institute of Radio Engineers, Jan. - 1969. - V. 37, - № 1. - P. 10-21.
8. Швець В. Т. Теорія ймовірностей і математична статистика. Одеса: ВМВ, PACS: 01.75.+m; 01.90.+g . УДК: 519.814; 519.243 2014 - 200 с. https://card-file.on-aft.edu.ua/bitstream/ 123456789/17874/3/000804A.pdf
9. Швець В. Т. Інформаційна ентропія і свобода вибору. // Conference proceeding. Part 1. XII International scientific and practical conference: Information technologies and automation – 2019. October 17-18, Odesa, - P. 22 - 25.

Shvets V. T.

ENTROPY AND ELECTIONS.
SOCIAL SYSTEMS ANALYSIS BY STATISTICAL PHYSICS METHODS

Summary

The paper proposes a formula for assessing the level of human freedom of choice during elections, similar to the formula for entropy in statistical physics and informational entropy in information theory. The formula is used to compare the freedom of elections in the presidential and parliamentary elections in Ukraine and the Russian Federation.Keywords: entropy, probability, freedom of choice, presidential elections in Ukraine, parliamentary elections in Ukraine.

Keywords: entropy, probability, freedom of choice, presidential elections in Ukraine, parliamentary elections in Ukraine.

Швець В. Т.

ЕНТРОПІЯ І ВИБОРИ
АНАЛІЗ СОЦІАЛЬНИХ СИСТЕМ МЕТОДАМИ СТАТИСТИЧНОЇ ФІЗИКИ

Резюме

У статті запропонована формула оцінки рівня свободи людини під час виборів, аналогічна формулі для ентропії у статистичній фізиці і інформаційній ентропії у теорії інформації. Формула застосована для порівняння рівня свободи на президентських і парламентських виборах в Україні і Російській федерації.
Ключові слова: ентропія, свобода вибору, президентські вибори в Україні, парламентські вибори в Україні.

Швец В. Т.

ЕНТРОПИЯ И ВЫБОРЫ.
АНАЛИЗ СОЦИАЛЬНЫХ СИСТЕМ МЕТОДАМИ СТАТИСТИЧЕСКОЙ ФИЗИКИ

Резюме

В статье предложена формула оценки уровня свободы человека во время выборов, аналогичная формуле для ентропии в статистической физике и информационной энтропии в теории информации. Формула использована для сравнения уровня свободы на президентских и парламентских выборах в Украине
Ключевые слова: энтропия, вероятность, свобода выбора, президентские выборыв Украине, парламентские выборы в Украине.

UDC 621.315.592

I.K. Doycho, L.M. Filevska, V.S. Grinevych

Odessa I.I. Mechnikov National University, str. Dvoryanska, 2, Odesa, Ukraine,
e-mail: viknawsvit@gmail.com

GAS SENSITIVITY OF SOME NANOPARTICLES ENSEMBLES IN POROUS GLASS

The importance of substances' surface development suitable for sensor technology by dispersing them to the level of nanoparticles' ensemble within a certain matrix has been demonstrated. It has been proven that the best matrix for the formation of the specified ensemble of nanoparticles is porous silicate glass. Methods of formation of ensembles of nanoparticles of some compounds in porous glass are briefly considered. The applicability of the mentioned systems for sensors is demonstrated by the example of their luminescent response sensitivity to the presence of ammonia or HCl vapours in the environment.

Introduction

The luminescence centers of materials useable as active elements of luminescent gas sensors are mostly located near the surface, and just the near-surface substance layers are affected by gas composition changes of the environment. Hence, the best registration of the specified changes, is in the maximum possible developement of the substance active surface which is achieved by dispersing the specified substance to nanometer sizes. As soon as it is inconvinient to operate with individual particles of nanometer sizes, it is reasonable to place them in a system of the appropriate size"tubes", which can be a matrix containing small cavities in the form of through pours. In this case an ensemble of nanoparticles is formed, consisting of the indicated small particles of the substance and the matrix itself, in which they are placed. The matrix properties must meet certain restrictions, due to which it will not affect the gas sensitivity of the studied substance and, moreover, will positively influence its luminescent properties. Such limitations include chemical inertness, mechanical durability, and its luminescent response may be present only in the spectrum regions that are not essential for the substance under investigation. Some authors use polymers [1-2] or gelatin [1, 3] as a matrix. These compounds do not luminesce and are quite chemically inert. Thanks to the peculiarities of their structure, they are able to keep the clusters of the studied substance formed inside them. However, these clusters can have arbitrary sizes and shapes, and their growth will not be restrained by polymer or gelatin, but on the contrary, they will uncontrollably form the backbone of the matrix by themselves. Sparse silicate glass with voids of nanometer size is free of this defects. The sizes of interpenetrating pours can vary from few nanometers to several hundred nanometers. In addition, the quartz skeleton of the compound is quite durable, so it limits the size of the particles that are formed, because they cannot exceed the size of the pours. The columnar structure of the glass allows to influence both the inner surface of the pours and the nanoparticles created inside them. In the most cases, such nanoparticles can be conveniently created by saturating the matrix with solutions of suitable substances. Thus, porous silicate glass perfectly meets the requirements formulated to the matrix, inspite of the fact that it does not exist in nature. It can be obtained from two-phase sodium-borosilicate glass by a not very complicated technology [4].

Types of porous silicate glass and the technology of their production

Two-phase sodium borosilicate glass has the complex chemical formula $SiO_2 \times [Na_2O \times B_2O_3]$. The melting temperature of such glass exceeds 750°C. In addition, the

melting point of the silicate component of the glass is much higher than the melting point of the sodium borate complex, and therefore there is a temperature at which the sodium borate component of the glass is in a liquid state, while its silicate component is simply very heated. A temperature of 650°C corresponds to this condition. If the charge for boiling two-phase glass, which has been brought to 750°C, is cooled adiabatically to 650°C, then the separation of phases occurs at the indicated temperature, the sodium-borate complex will still melt, forming large bubbles that will form the silicate skeleton. Due to the viscosity of the melt, it is kept in such conditions for several hundreds of hours, until both phases mutually completely dissolve in each other, and then it is slowly cooled to room temperature. The two-phase glass obtained is quite large (up to hundreds of nanometers) areas of mutually intertwined silicate and sodium borate phases. These phases, in particular, show unequal chemical stability, thanks to which a mixture of hydrofluoric, nitric and glacial acidic acids can be used to completely etch the sodium borate phase, while almost not affecting the silicate phase, which forms a quartz skeleton with through-through cavities in places of the etched sodium borate phase. These cavities have quite large dimensions, however, due to mutual dissolution, the rather small, powder-like particles of SiO_2 also got inside the sodium borate phase, and after its etching off should settle inside the resulting cracks. Such settled powdery particles are called residual silica gel. Chemically, they are completely identical to quartz skeleton and differ from it only in their fineness. The glass produced in such a way is conventionally called porous glass of type C. Such glass is unsuitable for a number of applications, because due to sufficiently large pours, particles of the investigated substance of significant size will form in it. Therefore, the sufficient expansion of its surface will remain impossible.

For the formation of smaller pours in the glass, the technological modes of two-phase glass production should be slightly changed. The charge for its melting must be cooled adiabatically to a lower temperature, which is close to the melting point of the sodium borate phase, but lower than it (about 490 °C). If the charge is kept at such a temperature for hundreds of hours, it will lead to the formation of rather small bubbles in the sodium borate phase and, after cooling to room temperature, phase separation will occur, as a result of which the two-phase glass will be small (about tens of nanometers) areas of interwoven silicate and sodium borate phases. After the etching of the unstable sodium borate phase in the above-described manner, a rather fine-cracked silicate glass will be formed, which will also contain residual silica gel in the pours. Glass created in such a way is conventionally called porous glass of type A.

The presence of silica gel inside the pours, depending on the conditions of a specific scientific problem, can be both desirable and harmful. Thus, the presence of silica gel makes the glass more finely porous, but at the same time reduces the free space for the formation of nanoparticles of the studied substance. On the other hand, the presence of silica gel improves the adsorption properties of glass, but worsens its mechanical properties (deformation of the sample may occur due to the swelling of the gel in a humid environment [5-7]). It is true that special treatment can improve the mechanical properties of glass, but this will not always have a positive effect on its other properties [8]. Within the scope of the surface development problem for a substance suitable as an active element of a certain sensor, the separating ability of silica gel is definitely useful, which prevents the process of aggregation of particles ensemble formed in the gaps [1, 9]. Nevertheless, for cases where the presence of silica gel in cracks is harmful, the method of leaching silica gel developed in [10] is quite applicable, which impoverishes the glass from this formation, or completely eliminates it. According to this technique, the finished glass is etched in an alkaline etchant based on KOH. This etchant interacts with the finely dispersed silica gel rather quickly and acts much more slowly on the continuous (at least spongy) walls of the matrix. Due to this, the majority of the silica gel is removed, while the walls of the matrix backbone are only slightly etched [4, 11]. Type A glass treated in this way is conventionally called type B glass, and type C glass is called type D glass.

The results of studying the structure of all 4 above-mentioned types of glasses using an electron microscope are shown in Fig. 1. It is clearly visible that the glasses of types A and B are finely porous, while the pours in glasses of types C and D are much larger. Particles of residual silica gel appear as white spots in the images corresponding to glasses A and C. In type C glass they are larger, in type B glasses they are almost invisible (this confirms that the leaching technique leads only to impoverishment of the glass with silica gel [4, 11]), and in type D glasses they are absent at all.
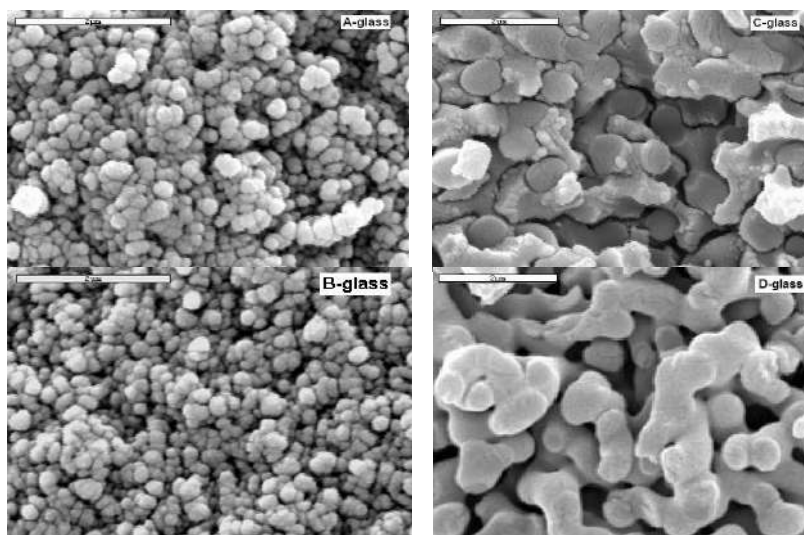
Fig. 1. Electron microscopic images of four poures types glass structures

Figure 2 shows the size distribution of pours for all specified types of glass. One can make sure, that in each of the glass types there are mainly two fractions of pours sizes, but any of the types contain small amounts of any pours from about 10 to over 100 nanometers.
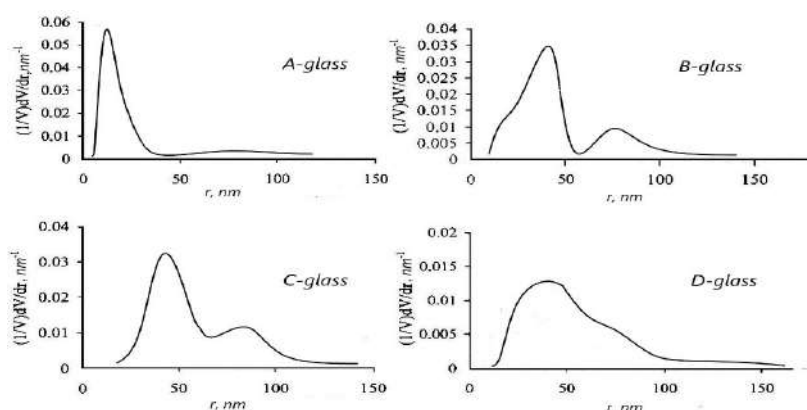
Fig. 2. Typical pours sizes distribution for four types of slotted glass

Formation of nanoparticles ensembles.

The formation methods of nanoparticles' ensembles in the porous glass matrix depend on a number of factors. The first of them, is the chemical composition of the particles' substance, the ensemble is to be formed. It should be taken into account that porous glass is almost pure quartz SiO_2, therefore the formation of silicon nanoparticles' ensemble, which are the component of the matrix, is possible through their chemical treatment [12-13]. For this, it should be based on the fact that silicon

69

is the main chemical component of both the framework of the porous glass and the residual silica gel in the pours. Both formations are chemically identical and differ only in dispersion. And since carbon in its chemical properties is similar to silicon, but more active, it is able to squeeze it out of the oxide at the appropriate temperatures. Thus, if the pours are saturated with carbon, under the right conditions it will push silicon out of the oxide, primarily from silica gel, as a more dispersed formation. Silicon will be in an energetically disadvantageous atomic state, and since carbon will turn into carbon dioxide, which is heavier than air and will prevent the re-oxidation of atomic silicon, the latter will have time to turn into silicon clusters, which will settle on the walls of the silicate skeleton, during the time required to remove CO2 from the pours like grape formations. In the future, the surface of these clusters will oxidize and a porous glass will be formed, enriched with silicon along the walls of the pours. This process is called carbon processing.

If it is necessary to form the nanoparticles' ensemble of a substance whose components are not included in the chemical composition of the matrix, but the specified substance is well soluble in water, alcohol or a special solvent that does not destroy the matrix, then the ensemble of nanoparticles can be formed by immersing the matrix into the appropriate solution. This will lead to the matrix impregnation with the subsequent formation of nanoparticles inside the pours. A classic example of such a substance is a group of dyes based on tetravalent stannum [4, 14]. These rather complex organic compounds are actually an aggregation of interwined benzene rings with nitrogen bridges and they are perfectly soluble in the organic solvent dimethylformamide (CH3)2NCO (abbreviated DMFA). By varying the concentration of the solution, the duration of the immersion and the temperature of the process, it is possible to obtain a whole nanoparticles' ensemble series of the specified molecular crystals with quite diverse properties, which can be particularly used in sensors.

In some cases, the substance itself is poorly soluble or insoluble in matrix-safe solvents. However, it can be synthesized as a result of the reaction of soluble substances. In this case, the specified synthesis should be performed directly inside the pours of the matrix. At the same time, after saturation of the matrix with a soluble component of the reaction, it is not necessary to interact with another substance, and sometimes it is enough to perform a thermosynthesis (as in the case of SnO_2 [15]) or coprecipitation (as in the case of RuO_2 [16]). It is worth to note that the above-mentioned carbon treatment, consisting of two stages, at the primary stage also represents the thermosynthesis of glucose, which is renewed to carbon in the form of graphite.

And finally, in some cases, after saturating the matrix with a soluble component of the reaction, it is necessary to place the saturated matrix in the solution of the second component of the reaction. This occurs when an ensemble of CdS [17] or AgBr [18] nanoparticles is formed. In these cases, after the completion of the reaction, the surface should be thoroughly cleaned so that the ensemble of nanoparticles does not shunt through it.

The nanoparticles' ensembles application in sensor technology

Highly dispersed ensembles of nanoparticles with a well-developed surface should be useful, first of all, as active elements for gas sensors. Nanoparticles' ensembles of dyes based on tetravalent stannum are especially applicable in this sense [19-20]. The molecules of these substances consist of two parts: a coordination node, which is a complex set of benzene rings, and a hydrazone fragment, which consists of one benzene ring located outside the coordination node and connected to it by an ordinary C-C bond. One of the hydrogen atoms of the hydrazone fragment is replaced by a certain group of atoms (e.g., the amine group NH3), which is analogous to a substitution impurity in semiconductors. At the same time, a ligand consisting of stannum and chlorine is contained inside the coordination unit, and is analogous to an impurity penetration in semiconductors. Both of these formations can be centers of light emission

Our studies demonstrate that the intensity of the dye with an amine ligand luminescence depends on the concentration of the solution

impregnating during the formation of nanoparticles' ensemble. This dependence is non-linear and has a maximum at a certain concentration, exceeding of which leads to a sharp decrease in luminescence [21]. Basing on this property, it is possible to register the presence of ammonia in the environment. In fact, if an ensemble of nanoparticles is created at a concentration that provides maximum luminescence, then in the presence of ammonia in the environment, the system will begin to behave as if it was formed at an overestimated concentration of the impregnating solution and its luminosity will drop sharply. This is the operation principle basis of the proposed ammonia transducer [22].

The coordination unit ligand itself is not enough active, for it is protected from all sides by a set of benzene rings. There are two types of ligands, $SnCl_4$ and $SnCl_3$. Both of them form a certain distribution of negative charge inside the dye molecule. In this case, the SnCl3 ligand corresponds to a more intense glow. The presence of HCl vapours in the environment enriches the coordination node with negative Cl- ions. This changes the charge distribution in the molecule to that typical for a dye with the $SnCl_4$ ligand, and the luminescence intensity of the system decreases sharply again. This property is the basis of the established action principle for the suggested hydrogen chloride vapor sensor [23].

After the actuation of both of these sensors, they should be subjected to low-temperature short-term annealing. to restore their performance This is the main drawback of these devices. This drawback does not occur in the case of using an ensemble of SnO_2 nanoparticles. This system is not sensitive to HCl vapors, but in the presence of ammonia in the environment it also sharply reduces the intensity of its emmitance. However, after being transferred to a clean atmosphere, within a short time it completely restores itself its performance . [24].

Conclusions

Porous silicate glass is the best matrix for creating ensembles of nanoparticles of all kinds of substances due to its durability, chem-ical inertness and separation properties of powder-like formations inside slots.

The molecular structure peculiarities of dyes based on tetravalent stannum make it possible to use them as active elements for some gas sensors.

In the dye molecule of the specified structure, there are two types of luminescence centers: a substituent in the hydrazide fragment, which is analogous to a substitution impurity in a semiconductor, and a ligand in the coordination node, which plays the role of a penetration impurity. The substituent is responsible for sensitivity to ammonia, and the ligand is responsible for sensitivity to HCl vapors.

The sensitivity principle of dye nanoparticle ensembles to the presence of these gases in the environment is manifested in their luminescence intensity decrease.

References

1. Meshkovsky I.K., 1998. The composite optical materials based on porous matrices, Sankt- Petersburg, 332 p.
2. Smyntyna V.A., Skobeeva V.M., Malushin N.V., The boundary influence on the optical and luminescent properties of the quantum dots of the CdS in a polymer// Fizika i khimiya tverdogo tela-2011-V12,N2-pp.355-358.
3. Smyntyna V.A., Skobeeva V.M., Malushin N.V. Influence of the Surface on the Spectrum of Luminescence NC CdS in Gelatine Matrix // Photoelectronics – 2012 – No.21 – pp.50-56.
4. Doycho I.K. Study of the photoluminescent properties of nanoparticles ensembles of dyes In the book: Non equilibrious processes in the sensor structures, Editor V.A.Smyntyna, p.p.120-170, ONU (Odessa Mechnikov national university),Odessa (2015).
5. Gevelyuk, S.A., Doycho, I.K., Rysiakiewicz-Pasek, E., Marczuk, K., Relative changes of porous glass dimensions in humid ambiance, Journal of Porous Materials, 7 (2000) 465-467.
6. Gevelyuk, S.A., Doycho, I.K., Lishchuk, D.V., Prokopovich, L.P., Safronsky, E.D., Rysiakiewicz-Pasek, E., Roizin, Ya.O., Linear extension of porous glasses with modi-

fied internal surface in humid environment, Optica Applicata, 30 (4) (2000) 605-611.

7. Gevelyuk, S.A., Doycho, I.K., Prokopovich, L.P., Rysiakiewicz-Pasek, E., Safronsky, E.D., Humidity dependencies of porous sol-gel and silica glass linear sizes, Material Science, 20 (2) (2002) 23-27.

8. Rysiakiewicz-Pasek E., Vorobyova V.A., Gevelyuk S.A., Doycho I.K., Mak V.T., Effect of potassium nitrate treatment on the adsorption properties of silica porous glasses, Journal of Non-Crystalline Solids 345–346, 2004, pp. 260–264.

9. Tyurin O.V., Bercov Y.M., Zhukov S.O., Levitskaya T.F., Gevelyuk S.A., Doycho I.K., Rysiakiewicz-Pasek E., Dye aggregation in porous glass, Optica Applicata, 40 (2) (2010) 311-321.

10. Mazurin O.V., Roskova G.P., Averianov V.I., Antropova T.V., 1991. Biphasic glasses: structure, properties, applications, NAUKA, Leningrad., 276 P.

11. *I. K. Doycho, V. S. Grinevych,* and *L. M. Filevska*. Porous Silica Glasses as a Model Medium for the Formation of Nanoparticles Ensembles: Review. Advanced Nanomaterials for Detection of CBRN, NATO Science for Peace and Security Series A: Chemistry and Biology, 2020, 283-294; https://doi.org/10.1007/978-94-024-2030-2_21

12. S.A.Gevelyuk, I.K.Doycho, L.P.Prokopovich, E.Rysiakiewicz-Pasek, K.Marczuk. The influence of anneal of incorporated carbon on the photoluminescence properties of porous glass and porous silicon // Polish Ceramic Bulletin 19, Ceramics 57 / Porous and Special Glasses (Proceedings of the 4-th International Seminar PGL'98) / edited by L.Stoch. – Polish Ceramic Society, Krakow: 1998. – p.59-64.

13. Gevelyuk, S.A., Doycho, I.K., Prokopovich, L.P., Rysiakiewicz-Pasek, E., Safronsky, E.D. Influence of carbon multiple treatments on the photoelectrical properties of porous glasses. Radiation Effects & Defects in Solids, 2003, Vol.158, pp.427-432. Doi: 10.1080/1042015022000037292

14. *I.K.Doycho, S.A.Gevelyuk, E.Rysiakiewicz-Pasek.* Photoluminescence of tautomeric forms of nanoparticle ensembles of dyes based on the 4-valence stannum complexes in porous silica glass // Photoelectronics. – 2015. – Vol.**24**. – pp.30-37.

15. *Gevelyuk S. A.; Grinevych V. S.; Doycho I. K.; Lepikh Ya.I.; Filevska L. M.* Photoluminescence of SnO_2 nanoparticle ensemble in porous glass with column structure // 2019 IEEE 8th International Conference on Advanced Optoelectronics and Lasers (CAOL). – 2019, – pp.416-419; doi: 10.1109/CAOL46282.2019.9019433

16. *Doycho I.K., Gevelyuk S.A., Filevska L.M., Grinevych V.S.* Catalysis of Wastewater Pollutants by Ruthenium Nanooxide in Porous Glass. Book of Abstracts of the 9th International, Conference Nanotechnology, and Nanomaterials (NANO 2021), August 25-27, 2021, Lviv, p.37. (если уже вышла отправленная в декабре статья в Шпрингере, можно заменить на неё)

17. Rysiakiewicz-Pasek, E., Polańska, J., Gevelyuk, S.A., Doycho, I.K., Mak, V.T., Zhukov, S.A., The photoluminescent properties of CdS clusters of different size in porous glasses, Optica Applicata, XXVIII (1) (2008) 93-100.

18. Doycho, I.K., Gevelyuk, S.A., Ptashchenko, O.O., Rysiakiewicz-Pasek, E., Tolmachova, T.N., Tyurin, O.V., Zhukov, S.O., Photoluminescence features of AgBr nanoparticles formed in porous glass matrixes, Optica Applicata, 40 (2) (2010) 323-332.

19. *Дойчо І.К., Гевелюк С.А., Лепіх Я.І., Рисякевич-Пасек Е..* Особливості газочутливості барвників на базі комплексів 4-валентного стануму // SEMST– 2017– Vol.14, № 1 – pp. 31-40.

20. *I.K.Doycho, S.A.Gevelyuk, Ya.I.Lepikh, E.Rysiakiewicz-Pasek.* Nature of gas sensitivity of dyes on the base of Sn(IV) complexes // Optica applicata. – 2019. – Vol. **49**. – No.3. – pp.427-436.

21. *S.A.Gevelyuk, E.Rysiakiewicz-Pasek, I.K.Doycho.* Dependence of photoluminescence of nanoparticle ensembles of stannum (IV) complexes in silica porous matrix on concentration of saturating solution // Photoelectronics. – 2016. – Vol.**25**. – pp.40-47.

22. Патент України на винахід №119092, Сенсор аміаку: МПК G01N 21/64 (2006.01) / *Гевелюк С.А., Дойчо І.К.,*

Леніх Я.І.; зареєстровано у Держреєстрі патентів на винаходи 25.04.2019.

23. Патент України на винахід №118415, Сенсор парів хлористого водню: МПКG01N 21/76 (2006.01) / *Леніх Я.І., Дойчо І.К., Гевелюк С.А.*; зареєстровано у Держреєстрі патентів на винаходи 10.01.2019.

24. *Gevelyuk S.A., Grinevych V.S., Doycho I.K., Filevska L.M.* The active environment influence on the luminescence of SnO_2 nanoparticles' ensembles in a porous matrix// Applied Physics A, 2020, 126(12) 919; DOI:10.1007/s00339-020-04101-4

Doycho I.K.,Filevska L.M., Grinevych V.S.

GAS SENSITIVITY OF SOME NANOPARTICLES ENSEMBLES IN POROUS GLASS

Summary The importance of substances' surface development suitable for sensor technology by dispersing them to the level of nanoparticles' ensemble within a certain matrix has been demonstrated. It has been proven that the best matrix for the formation of the specified ensemble of nanoparticles is porous silicate glass. Methods of formation of ensembles of nanoparticles of some compounds in porous glass are briefly considered. The applicability of the mentioned systems for sensors is demonstrated by the example of their luminescent response sensitivity to the presence of ammonia or HCl vapours in the environment.

Key words: gas sensitivity, photoluminescence, porous glass, ensembles of nanoparticles.

Дойчо І.К., Філевська Л.М., Гріневич В.С.

ГАЗОЧУТЛИВІСТЬ ДЕЯКИХ АНСАМБЛІВ НАНОЧАСТИНОК У ШПАРИСТОМУ СКЛІ

Реферат Продемонстровано важливість розгортання поверхні речовин, придатних для використання у сенсориці, шляхом диспергування їх до рівня ансамблю наночастинок всередині певної матриці. Доведено, що найкращою матрицею для формування зазначеного ансамблю наночастинок є шпаристе силікатне скло. Коротко розглянуто способи формування ансамблів наночастинок деяких сполук у шпаристім склі. Застосовність зазначених систем у сенсориці продемонстровано на прикладі чутливості їхнього люмінесцентного відклику до наявності аміаку або парів HCl у довкіллі.

Ключові слова: газочутливість, фотолюмінесценція, шпаристе скло, ансамблі наночастинок.

Дойчо И.К., Филевска Л.М., Гриневич В.С.

ГАЗОЧУВСТВИТЕЛЬНОСТЬ НЕКОТОРЫХ АНСАМБЛЕЙ НАНОЧАСТИЦ В ПОРИСТОМ СТЕКЛЕ

Реферат Продемонстрирована важность развертывания поверхности веществ, пригодных для использования в сенсорике, путем диспергирования их до уровня ансамбля наночастиц внутри определенной матрицы. Доказано, что наиболее предпочтительной матрицей для формирования указанного ансамбля наночастиц является пористое силикатное

стекло. Кратко рассмотрены способы формирования ансамблей наночастиц некоторых соединений в скважистом стекле. Применяемость указанных систем в сенсорике показана на примере чувствительности их люминесцентного отклика к наличию аммиака или паров HCl в окружающей среде.

V.A. Smyntyna, V.M. Skobeeva, K.A. Verheles.

I.I. Mechnikov National University of Odessa, Dvoryanskaya St. 2, 65082 Odessa, Ukraine,
E-mail: klara2010@meta.ua

INFLUENCE OF TECHNOLOGICAL CONDITIONS OF SYNTHESIS ON THE FORMATION OF PHOTOLUMINESCENCE SPECTRA OF CdS QDs

Here are presented the results of influence of two parameters of synthesis process of quantum dots sulfide cadmium (CdS QD) on the spectrum luminescence, namely, the acid-base balance of the growth solution and the correlation of reaction components (cadmium and sulfur salts). Carried out the syntheses in which the pH solution was changed in the interval of values from 2 to 10. There were also synthesized CdS QD with different ratios of the initial components. The results obtained by evidence of the fact that the technological process has a significant impact on the formation of bands luminescence CdS QDs.

Introduction

Quantum dots (QDs) are nanocrystals 2 to 10 nm in diameter synthesized from semiconductor materials.

Semiconductor CdS QDs have attracted considerable interest due to their unique properties, which are absent in bulk materials due to the effect of quantum confinement of charge carriers. For a number of areas of science and technology, colloidal quantum dots are a promising material. They are of particular interest as a basis for creating biomedical markers and sensors[1].

A necessary condition for the practical implementation of CdS QDs is the development of a technology for obtaining them with controlled properties. One of the simplest and technological methods of QDs synthesis is the colloidal chemical method. The colloidal method of synthesizing quantum dots attracts a lot of attention, as it provides an opportunity to precisely control the size and surface properties of the resulting nanoparticles. The properties of QDs obtained by this method depend on such parameters as the concentration of the starting materials, the pH of the growth solution, etc.

The greatest interest, from the point of view of application of quantum dots (QDs) of A_2B_6 compounds, is caused by their luminescent properties. A large number of works have been devoted to the study of the luminescence of CdS QDs, but the question of the nature of the centers that determine the luminescence and form the luminescence spectrum still remains relevant. Currently, the question of the nature of the luminescence centers and which luminescence bands are created by intrinsic and impurity lattice defects [2] remains relevant. Modern literary sources only mention the possibility of defects, but do not pay attention to the disclosure and description of their nature and the conditions of their creation in the process of synthesis [3]. This issue also includes the development of controlled synthesis, during which QD luminescence spectra can be predicted.

The colloidal-chemical synthesis of CdS QDs is influenced by a large number of factors related to the conditions of the synthesis (duration, rate of introduction of reaction components, synthesis temperature). The formation of luminescence centers in CdS QDs depends on many technological factors, including the concentration of cadmium and sulfur ions and their ratio, as well as the acid-alkaline balance in the aqueous growth solution of CdS QDs. The results of the influence of these factors are presented in this study.

1. Object and Research Methods

The studied nanocrystals of cadmium sulfide were obtained by a chemical method from solutions of cadmium and sulfur salts in a colloidal solution of gelatin. The formation of

CdS particles occurs as a result of the exchange reaction: $Cd(NO_3)_2+Na_2S=>CdS+2NaNO_3$.

To obtain a colloidal solution, 5% gelatin and equimolar concentrations of cadmium and sulfur salts were used. The volumes introduced into the colloidal solution of the components were the same. The pH values of the solutions were changed by adding a solution of alkali or hydrochloric acid to an aqueous solution of gelatin with cadmium nitrate to obtain the required pH values (2 ÷ 10).

Samples were also created in which the concentration of cadmium and sulfur ions and their ratio changed. The pH value during the synthesis process was constant and equal to 7. During the study, four combinations of solutions with different ratios of the initial components of cadmium and sulfur were created. The molar concentration ratio of the initial components $Cd(NO_3)_2/Na_2S$ was equal to: 1/4, 1/2, 1/1, 2/1. In each of these combinations, seven samples were obtained: with a constant volume of $CdNO_3$, namely 5 ml, but in each of them the volume of introduced Na_2S changed: 0.25; 0.5; 1; 2; 3; 4 and 5 ml.

The luminescence was excited by a pulse laser LCS-DTL-374QT with a light wavelength of 355 nm. Laser power - 35 mW.

2. Analysis of Results

2.1. The effect of the acid-base balance in an aqueous solution with QDs of CdS.

It is known that salts are hydrolyzed in aqueous solutions. In our case – hydrolysis of nitrate and sodium sulfate. The molar concentration of cadmium ions is calculated according to formulas (1-2) and graphically presented in Figure 1.

$$C_0 = [Cd^{2+}] + Cd(OH)^+ + Cd(OH)_2^0, \qquad (1)$$

$$\alpha_1 = \frac{|Cd^{2+}|}{C_{Cd(NO_3)_2}} = \frac{1}{1+\frac{k_1}{[H^+]}+\frac{k_1 k_2}{[H^+]^2}}; \quad \alpha_2 = \frac{k_1 \alpha_1}{[H^+]};$$

$$\alpha_3 = \frac{k_1 k_2 \alpha_1}{[H^+]^2}. \qquad (2)$$

where α – molar concentration of components; k is the ionization coefficient (taken from the table [4]).

It can be seen that at pH values <8, the concentration of cadmium ions in the solution is dominant, and up to pH = 6, it remains un-changed. At pH > 6, the concentration of cadmium ions decreases and $Cd(OH)^+$ is formed. At pH values greater than 9, cadmium hydroxide $Cd(OH)_2$ is formed.
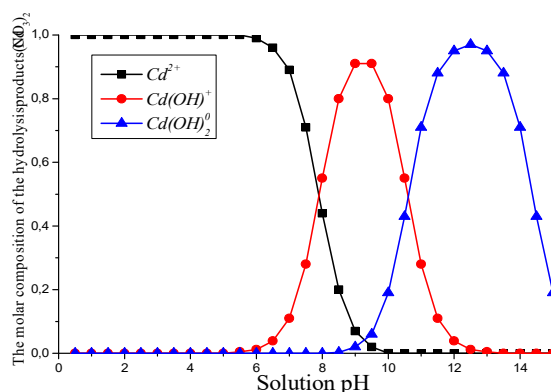
Fig. 1 – Dependence of the concentration of ions on the pH of the solution

Cadmium sulfide nanocrystals were synthesized at the following pH values of the solution: 2, 4, 7, 10.

Regarding the hydrolysis of sulfur sulfide, it is known that the hydrolysis of sulfur salts occurs at pH values>6. At lower pH values, the source of sulfur is impurity sulfur, which is present in gelatin.

In fig. 2 shows the normalized luminescence spectra of CdS QDs synthesized at different pH values. It can be seen that the luminescence spectra of samples obtained at low pH (2 and 4) and at pH (7 and 10) differ sharply. from. At low pH values, a short-wave luminescence band with a wavelength of $\lambda_{max} = (480 – 490)$ nm dominates, and at higher values, a long-wave band localized at $\lambda_{max} = (700 – 720)$ nm.

It was interesting to study the sensitivity of the luminescence spectrum of already grown CdS QDs to the acid-base composition of the colloidal solutions in which they are located, to determine whether the defect formation process is reversible as a result of a change in the pH of the solution, and how the pH value affects the change in QD size.

CdS QDs obtained at a neutral pH = 6 (initial sample) with an equimolar ratio of cadmium and sulfur ions with a wide luminescence band in the region (λmax = 667 nm) were chosen as the objects of the study. To the colloidal solution containing these QDs, solutions of alkali or hydrochloric acid were added to obtain pH (2, 4, 6, 8).
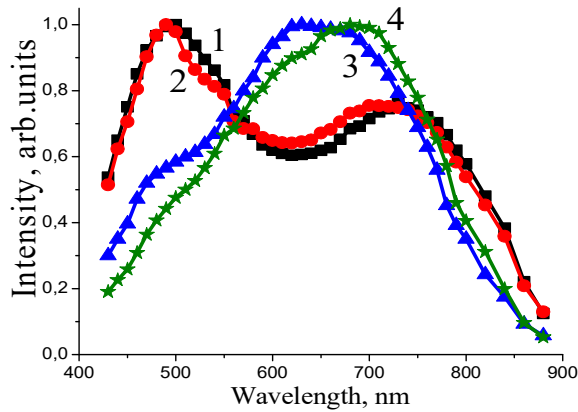
Fig. 2 – Normalized luminescence spectra of CdS QDs grown at different pH values of the solution: 2(1), 4(2), 7(3), 10(4)

As a result, colloidal solutions of CdS QDs were obtained, the color of which changed from yellow to orange (Fig. 3). It can be seen that the color of the solutions corresponding to pH = 2 and 4 is practically the same, which is confirmed by the data of the absorption spectra presented in Fig. 4.

Fig. 3 – Samples of CdS QDs obtained at different pH values

Extrapolation of the absorption curves to the energy axis gives the value of the effective band gap of nanocrystals at different pH, and, accordingly, the size of the particles can be determined: 2 and 4 (2.9 nm), 6 (3.5 nm), 8 (4 nm).

The average particle radius was estimated from optical absorption spectra.
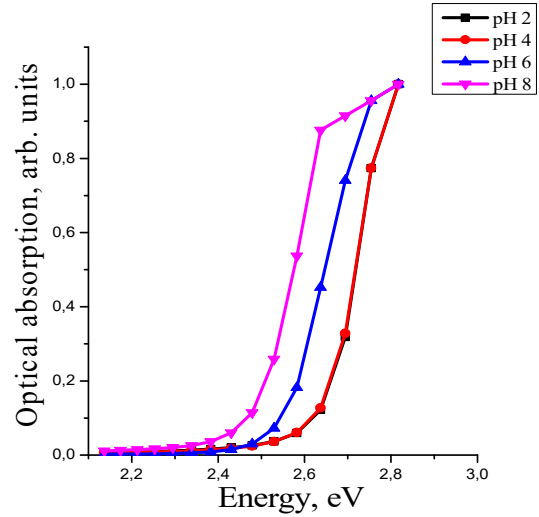
Fig. 4. Normalized absorption spectra of CdS QDs grown at different pH values of the solution: 2(1), 4(2), 6(3), 8(4)

According to the theory of interband absorption, the effective band gap of nanocrystals Eg* (the transition energy between the upper hole and lower electronic levels) increases with decreasing particle radius according to the law:

$$\hbar\omega = E_g^* + E_{l,n}^{e,h} \qquad (3)$$

where E_g^* - optical band gap width of bulk crystal; $E_{l,n}^{e,h}$ – dimensional quantization energy, which is inversely proportional to the square of the nanoparticle radius; l and n – orbital and principal quantum number. The dimensional quantization energy is defined as the difference between the effective band gap of a nanocrystal and a single crystal. It can be calculated using the formula (3):

$$E_{l,n}^{e,h} = h^2 \varphi_{l,n}^2 / 2 \, m_{e,h} r^2 \qquad (4)$$

where $m_{e,h}$– effective masses of an electron and a hole; r – average radius of the nanoparticle; $\varphi_{l,n}$– the root of the Bessel function (for quantum numbers $l = 0$ and $n = 1$, $\varphi_{0l} = 3,142$).[5]

The observed results can be explained by the following phenomena. A decrease in the size of QDs upon addition of hydrochloric acid (pH=2.4) may occur as a result of their dissolution, the size of QDs decreases from 3.5 nm to 2.9 nm. The reason for the increase in QDs size when alkali is added can be their coagulation, or the formation of a cadmium hydroxide shell.

Normalized luminescence spectra of samples measured after acid-alkaline treatment of already grown CdS QDs are shown in Fig. 5.

The obtained spectra repeat the results of the experiment on the influence of pH of the solution during the synthesis of nanocrystals [6].

In the spectra of nanocrystals with low pH (2 and 4), a short-wave luminescence band (570 nm) is detected. At high pH (6, 8), a long-wavelength band localized at a wavelength of λmax =690 nm dominates, the nature of which is associated with intrinsic defects in nanocrystals.

It was found that both in an acidic environment (pH=2.4) and in an alkaline environment (pH=8) the luminescence spectrum consists of two bands. The short-wave band (λmax = 580 nm) dominates in an acidic environment, and the long-wave band dominates in an alkaline environment (λmax = 683 nm).
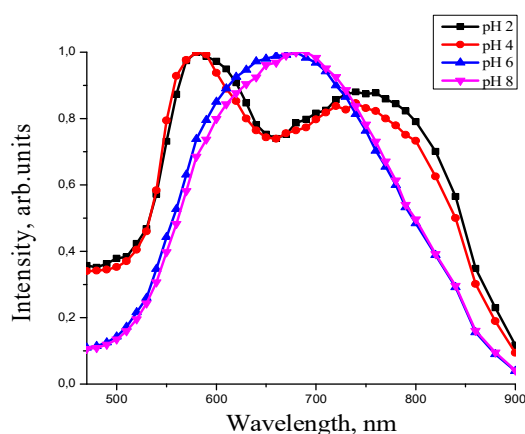
Fig. 5 – Normalized luminescence spectra of CdS QDs grown at different pH values of the solution: 2(1), 4(2), 6(3), 8(4).

In studies carried out earlier [6], when the acid-alkaline balance of the solution changed during the synthesis, a change in the spectrum was observed with the help of a change in the nature of surface defects. In this publication, the acid-base balance of a previously prepared solution with QDs was changed. In this case, it was noted that the change in the position of the luminescence spectrum correlates with the change in the size of the CdS QDs.

Thus, despite the different conditions of conducting the experiment regarding the effect of pH on the luminescence spectrum of CdS QDs, both obtained at different pH values during the synthesis and processed after synthesis, a qualitative correspondence between their luminescence spectra is observed.

2.2. The influence of the relative concentration of the starting components on the PL of CdS QDs

The graphs presented in Figure 6 correspond to the relative concentrations of $Cd(NO_3)_2/Na_2S$ components: 1/4, 1/2, 1/1, 2/1 (Figure 6 a, b, c, d, respectively). It can be seen that with an increase in the concentration of cadmium, the short-wavelength (λ_{max} = 490 nm) band becomes dominant, and in Fig. 6 (a), where the concentration of cadmium is quite low, this band is hardly noticeable.

This also confirms the nature of the evolution of the spectra of Figs. 6 (a, b, c, d) in which Na_2S:0.25 was added to the initial solution; 0.5; 1, 2; 3, 4 and 5 ml, (curves 1-7), respectively. Indeed, it can be seen that the addition of sulfur contributes to the increase in the intensity of the long-wave band. In the experiments, the samples containing the short-wave luminescence band (λ = 462 ÷ 493 nm) have an excess of cadmium, and the long-wave band (λ = 660 ÷ 711 nm) has an excess of sulfur.

Thus, the curves of the luminescence spectra in both experiments are composite, that is, they consist of several elementary bands. In this regard, the luminescence spectra were approximated by Gaussian curves, as a result of which three luminescence bands were detected in CdS QDs. Table 1 shows the schedule results.

Note that in the photoluminescence spectra of nanocrystals, a band is recorded in the region λ = 555 ÷ 598 nm. This band develops in nanocrystals, the synthesis of which was carried out at the same concentration of cadmium and sulfur ions.

Thus, the given results indicate that the luminescence of CdS QDs obtained by the method of colloidal chemistry is due to their own defects and it is related to the influence of the stoichiometric composition of cadmium and sulfur. Some discrepancy in the localization of the luminescence maxima of individual bands can be explained by the spread of QD size.
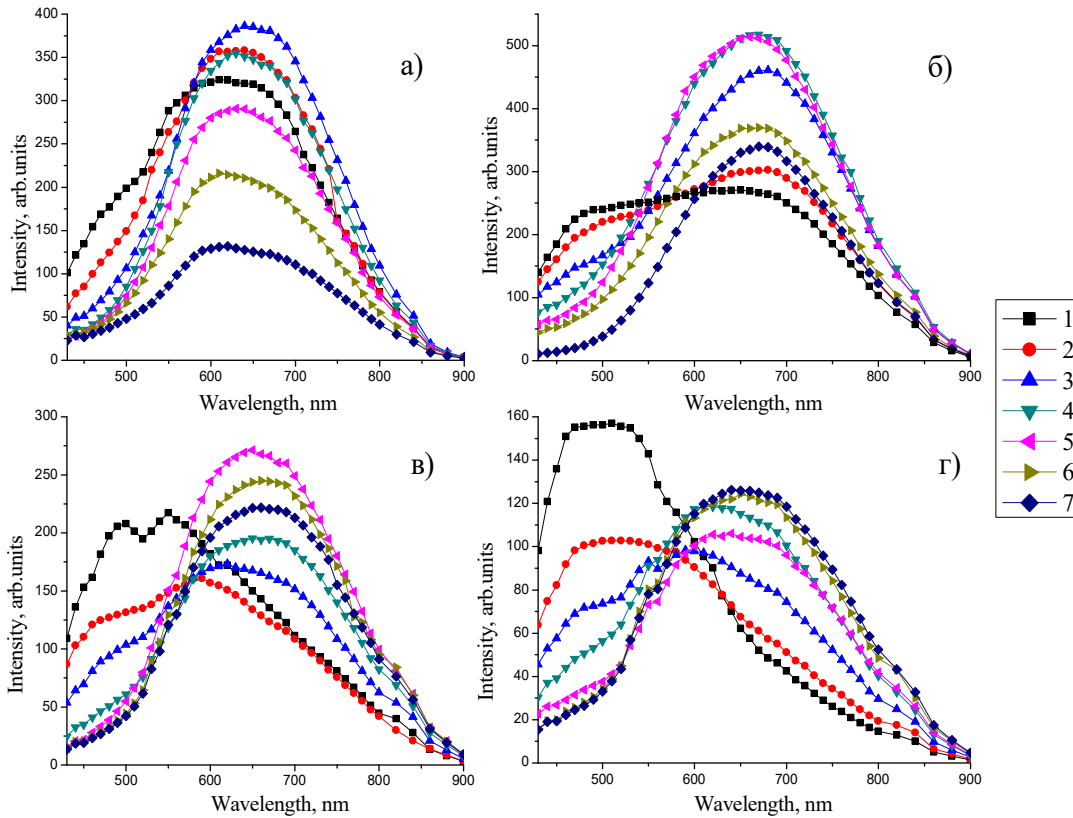
Fig. 6 – Luminescence spectra of CdS QDs obtained at the molar ratio of the initial components CdNO3 /Na2S: 1/4 (a); 1/2 (b); 1/1 (c); 2/1 (g).

Table 1. Dependence of the position of the maxima of the QD luminescence bands, obtained as a result of spectrum decomposition, on the pH value of the solution and at different ratios of the initial components.

The influence of the acid-base balance in an aqueous solution with CdS QDs (Fig. 2)				*The influence of the relative concentration of the initial components on the PL of CdS QDs (Fig. 6)*			
pH	λ_1, nm	λ_2, nm	λ_3, nm	$CdNO_3 /Na_2S$	λ_1, nm	λ_2, nm	λ_3, nm
2	490	-	716	*2/1 (curve 1)*	462	555	660
4	493	-	708	*1/1 (curve 3)*	462	573	690
7	483	592	694	*1/2 (curve 5)*	464	598	703
10	481	578	703	*1/4 (curve 7)*	-	593	711

Conclusions

The results of the research showed that the luminescence spectrum of CdS QDs depends on the acid-alkaline composition of the medium. At low pH values, the bands localized in the 500-580 nm region dominate, and at high values - in the 640÷680 nm region. It is shown that the luminescence spectrum can be changed both by changing the synthesis conditions and by changing the acid-base composition of colloidal nanocrystals.

The work also investigated the effect of two parameters of the QD synthesis process on their luminescence spectrum, namely: the acid-alkaline balance of the growth solution and the ratio of reaction components (cadmium and sulfur salts). Syntheses were carried out in which the pH of the solution varied in the range from 2 to 10. CdS QDs with different ratios of starting components were also synthesized. The obtained results indicate that the technological process has a significant effect

on the formation of cadmium sulfide QD radiation bands. In both cases, the radiation spectrum contained three bands localized in the wavelength range $\lambda_1 = 462 \div 493$ nm, $\lambda_2 = 555 \div 598$ nm, $\lambda_3 = 660 \div 711$ nm.

The observed features of the influence of the mentioned technological factors on the luminescence spectrum of CdS QDs are explained by the fact that the concentration of cadmium and sulfur ions is a determining parameter in the synthesis. In the first, the concentration of ions is regulated by the starting pH of the solution, and in the second, by the initial concentration of $Cd(NO_3)_2$ and Na_2S.

References

1. В. Г. Клюєв, Фам Тхі Хан Мьен, Ю. С. Бездітко, Природа центрів люмінесценції в нанокристалах CdS / Конденсовані середовища і міжфазні границі, Т. 16, № 1, 2014. – 27 с.
2. Ю. С. Бездітко, В. Г. Клюєв, Особливості формування нанокристалів CdS при фіксованому часі синтезу / Вісник ВДУ. Серія: Фізика. Математика, № 1, 2014. – 6 с.
3. Morphological and Optical Properties of CdS Quantum Dots Synthesized with different pH values /[Akeel M. Kadim, Wasan R. Saleh]. – Iraqi Journal of Science, Vol. 58, No.3A, 2017. –1207 p.
4. Гідроліз іонів металів у розведених розчинах / [В. А. Назарео, В. П. Антонович, Є. М. Невська]. - М .: Атомвидат – 1979. – 192 с.
5. Эфрос Ал. Л., Эфрос А. Л. «Межзонное поглощение света в полупроводниковом шаре», Физ. и техн. полупроводников. − 1982. − Т.16. В.7. − С. 1209−1214.
6. V. A. Smyntyna, V. M. Skobeeva, K. A. Verheles, N. V. Malushin. «Influence of technology on the formation of luminescence centers in QDs CdS», Journal of nano- and electronic physics. Sumy State University, 2019, Vol. 11 No 3, 05031(4pp) (2019).

V.A. Smyntyna, V.M. Skobeeva, K.A. Verheles.
I.I. Mechnikov National University of Odessa, Dvoryanskaya St. 2, 65082 Odessa, Ukraine,
E-mail: klara2010@meta.ua

INFLUENCE OF TECHNOLOGICAL CONDITIONS OF SYNTHESIS ON THE FORMATION OF PHOTOLUMINESCENCE SPECTRA OF CdS QDs

Summary
The purpose of the work is to study the influence of technological conditions of synthesis on the formation of photoluminescence spectra of CdS QDs. This article presents the results of the effect of pH on the luminescence of colloidal CdS QDs. A qualitative agreement was shown between the luminescence spectra of CdS QDs, both obtained at different pH values during synthesis, and CdS QDs subjected to treatment after synthesis. It was shown that the luminescence spectrum can be changed both by changing the synthesis conditions and by changing the acidity of colloidal CdS QDs. It are presented the results influence of two parameters of synthesis process of quantum dots sulfide cadmium (CdS QD) on the spectrum luminescence, namely, the acid-base balance of the growth solution and the correlation of reaction components (cadmium and sulfur salts). Carried out the syntheses in which the pH solution was changed in the interval of values from 2 to 10. There were also synthesized CdS QD with different ratios of the initial components. The results obtained by evidence of the fact that the technological process has a significant impact on the formation of bands luminescence CdS QDs . In both cases, the luminescence spectrum had three bands that are localized at $\lambda_1 = 462 \div 493$ nm, $\lambda_2 = 555 \div 598$ nm, $\lambda_3 = 660 \div 711$ nm. The observed features of the effect of these technological factors on the spectrum luminescence of CdS QDs are explained by the fact that, in the synthesis, the concentration of cadmium and sulfur ions is a determining parameter. In the first case, the ion concen-

tration is controlled by the pH value of the solution, and in the second, by the initial concentration of Cd (NO$_3$) $_2$ and Na$_2$S.

Keywords. cadmium sulfide quantum dots, absorption, photoluminescence, nanomaterials.

В.А. Сминтина, В.М. Скобєєва, К.О.Вергелес

Одеський національний університетімені І.І. Мечникова, 65082, Одеса, вул. Дворянська, 2,
E-mail: klara2010@meta.ua;

ВПЛИВ ТЕХНОЛОГІЧНИХ УМОВ СИНТЕЗУ НА ФОРМУВАННЯ СПЕКТРІВ ФОТОЛЮМІНЕСЦЕНЦІЇ КТ CdS

Реферат

Мета роботи полягає в дослідженні впливу технологічних умов синтезу на формування спектрів фотолюмінесценції КТ CdS. У роботі наведено результати впливу pH на люмінесценцію колоїдних КТ CdS. Показано якісну відповідність між спектрами люмінесценції КТ CdS, отриманих при різних значеннях pH під час синтезу, і КТ CdS, підданих обробці після синтезу. Також показано, що спектр люмінесценції можна змінювати як зміною умов синтезу, так і зміною кислотності колоїдних КТ CdS. Представлені результати впливу двох параметрів процесу синтезу квантових точок сульфіду кадмію (КТ CdS) на спектр люмінесценції, а саме, кислотно-лужного балансу ростового розчину і співвідношення компонентів реакції (солей кадмію і сірки). Здійснено низку експериментів з синтезом, в якому pH розчину змінювалася в інтервалі величин від 2 до 10. Також були синтезовані КТ CdS з різним співвідношенням вихідних компонентів. Отримані результати свідчать про те, що технологічний процес має суттєвий вплив на формування смуг випромінювання КТ CdS. В обох випадках спектр випромінювання містив три смуги, які локалізовані у $\lambda_1 = 462 \div 493$ нм, $\lambda_2 = 555 \div 598$ нм, $\lambda_3 = 660 \div 711$ нм. Спостережувані особливості впливу зазначених технологічних факторів на спектр люмінесценції КТ CdS пояснюються тим, що в синтезі визначальним параметром є концентрація іонів кадмію та сірки.У першому – концентрація іонів регулюється значенням pH розчину, а у другому – вихідною концентрацією Cd(NO$_3$)$_2$ та Na$_2$S.

Ключові слова. квантові точки сульфіду кадмію, поглинання, фотолюмінесценція, наноматеріали.

P. O. Kondratenko[1] , O. Yu. Khetselius[2]

[1]National Aviation University, 1, Komarov Ave, Kiev
[2]Odessa State Environmental University, 15, L'vovskaya str., Odessa
E-mail: okhetsel@gmail.com

SIMULATION CHAOTIC DYNAMICS OF RELATIVISTIC BACKWARD-WAVE OSCILLATOR WITH USING CHAOS THEORY AND QUANTUM NEURAL NETWORKS

Nonlinear simulation and forecasting chaotic evolutionary dynamics of such complex system as relativistic backward-wave oscillator is treated using the new combined method, based on the chaos theory algorithms, concept of geometric attractors, and algorithms for quantum neural network simulation. It has been performed modelling the dynamics of multilayer photon echo neural network for the case of noisy input sequence. It has been performed analysis, modelling and processing the temporal dependence of the output amplitude for the backward-wave oscillator, described by system of the nonstationary nonlinear theory equations for the amplitude of electromagnetic field and motion of a beam. The data on the Lyapunov's exponents, Kolmogorov entropy, correlation coefficient between the actual and neural networks prognostic rows, referred to a temporal dependence of the output signal amplitude of the nonrelativistic (relativistic) backward-wave oscillator are listed. The combining the advanced algorithms of the modern chaos theory, concept of a compact geometric attractors and one of the effective neural network algorithms, or, in a more general using an effective model of artificial intelligence etc, could provide very adequate and quantitatively correct description of temporal evolutionary dynamics of most complicated systems, in particular, in the field of modern ultrahigh-frequency electronics

1. Introduction.

It is well known that the multiple physical, chemical, biological, technical, communication, economical, geophysical and other systems (devices) demonstrate the typical complex chaotic behaviour. In many important situations typical dynamics of these systems is a world of strong nonlinearity. Naturally, there is a quite considerable number of works, devoted to an analysis, modelling and prediction evolutionary dynamics of different complex systems from the viewpoint of theory of dynamical systems and chaos, fractal sets of physics and other systems [1-11]. In a series of papers [10-20] the authors have attempted to apply some of these methods in a variety of the physical, geophysical, hydrodynamic problems. In connection with this, there is an extremely important task on development of new, more effective approaches to the nonlinear modelling and prediction of chaotic processes in different complex systems (e.g.[1-22]). Especial interest attracts research of regular and chaotic dynamics of nonlinear processes in various classes of devices of the so-called relativistic ultrahigh-frequency electronics (see, e.g. [1-8]). Earlier we have developed an effective approach to analysis, modelling and forecasting chaotic evolutionary dynamics of complex systems , which is based on the based on the chaos theory algorithms, concept of geometric attractors, and algorithms for quantum neural network simulation [17-20]. We are developing a new approach to analyze complex system dynamics based on the chaos theory methods and neural network algorithms [21-27]. The basic idea of the construction of the cited approach to prediction of chaotic processes in complex systems is in the use of the traditional concept of a compact geometric attractor in which evolves the fundamental dynamic characteristics, plus the implementation of neural network algorithms. The existing so far in the theory of chaos prediction models are based on the concept of an attractor, and are described in a number of papers (e.g. [17-24]). For example, very useful review of the subfield that has attracted great interest in the last years, namely, the application of various approaches from complex network theory in

the context of nonlinear time series analysis, has been presented in ref. [21,26] (see refs. therein). The time series mining focuses more on indexing, clustering, classification, segmentation, discovery, and forecasting [21]. According to [21], there has been a considerable amount of rapid developments of data mining tools initiated by the advent of big data and cloud computing reflecting the increasing size and complexity of available datasets. It should be underlined that hitherto however, there has been practically no multiple overlap between the nonlinear time series analysis and complex neural network methods (e.g. [13-15]).

In this paper we present the results of the nonlinear simulation and forecasting chaotic evolutionary dynamics of such complex system as relativistic backward-wave oscillator [5-7] using earlier developed new combined method [22-27], based on the chaos theory algorithms, concept of geometric attractors, and algorithms for quantum neural network simulation.

2. Mathematical approach

As the main fundamental ideas of the our combined approach, based on the chaos theory algorithms, concept of geometric attractors, and algorithms for quantum neural network simulation [17-20], here we will concern only the principally important items of this studying. As usually, let us remind that from a mathematical point of view, it is a fact that in the phase space of the system an orbit continuously rolled on itself due to the action of dissipative forces and the nonlinear part of the dynamics, so it is possible to stay in the neighbourhood of any point of the orbit y (n) other points of the orbit y^r (n), $r = 1,2,..., N_B$, which come in the neighbourhood y (n) in a completely different times than n.

According to ref. [22-24,27], in terms of the modern theory of neural systems, and neuro-informatics (e.g. [12,15]), the process of modelling the evolution of the system can be generalized to describe some evolutionary dynamic neuro-equations (miemo-dynamic equations). Considering the neural network with a certain number of neurons, as usual, we can introduce the operators S_{ij} synaptic neuron to neuron u_i u_j, while the corresponding

synaptic matrix is reduced to a numerical matrix strength of synaptic connections: $W = || w_{ij} ||$. The operator is described by the standard activation neuro-equation determining the evolution of a neural network in time:

$$s_i^{'} = sign(\sum_{j=1}^{N} w_{ij} s_j - \theta_i), \qquad (1)$$

where $1<i<N$. Naturally it easily to understand that a state of the neuron (the chaos-geometric interpretation of the forces of synaptic interactions, etc.) can be represented by currents in the phase space of the system and its the topological structure is obviously determined by the number and position of attractors. To determine the asymptotic behavior of the system it becomes crucial an information aspect of the problem, namely, the fact of being the initial state to the basin of attraction of a particular attractor. The domain of attraction of attractors are separated by separatrices or certain surfaces in the phase space. Their structure, of course, is quite complex, but mimics the chaotic properties of the studied object. Then, as usual, the next step is a natural construction parameterized nonlinear function $F (x, a)$, which transforms:

$$\mathbf{y}(n \rightarrow \mathbf{y}(n + 1) = \mathbf{F}(\mathbf{y}(n), \mathbf{a}), \qquad (2)$$

and then to use the different (including neural network) criteria for determining the parameters a (see below). Although, according to a classical theorem by Kolmogorov-Arnold-Moser, the dynamics evolves in a multidimensional space, the size and the structure of which is predetermined by the initial conditions, this, however, does not indicate a functional choice of model elements in full compliance with the source of random data. One of the most common forms of the local model is the model of the Schreiber type [3] (see also [17-20]).

The easiest way to implement this program is in considering the original local neighbourhood, enter the model(s) of the process occurring in the neighbourhood, at the neighbourhood and by combining together these local models, designing on a global nonlinear model. The latter describes most of the structure of the attractor. As shown

Schreiber [3], the most common form of the local model is very simple:

$$s(n+\Delta n)=a_0^{(n)}+\sum_{j=1}^{d_A} a_j^{(n)} s\big(n-(j-1)\tau\big) \quad (3)$$

where Δn is the time period for which a forecast. The coefficients $a_j^{(k)}$, may be determined by a least-squares procedure, involving only points $s(k)$ within a small neighbourhood around the reference point. Thus, the coefficients will vary throughout phase space. The fit procedure amounts to solving (d_A+1) linear equations for the (d_A+1) unknowns. When fitting the parameters a, several problems are encountered that seem purely technical in the first place but are related to the nonlinear properties of the system. If the system is low-dimensional, the data that can be used for fitting will locally not span all the available dimensions but only a subspace, typically. Therefore, the linear system of equations to be solved for the fit will be ill conditioned. However, in the presence of noise the equations are not formally ill-conditioned but still the part of the solution that relates the noise directions to the future point is meaningless. Other details of modelling techniques are described, for example, in refs. [22-26].

The new element of our approach is using the NNW algorithm in forecasting nonlinear dynamics of chaotic systems [9,10]. In terms of the neuro-informatics and neural networks theory the process of modelling the evolution of the system can be generalized to describe some evolutionary dynamic neuro-equations. Imitating the further evolution of a system within NNW simulation with the corresponding elements of the self-study, self-adaptation, etc., it becomes possible to significantly improve the prediction of its evolutionary dynamics. The fundamental parameters to be computed are the Kolmogorov entropy (and correspondingly the predictability measure as it can be estimated by the Kolmogorov entropy), the LE, the KYD etc. The LE are usually defined as asymptotic average rates and they are related to the eigenvalues of the linearized dynamics across the attractor. Naturally, the knowledge of the whole LE allows to determine other important invariants such as the Kolmogorov entropy and the attractor's dimension. The Kolmogorov entropy is determined by the sum of the positive LE. The estimate of the dimension of the attractor is provided by the Kaplan and Yorke conjecture $d_L=j+\sum_{i=1}^{j}\lambda_i/\square\lambda_{j+1}\vee$, where j is such that $\sum_{i=1}^{j}\lambda_i>0$ and $\sum_{i=1}^{j+1}\lambda_i<0$, and the LE are taken in descending order.

3. Standard dynamical model of a backward-wave oscillator and neural networks modelling.

Nonlinear dynamics of the system (the backward-wave oscillator) is usually described by system of the nonstationary nonlinear theory equations for the evolution in time and space for the amplitude of the electromagnetic field and the motion of the beam (single model BWT) (e.g.[7,8]):

$$\frac{\partial F}{\partial \tau}-\frac{\partial F}{\partial \xi}=-\frac{\mathscr{L}}{\pi}\int_0^{2\pi} e^{-i\theta_\alpha}\,d\alpha, \quad (4)$$

$$\frac{\partial^2\theta}{\partial \xi^2}=-\mathscr{L}^2\,\mathrm{Re}\,Fe^{i\theta_\alpha}$$

with the corresponding boundary and initial conditions:

$$\theta_\alpha\big|_{\xi=0}=\alpha, \quad \frac{\partial\theta_\alpha}{\partial\xi}\bigg|_{\xi=0}=0, \quad (5)$$

$$F\big|_{\xi=1}=0, \quad F\big|_{\tau=0}=F(\xi,0),$$

Here $\theta(\xi,\tau,\theta_0)$ is a phase of the electron, which runs in a space of interaction with phase θ_0 in a field, $F(\xi,\tau)$ dimensionless complex amplitude of the wave $E(x,t)=\mathrm{Re}[E(x,t)\exp(i\omega_0 t-i\beta_0 x)]$, $\xi=\beta_0 Cx$ — the dimensionless coordinate, $L=\beta_0 lC=2\pi CN$- the dimensionless length of the interaction space, l is a length of a system, N-

is a number of slow waves, covering over the length of system, $C = \sqrt[3]{I_0 K_0/(4U)}$ is the known Pierce parameter , I_0 is a current of beam, U is an accelerated voltage, K_0-resistance of link of the slowing system,

$$\tau = \omega_0 C (t - x/v_0)(1 + v_0/v_{\mathrm{rp}})^{-1}$$

(i.e. $\tau\tau - \xi/v_0$) is the dimensionless "retarded" time, C is modified gain parameter (see more details in refs. [2-8]). In refs. [5-8] there is presented the detailed information about numerical solution of the corresponding system and performed an analysis of the fundamental topological and dynamical invariants. For numerical simulation we have used a software package, based on the photon echo neural network, which imitates evolutionary dynamics of the complex system [15]. It has the following key features: multi-layering, possibility of introducing training, feedback and controlled noise. There are possible the different variants of the connections matrix determination and binary or continuous sigmoid response (and so on) of the model neurons. In order to imitate a tuition process we have carried out numerical simulation of the neural networks for recognizing a series of patterns (number of layers N=5, number of images p=640; the error function:

$$SSE = \sum_{p=1}^{p_{\max}} \{.. \sum_{k=}^{k_{\max}} [t(p,k) - O(p,k)]^2\},$$

$$(6)$$

where $O(p,k)$ – neural networks output k for image p and $t(p,k)$ is the trained image p for output κ; SSE is determined from a procedure of minimization; the output error is $RMS=sqrt(SSE/P_{max})$; As neuronal function there is used function of the form: $f(x)=1/[1+\exp(-\delta x)]$. In our calculation there is tested the function $f(x,T)=\exp[(xT)^4]$ too.

In order to check the possibilities of the (neural networks package NNW-13-2003 [15]) of the multilayer neural networks, it has been performed processing noisy input sequence.

Fig. 2 demonstrates the results of modeling the dynamics of multilayer neural network for the case of noisy input sequence [24]. The input signal was the Gaussian-like pulse with adding a noise with intensity D. At a certain value of the parameter D (the variation interval .0001-0.0040) the network training process and signal playback is optimal. The optimal value of D is 0.00168.
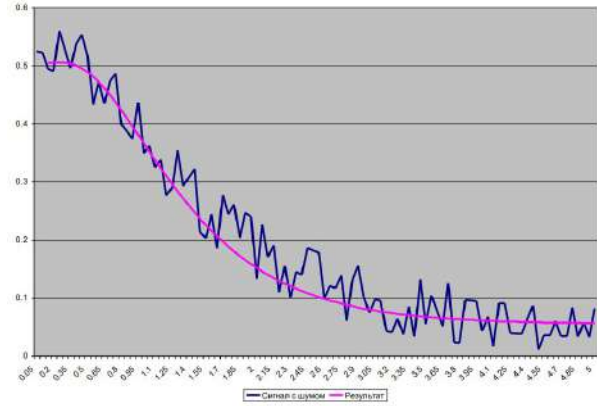
Figure 1. The results of modeling the dynamics of multilayer neural for the case of noisy input sequence (see text).

The farther step was in analysis, modelling and processing the temporal dependence of the out amplitude (solution of the system (4)-(5). For illustration we present the results of calculation the Lyapunov's exponents, the Kolmogorov entropy K_{entr} for the system, which is described by the system (4)-(5). The governing parameter L is equal 4.05.

Table 1. Numerical simulation data for the Lyapunov exponents (LE: $\lambda_1 - \lambda_4$) and the Kolmogorov entropy K (L=4.05)

λ_1	λ_2	λ_3	λ_4	K
0.261	0.0001	-0.0004	-0.528	0.26

In table 2 we present data on the correlation coefficient (r) between the actual and neural networks prognostic rows, referred to the temporal dependence of the output signal amplitude of the backward-wave oscillator (1) for L=4.05 (NN is number of neighbours for pre-ahead 100 points numerical series of the amplitude temporal dependence). The more details can be found in ref. [6,22-24]. One can see very closed coincidence between the actual and predicted row values for the temporal

dependence of the output signal amplitude of the backward-wave oscillator (tube).

Table 2. The correlation coefficient (r) between the actual and prognostic rows, referred to the temporal dependence of the output signal amplitude of the backward-wave oscillator (1) for L=4.05 (see text) .

NN	85	225	250
r	0.94	0.96	0.96

Analysis of the PC experiment results allows to make conclusion about sufficiently high-quality processing the input signals of very different shapes and complexity by the applied neural network. This is concerning the results of modelling the temporal dependence of the output signal amplitude of the backward-wave oscillator (1). We believe that the combining the advanced algorithms of the modern chaos theory, concept of a compact geometric attractors and one of the effective neural network algorithms, or, in a more general using an effective model of artificial intelligence etc, could provide very adequate, quantitatively correct description of temporal evolutionary dynamics of most complicated systems, in particular, in the field of modern ultrahigh-frequency electronics (see, e.g. [1-8]).

References

1. Benford J., Swegle, J., and Schamiloglu E., *High Power Microwaves*, 2nd ed. Taylor & Francis: N.-Y., **2006.**
2. Barker R. J. and Schamiloglu E Eds. *High-Power Microwave Sources and Technology*. Wiley: N.-Y., **2001**.
3. Ansari M.A., Thottappan M., Analysis, Design, and 3-D Simulation of a High-Efficiency Overmoded Nonuniform Relativistic Backward-Wave Oscillator. *IEEE Transactions On Electron Devices*, **2018.,** *65(3),* 1158-1163.
4. Levush B., Antonsen T.M., Bromborsky A., Lou W.R., Carmel Y., Theory of relativistic backward wave oscillator with end reflections. *IEEE Transactions on Plasma Sci.* **1992**, 20(3), 263-280.
5. Korovin, S.D., Kurkan, I.K., Rostov, V.V. *et al.* Relativistic backward wave oscillator with a discrete resonance reflector. *Radiophys. Quantum Electr.* **42,** 1047–1054 (1999).
6. Ryskin N.M., Titov V.N., Self-modulation and chaotic regimes of generation in a relativistic backward-wave oscillator with end reflections. *Radiophys.s Quantum Electr.***2001**, 44, 793- 806.
7. Bezruchko B.P., Bulgakova L.V., Kuznetsov S.P., Trubetskov D.I., Stochastical autovibrations and nonstability in the backward-wave tube. *Radiotechn. Electr.* **983**, N6, 1136-1139.
8. Glushkov A.V., Tsudik A.V., Ternovsky V.B., etal, Deterministic Chaos, Bifurcations and Strange Attractors in Nonlinear Dynamics of Relativistic Backward-Wave Tube. *Springer Proc. in Mathematics & Statistics*. **2021**, 363, 125-135.
9. Bunimovich L., Dynamical Systems, Ergodic Theory and Applications/ Bunimovich L.- Berlin: Springer, **2000.**
10. Sinai Y., *Ergodic Theory and Dynamical Systems*. Springer: Berlin, **2010**.
11. Lichtenberg, A., Liebermann, A., *Regular and chaotic dynamics*. Springer: N.-Y., **1992**.
12. Glushkov A.V.: *Methods of a chaos theory*. Astroprint: Odessa, **2012.**
13. Eckmiller, R., Malsburg, C. (Eds) *Neural Computers*, Springer: Berlin, **1998**.
14. Denker J. (Ed.) *Neural Networks for Computing*. AIP Publ.: N.-Y., **2000**.
15. Glushkov, A.V., Svinarenko, A.A., Loboda, A.V. *Theory of neural networks on basis of photon echo and its program realization.* TEC: Odessa. – 2004.
16. Khetselius, O.Yu. *Hyperfine structure of atomic spectra*. Astroprint: Odessa, **2008**
17. Abarbanel H., *Analysis of observed chaotic data.* Springer: N.-Y., **1996**.
18. Schreiber T., Interdisciplinary application of nonlinear time series methods. *Phys. Rep.* **1999**, 308, 1-64.
19. Kennel, M., Brown, R., Abarbanel, H. Determining embedding dimension for phase-space reconstruction using a geometrical construction. *Phys.Rev.A.* **1992**, *45*, 3403-3411.
20. Grassberger, P.; Procaccia, I. Measuring the strangeness of strange attractors. *Physica D*. **1983**, *9*, 189-208.

21. Zou Y, Donner R., Marwan N, Donges J., Kurths J, Complex network approaches to nonlinear time series analysis. *Phys. Rep.* **2019**, *787*, 1-79.

22. Khetselius, O., Forecasting evolutionary dynamics of chaotic systems using advanced non-linear prediction method. *In Dynamical Systems Applications;* Awrejcewicz, J. et al, Eds.; Łódz, **2013**; Vol T2, pp 145-152.

23. Khetselius O., New geometric attractor and neural networks approach to studying chaotic processes in photoelectronics systems. *Photoelectronics* **2013,** 22, 30-37.

24. Kondratenko P.A., Khetselius O.Yu., Ternovsky V.B., Zaichko P.A., Duborez A.V., Simulation chaotic dynamics of complex systems with using chaos theory, geometric attractors, and quantum neural networks. *Photoelectronics*. **2014,** *23,* 160-166.

25. Khetselius O.Yu., Brusentseva S.V., Tkach T.B. Studying interaction dynamics of chaotic systems within non-linear prediction method: Application to neurophysiology. *In Dynamical Systems Applications;* Awrejcewicz, J. et al, Eds.; Łódz, **2013**; Vol T2, pp 145-152.

26. Glushkov A.V., Khetselius O.Y., Nonlinear dynamics of complex neurophysiologic systems within a quantum-chaos geometric approach. *in: Glushkov A., Khetselius O., Maruani J., Brändas E. (Eds) Advances in Methods and Applications of Quantum Systems in Chemistry, Physics, and Biology*, Cham: Springer. **2021**, *33,* 291-303.

27. Glushkov A.V., Khetselius O.Yu., Kruglyak Yu.A., Ternovsky V.B., Ignatenko A.V., *Numerical methods in Quantum geometry and chaos theory, P.2.* TES: Odessa, **2015**.

Kondratenko P. O., Khetselius O. Yu.

SIMULATION CHAOTIC DYNAMICS OF RELATIVISTIC BACKWARD-WAVE OSCILLATOR WITH USING CHAOS THEORY AND QUANTUM NEURAL NETWORKS

Summary. Nonlinear simulation and forecasting chaotic evolutionary dynamics of such complex system as nonrelativistic (relativistic) backward-wave oscillator is treated using the new combined method, based on the chaos theory algorithms, concept of geometric attractors, and algorithms for quantum neural network simulation. It has been performed modeling the dynamics of multilayer photon echo neural network for the case of noisy input sequence. It has been performed analysis, modelling and processing the temporal dependence of the out amplitude for the backward-wave oscillator, described by system of the nonstationary nonlinear theory equations for the amplitude of the electromagnetic field and the motion of the beam. The data on the Lyapunov's exponents, Kolmogorov entropy and the correlation coefficient between the actual and neural networks prognostic rows, referred to the temporal dependence of output signal amplitude of the nonrelativistic (relativistic) backward-wave oscillator (tube) are listed. The combining the advanced algorithms of the modern chaos theory, concept of a compact geometric attractors and one of the effective neural network algorithms, or, in a more general using an effective model of artificial intelligence etc, could provide very adequate and quantitatively correct description of temporal evolutionary dynamics of most complicated systems, in particular, in the field of modern ultrahigh-frequency electronics.

Key words: Keywords: non-relativistic and relativistic backward-wave oscillator (tube), spectrum of radiation, spectroscopy, chaotic dynamics, concept of geometric attractor. quantum neural networks

Кондратенко П.О., Хецеліус О.Ю.

МОДЕЛЮВАННЯ ХАОТИЧНОЇ ДИНАМІКИ РЕЛЯТИВІСТСЬКОЇ ЛАМПИ ОБЕРНЕНОЇ ХВИЛІ З ВИКОРИСТАННЯМ ТЕОРІЇ ХАОСУ ТА КВАНТОВИХ НЕЙРОМЕРЕЖ

Резюме. Нелінійне моделювання та прогнозування хаотичної еволюційної динаміки такої складної системи, як лампа зворотної хвилі, розглядається за допомогою нового комбінованого методу, заснованого на алгоритмах теорії хаосу, концепції геометричних атракторів та квантово нейронно-мережевих алгоритмах моделювання. Проведено моделювання динаміки багатошарової фотонної нейромережі для випадку зашумленої вхідної послідовності. Проведено аналіз, моделювання та обробка часової залежності вихідної амплітуди для нерелятивістської (релятивістської) лампи, динаміка якої описується системою рівнянь нестаціонарної нелінійної теорії для амплітуди електромагнітного поля та руху пучка. Наведені дані про показники Ляпунова, ентропію Колмогорова, коефіцієнт кореляції між фактичним і нейронно-мережевими прогностичними даними часової залежності амплітуди вихідного сигналу розглянутої лампи зворотної хвилі тощо. Поєднання удосконалених алгоритмів сучасної теорії хаосу, концепції компактних геометричних атракторів і одного з ефективних нейронно-мережевих алгоритмів, або, у більш загальному сенсі, використання ефективної моделі штучного інтелекту тощо, може забезпечити дуже адекватний і кількісно коректний опис часової еволюційної динаміки найскладніших фізичних систем, зокрема, у сфері сучасної надвисокочастотної електроніки.

Ключові слова: нерелятивістська та релятивістська лампа зворотної хвилі, спектр випромінювання, спектроскопія, хаотична динаміка, концепція геометричного атрактору, квантові нейронні мережі

Tsudik A.V., Glushkov A.V.

Odessa State Environmental University, L'vovskaya str.15, Odessa
E-mail: tsudikav@gmail.com

SPECTROSCOPY AND DYNAMICS OF NONLINEAR PROCESSES IN RELATIVISTIC BACKWARD-WAVE TUBE WITH ACCOUNTING FOR EFFECTS OF SPACE CHARGE, DISSIPATION AND WAVE REFLECTIONS

An effective universal, approach to solving the problems of quantitative modelling and analysis of the fundamental characteristics of spectroscopy and dynamics of the nonlinear processes in relativistic microwave electronics devices, in particular, a relativistic backward wave tube (RBWT) has been developed and implemented. It has been performed modelling, analysis, and prediction of chaotic dynamics of RBWT with simultaneous consideration of not only relativistic effects, but also the effects of dissipation, presence of space charge, wave reflections at the ends of the decelerating system, etc in a wide range of changes at different values of control parameters, which are characteristic for the distributed relativistic electron-wave self-oscillating systems. From physical viewpoint the transition to chaos in the dynamics of the studied RBWT occurs according to the scenario everywhere in the sequence of period-doubling bifurcations, but with the growth of relativism, the dynamics become fundamentally complicated with the alternation of quasi-harmonic and chaotic regimes (including the appearance of the "beak" effect on the bifurcation diagram) and the transition everywhere intermittency to the high-D attractor.

1. Introduction

At the present time, the study of regular and chaotic dynamics of nonlinear processes in various classes of devices of the so-called relativistic ultra-high-frequency electronics definitely belongs to the number of extremely relevant and extremely complex directions in the physics of elements, systems and devices of electronics. It is well known that the development of relativistic microwave electronics and an increase in the pulse power of microwave radiation by several orders of magnitude was immediately caused by the appearance of high-current electronic accelerators [1-20]. The use of intense relativistic electron beams for the generation of microwave radiation already in the first experiments conducted led to the achievement of record levels of the output power of microwave generators [1-10]. At the moment, with the help of relativistic sources, practically the entire microwave range has been mastered, and for centimetre waves the level of pulse power is over 10^{10} W, for millimetre waves - 10^9 W. The main tasks of relativistic microwave electronics naturally include, first of all, the quantitative study of energy conversion mechanisms of high-intensity electron flows accelerated to relativistic velocities into powerful coherent electromagnetic radiation and, of course, their use in various devices for further application in various fields of science and technology, including, for the purposes of nano-sec location, special radio-technical applications, accelerators with an ultra-fast rate of particle energy collection. Powerful generators of chaotic oscillations of the microwave range are also of great applied interest in the tasks of plasma heating in controlled thermonuclear fusion installations, the construction of modern information transmission systems with such new possibilities as the use of dynamic chaos and other applications [1-6]. However, their application in practice faces a number of problems, in particular, it is about the need to increase the stability and efficiency of generation, increase the energy in the microwave pulse, maintain high coherence of radiation for high values of the generation power, the possibilities of wide adjustment of the generation frequency and so on.

The need to generate electromagnetic radiation of greater power contributed to the study of relativistic RBWT, which are actually the first devices implemented in a one-time mode based on a strong current electron accelerator. The peculiarity of RBWT is that the interaction of the microwave field with the electron beam is carried out through the synchronous harmonic of the wave, which propagates towards the electron flow. In contrast to non-relativistic BWT, the study of nonlinear dynamics of complex processes, different modes of functioning in RBWT is characterized by a significantly lower level of understanding. The inconsistency between the calculated and experimental values of the RBWT parameters is caused, in particular, by the use of simplified numerical models that do not adequately describe its relativistic dynamics, by an insufficiently correct approximation of accounting for only the 1st harmonic of the space charge, and by the observed decrease in the efficiency of the generator at an increase in the current of the high-current beam caused by the increase in the forces of the volume charge, etc.

Here we present a further development of an effective approach to solving the problems of quantitative modeling, analysis and forecasting of the characteristics of spectroscopy and the dynamics of nonlinear processes in relativistic microwave electronics devices, in particular, a relativistic backward wave tube (RBWT) [18-20]. There are presented the results of modelling, analysis, of the RBWT chaotic dynamics with simultaneous consideration of as relativistic effects, as also of the effects of dissipation, presence of space charge, wave reflections at the ends of the decelerating system, etc in a wide range of control parameters, which are characteristic for the distributed relativistic electron-wave self-oscillating systems.

2. Spectroscopy and dynamics of relativistic backward wave tube: Advanced model

Let us consider the system of equations of the dynamics of RWBT, which takes into account the influence of the space charge. It should be noted right away that when deriving the master equations of non-stationary nonlinear theory, in fact within the limits of the method of slowly changing amplitudes, the assumption is usually used that with the appropriate choice of independent variables $(\tau \propto t - x / v_0, \zeta \propto x)$. The equations of motion of electrons are written in the same form as in the stationary theory of RBWT [1-4,8-12,18-20]. The same is true when taking into account the influence of the space charge field [8,11,20]. Next, using the traditional notation of the space charge parameter introduced by Peirce, namely:

$$4QC = \left(\omega_p / \left(\omega_0 C \right) \right)^2, \qquad (1)$$

(where ω_p is a plasmas frequency, ω_0 – synchronization frequency, and C is the Peirce interaction parameter), it is possible to write down the system of equations of the dynamics of RBWT taking into account the influence of the space charge, leaving the excitation equation and boundary conditions unchanged. As a result, under the assumption of a wide beam, taking into account the movement of the influence of the space charge, we have the equation of dynamics:

$$\partial^2 \theta / \partial \zeta^2 = -L^2 \gamma_0^3 [(1 + \frac{1}{2\pi N} \partial \theta / \partial \zeta)^2$$
$$-\beta_0^2]^{\frac{3}{2}} Re[F \, exp(i\theta) +$$
$$+ \frac{4QC}{ik} \sum_{k=1}^{M} I_k \, exp(ik\theta)]$$

$$(2a)$$

$$\partial F / \partial \tau - \partial F / \partial \zeta + dF = -L \tilde{I}, \quad (2б)$$

$$I_k = -\frac{1}{\pi} \int_0^{2\pi} e^{-ik\theta} d\theta_0$$

$$(2c)$$

Note that in (2) the space charge field is represented by a Fourier series in terms of the variable θ, which characterizes the electron phase relative to the high-frequency filling of the wave field, and the finite number of members of the series M is taken into account.

in a number of works (see, e.g., [18-12,18-20]. According to this analysis, the physics of the effect is as follows: while the operating current of the BWT is relatively small, the space charge field does not play a significant role. But when the current increases, due to the occurrence of regrouping in the beam and due to feedback mechanism, from a certain point in time a new automodulation mode may appear in the system. Further, with the increase of the current due to the increase of the space charge, from a physical point of view, the existing Coulomb repulsion prevents the convergence of electrons and their mutual overtaking and, accordingly, the occurrence of rearrangement, which qualitatively should lead to the suppression of automodulation in the system. That is, the influence of the desired effect can be considered as a rather interesting means of qualitatively changing the intensity of one or another mode, in particular, automodulation or even the dynamic chaos mode. At the same time, it should be remembered that only in specific numerical or experimental studies of a certain BWT, an accurate quantitative picture of the impact of the effect can be established. It should be noted that there are currently no qualitative and quantitative data on the indicated effect for RBWT. Another significant factor that can affect the dynamics of real BWT is the effect of the presence of wave reflections at the ends of the decelerating system The qualitative physics of the effect is quite obvious (see, e.g., [1-4,9-12,20]). In fact, it is well known that at the end of the system, where the energy radiated by the beam arrives, only a certain part of it is transmitted to the output path, and the other part is transformed into reflected waves that transfer energy in the opposite direction (in the direction of electron motion). Since such waves are not synchronous with the beam in terms of their phase velocity, they should probably be expected to propagate without significant interaction with the electron beam. At the same time, having reached the opposite end of the system, the sought waves will be partially absorbed, partially reflected, and part of the energy will be transformed back into a working wave, that is, an additional feedback mechanism may take place. Further, if the

working and reflected waves are marked with "+" and "-" signs, i.e.:

$$E_{+} = \mathrm{Re}\left[\tilde{E}_{+}\left(x,t\right) e^{i\omega_0 t - i\beta_0 x} \right],$$

$$E_{-} = \mathrm{Re}\left[\tilde{E}_{-}\left(x,t\right) e^{i\omega_0 t + i\beta_0 x} \right].$$

(3)

then for the corresponding complex amplitudes the equations are true [14]:

$$v_{\mathrm{гр}}^{-1}\frac{\partial \tilde{E}_{+}}{\partial t} - \frac{\partial \tilde{E}_{+}}{\partial x} = -\frac{1}{2}\beta_0^2 K_0 \tilde{I}_1 \quad (4a)$$

$$v_{\mathrm{гр}}^{-1}\frac{\partial \tilde{E}_{-}}{\partial t} + \frac{\partial \tilde{E}_{-}}{\partial x} = 0 \quad (4b)$$

with boundary conditions at the ends of the retarding system

$$\tilde{E}_{-}\left(0,t\right) = R_0 \tilde{E}_{+}\left(0,t\right),$$

$$\tilde{E}_{+}\left(l,t\right) = R_l \tilde{E}_{-}\left(l,t\right) \quad (5)$$

where R_0 and R_l – complex reflection coefficients at the left and right ends of the deceleration system.

Since, the general solution for the amplitude of the reflected wave can be written as

$$\tilde{E}_{-}\left(x,t\right) = f\left(x - v_{\mathrm{гр}}t\right),$$

where f – arbitrary function, this variable can be excluded from consideration, leaving only the equations for the operating wave and the boundary condition with a delay:

$$v_{\mathrm{гр}}^{-1}\frac{\partial \tilde{E}_{+}}{\partial t} - \frac{\partial \tilde{E}_{+}}{\partial x} = -\frac{1}{2}\beta_0^2 K_0 \tilde{I}_1 , \quad (6)$$

$$\tilde{E}_{+}\left(l,t\right) = \rho e^{i\varphi}\tilde{E}_{+}\left(0,t - l / v_{\mathrm{гр}}\right).$$

Here ρ and φ are a modulus and a phase of the product of complex reflection coefficients $R_0 R_l = \rho e^{i\varphi}$.

The master system of equations for RBWT with taking into account wave reflections at the ends of the decelerating system, can be written in the following form:

$$\frac{\partial^2 \theta}{\partial \zeta^2} = -\mathrm{Re}\left[F \exp(i\theta) \right],$$

$$\partial F / \partial \tau - \partial F / \partial \zeta + \mathrm{d}F = \frac{-L}{\pi} \int_0^{2\pi} e^{-ik\theta} d\theta_0 \quad (7a)$$

$$\theta \big|_{\zeta=0} = \theta_0 , \quad \frac{\partial \theta}{\partial \zeta}\big|_{\zeta=0} = 0 , \quad (7b)$$

$$F(L,t) = \rho e^{i\varphi} F(0, \tau - sL), \quad (7c)$$

where $s = (1-u)/(1+u)$ — parameter of group desynchronization, $u = \upsilon_0 / \upsilon_{\mathrm{rp}}$ — dimensionless group velocity.

From a physical point of view, the parameter s (or u) is responsible for the frequency distance between adjacent modes that form an equidistant spectrum. It is obvious that the frequencies at which the amplitude of stimulated oscillations is maximal are the natural frequencies of the corresponding resonator. Given this condition, the equidistant spectrum will be:

$$\varphi_n = (2\pi n + \phi)/(1+s), \quad (8)$$

accordingly, the mode distribution is determined by the value $2\pi/(1+s)$.

Obviously, from the point of view of the influence on the dynamics of processes in the RBWT, it is worth expecting a quantitative influence of the presence of wave reflections at the ends of the retarding system of the BWT. But, one could guess that only in specific numerical or experimental studies of a certain RBWT there can be established a precise quantitative picture of the influence of this effect. To carry out numerical calculations with the aim of solving systems of differential equations of the type (2) and others, and further numerical modeling of the dynamics of nonlinear processes in RBWT, a set of programs is applied, which is based on the use of finite-difference schemes of the "predictor-corrector" type and the Thomson sweep method for solving the corresponding system of linear algebraic equations (e.g.[21-26]).

3. New physical results and conclusions

In this subsection, for the first time in the physics of RBWT, we will present the results of a full numerical simulation taking into account all above listed effects. As a master system, a system of differential equations with corresponding boundary conditions is taken: (2)–(7). It should be noted that in such a setting the problem turns out to be very difficult even from a numerical point of view, so below we specify all the input parameters, based, first, on the correspondence to the parameters of real devices (see [1-4,8-12]), secondly, fixing some parameters from the very beginning, keeping in mind the main goal - to investigate the nonlinear dynamics of a specific RBWT, taking into account most of the key physical effects in the chaotic regime, with the clarification and construction of the corresponding bifurcation diagrams in the "relativistic factor - bifurcation parameter" plane, proportional to the electron beam current $L = 2\pi C N / \gamma_0$.

The following initial values were taken as input parameters: relativistic factor $\gamma_0 = 1.5$ (further on, we will increase γ_0 by 2 and 4 times), electric length of the interaction space $N = k_0 l/(2\pi) = 10$, electron speed $v_0 = 0.75s$, $v_{\mathrm{rp}} = 0.25s$, dissipation parameter D=5dB, starting parameters of reflection: s=0.5, ρ=0.7, $0 < \varphi < 2\pi$. The choice of φ is due to the fact that the dependence on it is periodic. The influence of reflections leads to the fact that the bifurcation parameter L begins to depend on the phase φ of the reflection parameter. The obvious optimal values of the parameter (formula 8) are those for which φ_0 is close to the resonance frequencies, e.g., $\varphi_0 \sim \pi$. It is obvious that self-excitation of the system will

be difficult if φ_0 is located in the center of the interval between two natural frequencies. It is not difficult to estimate the most optimal and suboptimal phase values for self-excitation, respectively, $\varphi \sim 0.48\pi$ and $\varphi \sim 1.48\pi$. In the case of sufficiently large values of the parameter ρ (namely, this case should be considered the most interesting and complex, since for weak reflections the dynamics are similar to those discussed above, and the automodulation mechanism is related to the amplitude nonlinearity of the distributed system), the corresponding automodulation limit will obviously have a complex shape.

In the region $0<\varphi<\pi$ modes with indices n= -1,-2,-3 will be excited. As a result of the strong interaction, the second mode is suppressed, which leads to a two-frequency generation in the stationary mode. In the region $\pi<\varphi<2\pi$ self-modulation occurs for L values smaller than in the previous case. At the same time, the presence of dissipation will increase the corresponding L values.

Fig.1 shows the numerical data for the normalized field amplitude

$$F(\zeta,\tau) = \tilde{E} \, / \left(2\beta_0 U C^2 \right)$$

with the input parameters specified above. The corresponding theoretical results of test modeling of non-stationary processes in RBWT at the values of the bifurcation parameter L: (a) – 2.7, (b) – 3.5, (c) – 4.0.

It should be noted that, in contrast to the dynamics of RBWT, considered in the previous subsection, in the implemented model, all the considered effects have a significant impact. First, taking into account the effect of space charge leads to a certain suppression of automodulation, taking into account dissipation leads to an increase in the bifurcation parameter L, at which automodulation is realized.

The effect of strong reflection leads to a complex picture in the output spectrum of the system. From the beginning, there is a single-frequency generation corresponding to the first mode, but as L increases, this mode is suppressed by the second mode (n=-2).

At L=2.7 (see Fig. 1a), modes with n=-2, -4 have the largest amplitudes. With further growth of the bifurcation parameter L above 3,

both even and odd modes are excited (n=0, -1, -2, -3, -4); in fact, the automodulation mode is implemented, while two maxima of the field amplitude, spreading from the collector end to the gun end, are formed periodically along the length of the system, which is the reason for the doubling of the automodulation period.

(a)

(b)

(c)
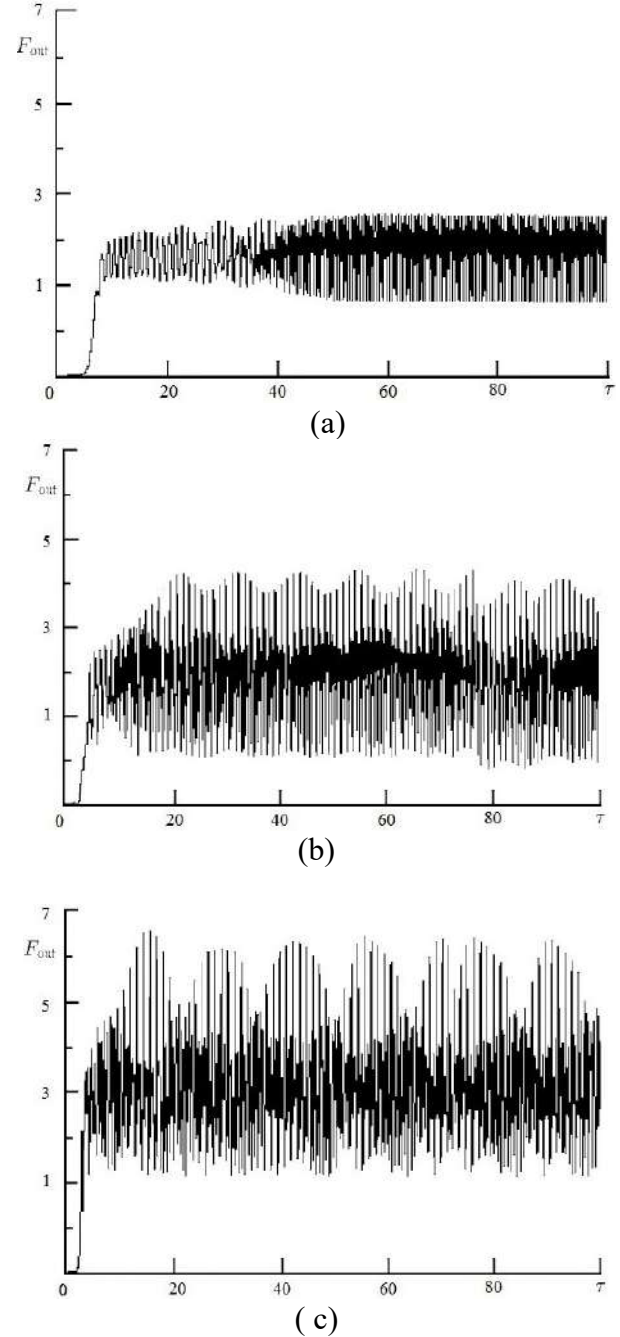
Figure 1. - Numerical data on the time dependence of normalized field amplitude $F(\zeta,\tau) = \tilde{E} \, / \left(2\beta_0 U C^2 \right)$ (our data with accounting for dissipation, a space charge, wave reflections) for bifurcation parameter (a) 2.7; (b)3.5; (c)4.0; (other parameters: γ_0=1.5, $N=\dot{\iota}10$, s=0.5, ρ=0.7, φ=1.3π).

In fig. 2 shows the calculated spectrum of the output signal for the value of the parameter L=3.9-4 (other parameters of the system are as follows: γ_0=1.5, $N=¿10$, s=0.5, ρ=0.7, φ =1.3π).
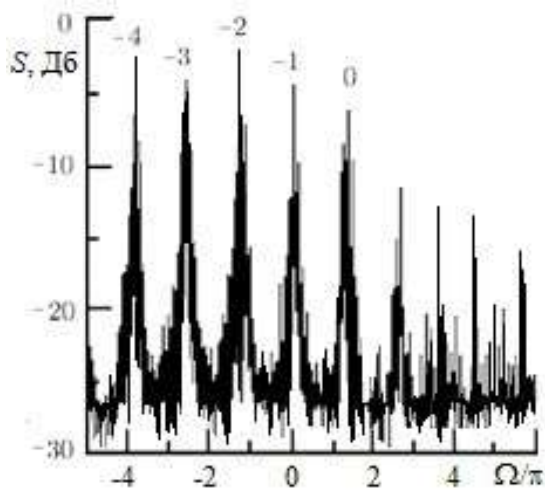
Figure 2 – Theoretical spectrum of the output signal for the value of the parameter L=3.9-4 (other parameters of the system are as follows: γ_0=1.5, $N=¿10$, s=0.5, ρ=0.7, φ=1.3π).

With a further increase in L, the quasi-periodic self-modulation mode is established again (Fig. 1b; period 13.8 ns) and, finally, a significantly chaotic mode appears (Fig. 1c). It is important that the results obtained by us are very well correlated with the results of [8,11], where the dynamics of the BWT is studied with taking into account the effect of reflections, but without taking into account the effect of dissipation and the influence of the space charge field, etc. It is of a great importance to underline that from physical viewpoint the transition to chaos in the dynamics of the studied RBWT occurs according to the scenario everywhere in the sequence of period-doubling bifurcations, but with the growth of relativism, the dynamics become fundamentally complicated with the alternation of quasi-harmonic and chaotic regimes (including the appearance of the "beak" effect on the bifurcation diagram) and the transition everywhere intermittency to the high-D attractor [15,16,18].

References

1. Ginzburg, N.S.; Zaitsev, N.A.; Ilyakov, E.; Kulagin, V.I.; Novozhilov, Yu. Rosenthal P., Sergeev V., Chaotic generation in backward wave tube of the megawatt power level. *Journ. of Techn.Phys*. **2001, 71,** 73-80.
2. Ginsburg, H. S.; Kuznetsov, S.P.; Fedoseyev, T.N. Theory of transients in relativistic BWO. *Izv. Vuzov. Ser. Radiophys*. **1978,** *21,* 1037-1052.
3. Glushkov, A.V. *Atom in an electromagnetic field*. KNT: Kiev, **2005**.
4. Levush B., Antonsen T.,Bromborsky A., Lou W., Relativistic backward wave oscillator: theory and experiment/ *Phys.Fluid*. **1992**, B4(7), 2293-2299.
5. Levush B., Antonsen T.M., Bromborsky A., Lou W.R., Carmel Y., Theory of relativistic backward wave oscillator with end reflections. *IEEE Transactions on Plasma Sci.* **1992**, 20(3), 263-280.
6. Glushkov, A.V. *Relativistic Quantum theory. Quantum mechanics of atomic systems*. Astroprint: Odessa, **2008**.
7. Glushkov A., Prepelitsa G., Svinarenko A., Zaichko P., Studying interaction dynamics of the non-linear vibrational systems within non-linear prediction method (application to quantum autogenerators) *In: Dynamical Systems Theory;* Awrejcewicz J. et al; Łódz, **2013**; Vol T1, pp 467-477.
8. Ryskin N.M., Titov V.N., Self-modulation and chaotic regimes of generation in a relativistic backward-wave oscillator with end reflections. *Radiophysics and Quantum Electronics.* **2001**, 44, 793-806.
9. Ryskin N.M., Titov V.N., The transition to the development of chaos in a chain of two unidirectionally-coupled backward-wave tubes. *Journ.Techn.Phys*. **2003**. 73, 90-94.
10. Kuznetsov A.P., Kuznetsov S.P., Ryskin N.M., Isaeva O.B., *Non-linearity: From oscillations to chaos*.-Moscow: NIS RHD.-2006.
11. Kuznetsov A.P., Shirokov A.P., Discretre model of relativistic backward-wave tube. *Russian J.of Phys. Ser.PND*. **1997**. 5, 76-83.

12. Kuznetsov S.P., Trubetskov D.I., Chaos and hyperchaos in backward-wave tube. *Russian Journ.of Phys. Ser.Radiophys.*- **2004**, XLVII(5), 1-8

13. Chernyakova, Y.G., Ignatenko A.V., Vitavetskaya L.A. Sensing the tokamak plasma parameters by means high resolution x-ray theoretical spectroscopy method: new scheme. *Sensor Electr. and Microsyst. Techn.* **2004**, *1*, 20-24

14. Ignatenko A., Svinarenko A., Prepelitsa G., Perelygina T., Optical bi-stability effect for multi-photon absorption in atomic ensembles in a strong laser field. *Photoelectronics*. **2009**, *18*, 103-105.

15. Grassberger, P. ; Procaccia, I. Measuring the strangeness of strange attractors. *Physica D*. **1983**, *9*, 189-208.

16. Khetselius, O., Forecasting evolutionary dynamics of chaotic systems using advanced non-linear prediction method *In Dynamical Systems Applications;* Awrejcewicz, J., Kazmierczak M., Olejnik, P., Mrozowski, J., Eds.; Łódz, **2013**; Vol T2, pp 145-152.

17. Khetselius, O.Yu. *Quantum structure of electroweak interaction in heavy finite Fermi-systems.* Astroprint: Odessa, **2011**.

18. Glushkov, A.V. Tsudik, D.A. Novak, O.B. Dubrovsky, Chaotic dynamics of relativistic backward-wave tube with accounting for space charge field and dissipation effects: New effects. *Photoelectronics.* **2018.** 27, 44-51.

19. Tsudik A.V., Glushkov A.V., Ternovsky V., Zaichko P., Advanced computing topological and dynamical invariants of relativistic backward-wave tube time series in chaotic and hyperchaotic regimes *Photoelectronics.* **2020.** Vol.29. P.110-117.

20. Glushkov A.V., Tsudik A.V., Ternovsky V.B., etal, Deterministic Chaos, Bifurcations and Strange Attractors in Nonlinear Dynamics of Relativistic Backward-Wave Tube. *Springer Proc. in Mathematics & Statistics*. **2021**, 363, 125-135.

21. Ivanova, E.P., Ivanov, L.N., Glushkov, A., Kramida, A. High order corrections in the relativistic perturbation theory with the model zeroth approximation, Mg-Like and Ne-Like Ions. *Phys. Scripta* **1985**, *32,* 513-522.

22. Khetselius, O.Yu. *Hyperfine structure of atomic spectra*. Astroprint: Odessa, **2008**

23. Glushkov, A.V., Ivanov, L.N. Radiation decay of atomic states: atomic residue polarization and gauge noninvariant contributions. *Phys. Lett. A* **1992,** *170,* 33-36.

24. Ivanova, E., Glushkov, A. Theoretical investigation of spectra of multicharged ions of F-like and Ne-like isoelectronic sequences. J. Quant. Spectr. and Rad. Tr. **1986**, *36*(2), 127-145.

25. Khetselius, O. Relativistic perturbation theory calculation of the hyperfine structure parameters for some heavy-element isotopes. *Int. J. Quant.Chem.* **2009,** *109,* 3330-3335.

26. Svinarenko, A.A., Mischenko, E.V., Loboda A.V., Dubrovskaya Yu.V., Quantum measure of frequency and sensing the collisional shift of the ytterbium hyperfine lines in medium of helium gas. *Sensor Electr. and Microsyst. Techn.* **2009**, N1, 25-29.

Tsudik A.V., Glushkov A.V.

SPECTROSCOPY AND DYNAMICS OF NONLINEAR PROCESSES IN RELATIVISTIC BACKWARD-WAVE TUBE WITH ACCOUNTING FOR EFFECTS OF SPACE CHARGE, DISSIPATION AND WAVE REFLECTIONS

Summary. An effective universal, approach to solving the problems of quantitative modeling, analysis and forecasting of the characteristics of spectroscopy and the dynamics of nonlinear processes in relativistic microwave electronics devices, in particular, a relativistic backward wave tube (RBWT) has been developed and implemented. It has been performed

modelling, analysis, and prediction of chaotic dynamics of RBWT with simultaneous consideration of not only relativistic effects, but also the effects of dissipation, presence of space charge, wave reflections at the ends of the decelerating system, etc in a wide range of changes at different values of control parameters, which are characteristic for the distributed relativistic electron-wave self-oscillating systems. From physical viewpoint the transition to chaos in the dynamics of the studied RBWT occurs according to the scenario everywhere in the sequence of period-doubling bifurcations, but with the growth of relativism, the dynamics become fundamentally complicated with the alternation of quasi-harmonic and chaotic regimes (including the appearance of the "beak" effect on the bifurcation diagram) and the transition everywhere intermittency to the high-D attractor.

Key words: relativistic theory, backward-wave tube, spectroscopy, chaotic dynamics

PACS 42.55.-f

Цудік А.В., Глушков О.В.

СПЕКТРОСКОПІЯ ТА ДИНАМІКА НЕЛІНІЙНИХ ПРОЦЕСІВ В РЕЛЯТИВІСТСЬКІЙ ЛАМПІ ЗВОРОТНОЇ ХВИЛІ З УРАХУВАННЯМ ЕФЕКТІВ ПРОСТОРОВОГО ЗАРЯДУ, ДИСИПАЦІЇ ТА ВІДБИТТЯ ХВИЛІ

Резюме. Розроблено новий ефективний універсальний підхід до вирішення задач кількісного моделювання, аналізу та прогнозування характеристик спектроскопії та динаміки нелінійних процесів у пристроях релятивістської мікрохвильової електроніки, зокрема? релятивістської лампи зворотного хвилі (РЛЗХ). Виконано моделювання та фізичний аналіз хаотичної динаміки РЛЗХ з одночасним врахуванням як релятивістських ефектів, так й ефектів дисипації, наявності просторового заряду, відбиття хвиль на кінцях системи, що сповільнюється, тощо, в при різних значеннях керуючих параметрів, характерних для розподілених релятивістських електронно-хвильових автоколивальних систем. З фізичної точки зору перехід до хаосу у динаміці досліджуваної РЛЗХ відбувається за сценарієм через послідовність біфуркацій подвоєння періоду, але з ростом релятивізму динаміка принципово ускладнюється і зводиться до чередування квазігармонійних та хаотичних режимів (включаючи появу нового феноменального ефекту «дзьоба» на відповідній біфуркаційній діаграмі) і в кінцевому результаті переходу через переривчастість до високорозмірного атрактору.

Ключові слова: релятивістська теорія, лампа зворотної хвилі, спектроскопія, хаотична динаміка

This article has been received in October 26, 2021

96

V.B. Ternovsky

Odessa National Maritime Academy, Didrikhson str. 4, Odessa

E-mail: ternovskyvb@gmail.com

OPTIMIZED RELATIVISTIC MANY-BODY PERTURBATION THEORY IN CALCULATIONS OF ATOMIC SPECTRAL AND RADIATION CHARACTERISTICS: Eu ATOM

The new formalism of the relativistic gauge-invariant perturbation theory (RMBPT-ODF) with the optimized Dirac-Fock approximation and a generalized energy approach is applied to the study of energy, radiation, and spectroscopic characteristics of a group of heavy atomic systems, in particular, energy levels and transition probabilities and oscillator strengths of the transitions $4f^7(^8S)6s^2 \, ^8S_{7/2} \, 4f^7(^8S)6s6p \, ^8P_{5/2,7.2,9.2}$, $4f^7(^8S)6s7p \, ^8P_{5/2,7/2}$, $4f^7(^8S)6s8p \, ^8P_{9/2,7/2}$ in spectrum of the europium atom Eu I. It is shown that the required formalism, in comparison with the standard non-optimized relativistic Hartree-Fock and Dirac-Fock methods, allows obtaining more accurate data both on energies and amplitudes and probabilities of radiative transitions, which is due to the use of the optimized zero ODF approximation, a fairly complete and effective account of complex many-body exchange-correlation effects. The contribution due to the polarization of the core reaches 30% of the value of the oscillator strength; the value of the calibration-invariant contribution to the radiation width is fractions of a percent, in contrast to all existing methods of modern atomic spectroscopy, for which the contribution reaches 5-50%.

1. Introduction

The study of energy, radiation, spectroscopic, and generally structural properties of heavy neutral and highly ionized atoms (so-called multiply charged ions) is of fundamental fundamental importance in many areas of atomic physics (theory of atomic spectra, spectroscopy, theory of spectral lines), astrophysics , plasma physics, laser physics, etc [1-34]. The development of new directions in the field of atomic optics and spectroscopy, laser physics and quantum electronics, such as precision spectroscopy of heavy and superheavy atoms and multi-charged ions, the latest astrophysical research, pulsed heating methods in experiments on controlled thermonuclear synthesis, the creation of fundamentally of new schemes of lasers in VUF, as well as further improvement and development of new experimental technologies, in particular with the use of new laser technologies, accelerators, etc., determines the urgent need to solve urgent and important tasks of atomic optics and laser physics on to a fundamentally new relativistic level of theoretical consistency and accuracy. In the last decade, relativistic theoretical spectroscopy of heavy both ordinary and exotic atomic systems, the so-called relativistic multielectron and hadronic atoms, as well as heavy multi-charged ions, which covers the ultraviolet and X-ray spectrum ranges, has been actively developing. It is well known that the study of the structure of the spectral lines of such atomic systems is of great interest for the further development of atomic and nuclear theories, as well as the theory of fundamental interactions, including electroweak and strong. Experiments to determine the properties of the splitting of spectral lines, in particular, the study of the characteristics of the ultrafine structure, make it possible to specify the values of the nuclear magnetic moments of various isotopes and to check the accuracy of various computational models used for the theoretical description of atomic nuclei in heavy systems [1-25].

Most of the standard methods of the theory, despite the known progress in their development, are not able to provide a simultaneous

precise description of all the listed groups of effects and corrections. Indeed, despite numerous attempts to develop precise methods for describing the spectra of heavy atomic systems (the mega-Dirac-Fock (DF=DF) method, the R-matrix method, the relativistic coupled-cluster method, various versions of the TK etc.; packages: "SUPERSTRUCTURE", "Dirac"-package, "Beta-package", "QED", "GRASP", "BERTHA", etc.), a whole set of problems of simultaneous high-precision calculation remains unsolved above mentioned effects. Moreover, there is no information about a rather large number of particularly heavy and superheavy atoms (as well as the corresponding multicharged ions) of Mendeleev's periodic table, and the situation related to the study of the characteristics of superheavy elements has acquired a particularly crisis character due to the lack of any reliable data. A similar complex of complex theoretical problems is also observed in the relativistic spectroscopy of heavy hadronic (in particular, kaonic) multi-electron atoms, for most of which no reliable spectroscopic data are given in the literature [26-29]. In our paper we present a formalism of the relativistic gauge-invariant perturbation theory (RMBPT-ODF) with the optimized Dirac-Fock (DF) approximation, which is applied to the study of energy, radiation, and spectroscopic characteristics of a group of heavy atomic systems, in particular, energy levels and transition probabilities and oscillator strengths of the transitions $4f^7(^8S)6s^2$ $^8S_{7/2}$ $4f^7(^8S)6s6p$ $^8P_{5/2,7.2,9.2}$, $4f^7(^8S)6s7p$ $^8P_{5/2,7\backslash2}$, $4f^7(^8S)6s8p$ $^8P_{9/2,7\backslash2}$ in spectrum of the europium atom Eu I. A generalized energy approach is used to calculate the transitions probabilities and oscillator strengths.

2. Relativistic many-body perturbation theory with optimized Dirac-Fock zeroth approximation

As the method of computing is earlier presented in detail, here we are limited only by the key topics [25-30]. The theoretical foundations of our method of combined relativistic RMBPT with optimized Dirac-Fock-Breit (ODF) zeroth approximation and generalized energy approach for consistent description and calculation of energetic, radiative, and spectroscopic characteristics of heavy multi-electron atomic systems with consistent, maximally precise consideration of relativistic, nuclear effects (including the effects of Breit-Rosenthal-Crawford-Schawlow, as well as Bohr-Weisskopf) and radiation QED corrections (including the radiative corrections for vacuum polarization, the self-energy part of the Lamb shift, as well as corrections of higher orders of PT, in particular, Källen-Sabry of order $\alpha^2(\alpha Z)$ and Wichmann-Kroll of order $\alpha(Z\alpha)^n$, etc. The starting basis for the development of our new - approach to the calculation of energy, radiation and spectroscopic characteristics of heavy atomic systems is the adiabatic formalism of Gell-Mann and Lowe and the ab initio PT formalism with using the Feynman diagram technique. The well-known S-matrix adiabatic formalism of Gell-Mann and Lowe leads to PT series on the coupling constant (in our case, the electromagnetic interaction) for shifts dE. The PT series are diagrammed in the standard way (using the usual technique of Feynman diagrams). At the same time, it is natural that new approximations in the theory of multi-electron systems are conveniently formulated as methods of summarizing Feynman diagrams of a certain type.

In the theory of the relativistic atom, there is a technique related to the diagonalization of the own matrix M for calculating the energy shifts dE of the states, and the corresponding matrix elements are complex. For a multi-electron atomic system in the relativistic theory, the energy shift of the excited state is represented in the standard complex form as [1,31-35]:

$$\Delta E = \mathrm{Re}\Delta E + i\,\mathrm{Im}\Delta E, \qquad (1a)$$

$$\mathrm{Im}\,\Delta E = -\Gamma/2, \qquad (1\text{б})$$

Their imaginary part of ΔE =dE is connected with the radiation decay (radiation) possibility. The whole calculation of the energies and decay probabilities of a non-degenerate excited state is reduced to the calculation and diagonalization of the complex matrix M.

The complex secular matrix M is represented in the form [1,31]:

$$M = M^{(0)} + M^{(1)} + M^{(2)} + M^{(3)}. \tag{2}$$

where $M^{(0)}$ is the contribution of the vacuum diagrams of all order of PT, and $M^{(1)}$, $M^{(2)}$, $M^{(3)}$ those of the one-, two- and three- quasiparticle diagrams respectively. $M^{(0)}$ is a real matrix, proportional to the unit matrix. It determines only the general level shift. We have assumed $M^{(0)} = 0$. The diagonal matrix $M^{(1)}$ can be presented as a sum of the independent one-quasiparticle contributions. For simple systems (such as alkali atoms and ions) the one-quasiparticle energies can be taken from the experiment. The first two order corrections to $\mathrm{Re}\, M^{(2)}$ have been analyzed previously using Feynman diagrams (look Ref. in [2,3]). In the second order, there are two kinds of diagrams: polarization and ladder ones.

The polarization diagrams take into account the quasiparticle interaction through the polarizable core, and the ladder diagrams account for the immediate quasiparticle interaction [31-36].

Some of the ladder diagram contributions as well as some of the three-quasiparticle diagram contributions in all PT orders have the same angular symmetry as the two-quasiparticle diagram contributions of the first order. These contributions have been summarized by a modification of the central potential, which must now include the screening (anti-screening) of the core potential of each particle by the two others. The additional potential modifies the one-quasiparticle orbitals and energies. The relativistic polarization potential [39] by Glushkov is used in our method.

In the QED theory, the photon propagator D(12) plays the role of this interaction. Naturally the analytical form of D(12) depends on the gauge, in which the electrodynamical potentials are written. Interelectron interaction operator with accounting for Breit interaction has been taken as follows:

$$V(r_i r_j) = \exp(i\omega r_{ij}) \cdot \frac{(1 - \alpha_i \alpha_j)}{r_{ij}}, \tag{3}$$

where, as usually, α_i are the Dirac matrices. In general, the results of all approximate calculations depended on the gauge. Naturally the correct result must be gauge-invariant. The gauge dependence of the amplitudes of the photoprocesses in the approximate calculations is a known fact and is investigated by Grant, Armstrong, Aymar and Luc-Koenig, Glushkov-Ivanov-Ivanova et al (see review in [9,32]). Grant has investigated the gauge connection with the limiting non-relativistic form of the transition operator and has formulated the conditions for approximate functions of the states, in which the amplitudes of the photo processes are gauge invariant (see review in [9]). These results remain true in the energy approach because the final formulae for the probabilities coincide in both approaches. Glushkov-Ivanov have developed a new relativistic gauge-conserved version of the energy approach [32]. In ref. [30,35-40] it has been developed its further generalization. Here we applied this approach for generating the optimized relativistic orbitals basis in the zeroth approximation of the many-body PT.

The fundamental point of our approach is the selection of the optimized Dirac-Fock (ODF) potential as the zero approximation, and the procedure for constructing a one-quasiparticle representation is based on the principle of constructing optimized atomic bases in compliance with the principle of gauge invariance, in particular, by minimizing gauge-invariant contributions to the radiative widths of the levels. Here it is important to emphasize that this procedure is implemented in this approach for the first time, in contrast to alternative approaches in relativistic spectroscopy of heavy atoms and ions, where zero approximations were built: unoptimized (standard) DF, Dirac-Hartree-Slater, Dirac-Kohn-Sham (DKS), X✔, relativistic HF, Hartree-Fock-Slater, as well as model methods (model potential, pseudopotential, etc.). The function of a certain state of the system (ASF) with the total angular momentum J, with its z-projection M and parity p has the form:

$$\Psi_s(JM^P) = \sum_m c_m(s)\Phi(\gamma_m JM^P) \tag{4}$$

$$\Phi(\gamma_m JM^P) = \sum_i d_i \begin{vmatrix} \psi_1(1) & \cdots & \psi_1(N) \\ \vdots & \ddots & \vdots \\ \psi_N(1) & \cdots & \psi_N(N) \end{vmatrix} \tag{5}$$

where c - configuration mixing factors for the state s; $\Phi(\gamma_m JM^P)$ - state functions of a certain configuration, that is, the Slater determinant of 4-component Dirac bispinors; ψ_i - one-electron relativistic wave functions.

The one-electron wave function can be defined as

$$\psi = \frac{1}{r}\begin{pmatrix} P_{n,\kappa}(r) \cdot \Omega_{\kappa,j}^{m_j}(\theta,\phi) \\ iQ_{n,\kappa}(r) \cdot \Omega_{-\kappa,j}^{m_j}(\theta,\phi) \end{pmatrix} \tag{6}$$

where $\Omega_{\kappa,j}^{m_j}(\theta,\phi)$ - angular 2-component spinor, $P(r)$ and $Q(r)$ are the major and minor radial parts of the wave function, respectively. The optimization of the PT one-electron basis has been fulfilled by means of introduction of the parameter to the exchange potential and further minimization of the gauge-non-invariant contributions into radiation width of atomic levels with using relativistic orbital bases, generated by the corresponding zeroth approximation Hamiltonian [1,32-36]. Other details can be found in Refs. [25-47].

3. Some results and conclusion

In this subsection, we present the results of the calculation of transition energies and probabilities of some transitions in the spectrum of heavy complex atoms (of the lanthanides group) of europium Eu I.

Table 1 shows the considered transitions, as well as the corresponding wavelengths that we calculated. In the table w we present the results of our calculations (column F) of oscillator strengths of electric dipole transitions together with available experimental data (columns E1, E2). For comparison, this table also shows the calculation results (see details in [1, 4,5,48]) within the framework of the popular and well-known Coulomb approximation (columns A, B, C correspond to the calibration of the photon propagator: Coulomb Babushkin, Feynmann) [3] and the multi-configurational DF method (column D), F – RMBPT with the empirical model potential zeroth approximation; G - the results of our calculation.

Table 1. Transitions and corresponding wave-lengths (in A) in the spectrum of EuI (our data)

N	Transition
1	$4f^7(^8S)6s^2\ ^8S_{7/2} \rightarrow 4f^7(^8S)6s6p\ ^8P_{5/2}$
2	$4f^7(^8S)6s^2\ ^8S_{7/2} \rightarrow 4f^7(^8S)6s6p\ ^8P_{7/2}$
3	$4f^7(^8S)6s^2\ ^8S_{7/2} \rightarrow 4f^7(^8S)6s6p\ ^8P_{9/2}$
4	$4f^7(^8S)6s^2\ ^8S_{7/2} \rightarrow 4f^7(^8S)6s7p\ ^8P_{5/2}$
5	$4f^7(^8S)6s^2\ ^8S_{7/2} \rightarrow 4f^7(^8S)6s7p\ ^8P_{9/2}$
6	$4f^7(^8S)6s^2\ ^8S_{7/2} \rightarrow 4f^7(^8S)6s7p\ ^8P_{7/2}$
7	$4f^7(^8S)6s^2\ ^8S_{7/2} \rightarrow 4f^7(^8S)6s8p\ ^8P_{9/2}$
8	$4f^7(^8S)6s^2\ ^8S_{7/2} \rightarrow 4f^7(^8S)6s8p\ ^8P_{7/2}$
9	$4f^7(^8S)6s^2\ ^8S_{7/2} \rightarrow 4f^7(^8S)6s8p\ ^8P_{5/2}$
N	Wavelength (in A)
1	4661,77
2	4627,15
3	4592,01
4	2743,16
5	2738,48
6	2731,33
7	2471,09
8	2461,68
9	2520,45

The analysis of the obtained data allows us to conclude that, firstly, our theory is in fairly good agreement with the experiment, much better in comparison with the well-known multiconfigurational DF method, as well as with the simplified Coulomb approximation.

Secondly, as can be seen, in the Coulomb approximation, the calculation data using different calibrations of the photon propagator are quite different from each other, while in our theory the difference in the data regarding the strength of the oscillators does not exceed 0.05% (for the Coulomb calibration and the Babushkin calibration).

Thirdly, the calculation demonstrated an extremely significant quantitative contribution (up to 30%) due to the effects of interelectron correlation (polarization and shielding interactions) as effects of the second and higher orders of the PT. Finally, the analysis shows that the experimental data for the transitions $4f^7(^8S)6s^2\,^8S_{7/2} \rightarrow 4f^7(^8S)6s7p\,^8P_{9/2}$ та $4f^7(^8S)6s^2\,^8S_{7/2} \rightarrow 4f^7(^8S)6s7p\,^8P_{7/2}$, obviously contain some error that in principle, it is explained by the extremely significant complexity of studying the specified spectrum.

Table 2 Oscillator strengths of series of transitions in the spectrum of EuI atom: experiment – E1, E2; A, B, C – Coulomb approximation (data correspond to gauge of photon propagator: Coulomb, Feynman, Babushkin), D – multiconfiguration DF method, F – RMBPT with empirical model potential zeroth approximation, G – our RMBPT-ODF data

N	A	B	C	D
1	0,205	0,264	0,469	0,280
2	0,272	0,350	0,622	0,374
3	0,342	0,439	0,781	0,540
4	0,0228	0,0293	0,052	
5	0,0381			
6	0,0303			
7	0,0157			
8	0,0098			
9	0,0075			
N	E1	E2	F	G
1	0,433	0,49	0,478	0,475
2	0,588	0,59	0,591	0,589
3	0,740	0,74	0,740	0,741
4	0,012		0,015	0,014
5	0,0024		0,028	0,025
6	0,0027		0,022	0,026
7	0,0015		0,0017	0,0016
8	0,0060		0,0063	0,0062
9	0,0045		0,0049	0,0047

Key to the adequate accuracy of the description of the spectroscopic characteristics of europium is the precise consideration of relativistic, radiation and exchange-correlation effects, the use of optimized orbital bases. A comparison of our results with the data of calculations within the relativistic PT with the Dirac-Kon-Shem approximation shows that there is a certain difference in the values of energies and transition probabilities, which is indeed connected with the different degree of consideration, including exchange-correlation corrections.

The main conclusion of our calculations is that the method of relativistic many-body perturbation theory RMBPT developed by us with the optimized Dirac-Fock zeroth approximation (ODF) has a fairly high theoretical consistency and precision, and can be used for calculations of such complex systems as atoms of lanthanides, actinides, in general, heavy and superheavy atoms as well as multicharged ions.

References

1. Grant I. *Relativistic Quantum Theory of Atoms and Molecules*. Oxford Univ. Press: Oxford, **2007**.
2. Glushkov, A.V. *Relativistic quantum theory. Quantum mechanics of atomic systems*. Astroprint: Odessa, **2008**.
3. Khetselius, O.Yu. *Hyperfine structure of atomic spectra*. Astroprint: Odessa, **2008**.
4. Khetselius, O.Yu. *Quantum structure of electroweak interaction in heavy finite Fermi-systems.* Astroprint: Odessa, **2011**.
5. Khetselius, O.Yu., Glushkov, A.V., Dubrovskaya, Yu.V., Chernyakova, Yu., Ignatenko, A.V., Serga, I., Vitavetskaya, L. Relativistic quantum chemistry and spectroscopy of exotic atomic systems with accounting for strong interaction effects. In: Concepts, *Methods and Applications of Quantum Systems in Chemistry and Physics*. Springer, Cham. **2018**, *31*, 71-91.
6. Khetselius O.Y., Ternovsky V.B., Dubrovskaya Y.V., Svinarenko A.A., Electron-β-Nuclear Spectroscopy of atomic systems and Many-Body perturbation theory approach to computing β-Decay Parameters In: *Glushkov A., Khetselius O., Maruani J., Brändas E.* (Eds) *Advances in Methods and Applications of Quantum Systems in Chemistry, Physics, and Biology, Ser.: Progress in Theoretical Chemistry and Physics*, Cham: **Springer**. **2021**, Vol.33, P. 59-89. https:.doi.org/ 10.1007/978-3-030-68314-6
7. Kunisz M.D., Coulomb approximation oscillator strengths for some transitions in rare

earths. *Acta Phys.Polon*. **1982**, 62, 285-296.

8. Kotochigova S.A., Identification of VUV absorption spectra of EuI 1. Calculation of states $4f^7 5d$ (9D)np. Opt.Spectr. **1983**, 55, 422-428.

9. Khetselius, O.Yu. Relativistic perturbation theory calculation of the hyperfine structure parameters for some heavy-element isotopes. *Int. Journ. Quant.Chem.* **2009,** *109,* 3330-3335.

10. Khetselius, O. Relativistic calculation of the hyperfine structure parameters for heavy elements and laser detection of the heavy isotopes. *Phys.Scr.* **2009,** *T135,* 014023.

11. Khetselius, O.Yu. Optimized relativistic many-body perturbation theory calculation of wavelengths and oscillator strengths for Li-like multicharged ions. Adv. Quant. Chem. **2019**, *78*, 223-251.

12. Dietz K., He✔ B.A., Single particle orbitals for configuration interaction derived from quantum electrodynamics. *Phys.Scripta*. **1989,** 39, 682-688.

13. Dubrovskaya, Yu., Khetselius, O.Yu., Vitavetskaya, L., Ternovsky, V., Serga, I. Quantum chemistry and spectroscopy of pionic atomic systems with accounting for relativistic, radiative, and strong interaction effects. *Adv. in Quantum Chem.* **2019,** Vol.78, pp 193-222.

14. Bystryantseva, A., Khetselius, O.Yu., Dubrovskaya, Yu., Vitavetskaya, L.A., Berestenko, A.G. Relativistic theory of spectra of heavy pionic atomic systems with account of strong pion-nuclear interaction effects: ^{93}Nb, ^{173}Yb, ^{181}Ta, ^{197}Au. *Photoelectronics*. **2016**, *25*, 56-61.

15. Khetselius, O., Glushkov, A., Gurskaya, M., Kuznetsova, A., Dubrovskaya, Yu., Serga, I., Vitavetskaya, L. Computational modelling parity nonconservation and electroweak interaction effects in heavy atomic systems within the nuclear-relativistic many-body perturbation theory. *J. Phys.: Conf. Ser.* **2017,** *905*(1), 012029.

16. Svinarenko, A., Khetselius, O., Buyadzhi, V., Florko, T., Zaichko, P., Ponomarenko, E. Spectroscopy of Rydberg atoms in a Black-body radiation field: Relativistic theory of excitation and ionization. *J. Phys.: Conf. Ser.* **2014**, *548*, 012048.

17. Khetselius, O.Y. Hyperfine structure of energy levels for isotopes ^{73}Ge, ^{75}As, ^{201}Hg. *Photoelectronics*. **2007,** *16*, 129-132.

18. Khetselius, O.Y., Gurnitskaya, E.P., Sensing the electric and magnetic moments of a nucleus in the N-like ion of Bi. *Sensor Electr. and Microsyst. Techn.* **2006**, *N3*, 35-39.

19. Khetselius, O.Yu., Lopatkin, Yu.M., Dubrovskaya, Yu.V, Svinarenko, A.A. Sensing hyperfine-structure, electroweak interaction and parity non-conservation effect in heavy atoms and nuclei: New nuclear-QED approach. *Sensor Electr. and Microsyst. Techn.* **2010,** 7(2), 11-19.

20. Florko, T.A., Tkach, T.B., Ambrosov, S.V., Svinarenko, A.A. Collisional shift of the heavy atoms hyperfine lines in an atmosphere of the inert gas. *J. Phys.: Conf. Ser.* **2012**, *397*, 012037.

21. Glushkov, A., Vitavetskaya, L. Accurate QED perturbation theory calculation of the structure of heavy and superheavy element atoms and multicharged ions with the account of nuclear size effect and QED corrections. *Herald of Uzhgorod Univ. Ser. Phys*. **2000**, *8*(2), 321-324.

22. Svinarenko, A. Spectroscopy of autoionization resonancesin spectra of barium. *Photoelectronics*. *2014*, *23*, 86-90.

23. Glushkov, A.V., Malinovskaya, S.V., Dubrovskaya, Yu.V., Sensing the atomic chemical composition effect on the beta decay probabilities. Sensor Electr. and Microsyst. Techn. **2005**, *2*(1), 16-20.

24. Glushkov, A.V., Khetselius, O.Yu., Svinarenko A.A. Theoretical spectroscopy of autoionization resonances in spectra of lanthanides atoms. *Phys. Scripta*. **2013**, *T153*, 014029.

25. Svinarenko, A., Glushkov, A, Khetselius, O., Ternovsky, V., Dubrovskaya Y., Kuznetsova A., Buyadzhi V. Theoretical spectroscopy of rare-earth elements: spectra and autoionization resonances. *Rare Earth Element*, Ed. J. Orjuela (InTech). **2017**, pp 83-104.

26. Khetselius O.Yu., Ternovsky V.B., Serga I.N. and Svinarenko A.A. Relativistic Quantum chemistry and Spectroscopy of some kaonic atoms: Hyperfine and Strong interaction effects. In: Glushkov A.V.,

Khetselius O.Y., Maruani J., Brändas E. (Eds) *Advances in Methods and Applications of Quantum Systems in Chemistry, Physics, and Biology, Ser.: Progress in Theor. Chemistry and Physics,* Cham: Springer. **2021**, Vol.33, P. 91-110.

27. Glushkov, A.V., Khetselius, O.Yu., Svinarenko A.A., Buyadzhi, V.V., Ternovsky, V.B, Kuznetsova, A., Bashkarev, P. Relativistic perturbation theory formalism to computing spectra and radiation characteristics: application to heavy element. *Recent Studies in Perturbation Theory*, ed. D. Uzunov (InTech). **2017**, 131-150.

28. Glushkov, A.V., Svinarenko, A.A., Ternovsky, V.B., Smirnov, A.V., Zaichko, P.A. Spectroscopy of the complex autoionization resonances in spectrum of helium: Test and new spectral data. *Photoelectronics*. **2015**, *24*, 94-102.

29. Ternovsky V.B., Theoretical studying Rydberg states spectrum of the uranium atom on the basis of relativistic many-body perturbation theory. *Photoelectronics.* **2019,** *28*, 39-45.

30. Glushkov, A.V., Ternovsky, V.B., Buyadzhi, V., Zaichko, P., Nikola, L. Advanced relativistic energy approach to radiation decay processes in atomic systems. *Photoelectr.* **2015**, *24*, 11-22.

31. Ivanov, L.N.; Ivanova, E.P. Method of Sturm orbitals in calculation of physical characteristics of radiation from atoms and ions. *JETP.* **1996,** *83,* 258-266.

32. Glushkov, A.V., Ivanov, L.N. Radiation decay of atomic states: atomic residue polarization and gauge noninvariant contributions. *Phys. Lett. A* **1992,** *170,* 33-36.

33. Glushkov, A.V.; Ivanov, L.N. DC strong-field Stark effect: consistent quantum-mechanical approach. *J. Phys. B: At. Mol. Opt. Phys.* **1993,** *26,* L379-386.

34. Glushkov, A.V. *Relativistic and correlation effects in spectra of atomic systems*. Astroprint: Odessa, **2006**.

35. Glushkov, A.V. Multiphoton spectroscopy of atoms and nuclei in a laser field: Relativistic energy approach and radiation atomic lines moments method. *Adv. in Quantum Chem.* **2019**, *78*, 253-285.

36. Glushkov, A., Loboda, A., Gurnitskaya, E., Svinarenko, A. QED theory of radiation emission and absorption lines for atoms in a strong laser field. *Phys. Scripta.* **2009,** *T135,* 014022.

37. Glushkov, A. Spectroscopy of cooperative muon-gamma-nuclear processes: Energy and spectral parameters *J. Phys.: Conf. Ser.* **2012,** *397,* 012011.

38. Glushkov, A.V. Spectroscopy of atom and nucleus in a strong laser field: Stark effect and multiphoton resonances. *J. Phys.: Conf. Ser*. **2014**, *548*, 012020.

39. Glushkov, A.V. Relativistic polarization potential of a many-electron atom. *Sov. Phys. Journal.* **1990**, *33(1)*, 1-4.

40. Glushkov, A., Svinarenko, A., Ignatenko, A. Spectroscopy of autoionization resonances in spectra of the lanthanides atoms. *Photoelectronics*. **2011**, *20*, 90-94.

41. Khetselius, O.Yu. Spectroscopy of cooperative electron-gamma-nuclear processes in heavy atoms: NEET effect. *J. Phys.: Conf. Ser*. **2012**, 3*97*, 012012.

42. Buyadzhi, V., Zaichko, P., Antoshkina, O., Kulakli, T., Prepelitsa, G., Ternovsky, V.B., Mansarliysky, V. Computing of radiation parameters for atoms and multicharged ions within relativistic energy approach: Advanced Code. *J. Phys.: Conf. Ser.* **2017**, *905*(1), 012003.

43. Glushkov, A., Gurskaya, M., Ignatenko, A., Smirnov, A., Serga, I., Svinarenko, A., Ternovsky, E. Computational code in atomic and nuclear quantum optics: Advanced computing multiphoton resonance parameters for atoms in a strong laser field. *J. Phys.: Conf. Ser*. **2017**, *905*, 012004. Glushkov, A.V., Ternovsky, V.B., Buyadzhi, V., Prepelitsa, G.P. Geometry of a Relativistic Quantum Chaos: New approach to dynamics of quantum systems in electromagnetic field and uniformity and charm of a chaos. *Proc. Int. Geom. Center*. **2014,** *7*(4), 60-71.

44. Moore C., *NBS Spectra Database*, NBS, Washington, **1987**.

V.B. Ternovsky

OPTIMIZED RELATIVISTIC MULTIPARTIC DISTURBANCE THEORY IN CALCULATIONS OF ATOMIC RADIATION AND SPECTRAL CHARACTERISTICS: Eu ATOM

Resume. The new formalism of the relativistic gauge-invariant perturbation theory (RMBPT-ODF) with the optimized Dirac-Fock approximation and a generalized energy approach is applied to the study of energy, radiation, and spectroscopic characteristics of a group of heavy atomic systems, in particular, energy levels and transition probabilities and oscillator strengths of the transitions $4f^7(^8S)6s^2$ $^8S_{7/2}$ $4f^7(^8S)6s6p$ $^8P_{5/2,7.2,9.2}$, $4f^7(^8S)6s7p$ $^8P_{5/2,7\backslash2}$, $4f^7(^8S)6s8p$ $^8P_{9/2,7\backslash2}$ in spectrum of the europium atom Eu I. It is shown that the required formalism, in comparison with the standard non-optimized Hartree-Fock and Dirac-Fock relativistic methods, allows obtaining more accurate data both on energies and amplitudes and probabilities of radiative transitions, which is due to the use of the optimized zero ODF approximation, a fairly complete and effective account of complex many-body exchange-correlation effects. The contribution due to the polarization of the core reaches 30% of the value of the oscillator strength; the value of the calibration-invariant contribution to the radiation width is fractions of a percent, in contrast to all existing methods of modern atomic spectroscopy, for which the contribution reaches 5-50%.

Key words: Relativistic theory, optimized Dirac-Fock method, study of energy and radiation characteristics, Eu atom

В.Б. Терновський,

ОПТИМІЗОВАНА РЕЛЯТИВІСТСЬКА БАГАТОЧАСТИНКОВА ТЕОРІЯ ЗБУРЕНЬ В ОБЧИСЛЕННЯХ АТОМНИХ СПЕКТРАЛЬНИХ ТА РАДІАЦІЙНИХ ХАРАКТЕРИСТИК: АТОМ Eu

Резюме. Новий формалізм релятивістської калібрувально-інваріантної теорії збурень (RMBPT-ODF) з оптимізованим нульовим наближенням Дірака-Фока та узагальнений енергетичний підхід застосовано до вивчення енергетичних, радіаційних і спектроскопічних характеристик групи важких атомних систем, зокрема, енергій рівнів та ймовірностей переходів та сил осциляторів $4f^7(^8S)6s^2$ $^8S_{7/2}$ $4f^7(^8S)6s6p$ $^8P_{5/2,7.2,9.2}$, $4f^7(^8S)6s7p$ $^8P_{5/2,7\backslash2}$, $4f^7(^8S)6s8p$ $^8P_{9/2,7\backslash2}$ атому європію EuI. Показано, що шуканий формалізм у порівнянні зі стандартними неоптимізованими релятивістськими методами Хартрі-Фока та Дірака-Фока дозволяє отримати більш точні дані як по енергіях, так й амплітудам та ймовірностям радіаційних переходів, що обумовлено використанням оптимізованого нульового наближення ODF, досить повним ефективним урахуванням складних багаточастинкових обмінно-кореляційних ефектів. Внесок за рахунок поляризації остову досягає 30% від значення сили осцилятора; величина калібрувально-неінваріантного внеску в радіаційну ширину складає долі проценту на відміну від усіх існуючих методів сучасної атомної спектроскопії, для яких внесок досягає 5-50%.

Ключові слова: Релятивістська теорія, оптимізований метод Дірака-Фока, вивчення енергетичних та радіаційних характеристик, атом Eu

O.Yu. Khetselius and Yu.V. Dubrovskaya

Odessa State Environmental University, L'vovskaya str., 15, Odessa
E-mail: dubrovskayayv@gmail.com

SPECTROSCOPY AND DYNAMICS OF HEAVY EXOTIC PIONIC ATOMIC SYSTEMS: ADVANCED RELATIVISTIC THEORY

An advanced relativistic approach is presented to studying spectroscopy and photodynamics of the exotic (pionic) atomic systems based on the Klein-Gordon-Fock equation approach and relativistic many-body perturbation theory with accounting for the fundamental electromagnetic and strong pion-nuclear interactions. The strong pion-nuclear interactions are taken into account by means of using the generalized strong pion-nuclear optical potential model with the effective Ericson-Ericson potential. The nuclear finite size effect is taken into consideration within the Fermi model. In order to take the nuclear quadrupole deformation effects on pionic processes into account we have used the model by Toki et al. The radiative corrections are effectively taken into account within the generalized Uehling-Serber approximation to treat the Lamb shift vacuum polarization part. The advanced data for the energy and spectral parameters for pionic atoms of the ^{173}Yb, ^{175}Lu, ^{197}Au, ^{208}Pb, ^{238}U with accounting for the radiation (vacuum polarization), nuclear (finite size of a nucleus) and the strong pion-nuclear interaction corrections are listed.

1. Introduction

Our work is devoted to the further development of the relativistic theoretical approach [1-3] to the description of spectra and different spectral parameters, in particular, radiative transitions probabilities for hadronic (pionic) atoms in the excited states with precise accounting for the relativistic, nuclear and radiative effects.

Here we present an advanced relativistic theory of spectra of the exotic (pionic) atomic systems based on the Klein-Gordon-Fock equation approach and relativistic many-body perturbation theory with accounting for the fundamental electromagnetic and strong pion-nuclear interactions. The latter has been performed by means of using the advanced strong pion-nuclear optical potential model with the generalized Ericson-Ericson potential. The nuclear finite size effect is taken into consideration within the Fermi model. In order to take the nuclear quadrupole deformation effects on pionic processes into account we have used the model by Toki et al. The radiative corrections are effectively taken into account within the generalized Uehling-Serber approximation to treat the Lamb shift vacuum polarization part. In order to take the contribution of the Lamb shift self-energy part into account we have used the generalized non-perturbative procedure, which generalizes the Mohr procedure and radiation model potential method by Flambaum-Ginges. The results of calculation of the energy and spectral parameters for pionic atoms of the ^{173}Yb, ^{175}Lu, ^{197}Au, ^{208}Pb, ^{238}U with accounting for the radiation (vacuum polarization), nuclear (finite size of a nucleus) and the strong pion-nuclear interaction corrections are presented.

As it is well known [1-22] spectroscopy of hadronic atoms already in the electromagnetic sector is extremely valuable area of research that provide unique data for different areas of physics, including nuclear, atomic, molecular physics, physics of particles, sensor electronic etc. While determining the properties of pion atoms in theory is very simple as a series of H such models and more sophisticated methods such combination chiral perturbation theory (PT), adequate quantitative description of the spectral properties of atoms in the electromagnetic pion sector (not to mention even the strong interaction sector) requires the development of High-precision approaches,

which allow you to accurately describe the role of relativistic, nuclear, radiation QED (primarily polarization electron-positron vacuum, etc.). pion effects in the spectroscopy of atoms.

The most popular theoretical models for pionic and kaonic atoms are naturally based on the using the Klein-Gordon-Fock equation, but there are many important problems connected with accurate accounting for as pion-kaon-nuclear strong interaction effects as QED radiative corrections (firstly, the vacuum polarization effect etc.). This topic has been a subject of intensive theoretical and experimental interest (see [1-23]). A development of the comprehensive theory of computing energy, spectral and radiation characteristics is of a great interest and importance in a modern theory of the hadronic atom spectra too [1-36].

2. Relativistic Spectroscopy of pionic atomic systems

Here we present a brief description of the key moments of our approach (more details can be found in Refs. [1-3]). As a negative pion is the Boson with spin 0, mass: m_{π^-} =139.57018 МэВ, r_{π^-}=0.672±0.08 fm, the relativistic particle wave functions are determined from solution of the Klein-Gordon-Fock equation with a general potential V_C, which includes an electric and polarization potentials of a nucleus (plus the strong pion-nuclear interaction potential). Generally speaking, the Klein-Gordon-Fock equation can be rewritten as the corresponding two-component equation [1-3]:

$$[-(\sigma_3 + i\sigma_2)\frac{\nabla^2}{2\mu} + \sigma_3\mu + (\sigma_3 + i\sigma_2)V_{opt}^{(0)} + V_C^{(0)}]\Psi_i = E_i\Psi_i,$$
(1)

where σ_i are the Pauli spin matrices and

$$\Psi_i = \frac{1}{2}\left(\begin{array}{c}(1 + (E - V_C^{(0)})/\mu)\phi_i \\ (1 - (E - V_C^{(0)})/\mu)\phi_i\end{array}\right).$$
(2)

This equation is equivalent to the stationary Klein-Gordon-Fock equation. The corresponding non-stationary Klein-Gordon-Fock equation can be written in the following standard form:

$$\mu^2 c^2 \Psi(x) = \{\frac{1}{c^2}[i\hbar\partial_t + eV_0(r)]^2 + \hbar^2\nabla^2\}\Psi(x)$$
(3)

where c is the speed of light, h is the Planck constant, $\smile$ is the reduced mass of the pion-nuclear system, and $\Psi_0(x)$ is the scalar wave function of the space-temporal coordinates. Usually one considers the central potential [$V_0(r)$, 0] approximation with the stationary solution:

$$\Psi(x) = \exp(\text{-i}Et/\hbar)\phi(x),$$
(4)

where $\phi(x)$ is the solution of the stationary equation:

$$\{\frac{1}{c^2}[E + eV_0(r)]^2 + \hbar^2\nabla^2 - \mu^2c^2\}\phi(x) = 0$$
(5)

Here E is the total energy of the system (sum of the mass energy mc^2 and binding energy ε_0). In principle, the central potential V_0 is the sum of the following potentials: the electric potential of a nucleus, vacuum-polarization potential. The strong interaction potential can be added below.

Generally speaking, an energy of the pionic atomic system can be represented as the following sum:

$$E \approx E_{KG} + E_{FS} + E_{QED} + E_N,$$
(6)

where E_{KG} is the energy of a pion in a nucleus (Z, A) with the point-like charge, E_{FS} is the contribution due to the nucleus finite size effect, E_{VP} is the radiation QED correction, E_N is the energy shift due to the strong interaction V_N.

Further let us consider in details the radiation or QED effects since their consistent and accurate accounting for is of a great importance and interest in spectroscopy of the pionic atomic systems. In order to take the radiation (QED) corrections into account, namely, the important effect of the vacuum polarization, one could use the procedure, which is in details presented, for example, in the Refs. [21-24]. Figure 1 illustrates the Feynman diagrams, which describe QED effect of the vacuum polarization: A1 – the Uehling-Serber term; A2, A3 – terms of order

$[\alpha(Z\alpha)\square^n$ (n=2,..); A4- the Källen-Sabry correction of order $\alpha^2(\alpha Z)$; A5 –the Wichmann-Kroll correction of order $\alpha(Z\alpha)^n$ (n=3).
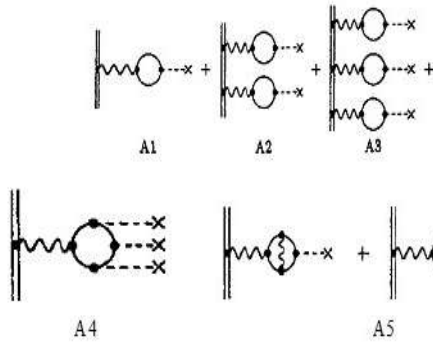
Figure 1. The Feynman diagrams, which describe QED effect of the vacuum polarization: A1 – the Uehling-Serber term; A2, A3 – terms of order $[\alpha(Z\alpha)\square^n$ (n=2,..); A4- the Källen-Sabry correction of order $\alpha^2(\alpha Z)$; A5 –the Wichmann-Kroll correction of order $\alpha(Z\alpha)^n$ (n=3).

An effect of the vacuum polarization is usually considered in the first PT theory order by means of the generalized Uehling-Serber potential with modification to account for the high-order radiative corrections. In particular, the generalized Uehling-Serber potential can be written as follows:

$$U(r)=-\frac{2Z\alpha^2}{3\pi r}\int_1^x dt\exp(-2rt/\alpha Z)(1+1/2t^2)\frac{\sqrt{t^2-1}}{t^2}\equiv-\frac{2Z\alpha^2}{3\pi r}C(g),$$
(7)

where $g=r/(\alpha Z)$. More correct and consistent approach is presented in Refs. [21-24].

The vacuum-polarization block includes the radiation potential of the standard vacuum-polarization contribution of the Uehling-Serber, supplemented by the contributions due to the Källen-Sabry [~$\alpha^2(\alpha Z)$ order] and Wichmann-Kroll [~$\alpha(Z\alpha)^n$order] corrections. The nuclear potential for the spherically symmetric density $\rho(r\vee R)$ can be presented as follows:

$$V_{nucl}(r|R)=-(1/r)\int_0^r dr'r'^2\rho(r'|R)+\int_r^x dr'r'\rho(r'|R)$$
(8)

In the concrete calculations one should use the formulas for the finite size nuclear potential and its derivatives on the nuclear radius. Here we use the known Ivanov-Ivanova et al method of differential equations (look details in Refs. [16-18,36,37]). The effective algorithm for definition of the potential $V_{nucl}(r\vee R)$ is used in Refs. [16,23,24] and reduced to solution of the following system of the differential equations (for the Fermi model):

$$V'_{nucl}(r,R)=(1/r^2)\int_0^r dr'r'^2\rho(r',R)\equiv(1/r^2)y(r,R)$$

,

$$y'(r,R)=r^2\rho(r,R),$$
(9)

$$\rho'(r)=(\rho_0/a)\exp$$
(10)

with the corresponding boundary conditions. The analogous expressions for determination of a density can be provided by the Gaussian model or within a consistent relativistic mean-field model [23].

In order to take into consideration the nuclear quadrupole deformation effects on pionic processes we used the model by Toki et al [19,20]:

$$\rho(r)=\rho_0(r)+\sum_{k\geq2}\sqrt{\frac{2k+1}{16\pi}}\rho_k(r)Y_k^0(\hat{r}),$$
(11)

where the quantity $\rho_k(r)$ is defined as follows:

$$\rho_k(r)=\sqrt{\frac{16\pi}{2k+1}}<JJ\left|\sum_{i=1}^A\frac{\delta(r-r_i)}{r^2}Y_K^0(\hat{r}_i)\right|JJ>$$
(12)

One should consider the case $k=2$, which corresponds to the nuclear quadrupole density. The Woods-Saxon-like form for the nuclear density distribution in the intrinsic frame is (see, e.g., [21]:

$$\bar{\rho}(r)=\rho_N/\left[1+\exp\left(\frac{r-R(\theta)}{a}\right)\right],$$
(13)

where

$$R(\theta)=R\left(1+\beta Y_2^0(\theta)\right),$$
(14)

ρ_N is the normalization constant, β is a quadrupole deformation parameter.

Further in order to calculate probabilities of the radiative transitions between energy level of the pionic atoms we have used the well-known relativistic energy approach (c. g.[16-18,23-28, 36-39]).

More simplified and sufficiently popular approach to treating the strong interaction in the pionic atomic system is provided by the well known optical potential model (see, e.g., [4,10]). Recall that in the model of optical potential for the description of pion-nuclear interaction the potential

$$V_{\pi N(opt)} = \mathrm{Re}V + i\,\mathrm{Im}V \qquad (15)$$

is used. Dedicated, as a rule, separate s-wave and p-wave pion-nuclear scattering are derived in accordance with the repulsive and attracting parts of the optical potential. In order to describe the strong πN interaction we use the optical potential model where the generalized Ericson-Ericson potential is as follows [4]:

$$V_{\pi N} = V_{opt}(r) = -\frac{4\pi}{2m}\left\{ q(r)\nabla \frac{\alpha(r)}{1 + 4/3\pi\xi\alpha(r)}\nabla \right\}, \qquad (16a)$$

$$q(r) = \left(1 + \frac{m_\pi}{m_N}\right)\left\{ b_0\rho(r) + b_1\left[\rho_n(r) - \rho_p(r)\right]\right\} +$$
$$+ \left(1 + \frac{m_\pi}{2m_N}\right)\left\{ B_0\rho^2(r) + B_1\rho(r)\delta\rho(r)\right\}, \qquad (16b)$$

$$\alpha(r) = \left(1 + \frac{m_\pi}{m_N}\right)^{-1}\left\{ c_0\rho(r) + c_1\left[\rho_n(r) - \rho_p(r)\right]\right\} +$$
$$+ \left(1 + \frac{m_\pi}{2m_N}\right)^{-1}\left\{ C_0\rho^2(r) + C_1\rho(r)\delta\rho(r)\right\}. \qquad (16c)$$

Here $\rho_{p,n}(r)$ – distribution of a density of the protons and neutrons, respectively, ξ– parameter ($\xi=0$ corresponds to case of "no correlation", $\xi=1$, if there are anticorrelations between nucleons); respectively isoscalar and isovector parameters $b_0, c_0, B_0, b_1, c_1, C_0$ B_1, C_1 – are corresponding to the s-wave and p-wave (repulsive and attracting potential member) scattering length in the combined spin-isospin space with taking into account the absorption of pions (with different channels for p-p pair $B_{0(pp)}$ and p-n pair $B_{0(pn)}$), the Lorentz-Lorenz effect in the p-wave interaction and isospin and spin dependence of an amplitude πN scattering:

$$b_0\rho(r) \to b_0\rho(r) + b_1\left[\rho_p(r) - \rho_n(r)\right], \qquad (17)$$

The description of numerical values of the potential parameters is in details described in Refs. [1-4,10-152]. Other details are in Refs. [1-3,34-40].

3. Results and conclusions

In Table 1 the advanced data on the *4f-3d, 5g-4f* transition energies for pionic atoms of the ^{173}Yb, ^{175}Lu, ^{197}Au, ^{208}Pb, ^{238}U are presented. There are also listed the measured values of the Berkley, CERN and Virginia laboratories and alternative data obtained on the basis of computing within alternative versions of the Klein-Gordon-Fock (KGF) theory with taking into account the finite size of the nucleus in the model uniformly charged sphere and the standard Uehling-Serber radiation correction [1-3,5,6, 14, 15, 34, 35].

Table 1. The 5g-4f and 4f-3d transition energies (keV) in the spectra of heavy pionic atoms (see text)

π-A		CERN Berkley E_{EXP}	E_{KGF+EM} [5,6,14]	E_{KGF-EM} [7,8]
^{173}Yb	5g-4f	-	-	-
^{197}Au	5g-4f	533.16 ± 0.20 532.5 ± 0.5	528.95	-
^{203}Tl	5g-4f	561.67 ± 0.25	559.65	559.681
^{202}Pb	5g-4f	575.56 ± 0.25	573.83	573.862
^{238}U	5g-4f	732.0 ± 0.4 731.4 ± 1.1	725.52	725.574
^{173}Yb	4f-3d	-	-	-
^{175}Lu	4f-3d	-	-	919.085
^{197}Au	4f-3d	1187.3 ± 1.9	-	-
^{208}Pb	4f-3d	1282 ± 2.2	-	-
π-A		E_N [5]	E_N [14, 15,34]	E_N, Our data
^{173}Yb	5g-4f	-	-	412.26
^{197}Au	5g-4f	532.87	531.88	533.08
^{203}Tl	5g-4f	560.93	-	561.63
^{202}Pb	5g-4f	575.21	-	575.78
^{238}U	5g-4f	729.80	-	730.92
^{173}Yb	4f-3d	-	-	838.67
^{175}Lu	4f-3d	-	-	923.14
^{197}Au	4f-3d	-	1167.92	1186.35
^{208}Pb	4f-3d	-	1261.23	1281.78

The analysis of the presented data confirms an importance of the consistent and correct accounting for the radiation (vacuum polarization) and the strong pion-nuclear interaction corrections. The contributions due to the nuclear finite size effect and electron screening correction should be accounted in a precise theory too. A correct treatment of the nuclear, relativistic, radiative and other effects could provide the physically reasonable agreement between experimental and theoretical data on the multi-electron pionic atoms.

References

1. O.Y. Khetselius, V.B. Ternovsky, I.N. Serga, A.A. Svinarenko, Relativistic Quantum Chemistry and Spectroscopy of Some Kaonic Atoms: Hyperfine and Strong-Interaction Effects In: *Glushkov A.V., Khetselius O.Y., Maruani J., Brändas E. (Eds) Advances in Methods and Applications of Quantum Systems in Chemistry, Physics, and Biology, Ser.: Progress in Theoretical Chemistry and Physics*, Cham: Springer. **2021,** *33,* 91-110.

2. Dubrovskaya Yu.V., Khetselius O.Yu., Vitavetskaya L.A., Ternovsky V.B., Serga I.N., Quantum Chemistry and Spectroscopy of Pionic Atomic Systems With Accounting for Relativistic, Radiative, and Strong Interaction Effects. *Advances in Quantum Chemistry* (Elsevier). **2019,** *78,* 193-222;

3. Khetselius, O.Yu., Glushkov, A.V., Dubrovskaya, Yu.V., Chernyakova, Yu.G., Ignatenko, A.V., Serga, I.N., Vitavetskaya, L. Relativistic quantum chemistry and spectroscopy of exotic atomic systems with accounting for strong interaction effects. In: *Wang YA, Thachuk M, Krems R, Maruani J (eds) Concepts, Methods and Applications of Quantum Systems in Chemistry and Phys.* Springer, Cham, **2018,** *31,*71-91.

4. Ericson, T.; Weise, W. *Pions and Nuclei;* Oxford: Clarendon; **1988**.

5. Iwasaki, M.; Trudel, A.; Celler, A.; Häusser, O.; Hayano, R. S.; Helmer, R.; Henderson, R.; Hirenzaki, S.; Jackson, K. P.; Kuno, Y.; Matsuoka, N.; Mildenberger, J.; Miller, C.A.; Outa, H.; Sakai, H.; Toki, H.; Vetterli, M.; Watanabe, Y.; Yamazaki, T.; Yen, S. Search for deeply bound pionic states in ^{208}Pb (*n, p*) reaction at T_n=418 MeV *Phys. Rev. C* **1991,** *43,* 1099.

6. Yamazaki, T.; Hayano, R. S.; Itahashi, K.; Oyama, K.; Gillitzer, A.; Gilg, H.; Knülle, M.; Munch, M.; Kienle, P.; Schott, W.; Geissel, H.; Iwasa, N.; Münzenberg, G. Discovery of deeply bound π⁻ states in the ^{208}Pb(*d,*^{3}He) reaction. *Z. Phys. A* **1996,** *355,* 219-221.

7. Backenstoss, G. Pionic atoms. *Ann. Rev. Nucl. Sci.* **1970,** *20*, 467.

8. Menshikov, L.I.; Evseev, M.K. Phys. Uspekhi. **2001,** *171,* 149–185.

9. Olaniyi, B.; Shor, A.; Cheng, S.; Dugan, G.; Wu, C.S. Electric quadrupole moments and strong interaction effects in piomic atoms of ^{165}Ho, ^{175}Lu, ^{176}Lu,^{179}Hf, ^{181}Ta. Nucl. Phys. A. **1982,** *403,* 572.

10. Erikcson, M.; Ericson, T.; Krell, M. Peculiarities of the pion-nuclear interaction. *Phys. Rev. Lett.* **1969,** *22,* 1189.

11. Seki, R.; Masutani K.; Jazaki, K. Unified analysis of pionic atoms and low-energy pion-nuclear scattering.- Hybrid analysis. *Phys. Rev. C.* **1983,** *27,* 1817.

12. Nose-Togawa, N.; Hirenzaki, S.; Kume, K. Pion-nucleus potential parameters and quadrupole effect in deeply bound pionic atom. *Nucl. Phys. A.* **1999,** *646,* 467-478.

13. Hatsuda T.; Kunihiro, T. Observed hadron properties for the study of QCD vacuum structure. *Phys. Rept.* **1994,** *247,* 221.

14. Taal, A.; David, P.; Hanscheid, H.; Koch, J.H.; de Laat, C.T. et al. Deeply bound 1s and 2p states in pionic atoms. *Nucl. Phys. A.* **1990,** *511,* 573-591.

15. de Laat, C.T.A.M.; Taal, A.; Konijn, J., David, P.; Hänscheid, H.; Risse, F.; Rösel, Ch.; Schrieder, W.; Petitjean, C. A study of the strong interaction effects on pionic 3d and 4f levels in ^{181}Ta, natRe, natPt, ^{197}Au, ^{208}Pb, ^{209}Bi and ^{237}Np. *Nucl. Phys. A.* **1991,** *523,* 453–458.

16. Ivanov, L.N.; Ivanova, E.P.; Aglitsky, E.V. Modern trends in the spectroscopy of multicharged ions. *Phys. Rep.* **1988,** *164,* 315–317.

17. Glushkov, A.V.; Ivanov, L.N. Radiation decay of atomic states: atomic residue polarization and gauge noninvariant

contributions. *Phys. Lett. A* **1992,** *170,* 33–36.

18. Ivanova, E.P. ; Glushkov, A.V. Theoretical investigation of spectra of multicharged ions of F-like and Ne-like isoelectronic sequences. *J. Quant. Spectr. Rad. Transfer.* **1986,** *36,* 127–145.

19. Toki, H.; Hirenzaki, S.; Yamazaki T.; Hayano, R. S. Structure and formation of deeply-bound pionic atoms. *Nucl. Phys. A* **1989,** *501,* 653.

20. Nose-Togawa, N.; Hirenzakia, S.; Kumea, K. Nuclear Quadrupole Effects in Deeply Bound Pionic Atoms. *Nucl. Phys. A* **1997,** *623,* 548–558.

21. Mohr, P.J. Energy Levels of H-like atoms predicted by Quantum Electrodynamics,10<Z<40. *Atom. Dat. Nucl. Dat. Tabl.* **1983***, 24,* 453.

22. Flambaum, V.V.; Ginges, J.S.M. Radiative potential and calculations of QED radiative corrections to energy levels and electromagnetic amplitudes in many-electron atoms. *Phys. Rev. A* **2005,** *72,* 052115.

23. Glushkov, A.V. *Relativistic Quantum theory. Quantum mechanics of atomic systems*; Astroprint: Odessa, **2008**.

24. Khetselius, O.Yu. *Quantum structure of electroweak interaction in heavy finite Fermi-systems.*Astroprint: Odessa, **2011**.

25. Glushkov, A.V.; Rusov, V.D.; Ambrosov, S.V.; Loboda, A.V. Resonance states of compound super-heavy nucleus and EPPP in heavy nucleus collisions *In New Projects and New Lines of Research in Nuclear Physics*; Fazio, G., Hanappe, F., Eds.; World Scientific: Singapore, **2003**, 126-132.

26. Glushkov, A.V. Energy approach to resonance states of compound superheavy nucleus and EPPP in heavy nuclei collisions *In Low Energy Antiproton Physics;* Grzonka, D., Czyzykiewicz, R., Oelert,W., Rozek, T., Winter, P., Eds.; AIP: New York, *AIP Conf. Proc.* **2005**, *796*, 206-210.

27. Khetselius, O.Yu. Relativistic Energy Approach to Cooperative Electron-γ-Nuclear Processes: NEET Effect *In Quantum Systems in Chemistry and Physics: Progress in Methods and Applications,* Series: *Progress in Theoretical Chemistry and Physics;* Nishikawa, K., Maruani, J., Brändas, E., Delgado-Barrio, G., Piecuch, P., Eds.; Springer: Dordrecht, **2012;** Vol. 26, pp. 217-229.

28. Khetselius, O.Yu. Relativistic perturbation theory calculation of the hyperfine structure parameters for some heavy-element isotopes. *Int. J. Quant. Chem.* **2009,** *109,* 3330–3335.

29. Khetselius, O.Yu. Relativistic calculation of the hyperfine structure parameters for heavy elements and laser detection of the heavy isotopes. *Phys. Scripta* **2009,** *135,* 014023.

30. Khetselius, O. Yu. *Hyperfine structure of atomic spectra*; Astroprint: Odessa, **2008**.

31. Khetselius, O.Yu. Atomic parity non-conservation effect in heavy atoms and observing P and PT violation using NMR shift in a laser beam: To precise theory. *J. Phys.: Conf. Ser.* **2009,** *194,* 022009.

32. Glushkov, A.V. Relativistic polarization potential of a many-electron atom. *Sov. Phys. Journal.* **1990**, *33(1),* 1-4.

33. Serga, I.N.; Dubrovskaya, Yu.V.; Kvasikova, A.S.; Shakhman, A.N; Sukharev, D.E. Spectroscopy of hadronic atoms: Energy shifts. *J. Phys.: Conf. Ser.* **2012,** *397,* 012013.

34. Serga, I.N.; Khetselius, O.Yu.; Vitavetskaya, L.A.; Bystryantseva A.N. Relativistic theory of spectra of pionic atomic system [208]Pb with account of strong pion-nuclear interaction effects. *Photoelectronics.* **2017**, *26*, 68-77.

35. Bystryantseva, A.N.; Khetselius, O.Yu.; Dubrovskaya, Yu.V.; Vitavetskaya, L.A.; Berestenko, A.G. Relativistic theory of spectra of heavy pionic atomic systems with account of strong pion-nuclear interaction effects: [93]Nb, [173]Yb, [181]Ta, [197]Au. *Photoelectronics.* **2016,** *25,* 56–61.

36. Ivanova, E.P.; Ivanov, L.N.; Glushkov, A.V.; Kramida, A.E. High Order Corrections in the Relativistic Perturbation Theory with the Model Zeroth Approximation, Mg-Like and Ne-Like Ions. *Phys. Scripta.* **1985,** *32,* 513.

37. Glushkov, A.V. Advanced Relativistic Energy Approach to Radiative Decay

Processes in Multielectron Atoms and Multicharged Ions. *In Quantum Systems in Chemistry and Physics: Progress in Methods and Applications, Series: Progress in Theoretical Chemistry and Physics*; Nishikawa, K., Maruani, J., Brandas, E., Delgado-Barrio, G., Piecuch, P., Eds.; Springer: Dordrecht, **2012**; Vol. 26, pp 231–252.

38. Glushkov, A.V. *Relativistic and Correlation Effects in Spectra of Atomic Systems;* Astroprint: Odessa, **2006.**

39. Khetselius, O.Yu. Determination of the hyperfine and electroweak interactions parameters and parity non-conservation amplitudes in heavy atoms and nuclei within nuclear-qed theory. *Photoelectronics*. **2011**, *20*, 12-17.

40. Svinarenko, A.A. Study of spectra for lanthanides atoms with relativistic many-body perturbation theory: Rydberg resonances. *J. Phys.: Conf. Ser.* **2014**, *548*, 012039.

PACS 36.10.-k

O.Yu. Khetselius, Yu.V. Dubrovskaya,

SPECTROSCOPY AND DYNAMICS OF HEAVY EXOTIC PIONIC ATOMIC SYSTEMS: ADVANCED RELATIVISTIC THEORY

Summary. An advanced relativistic approach is presented to studying spectroscopy and photodynamics of the exotic (pionic) atomic systems based on the Klein-Gordon-Fock equation approach and relativistic many-body perturbation theory with accounting for the fundamental electromagnetic and strong pion-nuclear interactions. The strong pion-nuclear interactions are taken into account by means of using the generalized strong pion-nuclear optical potential model with the effective Ericson-Ericson potential. The nuclear finite size effect is taken into consideration within the Fermi model. In order to take the nuclear quadrupole deformation effects on pionic processes into account we have used the model by Toki et al. The radiative corrections are effectively taken into account within the generalized Uehling-Serber approximation to treat the Lamb shift vacuum polarization part. The advanced data for the energy and spectral parameters for pionic atoms of the ^{173}Yb, ^{175}Lu, ^{197}Au, ^{208}Pb, ^{238}U with accounting for the radiation (vacuum polarization), nuclear (finite size of a nucleus) and the strong pion-nuclear interaction corrections are listed.

Keywords: relativistic theory, pionic atomic systems, spectroscopy and photodynamics

PACS 36.10.-k

О.Ю. Хецеліус. Ю.В. Дубровська

СПЕКТРОСКОПІЯ ТА ДИНАМІКА ВАЖКИХ ЕКЗОТИЧНИХ ПІОННИХ АТОМНИХ СИСТЕМ: УДОСКОНАЛЕНА РЕЛЯТИВІСТСЬКА ТЕОРІЯ

Резюме. Розроблено удосконалений релятивістський підхід до вивчення фундаментальних параметрів спектроскопії та фотодинаміки екзотичних (піонних) атомних систем на основі рівняння Клейна-Гордона-Фока та релятивістської теорії багаточастинкової збурень багатьох з урахуванням фундаментальних електромагнітних і сильних піон-ядерних взаємодій. Ефекти сильної піон-ядерної взаємодії враховуються за допомогою узагальненої моделі сильного піон-ядерного оптичного потенціалу з ефективним потенціалом Еріксона-Еріксона. Ядерний ефект скінченного розміру враховується в рамках моделі Фермі. З метою урахування впливу ядерної квадрупольної деформації на піонні динамічні процеси, використано модель Токі та ін. Радіаційні

поправки ефективно враховуються в рамках узагальненого наближення Улінга-Сербера для обробки частини поляризації вакууму Лемба. Наведені прецизійні дані для енергетичних і спектральних параметрів для піонних атомів 173Yb, 175Lu, 197Au, 208Pb, 238U з урахуванням радіаційних, ядерних (скінченний розмір ядра) поправок та ефектів сильної піон-ядерної взаємодії.

E.V. Ternovsky

Odessa State Environmental University, 15, Lvovskaya str., Odessa
E-mail: ternovskyev@gmail.com

RELATIVISTIC APPROACH TO COMPUTING WAVELENGTHS OF TRANSITIONS IN SPECTRA OF ATOMIC SYSTEMS IN PLASMAS

New relativistic approach to computing the spectral parameters of multicharged ions in plasmas for different values of the plasmas screening (Debye) parameter (respectively, electron density, temperature) is presented. The presented approach is based on the generalized relativistic energy approach combined with the optimized relativistic many-body perturbation theory with the Dirac-Debye screening hamiltonian as a zeroth approximation, adapted for application to study the energy and spectral parameters of atoms and ions in plasmas. The special exchange potential as well as the electron density with dependence upon the temperature are used. The wavelengths for a number of transitions, including (A): $E(1s2p\ ^1P_1)$-$E(1s^2\ ^1S)$; (B) $E(1s3p\ ^1P_1)\_E(1s^2\ ^1S)$; (C)AK: $E(1s2p\ ^3P_1)\_E(1s2s\ ^3S)$; (D): $E(1s3p\ ^3P_1)\_E(1s2s\ ^3S)$ of the helium in plasmas for various Debye lengths are calculated and compared with the corresponding data by Kar-Ho.

1. **Introduction.**

The properties of laboratory, thermonuclear (tokamak), laser-produced, astrophysical plasmas have drawn considerable attention over the last decades [1-5]. It is known that multicharged ions play an important role in the diagnostics of a wide variety of plasmas [1-23]. From the other side, studying spectra of ions in plasmas remains very actual in order to understand the plasma processes themselves. In most plasma environments the properties are determined by the electrons and the ions, and the interactions between them. It has stimulated a great number of papers, devoted to modelling the elementary processes in laser, collisionally pumped plasmas and construction of the first VUV and X-ray lasers with using plasmas of Li-, Ne-like ions as an active medium.

Such well-known atomic methods as the multi-configuration Dirac–Fock, R-, T-matrix, relativistic distorted-wave methods, coupled-cluster theories, and more simplified approaches such as the quantum defect and Coulomb approximations, pseudo- and model potential methods, the classical and quasiclassical models and others have been intensively applied to problems considered. At present time a considerable interest has been encapsu-lated to studying elementary atomic processes in plasmas environments because of the plasmas screening effect on the plasmas-embedded atomic systems. In many papers the calculations of various atomic and ionic systems embedded in the Debye plasmas have been performed [1-28]; a development of the advanced computational quantum methods and models for the further accurate computing wavelengths and oscillator strengths for the atomic systems in plasmas, including the Debye plasmas, remained a very actual and difficult problem (for example, see [1-42] and Refs. therein). To say strictly, solving of the whole problem requires a development of the quantum-electrodynamical approach as the most consistent one to problem of the Coulomb many-body system.

Nevertheless, there are known principal theoretical problems to be solved in order to receive the correct description of the elementary atomic processes in laser, collisionally pumped plasma. First of all, speech is about development of the advanced quantum-mechanical models for the further accurate computing oscillator strengths, electron-collisional strengths and rate coefficients for atomic ions in plasmas, including the Debye plasmas. As usually, a correct accounting for the relativistic, exchange-correlation, plasma environment ef-

fects is of a great importance. To say strictly, solving of the whole problem requires a development of the quantum-electrodynamical approach as the most consistent one to problem of the Coulomb many-body system.

In this paper, which goes on our work [15-20], we present New relativistic approach to computing the spectral parameters of multicharged ions in plasmas for different values of the plasmas screening (Debye) parameter (respectively, electron density, temperature) is presented. The presented approach is based on the generalized relativistic energy approach combined with the optimized relativistic many-body perturbation theory with the Dirac-Debye screening hamiltonian as a zeroth approximation, adapted for application to study the energy and spectral parameters of atoms and ions in plasmas. The special exchange potential as well as the electron density with dependence upon the temperature are used.

2. Theoretical Approach.

Some fundamental aspects of the approach developed were earlier presented (see, for example, Refs. [20-26]). Therefore, below we are limited only by the key and as a rule new points of a theory, following to Refs. [20-23]. Let us start our consideration from formulation relativistic many-body PT with the Debye shielding model Dirac Hamiltonian for electron-nuclear and electron-electron systems. Formally, a multielectron atomic systems (multielectron atom or multicharged ion) is described by the relativistic Dirac Hamiltonian (the atomic units are used) as follows:

$$H = \sum_i h(r_i) + \sum_{i>j} V\left(r_i r_j\right).$$

$$(1)$$

Here, $h(r)$ is one-particle Dirac Hamiltonian for electron in a field of a nucleus and V is potential of the inter-electron interaction. According to Refs. [6] it is useful to determine the interelectron potential with accounting for the retarding effect and magnetic interaction in the lowest order on parameter α^2 (α is the fine structure constant) as follows:

$$V\left(r_i r_j\right) = exp\left(i\omega_{ij} r_{ij}\right) \cdot \frac{\left(1 - \alpha_i \alpha_j\right)}{r_{ij}},$$

$$(2)$$

where ω_{ij} is the transition frequency; α_i, α_j are the Dirac matrices.

In order to take into account the plasmas environment effects already in the PT zeroth approximation we use the known Yukawa-type potential of the following form:

$$V(r_i, r_j) = (Z_a Z_b / |r_a - r_b|) exp\left(-\mu \cdot |r_a - r_b|\right) \quad (3)$$

where r_a, r_b represent respectively the spatial coordinates of particles, say, A and B and Z_a, Z_b denote their charges.

The potential (3) is well known (look, for example, [1-4,24] and Refs there) well known, for example, in the classical Debye-Hückel, theory of plasmas. The plasmas environment effect is modelled by the shielding parameter μ, which describes a shape of the long-rang potential. The parameter μ is connected with the plasma parameters such as the temperature θ and the charge density n as follows:

$$\mu \sim \sqrt{e^2 n / k_B T} \quad (4)$$

Here e is the electron charge and k_B is the Boltzman constant. The density n is given as a sum of the electron density N_e and the ion density N_k of the k-th ion species with the nuclear charge q_k : $n = N_e + \sum_k q_k^2 N_k$. It is very useful to remind the simple estimates for the shielding parameter.

For example, under typical laser plasma conditions of $T \sim 1keV$ and $n \sim 10^{23}$ cm^{-3} the parameter μ is of the order of 0,1 in atomic units. By introducing the Yukawa-type electron-nuclear attraction and electron-electron repulsion potentials, the Debye shielding model Dirac Hamiltonian for electron-nuclear and electron-electron subsystems is given in atomic units as follows [20-22]:

$$H = \sum_i [\alpha c p - \beta mc^2 - Z \exp(-\mu r_i)/r_i] +$$

$$+ \sum_{i>j} \frac{\left(1 - \alpha_i \alpha_j\right)}{r_{ij}} \exp(-\mu r_{ij})$$

$$(5)$$

where c is the velocity of light and Z is a charge of the atomic ion nucleus.

The formalism of the relativistic many-body PT is further constructed in the same way as the PT formalism in Refs. [20,24-32]. In the PT zeroth approximation one should use a mean-field potential, which includes the Yukawa-type potential (insist of the pure Coulomb one) plus exchange potential and additionally the correlation potential (for example, the Lundqvist-Gunnarson potential with the optimization parameter b can be used) as in Refs. [24-26]. As alternative one could use an optimized model potential by Ivanova-Ivanov (for Ne-like ions) [1,30], which is calibrated within the special ab initio procedure within the relativistic energy approach [24-27].

Let us concretize the corresponding mean-field potential. In particular, one of the possible versions $U(r)$ is as follows (sum of the Coulomb or Yukawa-type potential plus exchange potential:

$$U(r) = U_{Coul-Yuk}(r) + U_{ex}(r), \qquad (6)$$

With the exchange potential as follows:

$$U_{обм}(r) = \frac{4\pi}{T}\rho(r)\left[1 + 6\frac{\rho(r)}{T^{3/2}} + \frac{\pi^4}{3}\left(\frac{\rho(r)}{T^{3/2}}\right)^2\right]^{-1/3}, \qquad (7)$$

where $\rho(r)$ is an electron density.

The electron density can be presented as a sum of the following terms:

$$\rho(r) = \rho_1(r) + \rho_2(r), \qquad (8)$$

$$\rho_1(r) \sim \sum_{n,l} \Psi_{nl}(r)\square^2 \qquad (9)$$

$$\rho_1(r) = \frac{\sqrt{2}T^{3/2}}{\pi^2}\int \sqrt{y}\left[1 + \exp\left(y - \frac{U(r)}{T} + \eta\right)\right]^{-1} dy, \qquad (10)$$

$$y > \frac{1}{T}\left(U(r) + E_0\right), \qquad (11)$$

where $\eta = \frac{-\mu}{T}$, μ is a chemical potential and E_0 is a boundary between state of discrete spectrum and continuum.

The averaged numbers of fulfilling electron states can be determined on the basis of the Fermi-Dirac expression:

$$N_{nl} = 2(2l+1)\left[1 + \exp\left(\frac{1}{T}(E_{nl} + \mu)\right)\right]^{-1} \qquad (12)$$

The point of accounting for the many-body exchange-correlation corrections within a presented theory can be treated as in an usual perturbation theory for free multicharged ions. As usually, in the PT second order, there are two kinds of the exchange and correlation diagrams: polarization and ladder ones. The polarization diagrams take into account the quasiparticle interaction through the polarizable core, and the ladder diagrams account for the immediate quasiparticle interaction. An effective procedure of their accounting are in details described in Refs. [6-9,20-24]. The modified PC numerical code 'Superatom" [24-32] is used in all calculations. Other details can be found in Refs. [33-40].

3. Results and conclusions.

Below we will present our data on the wavelengths for a number of transitions, including (A): E(1s2p $^1P_1$)-E(1s^2 ^1S); (B) E(1s3p $^1P_1$)_E(1s^2 ^1S); (C)AK: E(1s2p $^3P_1$)_E(1s2s ^3S); (D): E(1s3p $^3P_1$)_E(1s2s ^3S) of the helium in plasmas for various Debye lengths and compare with the corresponding data by Kar-Ho [2]. It should be noted that Kar-Ho [2] have used the highly correlated basis functions for singly excited S, P, D states and CI-type basis functions for doubly excited meta-stable D states, and the plasmas effect has been taken into account by using a screened Coulomb (Yukawa) potential obtained from the Debye model that admits a variety of plasma conditions. The analysis shows that the presented data are in physically reasonable agreement with the theoretical data [2].

However, some difference between the corresponding results can be explained by using different relativistic orbital bases and by differences in the numerical realization of model for accounting for the screening effect as well as some numerical differences

Table 1. Transition wavelengths (in A ˚) of helium atom below the He+(1S) threshold for different Debye lengths (A): E(1s2p $^1P_1$)-E(1s^2 ^1S); (B) E(1s3p $^1P_1$)_E(1s^2 ^1S); (C)AK: E(1s2p $^3P_1$)_E(1s2s ^3S); (D): E(1s3p $^3P_1$)_E(1s2s ^3S); See text

$1/\mu$	[2]	(A)-this	(B)- this
∞	584.234	584.236	536.940
100	584.388	584.389	537.296
50	584.838	584.840	538.307
20	587.829	587.831	544.707
10	597.826	597.828	565.208
8	605.098	605.099	580.696
$1/\mu$	(B)- this	(C)-this	(D)-this
∞	536.940	10831.59	3889.372
100	537.296	10834.584	3901.312
50	538.307	10843.193	3935.133
20	544.707	10901.684	4155.382
10	565.208	11136.233	4985.283
8	580.696	11351.615	5831.351

References

1. Ivanova, E., Glushkov, A. Theoretical investigation of spectra of multicharged ions of F-like and Ne-like isoelectronic sequences. *J. Quant. Spectr. and Rad. Transfer*. **1986**, *36*(2), 127-145.

2. Sabyasachi Kar_, Y.K. Ho, Transition wavelengths for helium atom in weakly coupled hot plasmas. *J. Quant. Spectr. Rad. Transfer*. **2007**, *107*, 315–322.

3. Chensheng Wu, Yong Wu, Jun Yan, T. N. Chang, and Xiang Gao, Transition energies and oscillator strengths for the intrashell and intershell transitions of the C-like ions in a thermodynamic equilibrium plasma environment. *Phys. Rev. E,* **2022**, *105*, 015206

4. X. Lopez, C. Sarasola, and J. M. Ugalde, Transition Energies and Emission Oscillator Strengths of Helium in Model Plasma Environments, *J. Phys. Chem. A .* **1997**, *101* (10), 1804–1807.

5. Saha B., Fritzsche S. Influence of dense plasma on the low-lying transitions in Be-like ions: relativistic multiconfiguration Dirac–Fock calculation. *J. Phys. B: At. Mol. Opt. Phys.* **2007**, *40*, 259-270.

6. Yongqiang, Li Y., Wu, J., Hou, Y., Yuan, J. Influence of hot and dense plasmas on energy levels and oscillator strengths of ions: Be-like ions for *Z* = 26–36, *J. Phys. B:* *At. Mol. Opt. Phys*. **2008,** *41,* 145002.

7. Madhulita Das, Sahoo B. K., Sourav Pal. Relativistic spectroscopy of plasma embedded Li-like systems with screening effects in two-body Debye potentials. *J. Phys. B: At. Mol. Opt. Phys.* **2014,** *47*, 175701.

8. Han, Y.-C., Madsen, L.B. Comparison between length and velocity gauges in quantum simulations of high-order harmonic generation *Phys. Rev. A.* **2010**, *81*, 06343.

9. Gu, M. F. and Beiersdorfer, P., Stark shift and width of x-ray lines from highly charged ions in dense plasmas, *Phys. Rev. A* **2020,** 101, 032501.

10. C. J. Keane, B. A. Hammel, D. R. Kania, J. D. Kilkenny, R. W. Lee, A. L. Osterheld, *and* L. J. Suter, X-ray spectroscopy of high-energy density inertial confinement fusion plasmas. *Phys. Fluids B: Plasma Phys.* **1993**, *5*, 3328.

11. Glushkov A.V., Khetselius O.Yu., Loboda A.V., Ignatenko A., Svinarenko A., Korchevsky D., Lovett L., QED Approach to Modeling Spectra of the Multicharged Ions in a Plasma: Oscillator and Electron-ion Collision Strengths.. *AIP Conference Proceedings.* **2008**. 1058. 175-177

12. Ivanov, L.N., Ivanova, E.P., Aglitsky, E. Modern trends in the spectroscopy of multicharged ions. *Phys. Rep.* **1988,** *166*.

13. Bandrauk, A.D., Fillion-Gourdeau, F., Lorin, E. Atoms and molecules in intense laser fields: gauge invariance of theory and models *J. Phys. B: At. Mol. Opt. Phys.* **2013**, *46*, 153001

14. Glushkov, A.V., Malinovskaya, S.V., Prepelitsa, G.P., Ignatenko, V. Manifestation of the new laser-electron nuclear spectral effects in the thermalized plasma: QED theory of co-operative laser-electron-nuclear processes. *J. Phys.: Conf. Ser.* **2005,** *11,* 199-206.

15. Glushkov, A., Malinovskaya, S., Loboda, A., Shpinareva, I., Gurnitskaya, E., Korchevsky, D. Diagnostics of the collisionally pumped plasma and search of the optimal plasma parameters of x-ray lasing: calculation of electron-collision strengths and rate coefficients for Ne-like plasma. *J. Phys.: Conf. Ser.* **2005,** *11,* 188-

198.

16. Glushkov, A., Ambrosov, S., Loboda, A., Gurnitskaya, E., Prepelitsa, G. Consistent QED approach to calculation of electron-collision excitation cross sections and strengths: Ne-like ions. *Int. J. Quant. Chem.* **2005**, *104,* 562-569.

17. Ignatenko, A.V. Probabilities of the radiative transitions between Stark sublevels in spectrum of atom in an DC electric field: New approach. *Photoelectronics,* **2007**, *16*, 71-74.

18. Glushkov, A.V. Spectroscopy of atom and nucleus in a strong laser field: Stark effect and multiphoton resonances. *J. Phys.: Conf. Ser.* **2014**, *548*, 012020.

19. Glushkov, A.V., Ambrosov, S.V., Ignatenko, A. Non-hydrogenic atoms and Wannier-Mott excitons in a DC electric field: Photoionization, Stark effect, Resonances in ionization continuum and stochasticity. *Photoelect.,* **2001,** *10*, 103.

20. Glushkov, A., Buyadzhi, V., Svinarenko, A., Ternovsky, E.V., Advanced relativistic energy approach in electron-collisional spectroscopy of multicharged ions in plasma. *Concepts, Methods, Applications of Quantum Systems in Chemistry and Physics* (Springer). **2018**, *31*, 55-69.

21. Buyadzhi, V., Kuznetsova, A., Buyadzhi, A., Ternovsky, E.V., Tkach, T.B. Advanced quantum approach in radiative and collisional spectroscopy of multicharged ions in plasmas. Adv. in Quant. Chem. (Elsevier). **2019**, *78*, 171-191.

22. Ternovsky E.V., Mykhailov A.L New relativistic approach to computing spectral parameters of multicharged ions in plasmas. *Photoelectronics.* **2020,** *29*, 60-67.

23. Ternovsky E.V., Relativistic spectroscopy of multicharged ions in plasmas: Li-like ions. *Photoelectronics.* **2019**, *28*,105-112.

24. Glushkov, A.V. *Relativistic Quantum theory. Quantum mechanics of atomic systems;* Astroprint: Odessa, **2008**.

25. Khetselius, O.Yu. *Hyperfine structure of atomic spectra*. Astroprint: Odessa, **2008**.

26. Glushkov, A.V., Ivanov, L.N. Radiation decay of atomic states: atomic residue polarization and gauge noninvariant contributions. *Phys. Lett.A.* **1992,** *170,* 33.

27. Glushkov, A., Svinarenko, A., Ternovsky, V., Smirnov, A., Zaichko, P. Spectroscopy of the complex autoionization resonances in spectrum of helium: Test and new spectral data. *Photoelectr*. **2015**, *24*, 94.

28. Glushkov, A.V., Ivanov, L.N. Radiation decay of atomic states: atomic residue polarization and gauge noninvariant contributions. *Phys. Lett. A* **1992,** *170,* 33.

29. Glushkov, A.V.; Ivanov, L.N. DC strong-field Stark effect: consistent quantum-mechanical approach. *J. Phys. B: At. Mol. Opt. Phys.* **1993,** *26,* L379-386.

30. Ivanova, E.P., Ivanov, L.N., Glushkov, A., Kramida, A. High order corrections in the relativistic perturbation theory with the model zeroth approximation, Mg-Like and Ne-Like Ions. *Phys. Scripta* **1985**, *32,* 513-522.

31. Glushkov, A.V. *Relativistic and correlation effects in spectra of atomic systems*. Astroprint, Odessa, **2006.**

32. Khetselius, O.Yu. *Quantum structure of electroweak interaction in heavy finite Fermi-systems*. Astroprint: Odessa, **2011**.

33. Khetselius, O.Yu., Lopatkin, Yu.M., Dubrovskaya, Yu.V, Svinarenko, A.A. Sensing hyperfine-structure, electroweak interaction and parity non-conservation effect in heavy atoms and nuclei: New nuclear-QED approach. *Sensor Electr. and Microsyst. Techn*. **2010,** 7(2), 11-19.

34. Glushkov, A., Svinarenko, A., Ignatenko, A. Spectroscopy of autoionization resonances in spectra of the lanthanides atoms. *Photoelectronics*. **2011**, *20*, 90-94.

35. Khetselius, O.Yu. Relativistic perturbation theory calculation of the hyperfine structure parameters for some heavy-element isotopes. *Int. J. Quant. Chem.* **2009,** *109,* 3330–3335.

36. Khetselius, O. Relativistic calculation of the hyperfine structure parameters for heavy elements and laser detection of heavy isotope. *Phys. Scr.* **2009,** *135,*01402

37. Svinarenko, A.A., Glushkov, A.V., Khetselius, O.Yu., Ternovsky, V.B., Dubrovskaya, Yu., Kuznetsova, A., Buyadzhi, V. Theoretical spectroscopy of rare-earth elements: spectra and autoionization resonances. *Rare Earth Element*, Ed. J.Orjuela (InTech). **2017**, 83.

38. Glushkov, A.V., Khetselius, O.Yu., Svinarenko, A.A., Buyadzhi, V.V., Ternovsky, V.B, Kuznetsova, A., Bashkarev, P Relativistic perturbation theory formalism to computing spectra and radiation characteristics: application to heavy element. *Recent Studies in Perturbation Theory*, InTech. **2017**, 131.

39. Dubrovskaya, Yu., Khetselius, O.Yu., Vitavetskaya, L., Ternovsky, V., Serga, I. Quantum chemistry and spectroscopy of pionic atomic systems with accounting for relativistic, radiative, and strong interaction effects. *Adv. Quantum Chem.* **2019**, *78*, 193-222.

40. Khetselius, O.Yu., Glushkov, A.V., Dubrovskaya, Yu.V., Chernyakova, Yu.G., Ignatenko, A.V., Serga, I.N., Vitavetskaya, L. Relativistic quantum chemistry and spectroscopy of exotic atomic systems with accounting for strong interaction effects. In *Concepts, Methods and Applications of Quantum Systems in Chem. and Phys.* Springer. **2018**, *31*, 71.

Ternovsky E.V.

RELATIVISTIC APPROACH TO COMPUTING WAVELENGTHS OF TRANSITIONS IN SPECTRA OF ATOMIC SYSTEMS IN PLASMAS

Summary. New relativistic approach to computing the spectral parameters of multicharged ions in plasmas for different values of the plasmas screening (Debye) parameter (respectively, electron density, temperature) is presented. The presented approach is based on the generalized relativistic energy approach combined with the optimized relativistic many-body perturbation theory with the Dirac-Debye screening hamiltonian as a zeroth approximation, adapted for application to study the energy and spectral parameters of atoms and ions in plasmas. The special exchange potential as well as the electron density with dependence upon the temperature are used. The wavelengths for a number of transitions, including (A): $E(1s2p\ ^1P_1)$-$E(1s^2\ ^1S)$; (B) $E(1s3p\ ^1P_1)\_E(1s^2\ ^1S)$; (C)AK: $E(1s2p\ ^3P_1)\_E(1s2s\ ^3S)$; (D): $E(1s3p\ ^3P_1)\_E(1s2s\ ^3S)$ of the helium in plasmas for various Debye lengths are calculated and compared with the corresponding data by Kar-Ho.

Key words: atomic spectroscopy, plasmas, energy approach, relativistic theory

Терновський Є В.

РЕЛЯТИВІСТСЬКИЙ ПІДХІД ДО ОБЧИСЛЕННЯ ДОВЖИН ХВИЛЬ ПЕРЕХОДІВ У СПЕКТРАХ АТОМНИХ СИСТЕМ У ПЛАЗМІ

Резюме. Представлено новий релятивістський підхід до обчислення спектральних параметрів атомних систем у плазмі для різних значень параметра екранування (Дебая) плазми (відповідно, електронної густини, температури). Представлений підхід базується на узагальненому релятивістському енергетичному підході в поєднанні з оптимізованою релятивістською багаточастинковою теорією збурень з модельним гамільтоніаном Дірака-Дебая як нульовим наближенням теорії збурень, адаптованим для дослідження енергетичних та спектральних параметрів атомів та іонів у плазмі. Використовується спеціальний обмінний потенціал, а також електронна густина в залежності від температури. Довжини хвиль для ряду переходів, включаючи (A) $E(1s2p\ ^1P_1)$-$E(1s^2\ ^1S)$; (B) $E(1s3p\ ^1P_1)\_E(1s^2\ ^1S)$; (C)AK: $E(1s2p\ ^3P_1)\_E(1s2s\ ^3S)$; (D): $E(1s3p\ ^3P_1)\_E(1s2s\ ^3S)$ гелію в плазмі для різних довжин Дебая обчислюються та порівнюються з відповідними даними Кар-Хо.

Ключові слова: атомна спектроскопія, плазма, енергетичний підхід, релятивістська теорія

A.A. Kuznetsova, A. Sandler

Odessa National Maritime Academy, Odessa, 4, Didrikhsona str., Odessa
e-mail: kuznetsovaa232@gmail.com

THEORETICAL STUDY OF RYDBERG ALKALI ATOMIC SYSTEMS IN A BLACK-BODY RADIATION FIELD: RELATIVISTIC APPROACH

We present the results of studying the characteristics of Rydberg alkali atomic systems in a black-body (BBR; thermal) radiation field, in particular, BBR induced Stark shift coefficient k. As theoretical approach the combined generalized relativistic energy approach and relativistic many-body perturbation theory (PT) with ab initio Dirac zeroth approximation is applied. Application of theory to computing the spectral parameters of studied atomic systems have demonstrated physically reasonable agreement between the theoretical and experimental data. carefully. It should be noted that our method takes carefully into account such important factors as the implementation of a gauge invariance principle when calculating the corresponding matrix elements, the correct degree of consideration of complex exchange-correlation effects (primarily, the effect of polarization of the core), and also generates a fairly optimal one-quasiparticle representation in within the limits of many-body relativistic PT with ab initio zeroth Dirac-Fock (Kohn-Sham) approximation. In any case, the formalism developed in this work, as it follows from the given results, can be used for precise calculations of the Stark shift coefficient k, the BBR shift parameter β, and other parameters.

1. Introduction

Modern theoretical photo-optics and spectroscopy of atomic systems, laser physics, photoelectronics and related physical fields are characterized by rapid development, connected, on the one hand, with the unprecedented progress of modern experimental methods and technologies due to the appearance of intense and super-intense sources of coherent laser radiation, pulses from several tens of femtoseconds to units of picoseconds and the ability to achieve peak intensities from 10^{19} W/cm2 to promising relativistic and higher $\sim 10^{24}$ W/cm^2 (we are primarily talking about modern types of free electron lasers such as TESLA, XFEL etc.), the active use of beam-foil spectroscopy methods, magneto-optical traps with the production of single Rydberg atoms, collider and accelerator technology, etc. [1-25].

Relatively new topic of the modern theory is connected with consistent treating the Rydberg atoms in a field of the Blackbody radiation (BBR). It should be noted that the BBR is one of the essential factors affecting the Rydberg states in atoms [1].

The account for the ac Stark shift, fast redistribution of the levels' population and photoionization provided by the environmental BBR became of a great importance for successfully handling atoms in their Rydberg states. The vast majority of existing papers on the description of Rydberg atoms in the thermal radiation field (c.g. [1-32]) are based on the Coulomb hydrogen-like approximation, different versions of the quantum defect method, classical and quasiclassical model approaches, the model and pseudo – potential methods. consider the problem of calculating the shift in the frequency of atomic transitions induced by BBR radiation, which is of fundamental importance for the operation of, for example, atomic clocks. It is well known that the main contribution to systematic frequency shifts is due to the Stark shift.

The so-called BBR shift is one of the most important contributions at room temperature for many frequency standards. A detailed overview of the problem is given, e.g. in works [3-11, 20,21] and numerous sources cited there.

It should be noted that at the present time, the sought-after research has been transformed

into a separate highly intensive scientific field of research, and close attention is paid to theoretical developments, since the appropriate experimental measurements of BBR landslides are an extremely difficult academic task. In works [3-11,20], the current state of theoretical calculations of BBR shifts in various systems, which are of interest for the development of both microwave and optical frequency standards, is considered.

At the same time one should note that for heavy Rydberg atoms (both in the free state and in an external electromagnetic field) it is fundamentally important to accurately account for both relativistic and exchange-correlation effects. The quality and consistency of accounting for these effects also determine the accuracy of description of the energy and spectroscopic parameters of the heavy Rydberg atoms, including these atoms in a thermal radiation field. Naturally, the standard methods of the theoretical atomic physics, including the Hartree-Fock and Dirac-Fock approximations should be used in order to determine the thermal ionization characteristics of neutral and Rydberg atoms [1,2].

In this paper the results of studying the characteristics of Rydberg alkali atomic systems in a black-body (BBR; thermal) radiation field, in particular, BBR induced Stark shift coefficient k, on the basis of a new approach [20-22] are presented. As theoretical approach the combined generalized relativistic energy approach and relativistic many-body PT with ab initio Dirac zeroth approximation is applied (e.g.[23-33]).

2. Relativistic approach to atom in a Black-body radiation field

It is worth to remind that the electric field corresponding to thermal radiation according to Planck's law:

$$E^2(\omega)d\omega = \frac{8\alpha^3}{\pi} \frac{\omega^3 d\omega}{\exp(\omega/k_B T) - 1},$$

(1)

leads to non-resonant perturbation of atomic transitions, the corresponding electric field shift is then [7]:

$$\langle E^2 \rangle = (831.9 \text{ V/m})^2 \left(\frac{T(K)}{300}\right)^4.$$

(2)

The shift in the atomic transition frequency due to the action of an electric field is known to be related to the static polarizability as:

$$\delta\nu = -\frac{1}{2}(831.9 \text{ V/m})^2 \left(\frac{T(K)}{300}\right)^4 \alpha_0(1+\eta),$$

(3)

where η is an insignificant dynamic correction. It is not difficult to understand that the shift in the atomic transition frequency is actually the difference between the shifts of individual levels.

The key fundamental parameter is the β parameter of the relative BBR temperature-dependent atomic transition frequency shift, which is defined as [7,20]:

$$\frac{\delta\nu}{\nu_0} = \beta \left(\frac{T(K)}{T_0}\right)^4 \left(1 + \epsilon \left(\frac{T(K)}{T_0}\right)^2\right),$$

(4)

where, as usual, $T_0=300K$. The parameter β can be calculated directly on the basis of data on the Stark coefficient k according to the expression:

$$\beta = \frac{k}{\nu_0}(831.9 \text{ V/m})^2.$$

(5)

The fact is that the Stark coefficient is determined from the ratio for the frequency shift in a static electric field $\delta\nu=kE^2$. Accordingly, it can be related to the polarizability for the case of the initial and final states of the atomic system:

$$k = -\frac{1}{2}[\alpha_0(F) - \alpha_0(I)].$$

(6)

It is also worth quoting formulas that define a scalar and tensor polarizability, namely, a scalar polarizability can be standardly defined as (see, for example, [1,2]):

$$\alpha_{JF}^s(\omega) = \alpha_J^s(\omega) = \frac{1}{2J+1}\sum_{m_J=-J}^{m_J=J}\alpha_{Jm_J}(\omega)$$

$$= \frac{1}{2}\frac{c^3}{a_0^3}\sum_{J'}'\frac{2J_u+1}{2J_d+1}\frac{1}{(\omega_{J'J})^2}\frac{A_{J_u\to J_d}}{(\omega_{J'J})^2-\omega^2},$$

(7)

$$\omega_{J'J} = (E_{J'} - E_J)/\hbar$$

(8)

where I is the nuclear spin, J - total electronic moment.

Further let us give characteristics of the used generalized energy approach [9-20] and relativistic perturbation theory with the zeroth approximation [21-32] to computing the atomic radiation and spectral parameters. According to Ref. [11,22], the RMBPT zeroth order Hamiltonian of the Rydberg atomic system is as follows:

$$H_0 = \sum_i \{\alpha c p_i - \beta m c^2 + [-Z/r_i + $$
$$U_{MF}(r_i \mid b) + V_{XC}(r_i)]$$

(4)

where c is the velocity of light, α_i, α_j – the Dirac matrices, ω_{ij} –the transition frequency, Z is a charge of atomic nucleus. The general potential in (4) includes self-consistent Coulomb-like mean-field potential $U_{MF}(r_i \vee b)$, ab ibitio one-particle exchange-correlation (relativistic generalized exchange Kohn-Sham potential plus generalized correlation potential) $V_{XC}(r_i \vee b)$ with the gauge calibrated parameter b (it is determined within special relativistic procedure on the basis of relativistic energy approach (e.g. [1,2,21-26]).

The perturbation operator is as follows:

$$H^{PT} = \sum_{i>j} exp(i\omega_{ij}r_{ij})\cdot\frac{(1-\alpha_i\alpha_j)}{r_{ij}} - $$
$$\sum_i [U_{MF}(r_i) + V_{XC}(r_i \mid b)]$$

(5)

The multielectron interelectron exchange-correlation effects (the core polarization and screening effects, continuum pressure etc) are taken into consideration as the RMBPT second and higher orders contributions. The details of calculation of the corresponding matrix elements of the polarization and screening intere-

lectron interaction potentials are described in Refs. [9,22,33-38].

In order to calculate the values of A in (7) we use the known relativistic energy approach. Within it in the relativistic theory a radiation decay probability (ionization cross-section etc) is connected with the imaginary part of electron energy shift. The total energy shift of the state is usually presented in the form: $\Delta E = Re\Delta E + i\,\Gamma/2$, where Γ is interpreted as the level width, and a decay probability $P = \Gamma$. The imaginary part of electron energy shift is defined in the PT lowest order as:

$$Im\Delta E(B) = -\frac{e^2}{4\pi}\sum_{\substack{\alpha>n>f \\ [\alpha<n\le f]}}V_{\alpha n\alpha n}^{|\omega_{\alpha n}|},$$

(6)

where $(\alpha>n>f)$ for electron and $(\alpha<n<f)$ for vacancy. The matrix element is determined as follows [23-25]:

$$V_{ijkl}^{|\omega|} = \iint dr_1 dr_2 \Psi_i^*(r_1)\Psi_j^*(r_2)\frac{\sin|\omega|r_{12}}{r_{12}}(1- $$
$$-\alpha_1\alpha_2)\Psi_k^*(r_2)\Psi_l^*(r_1)$$

(7)

Their detailed description of the matrix elements and procedure for their computing is presented in Refs. [20-25]. The relativistic wave functions are calculated by solution of the Dirac equation with the potential, which includes the Dirac-Fock consistent field potential and additionally polarization potential [1]. The detailed procedures of calculation of the radial and angular integrals (amplitudes) in the matrix elements are described in Refs. [1,2,23,24,29-38]. All calculations are performed on the basis of the numeral code Superatom-ISAN (version 93).

3. Results and conclusions

Until now, a considerable number of works have been used to calculate the Stark shift coefficient k (10^{-10} Hz/(V/m)^2) and the BBR shift parameter β. Among the theoretical approaches used to calculate the specified parameters, various improved versions of the multi-particle relativistic PT method, taking

into account corrections up to higher PT orders, are repeatedly mentioned in this work. In table 1 there are presented the experimental and theoretical values of the Stark shift coefficient k (10^{-10} Hz/(V/m)^2) for transitions between components of the hyperfine structure of the ground state): Th1 – linearized coupled cluster method; Th2–the PT method with screened Coulomb interaction; Th3 is our RMBPT-DKS theory (see, e.g., [7,8,20]).

Table 1. The value of the Stark shift coefficient k (in 10^{-10} Hz/(V/m)^2): Th1 – linearized curled-cluster method; Th2 –TK method (PTSCI); Th3 -our RMBPT-DKS theory (see text)

^{23}Na	3s (F = 2 - F = 1)	Th1	-0.1285
		Th3	-0.126
		Exp	-0.124(3)
^{87}Rb	5s (F = 2 - F = 1)	Th1	-1.272
		Th2	-1.240
		Th3	-1.226
		Exp	-1.23(3)
^{133}Cs	6s (F = 2 - F = 1)	Th1	-2.271
		Th2	-2.260
		Th3	-2.245
		Exp1	-2.271(4)
		Exp2	-2.05(5)

The analysis of the presented data shows that, firstly, the theoretical results correlate reasonably well with each other. It is important to note that all theoretical calculations, as the most important component, include procedures for taking into account exchange-correlation corrections, although the classification of sought corrections and specific accounting schemes differ.

The method of connected clusters uses a standard methodology. It should be noted that in the PT method with screened Coulomb interaction (known as PTSCI), or the correlation potential method, the key approximation is the relativistic Hartree-Fock approximation using the correlation potential and random phase approximation. It should be noted that our method takes carefully into account such important factors as the implementation of a gauge invariance principle when calculating the corresponding matrix elements, the correct degree of consideration of complex exchange-correlation effects (primarily, the effect of polarization of the core). It is important to not too

that our method generates a fairly optimal one-quasiparticle representation in within the limits of many-body relativistic PT with ab initio zeroth Dirac-Fock (Kohn-Sham) approximation.

In any case, the formalism developed in this work, as it follows from the given results, can be used for precise calculations of the Stark shift coefficient k, the BBR shift parameter β, and other parameters.

References

1. Glushkov, A.V. *Relativistic Quantum theory. Quantum mechanics of atomic systems*. Astroprint: Odessa, **2008**.
2. Khetselius, O.Yu. *Hyperfine structure of atomic spectra*. Astroprint: Odessa, **2008**.
3. Safronova U.I., Johnson W., Derevianko A., Relativistic many-body calculations of energy levels, hyperfine constants, electric-dipole matrix elements, static polarizabilities for alkali-metal atoms. Phys.Rev.A.-1999.-Vol.60.-P.4476-4486.
4. Nascimento V.A., Caliri L.L., de Oliveira A.L., Bagnato V.S. , Marcassa L.G. Measurement of the lifetimes of S and D states below n=31 using cold Rydberg gas. *Phys.Rev.A*. **2006,** 74, 054501.
5. Beterov, I.I., Ryabtsev, I., Tretyakov D., Entin, V. Quasiclassical calculations of blackbody-radiation-induce depopulation rates and effective lifetimes of Rydberg *nS*, *nP*, and *nD* alkali-metal atoms with *n*~80. *Phys Rev A*. **2009,** 79, 052504.
6. Beterov I.I., TretyakovD.V., Ryabtsev I.I., Entin V.M., Ekers A., Bezuglov N.N., Ionization of Rydberg atoms by blackbody radiation. *New J. Phys*. **2009,** *11*, 013052
7. Safronova U., Safronova M. Third-order relativistic many-body calculations of energies, transition rates, hyperfine constants, blackbody radiation shift in ^{171}Yb^{+}. *Phys. Rev. A*. **2009**, *79*, 022512.
8. Safronova M.S., Porsev S.G., Safronova U.I., Kozlov M.G., Clark C.W., Blackbody-radiation shift in the Sr optical atomic clock. *Phys. Rev.A*. **2013**, 87, 012509.
9. Angstmann, E., Dzuba, V., Flambaum, V. Frequency shift of hyperfine transitions

due to blackbody radiation. *Phys. Rev. A.* **2006**, *74*, 023405.

10. Gallagher T.F., Cooke W.E. Interactions of Blackbody Radiation with atoms. *Phys. Rev. Let*t. **1979**, *42*, 835–839.

11. Lehman G. W. Rate of ionization of H and Na Rydberg atoms by black-body radiation. *J. Phys. B: At. Mol. Phys*. **1983**, *16*, 2145-2156.

12. D'yachkov L., Pankratov P. On the use of the semiclassical approximation for the calculation of oscillator strengths and photoionization cross sections. *J. Phys. B: At. Mol. Opt. Phys*. **1994**, *27*, 461-468.

13. Sukachev D., Fedorov S., Tolstikhina I., Tregubov D., Kalganova E, Vishnyakova G., Golovizin A., Kolachevsky N., Khabvarova K., Sorokin V., Inner -shell magnetic dipole transition in Tm atoms: A candidate for optical lattice clock. *Phys. Rev. A.* **2016**. 94, 022512.

14. Hirata S., Ivanov S, Bartlett R., Grabowski I. Exact-exchange time-dependent density-functional theory for static and dynamics polarizabilities. *Phys.Rev.A.* **2005**, *71*, 032507.

15. Glushkov A.V., Relativistic polarization potential of a many-electron atom. *Sov. Phys. Journ.* **1992**. *41*(9), 3-8

16. Glushkov A.V., Mansarliysky V.F., Khetselius O.Yu., Ignatenko A.V., Smirnov A.V., Prepelitsa G.P. Collisional shift of hyperfine line for thallium in an atmosphere of the buffer inert gas// Journal of Physics: C Series (IOP, UK). **2017,** *810*, 012027.

17. Mansarliysky V.F., Ternovsky E.V., Ignatenko A.V., Ponomarenko E.L. Optimized relativistic Dirac-Fock-Sturm approach to calculating polarizabilities and the hyperfine line shift and broadening for heavy atoms in the buffer gas. *Photoelectronics.* **2017**. 26, 41-47.

18. Khetselius O.Yu., Zaichko P.A., Smirnov A.V., Buyadzhi V.V., Ternovsky V.B., Florko T.A., Mansarliysky V.F. Relativistic many-body perturbation theory calculation of the hyperfine structure and oscillator strengths parameters for some heavy elements atoms and ions. In: *Quantum Systems in Physics, Chemistry, and Biology. Series: Progress in Theoretical Chemistry and Physics*, Eds. A.Tadjer, R.Pavlov, J.Maruani, E.Brändas, G.Delgado-Barrio (Springer). **2017.** *30*, 171-182.

19. Mansarliysky V.F. New relativistic approach to calculating the hyperfine line shift and broadening for heavy atoms in the buffer gas. *Photoelectronic*s. **2016**. 25, 73-78.

20. Glushkov A.V., Ternovsky V.B., Kuznetsova A.A., Tsudik A.V., Spectroscopy of Rydberg Atomic Systems in a Black-Body Radiation Field. In: *Mammino L., Ceresoli D., Maruani J., Brändas E. (eds) Advances in Quantum Systems in Chemistry, Physics, and Biology. Ser.: Progress in Theoretical Chemistry and Physics,* Cham: Springer. **2020**, Vol.32, P.51-63.

21. Zaichko P.A., Kuznetsova A.A., Tsudik A.V., Mansarliysky V.F., Relativistic calculation of the radiative transition probabilities and lifetimes of excited states for the rubidium atom in a Black-body radiation field. *Photoelectronics.* **2020**, 29, 126-133.

22. Kuznetsova A.A., Glushkov A.V., Ignatenko A.V., Svinarenko A.A., Ternovsky V.B., Spectroscopy of Multielectron Atomic Systems in a DC Electric Field. Advances in Quantum Chemistry (Elsevier). **2019**. Vol.*78*. P.287-306;

23. Glushkov, A.V. *Relativistic and correlation effects in spectra of atomic systems*. Astroprint: Odessa, **2006**.

24. Khetselius, O.Yu. *Quantum structure of electroweak interaction in heavy finite Fermi-systems.* Astroprint: Odessa, **2011**.

25. Ivanov, L.N.; Ivanova, E.P. Method of Sturm orbitals in calculation of physical characteristics of radiation from atoms and ions. *JETP.* **1996,** *83,* 258-266.

26. Glushkov, A.; Ivanov, L. Radiation decay of atomic states: atomic residue polarization and gauge noninvariant

contributions. *Phys. Lett.A* **1992**, *170,* 33.

27. Glushkov A.V.; Ivanov, L.N. DC strong-field Stark effect: consistent quantum-mechanical approach. *J. Phys. B: At. Mol. Opt. Phys.* **1993,** *26,* L379-386.

28. Glushkov A., Multiphoton spectroscopy of atoms and nuclei in a laser field: Relativistic energy approach and radiation atomic lines moments method. *Adv. in Quantum Chem.* **2019**, *78*, 253-285.

29. Glushkov, A.V.; Khetselius, O.Yu.; Svinarenko A. Theoretical spectroscopy of autoionization resonances in spectra of lanthanides atoms. *Phys. Scripta.* **2013**, *T153*, 014029.

30. Khetselius, O.Yu. Relativistic perturbation theory calculation of the hyperfine structure parameters for some heavy-element isotopes. *Int. Journ. Quant.Chem.* **2009,** *109,* 3330-3335.

31. Khetselius, O. Relativistic calculation of the hyperfine structure parameters for heavy elements and laser detection of the heavy isotopes. *Phys.Scr.* **2009,** *T135,* 014023

32. Khetselius, O.Yu. Optimized relativistic many-body perturbation theory calculation of wavelengths and oscillator strengths for Li-like multicharged ions. Adv. Quant. Chem. **2019**, *78*, 223-251.

33. Khetselius, O.Yu., Glushkov, A.V., Dubrovskaya, Yu.V., Chernyakova, Yu., Ignatenko, A.V., Serga, I., Vitavetskaya, L. Relativistic quantum chemistry and spectroscopy of exotic atomic systems with accounting for strong interaction effects. In: Concepts, *Methods and Applications of Quantum Systems in Chemistry and Physics*. Springer, Cham, **2018,** *31*, 71-91.

34. Dubrovskaya, Yu., Khetselius, O.Yu., Vitavetskaya, L., Ternovsky, V., Serga, I. Quantum chemistry and spectroscopy of pionic atomic systems with accounting for relativistic, radiative, and strong interaction effects. *Adv. in Quantum Chem.* **2019,** Vol.78, pp 193-222.

35. Bystryantseva A., Khetselius O.Yu., Dubrovskaya Yu., Vitavetskaya L.A., Berestenko A.G. Relativistic theory of spectra of heavy pionic atomic systems with account of strong pion-nuclear interaction effects: ^{93}Nb, ^{173}Yb, ^{181}Ta , ^{197}Au. *Photoelectronics.* **2016**, *25*, 56-61.

36. Khetselius, O., Glushkov, A., Gurskaya, M., Kuznetsova, A., Dubrovskaya Yu., Serga I., Vitavetskaya L. Computational modelling parity nonconservation and electroweak interaction effects in heavy atomic systems within the nuclear-relativistic many-body perturbation theory. *J. Phys.: Conf. Ser.* **2017,** *905*(1), 012029.

37. Khetselius O., Gurnitskaya E. Sensing the electric and magnetic moments of a nucleus in the N-like ion of Bi. *Sensor Electr. and Microsyst. Tech.* **2006**, *N3*, 35

38. Khetselius, O.Yu., Lopatkin Yu.M., Dubrovskaya, Yu.V, Svinarenko A.A. Sensing hyperfine-structure, electroweak interaction and parity non-conservation effect in heavy atoms and nuclei: New nuclear-QED approach. *Sensor Electr. and Microsyst. Techn.* **2010,** 7(2), 11-19.

A.A. Kuznetsova, A. Sandler

THEORETICAL STUDY OF RYDBERG ALKALI ATOMIC SYSTEMS
IN A BLACK-BODY RADIATION FIELD: RELATIVISTIC APPROACH

Summary. We present the results of studying the characteristics of Rydberg alkali atomic systems in a black-body (BBR; thermal) radiation field, in particular, BBR induced Stark shift coefficient k. As theoretical approach the combined generalized relativistic energy approach and relativistic many-body perturbation theory (PT) with ab initio Dirac zeroth approximation is applied. Application of theory to computing the spectral parameters of studied atomic systems have demonstrated physically reasonable agreement between the theoretical and experimental data. carefully. It should be noted that our method takes carefully into account such important

factors as the implementation of a gauge invariance principle when calculating the corresponding matrix elements, the correct degree of consideration of complex exchange-correlation effects (primarily, the effect of polarization of the core), and also generates a fairly optimal one-quasiparticle representation in within the limits of many-body relativistic PT with ab initio zeroth Dirac-Fock (Kohn-Sham) approximation. In any case, the formalism developed in this work, as it follows from the given results, can be used for precise calculations of the Stark shift coefficient k, the BBR shift parameter β, and other parameters.

Key words: Rydberg alkali atoms, relativistic theory, black-body radiation field.

Г.О. Кузнецова, А. Сандлер

ТЕОРЕТИЧНЕ ДОСЛІДЖЕННЯ РІДБЕРГІВСЬКИХ ЛУЖНИХ АТОМНИХ СИСТЕМ У ПОЛІ ВИПРОМІНЮВАННЯ ЧОРНОГО ТІЛА: РЕЛЯТИВІСТСЬКИЙ ПІДХІД

Резюме. Наведено результати дослідження характеристик рідбергівських лужних атомних систем у полі чорнотільного (BBR; теплового) випромінювання, зокрема індукованого BBR коефіцієнта штарківського зсуву k. В якості теоретичного підходу застосовано комбінований узагальнений релятивістський енергетичний підхід і релятивістську багаточастинкову теорію збурень з ab initio нульовим наближенням Дірака. Застосування теорії для обчислення спектральних параметрів досліджуваних атомних систем продемонструвало фізично обґрунтовану узгодженість між теоретичними та експериментальними даними. Запропонований підхід ретельно враховує такі важливі чинники, як реалізація принципу калібрувальної інваріантності при розрахунку відповідних матричних елементів радіаційних переходів, атомних поляризованостей, досить коректний ступінь врахування складних обмінно-кореляційних ефектів (насамперед, ефекту поляризації атомного остову), а також генерує досить оптимальне одноквазічастинкове представлення в межах релятивістської багаточастинкової теорії збурень із оптимальним нульовим наближенням Дірака-Фока (Кона-Шема). Розвинутий метод може бути використаний для подальших обчислень індукованого BBR коефіцієнта штарківського зсуву, параметра зсуву BBR та інших характеристик атомів у BBR полі.

Ключові слова: рідбергівські лужні атоми, релятивістська теорія, чорнотільне теплове випромінювання.

A.L. Mykhailov

Odessa State Environmental University, L'vovskaya str.15, Odessa
E-mail: mykhailovol94@gmail.com

ADVANCED STUDY OF SPECTRAL AND HYPERFINE STRUCTURE PARAMETERS FOR Li-LIKE MULTICHARGED IONS WITHIN RELATIVISTIC THEORY

The relativistic many-body perturbation theory with the optimized Dirac zeroth approximation is applied to calculation of some fundamental characteristics of the hyperfine structure of middle and heavy Li-like multicharged ions. The relativistic, exchange-correlation and other corrections are accurately taken into account. The optimized relativistic orbital basis set is generated in the optimal many-body perturbation theory approximation with performance of the gauge invariance principle. There are listed the calculated values of derivatives of the one-electron characteristics, including the hyperfine structure parameters, on nuclear radius for the Li-like multicharged ions with the corresponding analysis.

1. Introduction

In the last few decades a study of energy, spectral and radiation properties of the multicharged ions has a subject of significant interest for many physical, astrophysical and chemical applications. The levels energies, transitions probabilities, oscillator strengths and so on are very important in atomic physics (spectroscopy, spectral lines theory), astrophysics, plasma physics, laser physics, quantum electronics. They are very much needed in research of thermonuclear reactions, where the ionic radiation is one of the primary loss mechanisms and so on. The spectral lines belonging to the radiation of many multicharged ions have been identified in both solar flares and nonflaring solar active regions, observed in high-temperature plasmas, such as pinches and laser-produced plasmas, and in beam-foil spectra.

The multiple observations of satellite lines of the He-, Li-, Be-like multicharged ions in the solar corona and in laboratory plasmas have emphasized the need for accurate values of the energetic and spectroscopic parameters for multicharged ions (c.f.[1-15]).

Theoretical methods used to calculate the spectroscopic characteristics of heavy and superheavy ions may be divided into three main groups: a) the multi-configuration Hartree-Fock method, in which relativistic effects are taken into account in the Pauli approximation, gives a rather rough approximation, which makes it possible to get only a qualitative idea on the spectra of heavy ions. b) The multi-configuration Dirac-Fock (MCDF) approximation (the Desclaux program, Dirac package) [1-4] is, within the last few years, the most reliable version of calculation for multielectron systems with a large nuclear charge; in these calculations one- and two-particle relativistic effects are taken into account practically precisely.

Howver, it is well known that in the region of small Z (Z is a charge of the nucleus) the calculation error in the MCDF approximation is connected mainly with incomplete inclusion of the correlation and exchange effects which are only weakly dependent on Z; c) In the study of lower states for ions with $Z40$ an expansion into double series of the PT on the parameters $1/Z$, αZ (α is the fine structure constant) turned out to be quite useful. It permits evaluation of relative contributions of the different expansion terms: non-relativistic, relativistic, QED contributions as the functions of Z.

Nevertheless, the serious problems in calculation of the heavy elements spectra are connected with developing new, high exact meth-

ods of account for the QED effects, in particular, the Lamb shift (LS), self-energy (SE) part of the Lamb shift, vacuum polarization (VP) contribution, correction on the nuclear finite size for superheavy elements and its account for different spectral properties of these systems, including calculating the energies and constants of the hyperfine structure, derivatives of the one-electron characteristics on nuclear radius, nuclear electric quadrupole, magnetic dipole moments etc (c.f.[1-15]). In this work the relativistic many-body perturbation theory with the optimized Dirac zeroth approximation (e.g.[13-15]) is applied to calculation of some fundamental characteristics of the hyperfine structure of middle and heavy Li-like multicharged ions. There are listed the calculated values of derivatives of the one-electron characteristics, including the hyperfine structure parameters, on nuclear radius for the Li-like multicharged ions with the corresponding analysis. It should be noted that the Li-like ions was always a subject of intensive theoretical and experimental studying (e.g. [1-4, 13-15, 18]).

2. Relativistic theory of determination hyperfine structure parameters

The theoretical basis of the RMBPT with the Dirac-Kohn-Sham zeroth approximation was in details presented in papers [13-15] (see [2-4] too), and here we will only present the essential features. As usually, we use the charge distribution in atomic (ionic) nucleus $\rho(r)$ in the Gaussian approximation:

$$\rho(r \lor R) = \left(4\gamma^{3/2}/\sqrt{\pi}\right)\exp\left(-\gamma r^2\right) \qquad (1)$$

where $\gamma=4/\pi R^2$ and R is the effective nucleus radius. The Coulomb potential for the spherically symmetric density $\rho(r)$ is:

$$V_{nucl}(r|R) = -((1/r)\int_0^r dr' r'^2 \rho(r'|R) + \int_r^\infty dr' r' \rho(r'|R)) \quad (2)$$

Further consider the Dirac-like type equations for the radial functions F and G (components of the Dirac spinor) for a three-electron system $1s^2nlj$. Formally a potential $V(r|R)$ in these equations includes−electric and polarization potentials of the nucleus, V_X is the exchange

inter-electron interaction (in the zeroth approximation). The standard Kohn-Sham (KS) exchange potential is [2]:

$$V_X^{KS}(r) = -(1/\pi)[3\pi^2\rho(r)]^{1/3}.$$
$$\qquad (3)$$

In the local density approximation the relativistic potential is [33]:

$$V_X[\rho(r),r] = \frac{\delta E_X[\rho(r)]}{\delta\rho(r)},$$
$$\qquad (4)$$

where $E_X[\rho(r)]$ is the exchange energy of the multielectron system corresponding to the homogeneous density $\rho(r)$, which is obtained from a Hamiltonian having a transverse vector potential describing the photons. In this theory the exchange potential is [3,4]:

$$V_X[\rho(r),r] = V_X^{KS}(r)\cdot\{\frac{3}{2}\ln\frac{[\beta+(\beta^2+1)^{1/2}]}{\beta(\beta^2+1)^{1/2}} - \frac{1}{2}\},$$
$$\qquad (5)$$

where $\beta = [3\pi^2\rho(r)]^{1/3}/c$, c is the velocity of light. The corresponding one-quasiparticle correlation potential

$$V_C[\rho(r),r] = -0.0333\cdot b\cdot\ln[1+18.3768\cdot\rho(r)^{1/3}]$$
$$, \quad (6)$$

(here b is the optimization parameter; see below). The perturbation operator contains the relativistic potential of the interelectron interaction of the form:

$$V_{e-e}^{rel}(r_i,r_j) = \frac{(1-\alpha_i\alpha_j)}{r_{ij}}\exp(i\omega_{ij}r_{ij})$$
$$, \qquad (7)$$

(here α_i, α_j are the Dirac matrices, ω_{ij} is the transition frequency) with the subsequent subtraction of the exchange and correlation potentials. The rest of the exchange and correlation effects is taken into account in the first two orders of the PT (c.g.[2-4].

In Refs. [2-4,17-22] it was presented the effective relativistic formalism with ab initio optimization principle for construction of the optimal relativistic orbital basis set. The minimization condition of the gauge

dependent multielectron contribution of the lowest QED PT corrections to the radiation widths of the atomic levels is used. The alternative versions are proposed in refs. [30-37]. The general scheme of treatment of the spectra for Li-like ion is as follows. Consider the Dirac-type equations for a three-electron system $1s^2nlj$. Formally they fall into one-electron Dirac equations for the orbitals $1s1s$ and nlj with the potentials:

$$V(r)=2V(r\vee 1s)+V(r\vee nlj)+V_x(r)+V(r\vee R)$$
(8)

$V(r\vee R)$ includes the electrical and the polarization potentials of the nucleus; the components of the self-consistent Hartree-like potential, V_{ex} is the exchange inter-electron interaction (look below). The main exchange effect will be taken into account if in the equation for the $1s$ orbital we assume

$$V(r)=V(r\vee 1s)+V(r\vee nlj)$$
(9)

and in the equation for the nlj orbital

$$V(r)=2V(r\vee 1s)$$
(10)

The rest of the exchange and correlation effects will be taken into account in the first two orders of the PT by the total inter-electron interaction [13-15,18-20].

The used expression for $\rho(r\vee 1s)$ coincides with the precise one for a one-electron relativistic atom with a point nucleus. The finiteness of the nucleus and the presence of the second $1s$ electron are included effectively into the energy E_{1s}.

Actually, for determination of the properties of the outer nlj electron one iteration is sufficient. Refinement resulting from second iteration (by evaluations) does not exceed correlation corrections of the higher orders omitted in the present calculation.

The relativistic potential of core (the "screening" potential) $2V^{(1)}(r\vee 1s)=V_{scr}$ has correct asymptotic at zero and in the infinity. The procedures for accounting of the nuclear,

radiative QED corrections are in details presented in Refs. [2-4,13-24].

3. Results and Conclusions

Energies of the quadruple (W_q) and magnetic dipole (W_μ) interactions, which define a hyperfine structure (hfs), are calculated as follows [4]:

$$W_q=[\Delta+C(C+1)]B,$$

$$W_\mu=0,5\ AC,$$

$$\Delta=-(4/3)(4\chi-1)(I+1)/[i(I-1)(2I-1)],$$

$$C=F(F+1)-J(J+1)-I(I+1).$$
(11)

Here I is a spin of nucleus, F is a full momentum of system, J is a full electron momentum. Constants of the hyperfine splitting are expressed through the standard radial integrals:

$$A=\{[(4,32587)10^{-4}Z^2\chi g_I]/(4\chi^2-1)\}(RA)_{-2},$$
(12)

$$B=\{7.2878\ 10^{-7}\ Z^3Q/[(4\chi^2-1)I(I-1)\}\ (RA)_{-3},$$

Here g_I is the Lande factor, Q is a quadruple momentum of nucleus (in Barn); radial integrals are defined as follows [4,18]:

$$(RA)_{-2}=\int_0^\infty drr^2 F(r)G(r)U(1/r^2,R),$$

(13)

$$(RA)_{-3}=\int_0^\infty drr^2[F^2(r)+G^2(r)]U(1/r^3,R)$$

and calculated in the Coulomb units (=3,57 $10^{20}Z^2m^{-2}$; = 6,174 $10^{30}Z^3m^{-3}$ for valuables of the corresponding dimension). The radial parts F and G of two components of the Dirac function for electron, which moves in the potential $V(r,R)+U(r,R)$, are determined by solution of the Dirac equations (look above). In table 1 there are listed the calculated values of derivatives of the one-electron characteristics on nuclear radius (in cm^{-1}/cm) for 2l,3l,4l (l=0) states of the Li-like ions with minimally possible valus of j:

$$d\langle|V|\rangle /dR=Z^3DV\ (cm^{-1}/cm);$$

$$d\langle|U|\rangle /dR = Z^5 DU \text{ (cm}^{-1}\text{/cm)}, \quad (14)$$

$$dA/dR = Z^4 g_I DA \text{ (cm}^{-1}\text{/cm)}.$$

Here 1cm^{-1} is an energy unit and 1cm is a length unit.

Table 1 Derivatives of the one-electron characteristics on nuclear radius (in cm^{-1}/cm) for 2s,3s,4s states of the Li-like ions: $d\langle|V|\rangle /dR = Z^3 DV$, $d\langle|U|\rangle /dR = Z^5 DU$, $dA/dR = Z^4 g_I DA$

nlj Z		30	41	59
$2s_{1/2}$	DV	20+11	41 +11	121 +12
	DU	14+06	16 +06	20 +06
	DA	19+06	24 +06	44 +06
$3s_{1/2}$	DV	60+10	12 +11	35 +11
	DU	42+05	44 +05	60 +05
	DA	56+05	74 +05	12 +06
$4s_{1/2}$	DV	24+10	51 +10	13 +11
	DU	17+05	18 +05	24 +05
	DA	23+05	30 +05	55 +05
nlj Z		69	79	92
$2s_{1/2}$	DV	223 +12	415 +12	967 +12
	DU	25 +06	36 +06	64 +06
	DA	63 +06	101 +07	197 +07
$3s_{1/2}$	DV	65 +11	122 +12	293 +12
	DU	81 +05	10 +06	18 +06
	DA	18 +06	29 +06	57 +06
$4s_{1/2}$	DV	26 +11	50 +11	121 +12
	DU	32 +05	47 +05	80 +05
	DA	81 +05	11 +05	23 +05

Let us remember that here V is a potential of the elctron-nuclear interaction and U is the Serber-Uehling vacuum-polarization potential. Considered value of full moment is $j=3/2$ for deriviative of the constant B on nuclear radius $\partial B/\partial R$ and value $j=3/2$ for other operators. It should be noted that the corresponding characteristics are less sensitive to the nuclear size for states with the large values of moment

j. In any case cited effects are not observed in the modern experiment. In table 2 we present the calculated values of derivatives of the hfs constant B on nuclear radius (in cm^{-1}/cm); $dB/dR = -Z^4 QDB/[I(2I-1)]$.

Table 2 Deriviatives of the hfs constant B on nuclear radius (in cm^{-1}/cm) $dB/dR = -Z^4 QDB/[I(2I-1)]$.

Nlj	Z	20	41	59
$2p_{3/2}$	DB	02+02	11+02	17+02
$3p_{3/2}$	DB	19+01	37+01	57+01
$4p_{3/2}$	DB	03+01	11+01	21+01
nlj	Z	69	79	92
$2p3/2$	DB	27+02	40+02	71+02
$3p3/2$	DB	95+01	15+02	27+02
$4p3/2$	DB	38+01	60+02	12+02

Let us note that for derivatives in tables 1,2 the main member of degree dependence upon a charge Z is separated. The remained Z-dependence is directly connected with relativistic and nuclear (the finite nuclear charge) effects in the one-electron functions.

References

1. Grant I. *Relativistic Quantum Theory of Atoms and Molecules.* Oxford, 2007.
2. Glushkov, A.V. *Relativistic Quantum theory. Quantum mechanics of atomic systems.* Astroprint: Odessa, 2008.
3. Glushkov, A.V. *Relativistic and correlation effects in spectra of atomic systems.* Astroprint: Odessa, 2006.
4. Khetselius, O.Yu. *Hyperfine structure of atomic spectra.* Astroprint: Odessa, 2008.
5. Khetselius, O.Yu. Atomic parity non-conservation effect in heavy atoms and observing P and PT violation using NMR shift in a laser beam: To precise theory. *J. Phys.: Conf. Ser.* 2009, *194,* 022009
6. Khetselius, O.Yu. Hyperfine structure of radium. *Photoelectronics.* 2005, *14,* 83.
7. Khetselius, O.. Relativistic perturbation theory calculation of the hyperfine

structure parameters for some heavy-element isotopes. *Int. Journ. Quant. Chem.* 2009, *109,* 3330-3335.

8. Khetselius, O.Yu. Relativistic calculation of the hyperfine structure parameters for heavy elements and laser detection of the heavy isotopes. *Phys.Scripta.* 2009, *135,* 014023.

9. Khetselius, O.Yu. Optimized relativistic many-body perturbation theory calculation of wavelengths and oscillator strengths for Li-like multicharged ions. Adv. Quant. Chem. 2019, *78,* 223-251.

10. Khetselius O.Yu.; Gurnitskaya, E.P. Sensing the hyperfine structure and nuclear quadrupole moment for radium. *Sensor Electr. and Microsyst. Techn.* 2006, *2,* 25-29.

11. Khetselius, O.Yu.; Gurnitskaya, E.P. Sensing the electric and magnetic moments of a nucleus in the N-like ion of Bi. *Sensor Electr. and Microsyst. Techn.* 2006, *3,* 35-39.

12. Khetselius, O.Yu. *Quantum structure of electroweak interaction in heavy finite Fermi-systems.* Astroprint: Odessa, 2011.

13. Khetselius O.Yu., Glushkov A.V., Ternovsky E.V., Buyadzhi V.V., Mykhailov O.L. Hyperfine and Electroweak Interaction in Heavy Finite Fermi-Systems and Parity Non-conservation Effect. In*: Mammino L., Ceresoli D., Maruani J., Brändas E. (eds) Advances in Quantum Systems in Chemistry, Physics, and Biology. Ser.: Progress in Theor. Chem. and Phys.,* Cham: Springer. 2020, Vol.32, P.65-81.

14. Khetselius O., Mykhailov, A. Relativistic calculation of wavelengths and E1 oscillator strengths in li-like multicharged ions and gauge invariance principle. *Photoelectronics.* 2020, *29,* 134-142.

15. Mykhailov O.L., Efimova E., Ternovsky E.V., Serga I., Hyperfine structure parameters for Li-like multicharged ions within relativistic many-body perturbation theory *Photoelectronics.* 2019, *28,* 113-120.

16. Svinarenko, A.A. Study of spectra for lanthanides atoms with relativistic many-body perturbation theory: Rydberg resonances. *J. Phys.: Conf. Ser.* 2014, *548,* 012039.

17. Ivanova, E.P.; Ivanov, L.N.; Glushkov, A.V.; Kramida, A.E. High order corrections in the relativistic perturbation theory with the model zeroth approximation, Mg-Like and Ne-Like Ions. *Phys. Scripta* 1985, *32,* 513-522.

18. Ivanov, L. N.; Ivanova, E. P.; Aglitsky, E. V. Modern Trends in the Spectroscopy of Multicharged Ions. *Phys. Rep.* 1988, *166,* 315-390.

19. Glushkov, A.V.; Ivanov, L.N. Radiation decay of atomic states: atomic residue polarization and gauge noninvariant contributions. *Phys. Lett. A* 1992, *170,* 33-36.

20. Glushkov A.V.; Ivanov, L.N. DC strong-field Stark effect: consistent quantum-mechanical approach. *J. Phys. B: At. Mol. Opt. Phys.* 1993, *26,* L379-386.

21. Glushkov, A.V. Spectroscopy of atom and nucleus in a strong laser field: Stark effect and multiphoton resonances. *J. Phys.: Conf. Ser.* 2014, *548,* 012020

22. Glushkov A., Spectroscopy of cooperative muon-gamma-nuclear processes: Energy and spectral parameters *J. Phys.: Conf. Ser.* 2012, *397,* 012011

23. Glushkov, A. Multiphoton spectroscopy of atoms and nuclei in a laser field: relativistic energy approach and radiation atomic lines moments method// Adv. Quant.Chem. (Elsevier), 2018, *78,* doi.org/10.1016/bs.aiq.2018.06.004

24. Glushkov, A.V., Khetselius, O.Yu., Svinarenko A.A., Buyadzhi, V.V., Ternovsky, V.B, Kuznetsova, A., Bashkarev, P Relativistic perturbation theory formalism to computing spectra and radiation characteristics: application to heavy element. *Recent Studies in Perturbation Theory*, ed. D. Uzunov (InTech) 2017, 131-150.

PACS 31.15.A-;32.30.-r

A.L. Mykhailov

ADVANCED STUDY OF SPECTRAL AND HYPERFINE STRUCTURE PARAMETERS FOR Li-LIKE MULTICHARGED IONS WITHIN RELATIVISTIC THEORY

Summary. The relativistic many-body perturbation theory with the optimized Dirac zeroth approximation is applied to calculation of some fundamental characteristics of the hyperfine structure of middle and heavy Li-like multicharged ions. The relativistic, exchange-correlation and other corrections are accurately taken into account. The optimized relativistic orbital basis set is generated in the optimal many-body perturbation theory approximation with performance of the gauge invariance principle. There are listed the calculated values of derivatives of the one-electron characteristics, including the hyperfine structure parameters, on nuclear radius for the Li-like multicharged ions with the corresponding analysis.

Keywords: Relativistic theory, spectral and hyperfine structure parameters, Li-like multicharged ions

PACS 31.15.A-;32.30.-r

О.Л. Михайлов

УДОСКОНАЛЕНИЙ АНАЛІЗ ПАРАМЕТРІВ СПЕКТРІВ ТА НАДТОНКОЇ СТРУКТУРИ Li-ПОДІБНИХ БАГАТОЗАРЯДНИХ ІОНІВ В МЕЖАХ РЕЛЯТИВІСТСЬКОЇ ТЕОРІЇ

Резюме. Релятивістська багаточастинкова теорія збурень з оптимізованим нульовим наближенням Дірака застосована для обчислення фундаментальних характеристик надтонкої структури середніх і важких Li-подібних багатозарядних іонів. Релятивістські, обмінно-кореляційні та інші поправки враховані ефективно. Оптимізований релятивістський орбітальний базис генерується в оптимальному наближенні багаточастинкової теорії збурень із застосуванням принципу калібрувальної інваріантності. Наведені розрахункові значення похідних одноелектронних характеристик, у тому числі, параметрів надтонкої структури, від радіуса ядра для ряду Li-подібних багатозарядних іонів з відповідним аналізом.

Ключові слова: релятивістська теорія, параметри спектрів та надтонкої структури, Li-подібні багатозарядні іони

Svinarenko A.A., Nesterenko A.A.

Odessa State Environmental University - OSENU, L'vovskaya str.15, Odessa
E-mail: svinarenkoaa@gmail.com

THEORETICAL STUDYING SPECTRAL CHARACTERISTICS OF TM ATOM WITHIN OPTIMIZED RELATIVISTIC MANY-BODY THEORY

Theoretical studying Rydberg spectrum of complex lanthanide atom of Tm has been performed within the relativistic many-body perturbation theory and generalized relativistic energy approach. The zeroth approximation of the relativistic perturbation theory is provided by the optimized Dirac-Kohn-Sham-Breit ones. Optimization has been fulfilled by means of introduction of the special gauge parameter to the Fock and Kohn-Sham exchange potentials and further minimization of the gauge-non-invariant contributions into radiation width of atomic levels with using relativistic orbital sets, generated by the corresponding zeroth approximation Hamiltonian. The calculated energies and widths of autoionization resonant states $4f^{-1}_j$ $6s(J12)nsnp[J]$ of the Tm atom with n=25-35 are presented and compared with known theoretical results, received within other approaches. Two main types of the Rydberg autoionization resonances decay, namely, the classic Beutler-Fano decay channel and a new Ivanov et al reorientation-type decay channel ar4e studied. It is noted that, for example, for autoionization resonant states $4f^{13}_{5/2}6s_{1/2}(3)ns_{1/2}[J]$ with the considered values of n, the decay of resonances occurs along both channels, and it is extremely difficult to understand a priori which of them is dominant.

1. Introduction

The development of new directions in the field of optics and spectroscopy, laser physics and quantum electronics, such as precision spectroscopy of heavy and superheavy atoms and ions, the latest astrospectroscopic research, pulse heating methods in controlled thermonuclear fusion research, the creation of fundamentally new schemes of lasers in the VHF, X-ray regions of the spectrum, etc., determines the need to solve the urgent and important tasks of atomic optics and laser spectroscopy at a fundamentally new level of theoretical consistency and accuracy. In the last decade, the spectroscopy of multi-charged ions, covering the UV and X-ray D-ranges of the spectrum, has also been intensively developed. Significant progress in the development of experimental methods of research, in particular, a significant increase in the intensity and quality of laser radiation, the use of accelerators, heavy ion colliders, sources of synchrotron radiation and, as a result, the possibil-

ity of a precise study of increasingly energetic processes, stimulates the development of new in the theory of heavy atoms theoretical methods of calculating their characteristics, in particular, radiation and autoionization. It is known that autoionization states (AS) play a significant role in various elementary atomic processes such as autoionization, selective photoionization, scattering of electrons on atoms, atom - and ion - atom collisions, etc. The presence of AS in ions significantly affects the characteristics of the radiation spectrum of high-temperature astrophysical and laboratory plasma. Their radiative decay is accompanied by the formation of the most complex spectra of dielectron satellites to the resonance lines of ions of the next ionization multiplicity, which contain information about the state of the plasma used for its diagnosis, as well as when studying the physical conditions in the solar corona, etc. astrophysical objects [1–28]).

In many papers the standard Hartree-Fock (HF), Dirac-Fock (DF) methods, model poten-

tial (MP) approach, quantum defect approximation etc in the different realizations have been used for calculating energies and oscillator strengths. However, it should be stated that for the heavy alkali atoms (for example, such as lanthanides and actinides atoms) and particularly for their high-excited (Rydberg) states, there is not enough precise information available in literature. The multi-configuration Dirac-Fock method is the most reliable version of calculation for multielectron systems with a large nuclear charge. However, one should remember about very complicated structure of spectra of the lanthanides atoms and necessity of correct accounting for different correlation effects such as polarization interaction of the valent quasiparticles and their mutual screening, iterations of a mass operator etc.).

In this paper we present the results of studying the spectral characteristics of various autoionization states (AS) (including narrow and abnormally narrow) in a spectrum of the Tm atom. The method of study is an accurate, ab initio method of relativistic many-body perturbation theory for three-quasi-particle atomic systems with a gauge-invariant zeroth approximation [25-30] and an energy approach, which is based on S-matrix formalism of Gell-Mann and Low [31-38]. Optimization has been fulfilled by means of introduction of the special gauge parameter to the Fock and Kohn-Sham exchange potentials and further minimization of the gauge-non-invariant contributions into radiation width of atomic levels with using relativistic orbital sets, generated by the corresponding zeroth approximation Hamiltonian [35-38]. The calculated energies and widths of autoionization resonant states $4f^{-1}_j$ $6s(J12)nsnp[J]$ of the Tm atom with n=25-35 are presented and compared with known theoretical results, received within other approaches (e.g. [2,3,18,32-34]).

2. Theoretical method

As the method of computing is earlier presented in detail, here we are limited only by the key topics [25-30]. Generally speaking, the majority of complex atomic systems possess a dense energy spectrum of interacting states with essentially relativistic properties. In the theory of the non-relativistic atom a convenient field procedure is known for calculating the energy shifts ΔE of degenerate states. This procedure is connected with the secular matrix M diagonalization [10-22]. In constructing M, the Gell-Mann and Low adiabatic formula for ΔE is used. In contrast to the non-relativistic case, the secular matrix elements are already complex in the second order of the electrodynamical PT (first order of the interelectron interaction). Their imaginary part of ΔE is connected with the radiation decay (radiation) possibility. In this approach, the whole calculation of the energies and decay probabilities of a non-degenerate excited state is reduced to the calculation and diagonalization of the complex matrix M. The complex secular matrix M is represented in the form [31-38]:

$$M = M^{(0)} + M^{(1)} + M^{(2)} + M^{(3)}.$$

(1)

where $M^{(0)}$ is the contribution of the vacuum diagrams of all order of PT, and $M^{(1)}$, $M^{(2)}$, $M^{(3)}$ those of the one-, two- and three-quasiparticle diagrams respectively. $M^{(0)}$ is a real matrix, proportional to the unit matrix. For simple systems (such as alkali atoms and ions) the one-quasiparticle energies can be taken from the experiment. Substituting these quantities into (1) one could have summarized all the contributions of the one-quasiparticle diagrams of all orders of the formally exact QED PT. However, the necessary experimental quantities are not often available. The first two order corrections to $\mathrm{Re}\,M^{(2)}$ have been analyzed previously using Feynman diagrams (look Ref. in [1,2]). The contributions of the first-order diagrams have been completely calculated.

In the second order, there are two kinds of diagrams: polarization and ladder ones. The polarization diagrams take into account the quasiparticle interaction through the polarizable core, and the ladder diagrams take into account the immediate quasiparticle interaction [28-31,35-38]. Some of the ladder diagram contributions as well as some of the three-quasiparticle diagram contributions in all PT orders have the same angular symmetry as the two-quasiparticle diagram contributions of the first order. These contributions have been

summarized by a modification of the central potential, which must now include the screening (anti-screening) of the core potential of each particle by the two others.

Interelectron interaction operator with accounting for the Breit interaction has been taken as follows:

$$V(r_i r_j) = \exp(i\omega r_{ij}) \cdot \frac{(1 - \alpha_i \alpha_j)}{r_{ij}}, \quad (2)$$

where, as usually, α_i are the Dirac matrices.

The total probability of a λ-pole transition is the sum of the electrical P_λ^E (electric multipole decomposition) and magnetic P_λ^M (corresponding decomposition) parts and is calculated within the relativistic energy formalism [31-42]. In the energy approach with respect to the complex multielectron atomic system the energy shift in the complex form is: $\delta E = \text{Re}\delta E + i\,\text{Im}\delta E$, Im $\delta E = -P/2$, where P- probability of decay (transition). For a single quasiparticle atomic system ImδE and, accordingly, P in the 2nd perturbation theory order (the perturbation operator $U_{MF}(r_i \vee b)$ - $J_\mu(x)A^\mu(x)$, where A is the vector of the electromagnetic field potential, J is the current operator, U_{MF} is a mean-field potential) is proportional to the matrix element with Dirac bispinors ϕ_i^{EFMP} (ab initio RMP наближення):

$$V_{ijkl} = \iint d^3 r_1 d^3 r_2 \varphi_i^{EFMP^*}(r_1) \varphi_j^{EFMP^*}(r_2)[(1 - \alpha_1 \alpha_2)$$
$$\cdot \sin|\omega|r_{12}/r_{12}] \cdot \varphi_k^{EFMP}(r_2)\varphi_l^{EFMP}(r_1)$$

(3)

which are decomposed into a series of Bessel functions of the 1st kind (analog of multipole decomposition). In general, the results of all approximate calculations depended on the gauge. Naturally the correct result must be gauge-invariant. The gauge dependence of the amplitudes of the photo processes in the approximate calculations is a well known fact and is in details investigated by Grant, Armstrong, Aymar and Luc-Koenig, Glushkov-Ivanov et al (e.g., see reviews in [2,3,18,29,30] and Refs. therein). For simplicity, it is worth to remind that an autoionization decay in the one-quaiparticle

approximation can be represented as (i=l-$3\beta_1\beta_2 \rightarrow \beta_3 k$, where β_i (i=l-3) described a set of quantum numbers of bound states, k -a state of free electron. Decay is possible only into the state of the continuous spectrum, which coincides in terms of parity and total moment J with the original AS. The width of the state associated with AC decay is determined by the connection with the continuum states and actually $\Gamma \infty |V(\beta_1\beta_2, \beta_3 k)|^2$. i.e., is proportional to matrix element of the interaction operator (2). The latter is determined by the known sum

$$Q_a = Q_a^{Qul} + Q_a^{Br} \quad (3)$$

where respectively Q_a^{Qul} and Q_a^{Br} correspond to the Coulomb and Breit parts of the potential (2). These parts are expressed through the known atomic radial integrals R and known angular coefficients S. All details can be found in [2,28-38]. All calculations are performed with using the PC code Super atom [2,25-30,35].

3. The results and conclusions

The Tm spectrum is particularly complex. It is characterized by the position of the closely lying $4f^1 6snl$ Tm ionization limits and quite complex scheme of the autoionization decay of the $4f^{13}6snl$ Tm Rydberg states. The presence of 2 pairs of closely lying ionization limits (with vacancy states in the $4f^{14}$ core: : $4f_{7/2^{-1}} 4f_{5/2^{-1}}$) causes 2 main types of autoionization decay [2,34]:

i). the classic Beutler-Fano decay (BFD) channel −

$4f^1_{5/2}6s_{1/2}(J12)nl-4f^1_{7/2}6s_{1/2}[J12']$ Tm$^+$+leje,

n>7, J12=2;3, J12'=3;4

ii). A new reorientation-type decay channel (ROD) for AS spectroscopy -

$4f^1 j\, 6s_{1/2}(J12)nl-4f^1 j 6s_{1/2}[J12']Tm^+$+leje)
n>25, J12=3, J12'=2;4 j=5/2,7/2,

Here, ROD denotes the decay of AC of the reorientation type, (BFD) is the channel of the

Beutler-Fano decay known in theory. The 4f$^{-1}_{5/2}$ 6s$_{1/2}$nl states are subject to both BFD and ROD decay. In contrast to BFD decay, ROD decay is a low-energy process that preserves one-electron quantum numbers of the atomic core: 4fj^{-1} ,6s$_{1/2}$. ROD decay can be either monopole or quadrupole.

Below we present the calculated energies and widths of AS 4f$^{-1}_j$ 6s(J12)nsnp[J] of the Tm atom with n=25-35. The obtained results are presented in tables 1-4. Table 1 shows the calculated values of the widths $\Gamma 2$ (in cm^{-1}) and energies E2 (10 cm^{-1}) of the AS $4f^{13}_{7/2}6s_{1/2}(3)ns_{1/2}[J]$ of the Tm atom, for which ROD decay is the only channel of autoionization decay. For comparison, calculation data obtained by Ivanov et al. (E1,G1) [32-34] and Glushkov et al (E,G3) [2,18].

Table 1

Widths and energies of the AS $4f^{13}_{7/2}6s_{1/2}(3)ns_{1/2}[J]$ of the Tm atom

	J=5/2		
n	$\Gamma 1$	$\Gamma 3$	$\Gamma 2$
25	1.18(-5)	1.29(-5)	1.25(-5)
26	-	-	1.13(-5)
30	5.77(-6)	6.72(-6)	6.12(-6)
33	-	-	3.79(-6)
35	-	-	3.21(-6)
	J=5/2		
n	E1	E3	E2
25	4985	4981	4983
26	-	-	4975
30	4995	4993	4994
33	-	-	4996
35	-	-	4998
	J=7/2		
n	$\Gamma 2$		E2
25	1.58(-2)		4986
26	1.34(-2)		4988
30	3.98(-3)		4995
33	1.58(-2)		4998
35	3.18(-3)		5000

Table 2 shows our values of widths and energies of the AS $4f^{13}_{7/2}6s_{1/2}(3)np_j[J]$ and AS $4f^{13}_{5/2}6s_{1/2}(2)ns_{1/2}[J]$, for which the ROD is a single decay channel for AS studied.

Table 2.

Widths and energies of the AS $4f^{13}_{7/2}6s_{1/2}(3)np_j[J]$ of the Tm atom (our data)

(j,J)	(3/2,3/2)		(1/2,5/2)	
n	$\Gamma 2$	E2	$\Gamma 2$	E2
25	4.68(-5)	49862	1.40(-1)	49858
26	4.22(-5)	49877	1.33(-1)	49874
30	2.42(-5)	49939	1.03(-1)	49937
33	1.80(-5)	49971	7.54(-2)	49968
35	1.39(-5)	49992	5.72(-2)	49990
(j,J)	(3/2,5/2)		(1/2,7/2)	
n	$\Gamma 2$	E2	$\Gamma 2$	E2
25	1.92(-1)	49865	3.72(-2)	49848
26	1.75(-1)	48979	3.45(-2)	49863
30	1.07(-1)	49941	2.38(-2)	49938
33	8.20(-2)	49972	2/12(-2)	49961
35	6.59(02)	49993	1.76(-2)	49982
(j,J)	(3/2,7/2)		(3/2,9/2)	
n	$\Gamma 2$	E2	$\Gamma 2$	E2
25	3.46(-1)	49867	3.98(-1)	49869
26	3.24(-1)	49884	3.71(-1)	49886
30	2.38(-1)	49952	2.62(-1)	49953
33	2.05(-1)	49977	2.26(-1)	49978
35	1.56(-1)	49992	1.729(-1)	49993

Table 3 shows our values of widths and energies (in cm^{-1}) of the $4f^{13}_{5/2}6s_{1/2}(2)ns_{1/2}[J]$ AS.

Table 3.

Widths and energies of the AS $4f^{13}_{5/2}6s_{1/2}(2)ns_{1/2}[J]$ of the Tm atom (our data)

	J=3/2	J=3/2
n	$\Gamma 2$	E2
25	2.64(-5)	5836
30	1.27(-5)	5845
35	8.89(-6)	5850
	J=5/2	J=5/2
n	$\Gamma 2$	E2
25	5.32(-5)	5838
30	2.78(-5)	5846
35	1.54(-5)	5852

Analysis of the data shows that the computational method used provides a physically reasonable agreement between the theoretical and experimental data. However, comparison of the corresponding results for widths demonstrates again sufficiently large discrepancy. In our opinion, this fact is explained by

insufficiently exact estimates of the radial integrals, using the non-optimized basises and some other additional calculation approximations. Table 4 shows the calculated widths and energies of the $4f_{5/2}^{13}6s_{1/2}(3)ns_{1/2}[J]$, states, for which autoionization decay can pass through both channels: ROD and BFD.

Table 4. Widths and energies of the AS $4f_{5/2}^{13}6s_{1/2}(3)ns_{1/2}[J]$ of the Tm atom (our data)

	Γ2 J=5/2		Γ2 J=7/2	
n	Γ(ROD)	Γ(BFD)	Γ(ROD)	Γ(BFD)
25	1.39(-2)	2.85(-5)	1.36(-5)	5.41(-5)
30	3.32(-3)	1.52(-5)	6.81(-6)	2.78(-5)
35	1.01(-3)	8.68(-6)	3.53(-6)	1.56(-5)

It is important to note that for AS $4f_{5/2}^{13}6s_{1/2}(3)ns_{1/2}[J]$ (table 4) with the considered values of n, the decay of resonances occurs along both channels, and it is extremely difficult to understand a priori which of them is dominant.

References

1. Grant I. *Relativistic Quantum Theory of Atoms and Molecules*. Oxford Univ. Press: Oxford, 2007.
2. Glushkov, A.V. *Relativistic Quantum theory. Quantum mechanics of atomic systems*. Astroprint: Odessa, 2008.
3. Khetselius, O.Yu. *Hyperfine structure of atomic spectra*. Astroprint: Odessa, 2008.
4. Glushkov, A.V.; Malinovskaya, S.V.; Loboda, A.V.; Shpinareva, I.M.; Prepelitsa, G.P. Consistent quantum approach to new laser-electron-nuclear effects in diatomic molecules. *J.Phys.: Conf. Ser.* 2006, *35,* 420-424.
5. Glushkov, A.V. Operator Perturbation Theory for Atomic Systems in a Strong DC Electric Field. *In Advances in Quantum Methods and Applications in Chemistry, Physics, and Biology, Series: Progress in Theoretical Chemistry and Physics*; Hotokka, M., Brändas, E., Maruani, J., Delgado-Barrio, G., Eds.; Springer: Cham, 2013; Vol. 27, pp 161–177.
6. Glushkov, A.V.; Ambrosov, S.V.; Ignatenko, A.V.; Korchevsky, D.A. DC strong field stark effect for nonhydrogenic atoms: Consistent quantum mechanical approach. *Int. Journ. Quant. Chem.* 2004, *99,* 936-939.
7. Glushkov, A.V.; Kondratenko, P.A.; Buyadgi V.V.; Kvasikova, A.S.; Sakun, T.N.; Shakhman, A.S. Spectroscopy of cooperative laser electron-γ-nuclear processes in polyatomic molecules. *J. Phys.: Conf. Ser.* 2014, *548*, 012025.
8. Malinovskaya, S.V.; Dubrovskaya, Yu.V.; Vitavetskaya, L.A. Advanced quantum mechanical calculation of the beta decay probabilities. *AIP Conf. Proc.* 2005, *796,* 201-205.
9. Glushkov, A.V.; Malinovskaya, S.V.; Chernyakova Y.G.; Svinarenko, A.A. Cooperative laser-electron-nuclear processes: QED calculation of electron satellites spectra for multi-charged ion in laser field. *Int. Journ. Quant. Chem.* 2004, *99,* 889-893.
10. Glushkov, A.V.; Malinovskaya, S.V.; Prepelitsa, G.; Ignatenko, V. Manifestation of the new laser-electron nuclear spectral effects in the thermalized plasma: QED theory of co-operative laser-electron-nuclear processes. *J. Phys.: Conf. Ser.* 2005, *11,* 199-206.
11. Glushkov, A.V.; Malinovskaya, S.V.; Loboda, A.V.; Shpinareva, I.M.; Gurnitskaya, E.P.; Korchevsky, D.A. Diagnostics of the collisionally pumped plasma and search of the optimal plasma parameters of x-ray lasing: calculation of electron-collision strengths and rate coefficients for Ne-like plasma. *J. Phys.: Conf. Ser.* 2005, *11,* 188-198.
12. Florko, T.A.; Tkach, T.B.; Ambrosov, S.V.; Svinarenko, A.A. Collisional shift of the heavy atoms hyperfine lines in an atmosphere of the inert gas. *J. Phys.: Conf. Ser.* 2012, *397*, 012037.
13. Karaçoban, B.; Özdem, L. Energies, Landé Factors, and Lifetimes for Some Excited Levels of Neutral Ytterbium. *Acta Phys.Pol.A.* 2011, *119*, 342-353.
14. Khetselius, O.Yu. Relativistic Energy Approach to Cooperative Electron-γ-Nuclear Processes: NEET Effect *In Quantum Systems in Chemistry and Physics, Series: Progress in Theoretical*

Chemistry and Physics; Nishikawa, K., Maruani, J., Brändas, E., Delgado-Barrio, G., Piecuch, P., Eds.; Springer: Dordrecht, 2012; Vol. 26, pp 217-229.

15. Khetselius, O.Yu. Relativistic perturbation theory calculation of the hyperfine structure parameters for some heavy-element isotopes. *Int. Journ. Quant.Chem.* 2009, *109,* 3330-3335.

16. Khetselius, O.Yu. Relativistic calculation of the hyperfine structure parameters for heavy elements and laser detection of the heavy isotopes. *Phys.Scripta.* 2009, *135,* 014023.

17. Khetselius, O.Yu. Optimized Perturbation Theory for Calculating the Hyperfine Line Shift and Broadening of Heavy Atoms in a Buffer Gas. *In Frontiers in Quantum Methods and Applications in Chemistry and Physics*, *Series: Progress in Theoretical Chemistry and Physics;* Nascimento, M., Maruani, J., Brändas, E., Delgado-Barrio, G., Eds.; Springer: Cham, 2015; Vol. 29, pp. 55-76.

18. Khetselius, O.Yu. *Quantum structure of electroweak interaction in heavy finite Fermi-systems.* Astroprint: Odessa, 2011.

19. Khetselius, O.Yu. Optimized relativistic many-body perturbation theory calculation of wavelengths and oscillator strengths for Li-like multicharged ions. Adv. Quant. Chem. 2019, *78,* 223-251.

20. Khetselius, O.Yu. Hyperfine structure of radium. *Photoelectronics.* 2005, *14,* 83-85.

21. Khetselius O.Yu.; Gurnitskaya, E.P. Sensing the hyperfine structure and nuclear quadrupole moment for radium. *Sensor Electr. and Microsyst. Techn.* 2006, *2,* 25-29.

22. Khetselius, O.Yu. Atomic parity non-conservation effect in heavy atoms and observing P and PT violation using NMR shift in a laser beam: To precise theory. *J. Phys.: Conf. Ser.* 2009, *194,* 022009

23. Glushkov, A.V.; Malinovskaya S.V. Co-operative laser nuclear processes: border lines effects *In New Projects and New Lines of Research in Nuclear Physics.* Fazio, G., Hanappe, F., Eds.; World Scientific: Singapore, 2003, 242-250.

24. Glushkov, A.V. Spectroscopy of atom and nucleus in a strong laser field: Stark effect and multiphoton resonances. *J. Phys.: Conf. Ser.* 2014, *548,* 012020.

25. Glushkov, A.V. *Relativistic and Correlation Effects in Spectra of Atomic Systems.* Astroprint: Odessa, 2006.

26. Glushkov, A.V.; Khetselius, O.Yu.; Svinarenko A.A. Theoretical spectroscopy of autoionization resonances in spectra of lanthanides atoms. *Phys. Scripta.* 2013, *T153*, 014029.

27. Svinarenko, A.A. Study of spectra for lanthanides atoms with relativistic many-body perturbation theory: Rydberg resonances. *J. Phys.: Conf. Ser.* 2014, *548,* 012039.

28. Svinarenko, A., Glushkov, A, Khetselius, O., Ternovsky, V., Dubrovskaya Y., Kuznetsova A., Buyadzhi V. Theoretical spectroscopy of rare-earth elements: spectra and autoionization resonances. *Rare Earth Element*, Ed. J. Orjuela (InTech). 2017, pp 83-104.

29. Glushkov, A.V., Khetselius, O.Yu., Svinarenko A.A., Buyadzhi, V.V., Ternovsky, V.B, Kuznetsova, A., Bashkarev, P. Relativistic perturbation theory formalism to computing spectra and radiation characteristics: application to heavy element. *Recent Studies in Perturbation Theory*, ed. D. Uzunov (InTech). 2017, 131-150.

30. Glushkov, A.V. Relativistic polarization potential of a many-electron atom. *Sov. Phys. Journal.* 1990, *33(1)*, 1-4.

31. Ivanov, L.N.; Ivanova, E.P. Atomic ion energies for Na-like ions by a model potential method $Z = 25–80$. *Atom. Data Nucl. Data Tabl.* 1979, *24,* 95-109.

32. Bekov, G.I.; Vidolova-Angelova, E.P.; Ivanov, L.N.; Letokhov, V.S.; Mishin V.. Laser spectroscopy of narrow doubly excited autoionization states of ytterbium atoms. *JETP.* 1981, *53,* 441-447

33. Vidolova-Angelova E., Ivanov L.N., Ivanova E.P., Angelov D.A., Relativistic perturbation method for investigating the radiation decay of highly excited many electron atoms: Tm atom. *J.Phys.B: At. Mol. Opt. Phys.* 1986, 19, 2053-2069.

34. Vidolova-Angelova E., Ivanov L.N., Autoionizing Rydberg states of thulium. Re-orientation decay due to monopole

interaction. J.*Phys.B:At. Mol. Opt.Phys.* 1991, 24, 4147-4158.

35. Ivanova, E.P.; Ivanov, L.N.; Glushkov, A.V.; Kramida, A.E. High order corrections in the relativistic perturbation theory with the model zeroth approximation, Mg-Like and Ne-Like Ions. *Phys. Scripta* 1985, *32,* 513-522.

36. Glushkov, A.V.; Ivanov, L.N.; Ivanova, E.P. Autoionization Phenomena in Atoms. *Moscow University Press*, Moscow, 1986, 58-160

37. Glushkov, A.V.; Ivanov, L.N. Radiation decay of atomic states: atomic residue polarization and gauge noninvariant contributions. *Phys. Lett. A* 1992, *170,* 33-36.

38. Glushkov A.V.; Ivanov, L.N. DC strong-field Stark effect: consistent quantum-mechanical approach. *J. Phys. B: At. Mol. Opt. Phys.* 1993, *26,* L379-386.

39. Glushkov, A.V. Negative ions of inert gases. *JETP Lett.* 1992, *55,* 97-100.

40. Glushkov, A.V. Energy approach to resonance states of compound superheavy nucleus and EPPP in heavy nuclei collisions *In Low Energy Antiproton Physics;* Grzonka, D., Czyzykiewicz, R., Oelert,W., Rozek, T., Winter, P., Eds.; AIP: New York, *AIP Conf. Proc.* 2005, *796*, 206-210.

41. Glushkov, A.V. Advanced Relativistic Energy Approach to Radiative Decay Processes in Multielectron Atoms and Multicharged Ions. *In Quantum Systems in Chemistry and Physics: Progress in Methods and Applications, Series: Progress in Theoretical Chemistry and Physics*; Nishikawa, K., Maruani, J., Brandas, E., Delgado-Barrio, G., Piecuch, P., Eds.; Springer: Dordrecht, 2012; Vol. 26, pp 231–252.

42. Glushkov, A.V. Multiphoton spectroscopy of atoms and nuclei in a laser field: Relativistic energy approach and radiation atomic lines moments method. *Adv. in Quantum Chem.* 2019, *78*, 253-285.

43. Glushkov, A.V. Spectroscopy of cooperative muon-gamma-nuclear processes: Energy and spectral parameters *J. Phys.: Conf. Ser.* 2012, *397,* 012011

44. Glushkov, A.V.; Gurskaya, M.Yu.; Ignatenko, A.V.; Smirnov, A.V.; Serga, I.N.; Svinarenko, A.A.; Ternovsky, E.V. Computational code in atomic and nuclear quantum optics: Advanced computing multiphoton resonance parameters for atoms in a strong laser field. *J. Phys.: Conf. Ser.* 2017, *905*, 012004.

Svinarenko A.A., Nesterenko A.A.

THEORETICAL STUDYING SPECTRAL CHARACTERISTICS OF TM ATOM WITHIN OPTIMIZED RELATIVISTIC MANY-BODY THEORY

Summary. Theoretical studying Rydberg spectrum of complex lanthanide atom of Tm has been performed within the relativistic many-body perturbation theory and generalized relativistic energy approach. The zeroth approximation of the relativistic perturbation theory is provided by the optimized Dirac-Kohn-Sham-Breit ones. Optimization has been fulfilled by means of introduction of the special gauge parameter to the Fock and Kohn-Sham exchange potentials and further minimization of the gauge-non-invariant contributions into radiation width of atomic levels with using relativistic orbital sets, generated by the corresponding zeroth approximation Hamilton. The calculated energies and widths of autoionization resonant states $4f^{-1}_j\, 6s(J12)nsnp[J]$ of the Tm atom with n=25-35 are presented and compared with known theoretical results, received within other approaches. Two main types of the Rydberg autoionization resonances decay, namely, the classic Beutler-Fano decay channel and a new Ivanov et al reorientation-type decay channel ar4e studied. It is underlined that, for example, for autoionization resonant states $4f^{13}_{5/2}6s_{1/2}(3)ns_{1/2}[J]$ with the considered values of n, the decay

of resonances occurs along both channels, and it is extremely difficult to understand a priori which of them is dominant.

Свинаренко А.А., Нестеренко А.А.

ТЕОРЕТИЧНЕ ВИВЧЕННЯ СПЕКТРАЛЬНИХ ХАРАКТЕРИСТИК Tm-АТОМА НА ОСНОВІ ОПТИМІЗОВАНОЇ РЕЛЯТИВІСТСЬКОЇ ТЕОРІЇ

Резюме. Теоретичне дослідження рідбергівського спектру складного атома (з лантаноідів) Tm виконано в рамках оптимізованої релятивістської багаточастинкової теорії збурень і узагальненого релятивістського енергетичного підходу. Нульове наближення релятивістської теорії збурень визначається оптимізованим наближенням Дірака-Кона-Шам-Брейта. Оптимізацію виконано шляхом введення спеціального калібрувального параметра до обмінних потенціалів Фока та Кона-Шема та подальшої мінімізації калібрувально-неінваріантних внесків в радіаційну ширину атомних рівнів з використанням релятивістських орбітальних наборів, породжених відповідним гамільтоніаном нульового наближення. Наведено розраховані енергії та ширини автоіонізаційних станів $4f^{-1}_j 6s(J12)nsnp[J]$ атома Tm з головним квантовим числом n=25-35 та порівняно з відомими теоретичними результатами, отриманими в рамках інших підходів. Досліджено два основних типи розпаду рідбергівських автоіонізаційних резонансів, а саме, класичний канал розпаду Бейтлера-Фано та новий канал розпаду реорієнтаційного типу, відкритий Івановим-Летоховим та інш. Зазначено, що, наприклад, для автоіонізаційних резонансів з розглянутими значеннями n розпад резонансів відбувається по обох каналах, і апріорі зрозуміти, який з них є домінуючим, надзвичайно важко.

Ключові слова: релятивістська теорія збурень, оптимізоване нульове наближення, спектроскопія, атом Tm

A.V. Tjurin[1], V.G. Shevchuk[1] , I.I. Bilan[2]

[1]I.I. Mechnikov Odessa National University, 2, Dvoryanskaya str., Odessa
[2]Odessa National Maritime Academy, 4, Didrikhson str., Odessa
E-mail: bilanigorivan@gmail.com

NON-LINEAR ANALYSIS OF CHAOTIC SELF-OSCILLATIONS IN BACKWARD-WAVE TUBE

The paper presents the results of the analysis and modelling of topological and dynamic invariants for the regimes of chaotic self-oscillations in the backward-wave oscillator, in particular, the analysis of chaotic time series for the amplitude of the output signal, which is the solution of the equations of the non-stationary nonlinear theory for the O-type backward-wave oscillator (without taking into account space charge, relativistic effects, energy losses, etc.). The main attention is paid to the calculation and analysis of the spectrum of Lyapunov exponents based on the Sano-Savada algorithm. Numerical data of the Lyapunov backward-wave oscillator calculated for the time series of the amplitudes of the output signal are given, which definitely indicate the presence of elements of advanced chaos in the dynamics of the system.

1. At present time study the powerful generators of chaotic oscillations of microwave range are of a great interest for radar, plasma heating in fusion devices, modern systems of information transmission using dynamic chaos and many other applications. Among the most studied of vacuum electronic devices with complex dynamics are backward-wave oscillators, for which the possibility of generating chaotic oscillations has been theoretically and experimentally found [1-12]. The backward-wave oscillator is an electronic device for generating electromagnetic vibrations of the superhigh frequencies range. Above nost interesting for our study papers one should pay the attention on the following works.

Firstly, the papers [4,5] contain very important results. The authors of these works have solved the equations of nonstationary nonlinear theory for the O-type backward-wave oscillator without account of the spatial charge, relativistic effects, energy losses etc. It has been shown that the finite-dimension strange attractor is responsible for chaotic regimes in the backward-wave oscillator. The authors have in details presented the numerical data on the different dynamical characteristics of the non-relativistic backward-wave oscillator, namely, phase portraits, statistical

quantifiers for a weak chaos arising via period-doubling cascade of self-modulation and the same characteristics of two non-relativistic backward-wave oscillator. It is shown that the chaos formed in the dynamics of the oscillator is characterized by more than one positive Lyapunov exponent (developed chaos or hyperchaos). the Lyapunov correlation dimensions as well as in general a whole set of the dynamical and topological characteristics of the strange attractor are also calculated.

Naturally the quantitative study of the dynamical and topological characteristics of the strange attractors in dynamics of the nonrelativistic and relativistic backward-wave oscillators have been performed in many papers (e.g. [1-12] and refs. therein) Depending on the key control parameters of the system, many researchers have discovered a rather complex scheme of alternating regular, auto-modulation, and chaotic (hyperchaotic) generation modes, and in the end, the processes ended with a transition to highly irregular broadband chaotic (hyperchaotic) oscillations with a sufficient spectrum.

In the last decade, a large number of numerical studies have been carried out using ideas derived from the science of chaos to characterize, model and predict the regular and

chaotic dynamics of various electronics systems, including the studies of the dynamics of backward wave oscillators listed above (see [1-6,24]). The results of such studies are very encouraging, since they not only showed that the dynamics of complex and regular and chaotic phenomena can be understood with a sufficiently high accuracy from the quantitative point of view, but also proved sufficiently efficient models for predicting the dynamics (time series) of complex chaotic systems, at least in the first approximation (e.g.[7-22]).

A variety of different techniques for characterizing chaotic dynamics of the nonlinear systems identifying the presence of chaotic elements is used [1,2]. Usually a mutual information approach, correlation integral analysis, false nearest neighbour algorithm, Lyapunov exponent's analysis, and surrogate data method and others are used for comprehensive characterization. The fundamental quantities to characterize chaotic behaviour of the complex dynamical systems are the exponential divergence of nearby orbits (computing positive Lyapunov exponents'), positive finite Kolmogorov entropy, and a noninteger dimension of the attractor [7-26]. These characteristics are usually invariant under the corresponding smooth transformation of coordinates. There are several determination schemes among these quantities, and if the Lyapunov spectrum can be determined, the rest can be estimated as equalities or upper or lower bounds. So, the definition of the highest Lyapunov exponents, as well as the full spectrum of the Lyapunov exponents is an important task in the nonlinear analysis of the complex dynamical distributed. It is well known that the Lyapunov exponents are a quantitative measure sensitivity to the values of the initial conditions. Since the Lyapunov exponents are defined as asymptotic average rates, they are independent of the initial conditions, and therefore they do comprise an invariant measure of attractor There are several different methods for computing the Lyapunov exponents [e.g.2,3,13-25]). One of the most spread algorithms to compute the leading Lyapunov exponents is Benettin algorithm [21] (see also [4,5]. The generalized algorithm allows to compute the full spectrum of Lyapunov. The disadvantage of the algorithm is that its applicability is only in those cases where when the corresponding evolutionary equations of the studied dynamical system known; besides, it is possible to measure all of it phase coordinates, which is not always possible.

Another approach is in computing the senior indicator for a sample from a single coordinate. The algorithm named after Wolf et al [20] calculates the leading Lyapunov exponent from sampled from a single coordinate, and is used when the equations are unknown evolution of the system. This algorithm gives quite satisfactory results, but requires very large samples, which is problematic for real data sets. In the last years it has become very popular computing the full Lyapunov spectrum using neural networks algorithms (e.g. [3,7-11,23-26] and reds therein). The use and optimization of neural networks is one of the directions in improving the performance and accuracy of algorithms for calculating Lyapunov exponents. Besides, it should be noted that in the latter it could be possible to organize a training a neural network on samples, which allows use short samples or noisy data. This gives significant advantages over classical methods. At last , it is necessary to add that in order to increase an accuracy of computing the Lyapunov exponents, one should use various orthogonalization methods , for example, the classical Gram-Schmidt method and the modified Gram-Schmidt method.

This paper is devoted to numerical studying the chaotic self-oscillations regimes in the backward-wave tube, namely, to application of the some numerical analysis techniques to analysis of the chaotic time series as solutions of the equations of nonstationary nonlinear theory for the O-type backward-wave oscillator. The main attention is paid to computing and analysing a spectrum of the Lyapunov exponent's within the Sano-Sawada method [23] (see other details in refs. [2,9,10]). The advanced numerical data on the Lyapunov exponents of computed for the time series of output signal amplitudes, which are the solutions of nonstationary nonlinear theory for the O-type backward-wave oscillator

without account of the spatial charge, relativistic effects, energy losses etc.

2. The main mathematical object of the numerical investigation is the time or other series of the amplitude of the dynamic parameter of the system, which is to be carried out, we introduce it formally:

$$x(t_0 + n\Delta t) = x(n), \qquad (1)$$

where t_0 – some initial point in time, Δt is the time interval during which further members of the time series are selected, $t_0 + n\Delta t$ – "i" point in time.

By definition, the procedure of construction (restoration) from a scalar time series $\{ s_i \}$ to a series of state vectors $\{ y_i \}$ is called phase trajectory reconstruction. It should be noted that depending on the class of the problem, more precisely, the system or device under investigation, any dynamic parameters can act as y(n),

Further it is usually necessary to reconstruct phase space using as well as possible information contained in the dynamical parameter s(n), where n the number of the measurements. Such a reconstruction results in a certain set of d-dimensional vectors y(n) replacing the scalar measurements. Packard et al. [7] introduced the method of using time-delay coordinates to reconstruct the phase space of an observed dynamical system. The direct use of the lagged variables $x(n + \tau)$, where τ is some integer to be determined, results in a coordinate system in which the structure of orbits in phase space can be captured. Then using a collection of time lags to create a vector **x** in d dimensions,

$$\mathbf{x}(n) = [x(n), x(n + \tau), x(n + 2\tau), \ldots,$$

$$x(n + (d-1)\tau)], \qquad (2)$$

the required coordinates are provided.

In a nonlinear system, the **x**$(n + j\tau)$ are some unknown nonlinear combination of the actual physical variables that comprise the source of the measurements. The dimension d is called the embedding dimension, dE. If τ is chosen too small, then the coordinates $x(n + j\tau)$ and $x(n + (j + 1)\tau)$ are so close to each other in numerical value that they cannot be distinguished from each other. Similarly, if τ is too large, then $x(n + j\tau)$ and $x(n + (j + 1)\tau)$ are completely independent of each other in a statistical sense. Also, if τ is too small or too large, then the correlation dimension of attractor can be under- or overestimated respectively [8,18]. The autocorrelation function and average mutual information can be applied here.

Usually the main aim of the embedding dimension determination is to reconstruct a Euclidean space R_d large enough so that the set of points dA can be unfolded without ambiguity. There are several standard approaches to reconstruct the attractor dimension (see, e.g., [2,3,11-17]). The correlation integral analysis is one of the widely used techniques to investigate the signatures of chaos in a time series. The analysis uses the correlation integral, C(r), to distinguish between chaotic and stochastic systems. To compute the correlation integral, the algorithm of Grassberger and Procaccia [16] is the most commonly used approach.

The Lyapunov exponents are the dynamical invariants of the nonlinear system. In a general case, the orbits of chaotic attractors are unpredictable, but there is the limited predictability of chaotic physical system, which is defined by the global and local Lyapunov exponents. A negative exponent indicates a local average rate of contraction while a positive value indicates a local average rate of expansion.

In our case the quantity If $\{x_n)$ (n=1,2, . . .) denote a time series of some physical quantity measured at the discrete time interval (0 in fact this is an output signal amplitudes, which are the solutions of nonstationary nonlinear theory for the O-type backward-wave oscillator).

Further, according to the the Sana-Sawada algorithm [23], one should consider a small ball of radius ε centered at the orbital point x,, and find any set of points $\{x_i)$ (i =1,2, . . . , N) included in this ball, i.e.:

$$\{y_i)= \{|x_{ki}—x_i| \| x_k —x_i \| < \varepsilon,\}, \qquad (3)$$

where y_i is the displacement vector between x_k and x_i. After the evolution of a time interval $\tau = m\Delta t$ t, the orbital point x_j will proceed to x_{j+m} and neighboring points $\{x_k\}$ to

{x_{k+m}}. The displacement vector y'=x,,—x is thereby mapped to

$$\{z_i\} = \{|x_{ki}-x_i| \; \| \; x_k - x_i \| < \varepsilon,\}, \qquad (4)$$

According to Ref. [23], if the radius ε is small enough for the displacement vectors {y} and {z} to be regarded as good approximation of tangent vectors in the tangent space, evolution of y' to z' can be represented by some matrix A, as: $z^i = A_j \; y^i$.

Further one should proceed proceed to the optimal estimation of the linearized flow map A; from the data sets {y} and {z}. According to Ref. [23], a plausible procedure for optimal estimation is the least-square-error algorithm, which minimizes the average of the squared error norm between z and Ay with respect to all components of the matrix A is as follows:

$$\min \bar{S}(A_j) = \min\left(\frac{1}{N}\right) \sum_{m=1}^{N} \|zi - Ajyi\| ** 2$$

The Lyapunov exponents can be computed in a standard way as the corresponding limit of a sum $ln\|Ajej\|$. Other details can be found in Refs. [23,24]. In fact, if one manages to derive the whole spectrum of Lyapunov exponents, other invariants of the system, i.e. Kolmogorov entropy and attractor's dimension can be found. The Kolmogorov entropy, K, measures the average rate at which information about the state is lost with time. An estimate of this measure is the sum of the positive Lyapunov exponents. The inverse of the Kolmogorov entropy is equal to the average predictability.

Let us present some obtained results. All input data have been taken from ref. [4,5,24].

In Table 1 we present our data on the correlation dimension d_2, the embedding dimension determined based on the algorithm of false nearest neighboring points (d_N) with percentage of false neighbors (%) calculated for different values of time lag ▲ for two regimes of of chaotic self-oscillations in the backward-wave oscillator, in particular, for the amplitude of the output signal for L=4.1 (I) and L=6.1 (II). Here L is normalized backward-wave oscillator length , which plays a role of the main control (governing) parameter of the backward-wave oscillator (e.g.[4,5]). The corresponding amplitude of the output signal is the solution of the equations of the non-stationary nonlinear theory for the O-type backward-wave oscillator (without taking into account space charge, energy losses, etc.) (e.g.[4,24]).

Table 1. Correlation dimension d_2, the dimension of the attachment determined based on the algorithm of false nearest neighboring points (d_N) with percentage of false neighbors (%) calculated for different values of time lag τ

Chaos (I)			Hyperchaos (II)		
τ	d_2	(d_N)	τ	d_2	(d_N)
60	3.6	5 (5.5)	67	7.2	10 (12)
6	3.1	4 (1.1)	10	6.4	8 (2.1)
8	3.1	4 (1.1)	12	6.4	8 (2.1)

In Table 2 we list the results of computing the Lyapunov's exponents and Kolmogorov entropy K_{entr}.

Table 2. Numerical parameters of the chaotic self-oscillations in the backward-wave tube: $\lambda_1 - \lambda_4$ are the Lyapunov exponents in descending order, K is Kolmogorov entropy

Regime	λ_1	λ_2	K
Chaos (L=4.2)	0.261	0.0001	0.26
Hyperchaos (L=6.1)	0.514	0.228	0.74
Regime	λ_3	λ_4	K
Chaos (L=4.2)	−0.0004	−0.528	0.26
Hyperchaos (L=6.1)	0.0000	−0.0002	0.74

One could see the that the Lyapunov exponents have as positive as negative values. So, the main conclusion is that the chaos formed in the dynamics of the oscillator is characterized by more than one positive Lyapunov exponent (developed chaos or hyperchaos). The received data are quite satisfactory agreed with the corresponding results of [4,24]. However, some difference in values of the Lyapunov exponents is connected with using another algorithm.

References

1. Berezin V. M., Buryak V. S., Gutzeit E. M., Maran V. P. *Microwave electronic devices.* M .: Higher school, **1985**.
2. Ott E. Chaos in dynamical systems. Cambridge: Univ.Press, 2002.
3. Glushkov A.V.: *Methods of a chaos theory*. Odessa: Astrorpint, **2012.**
4. Kuznetsov S.P., *Dynamical Chaos.* M: Nauka, **2001**.
5. Kuznetsov S.P., Trubetskov D.I., Chaos and hyperchaos in the backward-wave tube. *Izv.Vuzov. Ser. Radiophys*. **2004** *XLVII*, 1-17.
6. Glushkov A.V., Tsudik A.V., et al, Deterministic Chaos, Bifurcations and Strange Attractors in Nonlinear Dynamics of Relativistic Backward-Wave Tube. In: *Awrejcewicz J. (ed) Perspectives in Dynamical Systems II: Mathematical and Numerical Approaches. Series: Springer Proceedings in Mathematics & Statistics*, **2021**, *363*, 125-135.
7. Glushkov A.V., Khetselius O.Y., Nonlinear Dynamics of Complex Neurophysiologic Systems within a Quantum-Chaos Geometric Approach. *In: Glushkov A., Khetselius O., Maruani J., Brändas E. (Eds) Advances in Methods and Applications of Quantum Systems in Chemistry, Physics, and Biology*, Cham: Springer. **2021**, *33,* 291-303
8. Glushkov A., Prepelitsa G., Khetselius O., Kuzakon V., Solyanikova E., Svinarenko A., Modeling of interaction of non-linear vibrational systems on basis of temporal series analyses (application to semiconductor quantum generators). *Dynamical Systems - Theory and Applications.* **2011,** BIF-110.
9. Glushkov, A., Prepelitsa, G., Svinarenko, A., Zaichko, P., Studying interaction dynamics of the non-linear vibrational systems within non-linear prediction method (application to quantum autogenerators) *In: Dynamical Systems Theory;* Awrejcewicz et al Eds.; Łódz, **2013**; Vol T1, 467-477.
10. Prepelitsa G., Brusentseva S., Duborez A., Khetselius O., Bashkaryov P., New nonlinear analysis, chaos theory and information technology approach to studying dynamics of chain of quantum autogenerators. *Photoelectronics* . **2016,** *25*, 85-90.
11. Glushkov, A.V., *Atom in an electromagnetic field*. Kiev: KNT, **2005**.
12. Glushkov, A.; Gurskaya, M.; Ignatenko, A.; Smirnov, A.; Serga, I.; Svinarenko, A.; Ternovsky E. Computational code in atomic and nuclear quantum optics: Advanced computing multiphoton resonance parameters for atoms in a strong laser field. *J. Phys.: Conf. Ser*. **2017**, *905*, 012004.
13. Abarbanel H., Brown R., Sidorowich J., Tsimring L., The analysis of observed chaotic data in physical systems. *Rev Modern Phys*. **1993**, *65*, 1331–1392.
14. Kennel M., Brown R., Abarbanel H., Determining embedding dimension for phase-space reconstruction using geometrical construction. *Phys. Rev.A*. **1992**, *45*, 3403–3411.
15. Havstad J., Ehlers C., Attractor dimension of nonstationary dynamical systems from small data sets. *Phys Rev A*. **1989**, *39*, 845–853.
16. Grassberger P., Procaccia I., Measuring the strangeness of strange attractors. Physica D. **1983,** *9*, 89–208.
17. Mañé R., On the dimensions of the compact invariant sets of certain non-linear maps. *Lecture notes in mathematics*. **1981**, *898*, 230–242.
18. Parker T.S., Chua L.O. *Practical numerical algorithms for chaotic systems*. Springer-Verlag, **1989**.
19. Golub G.H., van Loan C.F. *Matrix computations*. Third Edition. The Johns Hopkins. Univ. Press: Baltimore, **1996**.
20. Wolf A., Swift J.B., Swinney H.L., Vastano J.A. Determining Lyapunov exponents from a time series. *Physica,* **1985**, *D16*, 285-317
21. Benettin G., Galgani L., Strelcyn J.M. Kolmogorov entropy and numerical experiments. *Phys. Rev.*A **1976**, *14*, 2338 - 2345.
22. Khetselius O.Yu., New geometric attractor and neural networks approach to studying chaotic processes in photoelectronics

systems. *Photoelectronic*s, **2013,** 22, 30-37.

23. Sano M., Sawada Y., Measurement of Lyapunov spectrum from a chaotic time series. Phys. Rev.Lett. **1985**, 55, 1082–1085.

24. Prepelitsa G.P., Buyadzhi V.V., Ternovsky V.B. Non-linear analysis of chaotic self-oscillations in backward-wave tube. *Photoelectronics*.-**2013**, *22*, 103-107.

25. Geist K., Parlitz U., Lauterborn W. Comparision of different methods for computing Lyapunov exponents. *Prog. Theor. Phys.* **1990**, *83* (5), 875.

26. Kuptsov P.V., Computation of lyapunov exponents for spatially extended systems: advantages and limitations of various numerical methods. *Izv. Vuzov PND*. **2010**, *18*(5), 93-98.

Tjurin A.V., *V.G. Shevchuk, I.I. Bilan*

NON-LINEAR ANALYSIS OF CHAOTIC SELF-OSCILLATIONS IN BACKWARD-WAVE TUBE

Summary. The paper presents the results of the analysis and modelling of topological and dynamic invariants for the regime of chaotic self-oscillations in the backward-wave oscillator, in particular, the analysis of chaotic time series for the amplitude of the output signal, which is the solution of the equations of the non-stationary nonlinear theory for the O-type backward-wave oscillator (without taking into account space charge, relativistic effects, energy losses, etc.). The main attention is paid to the calculation and analysis of the spectrum of Lyapunov exponents based on the Sano-Savada algorithm. Numerical data of the Lyapunov backward-wave oscillator calculated for the time series of the amplitudes of the output signal are given, which definitely indicate the presence of elements of advanced chaos in the dynamics of the system.

Key words: non-relativistic and relativistic backward-wave tube, spectrum and dynamics, non-linear methods, optical chaos, Lyapunov exponents

Тюрін О.В., Шевчук В.Г., Білан І.І.

НЕЛІНІЙНИЙ АНАЛІЗ ХАОТИЧНИХ АВТОКОЛИВАЛЬНИХ РЕЖИМІВ У ЛАМПІ ЗВЕРНЕНОЇ ХВИЛІ

Резюме. В роботі представлені результати аналізу та моделювання топологічних і динамічних інваріантів для режиму хаотичних автоколивань в лампі зворотної хвилі, зокрема, виконаний аналіз хаотичних часових рядів для амплітуди вихідного сигналу, яка є розв'язком рівнянь нестаціонарної нелінійної теорії для лампи зворотної хвилі О-типу (без урахування просторового заряду, релятивістських ефектів, втрат енергії тощо). Основна увага приділена обчисленню та аналізу спектра показників Ляпунова на основі алгоритму Сано-Савади. Наведено чисельні дані показників Ляпунова розрахованих для часового ряду амплітуд вихідного сигналу, які безумовно вказують на наявність елементів розвиненого хаосу в динаміці системи.

Ключові слова: нерелятивістська та релятивістська лампа зворотної хвилі, спектр і динаміка, нелінійні методи, оптичний хаос, показники Ляпунова

T.B. Tkach[1], A.S. Kvasikova[2], I.M. Shpinareva[3]

[1]Odessa State Environmental University, 15, Lvovskaya str., Odessa
[2]State University of Intel. Technologies & Telecommunications, 1, Kuznechna str., Odessa
[3]I.I. Mechnikov Odessa National University, 2, Dvoryanskaya str., Odessa
e-mail: kvasikovaas@gmail.com

ON SOME NUMERICAL MODEL TO SOLVING DYNAMICAL EQUATIONS OF NONRELATIVISTIC AND RELATIVISTIC BACKWARD-WAVE TUBE

It is developed an effective computational approach to solution the master corresponding system of differential equations, which describe the nonlinear stationary and non-stationary electromagnetic processes in the nonrelativistic and relativistic backward-wave tubes (carcinotrons) with maximal accounting for the different physical factors such as the relativistic effects, effects of dissipation, the presence of a space charge, wave reflections at the ends of the slowing system, stochastic factors by means including the special elements in a whole system etc as well as the detailed investigation of characteristics (dynamical and topological invariants) of dynamics of a carcinotron in automodulation and chaotic regimes with construction the corresponding bi-furcation diagrams. Below in order to further solve the master system of dynamical equations for carcinotron it is presented in brief the realizing numerical scheme, based on the use of the conservative finite-difference schemes of the "predictor-corrector" type and the sweep algorithm.

1. Introduction

One of the most quickly developing directions of the modern physical, quantum, sensor and phototo-electronics is theoretical and experimental study of physical processes in systems and devices of relativistic microwave range electronics, including the backward-wave tubes (lamps, oscillators) their chains and others under different regimes of their functionating (for example, look [1-12]).

It is known that the backward-wave tubes or carcinotrons are an electronic devices for generating electromagnetic oscillations in the microwave range, in which a beam of electrons interacts with an electromagnetic wave in a retarding system in situations where the phase speed of the wave is close to the speed of electrons, and the group speed is opposite in direction [1–8]. Thanks to the first condition, the electrons are exposed to the effective action of the wave field: clumps are formed in the beam, and a high-frequency component of the current appears. Surely, at the present time there are developed a great number of different simple and quite

complicates stationary and nonstationary models to describe the nonlinear electromagnetic processes in the nonrelativistic and relativistic backward-wave tubes (for example, look [1-8] and refs therein).

There have been presented quite much numerical approaches to find numerical solutions of the stationary and nonstationary systems of differential equations which are describe the nonlinear electromagnetic processes in the nonrelativistic and relativistic backward-wave tubes [3-8].

It should be stated that the implementation of mathematical models on computers takes place using the methods of applied mathematics, which, of course, are constantly being improved along with progress in the field of computer technology. The solution of the mathematical model of the problem, which should provide the criterion of efficiency and optimality, can be obtained faster with the help of a suitable efficient algorithm. Any reduction of the problem of relativistic microwave range (little and large power) electronics, including the backward-wave tubes, is usually reduced to the solution of

algebraic equations of one or another structure (for example, look details in [9-16]).

As a result, most methods of applied mathematics are related to reducing the problem to a system of algebraic equations and their subsequent solution. One of the fairly widespread methods of solving problems in mathematical physics and applied mathematics is the finite difference method [15] (see also [16-20]).

In recent years, the problem of wide application of various methods of constructing difference schemes in the problems of mathematical physics, physics of systems, elements and devices, including physical and quantum electronics [3-12].

The main aim of our work is develop effective computational approach to solution the master corresponding system of differential equations, which describe the nonlinear stationary and non-stationary electromagnetic processes in the nonrelativistic and relativistic backward-wave tubes with maximal accounting for the different physical factors such as the relativistic effects, effects of dissipation, the presence of a space charge, wave reflections at the ends of the slowing system, stochastic factors by means including the special elements in a whole system etc as well as the detailed investigation of characteristics (dynamical and topological invariants) of dynamics of the backward-wave tube in regular, automodulation and chaotic regimes with construction the corresponding bi-furcation diagrams. Below in order to further solve the system of differential equations for the backward-wave tube it is in brief described the realizing numerical scheme, based on the use of the conservative finite-difference schemes of the "predictor-corrector" type and the method of the sweep method.

2. Standard system of differential equations for a backward-wave tube

In the ref. [1-8] it has presented the detailed explanation of the master systems of equations describing the fundamental processes in the system, so we should only present the corresponding system in the suitable form. According to ref. [3-6], the component of the wave field that interacts with the electron beam can be represented as

$$E(x,t) = R\left[\widetilde{E}(x,t)e^{i\omega_0 t - i\beta_0 x}\right],$$

where $\widetilde{E}(x,t)$ is a slowly varying complex function.

The high-frequency current arising in the electron beam as a result of the action of the wave field on it is represented in the following form [5]:

$$I(x,t) = Re\left[I_1(x,t)e^{i\omega_0\left(t-\frac{x}{v_0}\right)} + I_2(x,t)e^{2i\omega_0(t-x/v_0)} + \ldots\right], \quad (1)$$

where $I_1(x,t)$, $I_2(x,t)\ldots$ – slow amplitudes of the first, second and subsequent harmonics. First master equation can be written in the standard form (see details in Refs. [3-5]):

$$\frac{1}{v_{ep}}\frac{\partial \widetilde{E}}{\partial t} - \frac{\partial \widetilde{E}}{\partial x} = \frac{-1}{2}\beta_0^2 K_0 \widetilde{I}_1, \quad (2)$$

where K_0 – the coupling resistance of the retarder system for the working spatial harmonic at the frequency ω_0.

The second component of the self-consistent theory is the formulation of the electron motion equation which has the standard form [7,8]:

$$w\frac{d^2 x}{dt^2} = \frac{e}{m_0}Re\left[\widetilde{E}(x,t)e^{i\omega_0 t - i\beta_0 x}\right] \quad (3)$$

Further usually one could define $t(x,t_0) = t_0 + x/v_0 + \tilde{t}(x,t_0)$ as a time of arrival at the point x of the electron that flew into the interaction space at the moment t_0.

Due to the slowness of the change of the complex amplitude in time and the smallness of the change in the speed of electrons in the process of interaction, one has the right to replace in the right part $\widetilde{E}(x,t(x,t_0))$ на

147

$\tilde{E}\left(x, t_0 + x/\upsilon_0\right)$ и $\left(\partial t/\partial x\right)^3_{t_0}$ on υ_0^{-3}, and further it can be written as:

$$\left(\partial^2 \tilde{t}/\partial x^2\right)_{t_0} = -\frac{e}{m\upsilon_0^3} Re\left[\tilde{E}(x, t + x/\upsilon_0)e^{i\omega_0(t_0 + \tilde{t}(x, t_0))}\right]. \quad (4)$$

After reduction to dimensionless variables and parameters, the equations and boundary conditions take the following form [4-7]:

$$\partial^2\theta/\partial\zeta^2 = -R\left[F exp\left(i\theta\right)\right],$$

$$\partial F/\partial\tau - \partial F/\partial\zeta = \tilde{I},$$

$$\tilde{I} = \frac{-1}{\pi} \int_0^{2\pi} e^{-i\theta} d\theta_0, \quad (5)$$

$$\theta\,\square_{\zeta=0} = \theta_0, \ \partial\theta/\partial\zeta\,\square_{\zeta=0} = 0,$$

$$F\,\square_{\zeta=L} = 0, \quad (6)$$

where $\zeta = \beta_0 Cx$, $\quad (7)$

$$\tau = \omega_0 C\left(t - x/\upsilon_0\right)\left(1 + \upsilon_0/\upsilon_{gp}\right)^{-1} -$$

are the dimensionless independent variables are coordinate and "local time". Due to the introduction of "local time", which is counted at each point of the space of interaction with the displacement x/υ_0, there is no derivative in the equation of motion by τ which facilitates the construction of a difference scheme for the numerical solution of the system of equations. This is also convenient in the sense that in the dimensionless form of the equations, the parameter of the ratio of the group velocity to the beam velocity is excluded, which now appears only in the coefficient connecting dimensional and dimensionless time. As usually, the value $\theta(\zeta, \tau, \theta_0)$ characterizes the phase relative to the wave for an electron that has flown into the space of interaction with the phase θ_0 , and

$$F\left(\zeta, \tau\right) = \tilde{E}/\left(2\beta_0 UC^2\right)$$

is the dimensionless complex amplitude of the high-frequency wave field. Pierce's parameter

$$C = \sqrt[3]{I_0 K_0/(4U)},$$

where is I_0 the constant component of the beam current, U is the accelerating voltage, assumed to be small.

3. Numerical differences scheme

In order to further solve the system of differential equations for the backward-wave tube it has been developed a numerical scheme, which is based on the use of finite-difference schemes of the "predictor-corrector" type and the method of the sweep method (see details in refs. [3-7]). The finite-difference scheme has been constructed and analogous the scheme [5,6]. Namely, the following substitutions have been applied:

$$[Q = exp(i\theta)] ,$$

$$X = (1/L)d\theta)/d\zeta, \quad (8)$$

the corresponding master system:

$$\partial^2\theta/\partial\zeta^2 = -Re[F\, exp(i\theta)],$$

$$\partial F/\partial\tau - \partial F/\partial\zeta = \tilde{I},$$

$$\tilde{I} = -\frac{1}{\pi}\int_0^{2\pi} e^{-i\theta}\, d\theta_0, \quad (9)$$

has the following form:

$$\frac{\partial Q}{\partial} = iLXQ$$

$$\quad (10)$$

$$\frac{\partial X}{\partial} = -LRe\left(FQ\right)$$

Further the initial filed distribution is determined in the points of the net on the coordinate. The known method of largest particles is used. As usually the initial distribution of a field is determined by the distribution of the main amplitude mode. For each particle (index j) and each time moment (index i) it is solving the equation of motion according to the standard predictor—corrector scheme:

$$X_{i+\frac{1}{2}}^j = X_i^j + LP_i^j\frac{d}{2} = X_i^j + DP_i^j$$

$$\quad (11)$$

$$Q^j_{i+\frac{1}{2}} = Q^j_i + iL\, X^j_i Q^j_i \frac{d}{2} = Q^j_i + iDL\, X^j_i Q^j_i$$

where

$$D = L\frac{d\zeta}{2},$$
$$P = -Re[FQ]$$

is a particle acceleration

Then it has been calculating (at the next step):

$$P^j_{i+\frac{1}{2}} = -Re\{[(F_i + F_{i+1})/2]QX^j_{i+\frac{1}{2}}\},$$

$$X^j_{i+1} = X^j_i + LP^j_{i+1/2}d\zeta = X^j_i + 2DP^j_{i+1/2},$$

$$Q^j_{i+1} = Q^j_i + iLX^j_{i+1/2}Q^j_{i+1/2}d\zeta$$
$$= Q^j_i + 2iDLX^j_{i+1/2}Q^j_{i+1/2}, \quad (12)$$

The values of the first harmonic of the current in each node are determined by the standard expression:

$$I_i = (2/J)\sum_{j=1}^{J} Q^j_i$$

After determining the current values at each point of the grid, the induced field is then determined. To solve the excitation equation, a second-order scheme is used; accordingly, the iterative procedure for calculating the next time value of the field at each node along the coordinate has the form:

$$F^{l+1}_i = a_1 F^l_{i+1} + a_2 F^l_i + a_3 F^l_{i-1}$$
$$- D[b_1 I^l_{i+} b_2 I^{l-1}_i + b_3 I^l_{i-1}] \quad (13)$$

Other details can be found in the refs. [3-10]. In conclusions let us note that it is supposed the further generalization and development more advanced approach with maximal accounting for the different physical factors (such as the relativistic effects, effects of dissipation, the presence of a space charge, wave reflections at the ends of the slowing system, stochastic factors by means including the special elements in a whole system etc) as well as the further detailed numerical investigation of characteristics (dynamical and topological invariants) of dynamics of nonrelativistic and relativistic backward-wave tubes (carcinotrons) in different regular, automodulation and chaotic (hyperchaotic) regimes with construction the corresponding

bi-furcation diagrams and understanding the features of so called (generally speaking) self-oscillating distributed dynamical systems, which are characterized by the absence of rigid scenarios of the transition to chaos, in contrast to common known scenarios in more simple systems.

References

1. Levush B., Antonsen T.M., Bromborsky A., Lou W.R., Carmel Y., Theory of relativistic backward wave oscillator with end reflections. IEEE Transactions on Plasma Sci. 1992, 20(3), 263-280.
2. Levush B., Antonsen T.M., Bromborsky A., Lou W.R., Carmel Y., Theory of relativistic backward wave oscillator with end reflections. IEEE Trans, on Plasma Sci. 1992, 20(3), 263-280.
3. Glushkov A.V., Tsudik A.V., Ternovsky V.B., etal, Deterministic Chaos, Bifurcations and Strange Attractors in Nonlinear Dynamics of Relativistic Backward-Wave Tube. Springer Proc. in Mathematics & Statistics. 2021, 363, 125-135.
4. Ginzburg H.S., Kuznetsov S.P., and T. N. Fedoseeva T.N., Theory of transient processes in a relativistic BWO. Izv. Univ. Radiophys. 1978, 21, 1037-1052.
5. Bezruchko B.P., Bulgakova L.V., Kuznetsov S.P., Trubetskov D.I., Stochastic self-oscillations and instability in a backward wave lamp. Radio engineering and Electr. 1983, 26, 1136-1139.
6. Astakhov S.A., Bezruchko B.P., Zborovsky A.V., Trubetskov D.I., Study of complex dynamics of the system "electron beam-backward wave with reflections (experimental computer simulations). In: Conf. Materials "Advances in Electron industry". 1998 (5p.).
7. Kuznetsov S.P., Shirokov A.P. Discrete model of a relativistic backward wave lamp. Izv. Vuzov – Appl. Nonlinear Dynamics. 1997, 5, 76–84.
8. Kuznetsov S.P., Non-linear dynamics of the restoration lamp: self-modulation, multistability, control Izv. Vuzov – Appl. Nonlinear Dynamics. 2006, 14(4), 76–84.
9. Kuznetsov S.P., Trubetskov D.I., Chaos and

hyperchaos in backward-wave tube. Rus. J. Phys. Ser. Radiophys.-2004, XLVII(5), 1-8

10. Vitavetskaya L.A., Chernyakova Y.G, Ignatenko A.V., Mishchenko E.V., etal, Generalized conservative difference scheme for the problem of laser pulse propagation in a nonlinear medium. Herald of OSENU. 2009, N7, 241-245.

11. Chan Z., Wang J., Wang ., Qiao H., Zhang D., Guo W., An optimization method of relativistic backward wave oscillator using particle simulation and genetic algorithms. Phys. Plasmas. 2013, 20, 113103.

12. Trofimov V.A. Nonlinear wave equation of laser optics of femtosecond pulses. Differ. Equations. 1998, 34(7),1002-1004.

13. Varentsova S., Volkov A., Trofimov V., Conservative difference scheme for problem of femtosecond laser pulse propagation in a cubic-nonlinear medium. Zh. Vych. Math. & Math. Phys. 2003, 43(11), 1709-1721.

14. Rostov V. V., Totmeninov E. M., Yalandin M., Powerful relativistic microwave generators based on a backward -wave lamp

with a modulating resonant reflector, Journal of Techn. Phys. 2008, 78(11), 85–92.

15. Totmeninov E.M. etal,, Relativistic backward wave lamp with a mechanical frequency tuning band. Journal of Technical Physics. 2011, 81(7), 111–114.

16. Goykhman M. B. et al, Relativistic backward wave lamp with smooth adjustment of the duration of output radiation pulses. Journal of technical physics. Journal of Technical Physics. 2012, 82(6), 111– 114.145–148.

17. Marchuk G, Methods of computational mathematics. Nauka: M, 1980.

18. Glushkov A., Shpinareva I., Ambrosov S, Calculational Methods of dynamics of continuous mediums. TES: Odessa, 2004.

19. Glushkov A., Kruglyak Y., Chernyakova Y., Linear algebra. TES: Odessa, 2004.

20. Glushkov A.V., Khetselius O.Yu., Kruglyak Yu. A., Ternovsky V.B., Ignatenko A.V., Numerical methods in Quantum geometry and chaos theory, P.2. TES: Odessa, 2015.

PACS: 41.20.-q, 41.20.Jb, 41.60.Dk

Tkach T.B., Kvasikova A.S., Shpinareva I.M.

ON SOME NUMERICAL MODEL TO SOLVING DYNAMICAL EQUATIONS OF NONRELATIVISTIC AND RELATIVISTIC BACKWARD-WAVE TUBE

Summary. It is developed an effective computational approach to solution the master corresponding system of differential equations, which describe the nonlinear stationary and non-stationary electromagnetic processes in the nonrelativistic and relativistic backward-wave tubes (carcinotrons) with maximal accounting for the different physical factors such as the relativistic effects, effects of dissipation, the presence of a space charge, wave reflections at the ends of the slowing system, stochastic factors by means including the special elements in a whole system etc as well as the detailed investigation of characteristics (dynamical and topological invariants) of dynamics of a carcinotron in automodulation and chaotic regimes with construction the corresponding bi-furcation diagrams. Below in order to further solve the master system of dynamical equations for carcinotron it is presented in brief the realizing numerical scheme, based on the use of the conservative finite-difference schemes of the "predictor-corrector" type and the sweep algorithm.

Key words: nonrelativistic and relativistic backward-wave tubes, carcinotrons, computational approach, chaotic dynamics, difference scheme and sweep algorithm

PACS 31.15.A-; 32.30.-r

Ткач Т.Б., Квасикова А.С., Шпінарева І.М.

ПРО ДЕЯКУЮ ЧИСЛОВУ МОДЕЛЬ ДО РОЗВ'ЯЗУВАННЯ ДИНАМІЧНИХ РІВНЯНЬ НЕРЕЛЯТИВІСТСЬКОЇ ТА РЕЛЯТИВІСТСЬКОЇ ЛАМПИ ЗВОРОТНОЇ ХВИЛІ

Резюме. Розроблється ефективний обчислювальний підхід до розв'язання відповідної мастерної системи динамічних рівнянь, які описують нелінійні стаціонарні та нестаціонарні електромагнітні процеси в нерелятивістських та релятивістських лампах зворотної хвилі (карсинотронах) з подальшим максимальним урахуванням різних фізичних факторів, таких як релятивістські ефекти. , ефекти дисипації, наявність просторового заряду, відбиття хвилі на кінцях сповільнюваної системи, стохастичні фактори за допомогою включення спеціальних елементів у всю систему тощо, а також дослідженням характеристик (динамічних і топологічних інваріантів) динаміка карсинотрона в автомодуляційному та хаотичному режимах з побудовою відповідних біфуркаційних діаграм. Для розв'язування головної системи динамічних рівнянь карсинотрона наведено реалізуєму чисельну схему, яка заснована на використанні консервативної різницевої схеми типу «предиктор-коректор» та алгоритму розгортки.

Ключові слова: нерелятивістські та релятивістські лампи зворотної хвилі, карсинотрон, обчислювальний підхід, хаотична динаміка, різницева схема та алгоритм розгортки

A.V. Glushkov[1], A.A. Kuznetsova[2]
[1]Odessa State Environmental University, L'vovskaya str.15, Odessa
[2]Odessa National Maritime Academy, Didrikhson str. 4, Odessa
E-mail: glushkovav@gmail.com

RELATIVISTIC ENERGY APPROACH TO ATOMIC SYSTEMS IN A STRONG ELECTROMAGNETIC FIELD IN PLASMAS

The fundamentals of a consistent relativistic approach to determination of radiation and spectral characteristics of the atomic systems (atoms, multicharged ions in plasmas conditions) in a strong external electromagnetic field (EMF), which is based on a relativistic energy formalism (REA) (adiabatic Gell-Mann and Low formalism) and relativistic many-body perturbation theory (RMBPT) formalism for atomic systems in a plasmas are presented. Within an energy approach in relativistic approximation the Gell-Mann and Low formula expresses the imaginary part of an atomic level energy shift δE through the QED scattering matrix, which includes an interaction as with an EMF as with the photon vacuum field (spontaneous radiative decay). It results in possibility of an uniform simultaneous consideration of spontaneous and (or) induced, radiative processes and their interference. The radiation atomic lines position and shape fully determine a spectroscopy of the plasmas atomic systems in an EMF. The effective modified technique, based on the Ivanova-Ivanov method of differential equations, for computing the infinite sums in expressions for a spectral line shifts and broadening is shortly described. The fundamentals of a formalism of the relativistic gauge-invariant RMBPT with the optimized Dirac-Kohn-Sham (DKS) and Debye-Hückel zeroth approximations are presented.

1. Introduction

Spectroscopy of atomic and molecular systems in a strong electromagnetic field belongs to one of the most relevant and practically important directions of modern optics and spectroscopy, in particular, as one of the main sources of spectroscopic information for atomic, molecular, nuclear physics, laser physics, quantum and photo-electronics, plasma physics, astrophysics, etc. In recent years, great interest in both the theoretical fundamental and its numerous applied aspects has grown dramatically. This is due to many reasons, and first of all, we are talking about significant progress in the development of new experimental research methods, in particular, a significant increase in the intensity and quality of laser radiation, the use of accelerators, heavy ion colliders , sources of synchrotron radiation, neutron sources, etc. (e.g.[1-26]), which opens completely new opportunities for the study of increasingly energetic processes, stimulates the development of new theoretical methods for calculating their characteristics in spectroscopy due to collisions of electrons, photons, atoms, molecules. It's appropriate to remind that in many modern plasma experiments (using tokamak plasma, laser plasma, etc.), as well as in astrophysical, space, laboratory, etc. electric fields of various classes are available in the plasma, including quasi-monochromatic electric fields with a relative width of the frequency band, broadband electric fields, finally, the specified environment is influenced by powerful electromagnetic pulses, which as a result induce extremely complex from a theoretical point of view, physical processes in plasma.

In this paper we present the fundamentals of a consistent approach to atomic systems (atoms, multicharged ions in plasmas conditions) in a strong external electromagnetic field (EMF), which is based on a relativistic energy formalism (REA) (adiabatic Gell-Mann and Low formalism) [23-34] and relativistic many-body perturbation theory (RMBPT) formalism for atomic systems in a plasmas (e.g. [35-37]). Within an energy approach in relativistic approximation the Gell-Mann and Low formula expresses the imaginary part of an

atomic level energy shift δE through the QED scattering matrix, which includes an interaction as with an EMF as with the photon vacuum field (spontaneous radiative decay). The fundamentals of a new formalism of the relativistic gauge-invariant RMBPT with the optimized Dirac-Kohn-Sham and Debye-Hückel zeroth approximations are presented.

2. Relativistic energy approach to atomic systems in an electromagnetic field in plasmas

The theoretical basis of the relativistic energy approach in atomic spectroscopy was widely discussed earlier (see, e.g. [21-32]) and here we will focus on the key topics following to Refs. [22,27-29,32]. Let us note that in the theory of the non-relativistic atom a convenient field procedure is known for calculating the energy shifts δE of degenerate states. This procedure is connected with the secular matrix M diagonalization [27,28]. In constructing M, the Gell-Mann and Low adiabatic formula for δE is used. In relativistic version of the Gell-Mann and Low formula δE is connected with electrodynamical scattering matrice, which includes interaction with a laser field. Naturally, in relativistic theory the secular matrix elements are already complex in the second perturbation theory (PT) order. Their imaginary parts are connected with radiation decay possibility. The total energy shift is usually presented in the form [27-29]:

$$\delta E = \mathrm{Re}\,\delta E + i\mathrm{Im}\,\delta E,$$

(1a)

$$\mathrm{Im}\,\delta E = -\Gamma / 2,$$

(1b)

where Γ is the level width (decay possibility). As it was said, spectroscopy of an atom in a laser field is fully determined by position and shape of the radiation emission and absorption lines. The lines moments M_n are strongly dependent upon the laser pulse quality: intensity and mode constitution [7-13,23,24,27-32]. Let us describe the interaction "atom -EMF" by the following potential:

$$V(r,t) = V(r)\int d\omega f(\omega - \omega_0) \sum_{n=-\infty}^{r} \cos(\omega_0 t + \omega_0 n\tau)$$

(2)

Here ω_0 is the central EMF radiation frequency, n is the whole number. The potential V represents the infinite duration of EMF pulses with known frequency τ. Next we will consider the interaction of an atom with a single pulse. The function $f(\omega)$ is a Fourier component of the EMF pulse. The condition:

$$\int d\omega f^2(\omega) = 1$$

(3)

normalizes potential $V(r,t)$ on the definite energy in the pulse. It is worth to comment that the EMF pulses with Lorentzian, Gaussian or more complicated shape can be considered. As it was indicated in Ref. [28-32], the main program results in the calculating an imaginary part of energy shift $\mathrm{Im}\,\delta E_\alpha(\omega_0)$ for any atomic level as the function of the central laser frequency ω_0. An according function has the shape of the resonance, which is connected with the transition α-s (α, s-discrete levels) with absorption (or emission) of the "k" number of photons. We will calculate the following quantities for the multiphoton resonance:

$$\delta\omega(s-\alpha \mid k) = \int d\omega \mathrm{Im}\,\delta E_\alpha(\omega)\,(\omega - \omega_{s\alpha}/k)/N,$$

(4)

$$M_n = \int d\omega \mathrm{Im}\,\delta E_\alpha(\omega)\,(\omega - \varpi_{s\alpha}/k)^n/N,$$

(5)

$$N = \int d\omega \mathrm{Im}\,\delta E_\alpha(\omega),$$

(6)

$$\varpi_{s\alpha} = \omega_{s\alpha} + k \cdot \delta\omega(s-\alpha \mid k)$$

(7)

where N is the normalizing multiplier; $\omega_{s\alpha}$ is position of the non-shifted line for transition s-α, $\delta\omega(s-\alpha|k)$ is the line shift under k-photon absorption. To determine the quantities M_n, one should need to obtain an expansion of E_α to the following PT series:

$$\delta E_\alpha = \sum \delta E_\alpha^{(2k)}(\omega_0).$$

(8)

An external EMF shifts and broadens the atomic levels. The standard quantum approach relates complex eigenenergies $\delta E = \delta E_r + i\Gamma/2$

and complex eigenfunctions to the corresponding resonances [12,24,32]. The field effects drastically increase upon going from one excited level to another. The highest levels could overlap forming a "new continuum" with lowered boundary. In the case of a strong field, its potential should appear in the Dirac equations already in the zeroth-order approximation (the solution is Dirac-Volkov type function). On the other hand, it is convenient to use methods such as operator PT with included well known "distorted-waves" zeroth approximation" in the frame of the formally exact PT.

As usually [32], next one should use the known Gell-Mann and Low adiabatic formula for δE_α with QED scattering matrix. According to [27-32], the representation of the S- matrix in the form of PT series induces the expansion for δE_α:

$$\delta E_\alpha(\omega_0) = \lim_{\gamma \to 0} \gamma \sum_{k_1 k_2 \ldots k_l} c(k_1, k_2, \ldots, k_l) J_\gamma(k_1, k_2, \ldots, k_l),$$

(9)

$$J_\gamma(k_1, k_2, \ldots, k_l) = \prod_{j=1}^l S_\gamma^{(k_j)},$$

(10)

$$S_\gamma^{(n)} = (-1)^n \int_{-\infty}^0 dt_1 \ldots \int_{-\infty}^{t_n-1} dt_n \langle \Psi_\alpha | V_1 V_2 \ldots V_n | \Psi_\alpha \rangle,$$

(11)

$$V_i = \exp(iH_0 t_i) V(r t_i) \exp(-iH_0 t_i) \exp(\gamma t_i)$$

(12)

where S_γ is QED scattering matrix, γ is an adiabatic parameter, H_0 is the unperturbed atomic Hamiltonian (below it will be defined for atomic systems in the Debye plasmas), $c(k_1, k_2, \ldots, k_n)$ are the numerical coefficients. The details of rather cumbersome transformations are presented in Refs. [32], where the structure of matrix elements $S_\gamma^{(n)}$ is also described. As an example, let us note that $S_\gamma^{(2)}$ can be determined as follows:

$$S_\gamma^{(2)} \sim \int_{-\infty}^0 dt_1 \int_{-\infty}^0 dt_2 \exp[\gamma(t_1 + t_2)] \langle \Psi_\alpha | \exp(iH_0 t_1) V(r t_1) \cdot$$

$$\cdot \exp(-iH_0 t_1) \exp(iH_0 t_2) V(r t_2) \exp(-iH_0 t_2) | \Psi_\alpha \rangle.$$

(13)

After some transformations one can get the expressions for line moments. The final results for quantities (5) for the Gaussian shape laser pulse are as follows:

$$\delta\omega(s - a | k) = [\pi\Delta / (k+1) k][E(s, \omega_{s\alpha} / k) - E(\alpha, \omega_{s\alpha} / k)],$$

$$M_2 = \Delta^2/k ,$$

$$M_3 = \{4\pi\Delta^3 / [k(k+1)]\}[E(s, \omega_{s\alpha} / k) - E(\alpha, \omega_{s\alpha} / k)],$$

(14)

where

$$E(j, \omega_{s\alpha} / k) = \frac{1}{2} \sum_{s_i} V_{js_i} V_{s_i j} [\frac{1}{\omega_{js_i} + \omega_{s\alpha} / k} + \frac{1}{\omega_{js_i} + \omega_{s\alpha} / k}]$$

(15)

The summation in (15) is over all atomic states. The equations (1)-(15) describe the main characteristics of the radiative emission and absorption line of atomic system near the resonant EMF frequency $\omega_{s\alpha}/k$. The corresponding expressions for the Lorentzian shape laser pulse are given in Refs. [23,32]. For the soliton-like pulse it is necessary to use some approximations to simplify the expressions and perform the numerical calculation [32]. The next serious problem is calculation of the sum (15), which includes infinite summations over the complete set of unperturbed (or distorted in the zeroth approximation in a case of a strong EMF) atomic states. One of the most widespread methods for calculating the sums (20) is the Green function method (look below). However, as it was indicated in Refs. [23,25,27-30], the more preferable and effective method is based on the advanced algorithm of differential equations, initially developed by Ivanova-Ivanov [28]. It is worth to note that this method has been frequently used earlier in calculations of different atomic system energy and spectroscopic characteristics (see, e.g., [23-34]). The necessary sums can be expressed through sums of the following one-electron matrix elements:

$$S = \sum_{n_1} \langle n\chi m | V | n_1 \chi_1 m_1 \rangle \langle n_1 \chi_1 m_1 | V | n\chi m \rangle / (\varepsilon_{n_1 \chi_1 m_1} - \varepsilon)$$

(16)

where $(n\mu m)$ – quantum numbers of one-electron states, $\varepsilon = \varepsilon_{n\chi m} + \omega_{s\alpha}/k$ is the energy parameter. One-electron energies $\varepsilon_{n\chi m}$ include the rest energy $(\alpha Z)^{-2}$, where α is the fine structure constant and Z is charge of a nucleus. Here and below we use the Coulomb units (1 C.u.=Z^2 a.u.e.; a.u.e.= 1 atomic unit of energy). For definiteness, let us concretize an

154

interaction of atom with a EMF. In particular, for the typical dipole interaction the corresponding potential is:

$$V(\mathbf{r})=(\mathbf{a},\boldsymbol{\alpha}), \qquad (17)$$

where $\mathbf{a}$ is a vector of polarization of radiation; $\boldsymbol{\alpha}$ is a vector of the Dirac matrices.

One should introduce a bi-spinor of the following form [28-32]:

$$\Psi_{\chi_1 m_1} = \sum_{n_1} \phi_{n_1 \chi_1 m_1} \langle n_1 \chi_1 m_1 |V| n \chi m \rangle / \left(\varepsilon_{n_1 \chi_1 m_1} - \varepsilon \right) \qquad (18)$$

The radial parts F, G of a bi-spinor Ψ satisfy the system of the following differential equations [28,32]:

$$-F'/\alpha Z + (1+\chi_1)F/\alpha Z r + A_- G = C\left(\mathbf{a}\big| j_1 l_1 m_1, \ \tilde{j} \tilde{l} m\right) f_{n\chi}/\alpha Z \qquad (19a)$$

$$G'/\alpha Z + (1-\chi_1)G/\alpha Z r + A_+ F = C\left(\mathbf{a}\big| j_1 l_1 m_1, \ \tilde{j} \tilde{l} m\right) g_{n\chi}/\alpha Z \qquad (19b)$$

$$A_{\pm} = U_{MF}(r) \pm 1/(\alpha Z)^2 - \varepsilon \qquad (20)$$

Here Z is a nuclear charge, α is the fine structure constant, F and G are the components of the bi-spinor (18); $U_{MF}(r)$ is some atomic mean-field potential (see possible expressions, e.g., in Refs. [23-25]). The final expression for the sum (16) can be written as follows:

$$S = \int dr \ r^2 \left[f_{n\chi_1} \cdot G(r) \cdot C[(a|jlm, j_1 \tilde{l}_1 m_1)] \right.$$
$$\left. + g_{n\chi} \cdot F(r) \cdot C(a|j\tilde{l}m_1, j_1 l_1 m_1) \right] \qquad (21)$$

The alternative approach to calculating (16) is based on the using method of the Green's function of Dirac equation and presented, for example, in Ref. [32] in the Dirac-Kohn-Sham model of multielectron atom. The Green's function is defined as the solution of the inhomogeneous Dirac equation:

$$\left(\hat{H} - \zeta\right) G_E(r_1 r_2) = \delta(r_1 - r_2), \qquad (22)$$

where $\hat{H}$ is the Dirac Hamiltonian, ζ is an energy parameter. The known spectral decomposition of the Green's function is as follows:

$$G(r_1 r_2 \vee E) = \sum_{n\chi m} \Psi_{n\chi m}(r_2) \Psi_{n\chi m}(r_1)/(E_{n\chi} - E) \qquad (23)$$

where one can usually allocate partial contributions with a fixed χ (Dirac's angular quantum number), each of which is a product of the radial $G(r_1 r_2 \vee E, \chi)$ and angular parts. In the relativistic theory, the Green's function is a 4-component matrix:

$$G(r_1 r_2 \,|\, E, \chi) = \begin{pmatrix} \hat{F}(r_>)F(r_<) & \hat{F}(r_>)G(r_<) \\ \hat{G}(r_>)F(r_<) & \hat{G}(r_>)G(r_<) \end{pmatrix}, \qquad (24)$$

where $r_\square(r_\square)$ is more (less) of r_1, r_2. According to Ref. [32], the system of the corresponding Dirac equations for F and G component in the Dirac-Kohn-Sham approximation is as follows:

$$F' = -(\chi + |\chi|)F/r + \tilde{\alpha} \cdot \left[V_N(r) + V^{\text{DKS}}(r) - i\xi - \tilde{\alpha}^{-2}\right]G,$$
$$G' = (\chi - |\chi|)G/r - \tilde{\alpha} \cdot \left[V_N(r) + V^{\text{DKS}}(r) - i\xi + \tilde{\alpha}^{-2}\right]F, \qquad (25)$$

$$\tilde{F}' = -(\chi + |\chi|)\tilde{F}/r + \tilde{\alpha} \cdot [V_N(r) + V^{DKS}(r) - i\xi - \tilde{\alpha}^{-2}]\tilde{G},$$
$$\tilde{G}' = (\chi + |\chi|)\tilde{G}/r - \tilde{\alpha} \cdot [V_N(r) + V^{DKS}(r) - i\xi + \tilde{\alpha}^{-2}]\tilde{F}, \qquad (26)$$

where $\tilde{\alpha} = \alpha Z$, $V_N(r)$ is the potential of a nucleus. The functions (F, G) represent the first fundamental solution, which is regular for $r \to 0$ and singular for $r \to \infty$. Any combination $(\tilde{F}, \tilde{G}) + X r^{2|\chi|}(F, G)$ satisfies the above written equations for $(\tilde{F}, \tilde{G})$ and represents singular solution at zero [29,32]. The right chosen combination $(\widehat{F}, \widehat{G})$ for the single value of the mixing coefficient X (regular for $r \to \infty$) is second fundamental solution $(\widehat{f}, \widehat{g})$. The corresponding condition is as follows:

$$(F, G) \sim \exp(-Ar);, \ A = \left(\tilde{\alpha}^{-2} + \xi^2 \tilde{\alpha}^2\right)^{1/2}. \quad (27)$$

Other details can be found in Refs. [26-32].

3. Relativistic Debye model for atomic systems in plasmas

Below we shortly present the fundamentals of a relativistic many-body perturbation theory (RMBPT) with the Debye shielding model Hamiltonian for electron-nuclear and electron-electron systems [35-37]. The optimized one-electron representation in the PT zeroth approximation is constructed by means of the correct treating the gauge dependent multielectron contribution of the lowest PT corrections to the radiation widths of atomic levels. Within the known model by Debye and Hückel (e.g. [2-4,35], a plasmas environment effect is modelled by the shielding parameter μ, which describes a shape of the long-rang potential. An interaction potential between two charged particles in a plasmas can me described by the known Yukawa-type potential. A difference between the Yukawa type potential and standard Coulomb potential is in account for the effect of plasma, which is modeled by the shielding parameter. This parameter μ is connected with the plasma parameters such as the temperature T and the charge density n is as follows:

$$\mu \sim \sqrt{e^2 n / k_B T} \qquad (28)$$

Here e is the electron charge and k_B is the Boltzman constant. The density n is given as a sum of the electron density N_e and the ion density N_k of the k-th ion species with the nuclear charge q_k : $n = N_e + \sum_k q_k^2 N_k$. It is very useful to remind the simple estimates for the shielding parameter. For example, under typical laser plasma conditions of $T \sim$ 1keV and n$\sim 10^{23}$ cm^{-3} the parameter μ is of the order of 0,1 in atomic units. By introducing the Yukawa-type electron-nuclear attraction and electron-electron repulsion potentials, the Debye shielding model Dirac Hamiltonian for electron-nuclear and electron-electron subsystems is given in atomic units as follows (e.g. [35,36]):

$$H = \sum_i [\alpha c p - \beta m c^2 - Z \exp(-\mu r_i)/r_i] + \sum_{i>j} \frac{(1-\alpha_i \alpha_j)}{r_{ij}} \exp(-\mu r_{ij}) \qquad (29)$$

where c is the velocity of light and Z is a charge of the atomic ion nucleus. The formalism of the relativistic many-body PT for atoms in a plasmas is further constructed in the same way as the analogous RMBPT formalism for the free relativistic atomic systems (e.g. [25-32]). However, in the PT zeroth approximation of our RMBPT version we use a mean-field potential, which includes the Yukawa-type potential (insist of the pure Coulomb one) plus exchange Kohn-Sham potential and additionally the Lundqvist-Gunnarson correlation potential (with the optimization parameter b) as in Refs. [16-23,25,32]. As alternative one could use an optimized model potential by Ivanova-Ivanov (for Ne-like ions) [6], which is calibrated within the special ab initio procedure within the relativistic energy approach [28,31]. As usually, a standard field procedure is used for calculating the energy shifts δE of degenerate states of atomic system. This procedure is connected with the secular matrix M diagonalization [27,29]. In constructing M, the Gell-Mann and Low adiabatic formula for δE_α is used. The secular matrix elements are already complex in the PT second order (the first order on the inter-electron interaction). Their imaginary parts are connected with the radiation decay (transition, scattering, ionization etc) possibility. It is important to note that the computing the energies and radiative transition matrix elements is reduced to calculation and the further diagonalization of the complex matrix M .and determination of matrix of the coefficients with eigen state vectors $B_{ie,iv}^{IK}$ [27-29]. To calculate all necessary matrix elements one must use a basis of the one-quasiparticle relativistic functions. Namely this basis is proposed to use in computing radiation spectral lines characteristics of atomic systems in a plasmas. This is a novelty element of a whole theory.

4. Conclusions

To conclude let us note that in this paper we shortly present the fundamentals of a new, consistent relativistic approach to determination of radiation and spectral characteristics of the atomic systems (atoms, multicharged ions in plasmas conditions) in a

strong external EMF, which is based on a adiabatic Gell-Mann and Low formalism and RMBPT formalism for atomic systems in a plasmas. Within an REA the known Gell-Mann and Low formula expresses the imaginary part of an atomic level energy shift δE through the QED scattering matrix, which includes an interaction as with an EMF as with the photon vacuum field (spontaneous radiative decay). The fundamentals of a new formalism of the relativistic gauge-invariant RMBPT with optimized Dirac-Kohn-Sham and Debye-Hückel zeroth approximations and consistent technique for generating an optimized single-quasiparticle representation for atomic systems in the Debye plasmas are presented. It is well known that an adequate description of the radiation and spectral parameters requires using optimized basis's of relativistic wave functions. The approach presented includes an effective ab initio optimization basis construction p[procedure in a natural way. There is used the minimization of the gauge dependent multielectron contribution of the lowest RMBPT corrections to radiation widths of atomic levels, which is determined by imaginary part of an energy shift δE. In the RMBPT higher orders there appear diagrams, whose contribution into ImδE accounts for the polarization effects. This contribution describes collective effects and it is dependent upon electromagnetic potentials gauge (gauge non-invariant contribution δE_{ninv}). This value is considered to be the typical representative of electron correlation effects, whose minimization is a reasonable criteria in the searching for the RMBPT optimal one-electron basis [23-27]. In conclusion, it should be noted the approach presented can be applied to many actual problems modern nuclear physics too as well as astrophysics, laser physics and quantum, photoelectronics (e.g. [5,6,23,38-40]).

References:

1. Glushkov, A.V., Khetselius, O.Y., Maruani, J., Brändas, E. (Eds.) *Advances in Methods and Applications of Quantum Systems in Chemistry, Physics, and Biology. Series: Progress in Theoretical Chem. and Phys.* Cham: Springer. Vol.33, 2021.

2. Oks, E., *Stark Broadening of Hydrogen and Hydrogenlike Spectral Lines in Plasmas: The Physical Insight.* Oxford: Alpha Science Int, 2006.

3. Oks E., Dalimier E., Stamm R., Stehle C., Gonzalez M., Spectral Line Shapes in Plasmas and Gases, ed *Int. J. Spectr.* 2010, *1,* 852581.

4. Griem R., *Spectral Line Broadening by Plasmas.* Academic Press: N-Y., 1974.

5. Bagratashvili V.N., Letokhov V.S., Makarov A.A., Ryabov E.A. *Multiple Photon infrared Laser Photophysics and Photochemistry.* Harwood Acad.Publ.: N.-Y., 1995.

6. Khetselius, O.Yu. *Quantum structure of electroweak interaction in heavy finite Fermi-systems.* Astroprint: Odessa, 2011

7. Delone N., Krainov, V.P., *Multiphoton Processes*; Springer: N.-Y., 1994.

8. Fedorov, M.V. Stabilization of atom in a strong laser field. *Phys. Uspekhi.* 1999, *169(1),* 66—71.

9. Akulin V.M., Karlov N.V., *Intense resonant interactions in quantum electronics*, Nauka: Moscow, 1987

10. Mittleman, M. *Introduction to the Theory of Laser-Atom Interactions;* Plenum Press: N.Y., 1982.

11. *Atoms in Intense Laser Fields*, Gavrila, M., Ed.; Acad. Press: San Diego, 1992.

12. Glushkov A.V., Ivanov, L.N. DC strong-field Stark effect: consistent quantum-mechanical approach. *J. Phys. B: At. Mol. Opt. Phys.* 1993, *26,* L379-386.

13. Kulander, K.C.; Lewenstein, M. Multiphoton and Strong-Field Processes. *In Atomic, Molecular, & Optical Physics Handbook*, Drake, G. W. F., Ed.; AIP Press: New York, 1996, pp 828-838.

14. Khetselius, O.Yu. *Hyperfine structure of atomic spectra.* Astroprint: 2008.

15. Khetselius, O.Yu. Relativistic perturbation theory calculation of the hyperfine structure parameters for some heavy-element isotopes. *Int. Journ. Quant. Chem.* 2009, *109,* 3330-3335.

16. Khetselius, O.Yu. Relativistic calculation of the hyperfine structure parameters for heavy elements and laser detection of the heavy isotopes. *Phys.Scripta.* 2009, *135,*

014023.

17. Khetselius, O.Yu. Optimized relativistic many-body perturbation theory calculation of wavelengths and oscillator strengths for Li-like multicharged ions. Adv. Quant. Chem. 2019, *78*, 223-251.

18. Svinarenko, A. Study of spectra for lanthanides atoms with relativistic many-body perturbation theory: Rydberg resonances. *J. Phys.: Conf. Ser.* 2014, *548,* 012039.

19. Florko, T.A., Tkach, T.B., Ambrosov, S.V., Svinarenko, A.A. Collisional shift of the heavy atoms hyperfine lines in an atmosphere of the inert gas. *J. Phys.: Conf. Ser*. 2012, *397*, 012037.

20. Grant I. *Relativistic Quantum Theory of Atoms and Molecules*. Oxford Univ. Press: Oxford, 2007.

21. Ivanova, E.P.; Grant, I.P. Oscillator strength anomalies in the neon isoelectronic sequence with applications to x-ray laser modeling. *J. Phys.B: At. Mol. Opt. Phys.* 1998, *31,* 2871-2880.

22. Ivanov, L.N.; Letokhov, V.S. Selective ionization of atoms by a light and electric field. *Quant. Electr*.(in Russian) 1975*, 2,* 585-590.

23. Glushkov, A.V. *Relativistic Quantum theory. Quantum mechanics of atomic systems*. Astroprint: Odessa, 2008.

24. Glushkov, A.V. *Atom in an electromagnetic field*. KNT: Kiev, 2005.

25. Glushkov, A.V. *Relativistic and Correlation Effects in Spectra of Atomic Systems*. Astroprint: 2006.

26. Ivanova, E., Glushkov, A. Theoretical investigation of spectra of multicharged ions of F-like and Ne-like isoelectronic sequences. J. Quant. Spectr. and Rad. Tr. 1986, *36*(2), 127-145.

27. Ivanova, E.P., Ivanov, L.N., Glushkov, A., Kramida, A. High order corrections in the relativistic perturbation theory with the model zeroth approximation, Mg-Like and Ne-Like Ions. *Phys. Scripta* 1985, *32,* 513-522.

28. Glushkov, A., Ivanov, L. Radiation decay of atomic states: atomic residue polarization and gauge noninvariant contributions. *Phys.Lett.A*.1992, *170,* 33

29. Ivanov, L.N., Ivanova, E.P., Knight, L. Energy approach to consistent QED theory for calculation of electron-collision strengths: Ne-like ions. *Phys. Rev. A.* 1993, *48,* 4365-4374

30. Glushkov, A.V. Energy approach to resonance states of compound superheavy nucleus and EPPP in heavy nuclei collisions. In Low Energy Antiproton Physics. AIP: New York, *AIP Conf. Proc*. 2005, *796*, 206-210

31. Glushkov, A.V. Advanced relativistic energy approach to radiative decay processes in multielectron atoms and multicharged ions. In: *K.Nishikawa, J. Maruani, E. Brändas, G. Delgado-Barrio, P.Piecuch (Eds) Quantum Systems in Chemistry and Physics*: *Progress in Methods and Applications. Series: Progress in Theoretical Chem. and Phys.* Dordrecht: Springer. 2012, *26*, 231–252.

32. Glushkov, A. Multiphoton spectroscopy of atoms and nuclei in a laser field: Relativistic energy approach and radiate-on atomic lines moments method. *Adv. in Quantum Chem.* 2019, *78*, 253-285.

33. Glushkov, A.V., Operator Perturbation Theory for Atomic Systems in a Strong DC Electric Field. In: *M. Hotokka, J.Maruani, E. Brändas,, G.Delgado-Barrio (Eds) Advances in Quantum Methods and Applications in Chemistry, Physics, and Biology. Series: Progress in Theoretical Chem. and Phys.* Cham: Springer. 2013, *27*, 161–177.

34. Glushkov, A. Spectroscopy of coope-rative muon-gamma-nuclear processes: Energy and spectral parameters *J. Phys.: Conf. Ser.* 2012, *397,* 012011.

35. Malinovskaya S., Glushkov A., Khetselius O.,Lopatkin Yu., Loboda A., Svinarenko A., Nikola L., Perelygina T., Generalized energy approach to calculating electron collision cross-sections for multicharged ions in a plasma: Debye shielding model. Int. J. Quant. Chem. 2011, *111*(2), 288-296.

36. Glushkov A, Buyadzhi V, Svinarenko A, Ternovsky E., Advanced relativistic energy approach in electron-collisional spectroscopy of multicharged ions in plasma. In: *Y.A. Wang, M. Thachuk, R. Krems, J.Maruani, Concepts, Methods and Applications of Quantum Systems in*

Chemistry and Physics. Series: Progress in Theoretical Chem. and Phys. Cham: Springer. 2018, *31*, 55-69.

37. Ternovsky E., Relativistic spectroscopy of multicharged ions in plasmas: Li-like ions. *Photoelectr.* 2019. *28*, 105-112.

38. Khetselius, O.Y., Spectroscopy of cooperative electron-gamma-nuclear processes in heavy atoms: NEET effect *J. Phys.: Conf. Ser.* 2012, *397,* 012012.

39. Khetselius, O.Yu. Relativistic Energy Approach to Cooperative Electron-γ-Nuclear Processes: NEET Effect. In: *K.Nishikawa, J. Maruani, E. Brändas*, G.

Delgado-Barrio, P.Piecuch (Eds) Quantum Systems in Chemistry and Physics: *Progress in Methods and Applications. Series: Progress in Theoretical Chem. and Phys.* Dordrecht: Springer. 2012, *26,* 217-229.

40. Dubrovskaya, Yu., Khetselius, O.Yu., Vitavetskaya, L., Ternovsky, V.B., Serga, I.N., Quantum chemistry and spectroscopy of pionic atomic systems with accounting for relativistic, radiative, and strong interaction effects. *Adv. Quantum Chem.* 2019, *78*, 193-222

PACS 32.30.-r

Glushkov A.V., Kuznetsova A.A.

RELATIVISTIC ENERGY APPROACH TO ATOMIC SYSTEMS IN A STRONG ELECTROMAGNETIC FIELD IN PLASMAS

Summary. The fundamentals of a consistent relativistic approach to determination of radiation and spectral characteristics of the atomic systems (atoms, multicharged ions in plasmas conditions) in a strong external electromagnetic field (EMF), which is based on a relativistic energy formalism adiabatic Gell-Mann and Low formalism) and relativistic many-body perturbation theory (RMBPT) formalism for atomic systems in a plasmas are presented. Within an energy approach in relativistic approximation the Gell-Mann and Low formula expresses the imaginary part of an atomic level energy shift δE through the QED scattering matrix, which includes an interaction as with an EMF as with the photon vacuum field (spontaneous radiative decay). It results in possibility of an uniform simultaneous consideration of spontaneous and (or) induced, radiative processes and their interference. The radiation atomic lines position and shape fully determine a spectroscopy of the plasmas atomic systems in an EMF. The effective modified technique, based on the Ivanova-Ivanov method of differential equations, for computing the infinite sums in expressions for a spectral line shifts and broadening is shortly described. The fundamentals of a new formalism of the relativistic gauge-invariant RMBPT with the optimized Dirac-Kohn-Sham and Debye-Hückel zeroth approximations and consistent technique for generating an optimized single-quasiparticle representation for atomic systems in the Debye plasmas are presented.

Keywords: Relativistic energy approach, many-body perturbation theory, atomic systems, plasmas environment, electromagnetic field,

PACS 32.30.-r

Глушков О.В., Кузнецова Г.О.

РЕЛЯТИВІСТСЬКИЙ ЕНЕРГЕТИЧНИЙ ПІДХІД ДО АТОМНИХ СИСТЕМ У СИЛЬНОМУ ЕЛЕКТРОМАГНІТНОМУ ПОЛІ В ПЛАЗМІ

Резюме. Розроблені основи послідовного підходу до визначення енергетичних, радіаційних та спектроскопічних характеристик атомних систем (атомів, багатозарядних іонів у плазмових умовах) у сильному зовнішньому електромагнітному полі (ЕМП), який базується на релятивістському енергетичному формалізмі (адіабатичний формалізм Гелл-Мана та Лоу) і релятивістській багаточастинковій теорії збурень (RMBPT) для атомних систем у плазмі. У рамках релятивістського енергетичного підходу формула Гелл-Манна і Лоу виражає уявну частину зсуву енергії атомного рівня через КЕД матрицю розсіювання, яка включає взаємодію як з ЕМП, так і з фотонним вакуумом (останнє відповідає за спонтанний радіаційний розпад в системі). В межах розробленої теорії є можливим послідовне одночасне урахування спонтанних і (або) індукованих радіаційних процесів та їх інтерференції. Положення і форма атомних ліній випромінювання повністю визначають спектроскопію атомних систем в плазми у зовнішньому ЕМП. Описано ефективну модифіковану техніку, засновану на методі диференціальних рівнянь Іванової-Іванова, для обчислення нескінченних сум у виразах для зсуву та уширення спектральних ліній, та (або) виразів, що відповідають другому порядку RMBPT. Представлені основи нового формалізму релятивістської калібрувально-інваріантної RMBPT з оптимізованими нульовим наближенням Дірака-Кона-Шема та Дебая-Хюккеля і визначено послідовну схему генерації оптимізованого одноквазічастинкового представлення для атомних систем у плазмовому середовищу.

Ключові слова: релятивістський енергетичний підхід, релятивістська багаточастинкова теорія збурень, атомні системи, плазмове середовище, електромагнітне поле

PACS. 33.70.-w, 33.70.Jg

Yu.M. Lopatkin[1], T.M. Sakun[2]

[1]Sumy State University, 2, Ryms'koho-Korsakova str., Sumy
[2]National Aviation University, 1, Komarov Ave, Kiev
e-mail: lopatkinyurim@i.ua

RELATIVISTIC SPECTROSCOPY OF ATOMIC SYSTEMS: SPECTRAL LINES BROADENING AND SHIFT FOR HEAVY ELEMENTS IN THE BUFFER GAS AND PLASMAS ENVIRONMENT

It has been developed a modified relativistic approach to describing the shift and broadening due to collisions of spectral lines of hyperfine structure for alkali atoms in an atmosphere of buffer (inert) gases. The approach is based on the generalized kinetic theory of spectral lines, exchange, relativistic perturbation theory with the Dirac-Hartree-Slater zeroth approximation and accounting for the complicated correlation effects by means of using the many-body polarization density-dependent functionals. The basic expressions for the collision shift and broadening hyperfine structure spectral lines are taken from the kinetic theory of spectral lines. The exchange perturbation theory (the modified version EL-HAV) has been used to calculate the corresponding potentials. The results of calculating the interatomic potentials, local shifts, temperature dependent spectral line shifts for the systems of the Rb, Cs-He are listed and compared with available theoretical and experimental data. The important feature of our scheme is correct taking into account the correlation (polarization) effects with using special effective functionals from. The difference between our theoretical data and other calculation results can be explained by using different perturbation theory versions and different approximations for calculating the wave functions basis's.

1. Introduction

The behavior of atomic and molecular systems in different gas and plasmas environments is an actual problem of modern physics, namely, molecular, physics, photoelectronic, optics and spectroscopy etc. On the one hand, sources of high-energy (e.g. ultraviolet) radiation have become widely used, including the technique of picosecond and femtosecond laser pulses. In particular, dyes have become widely used in various fields of optics , spectroscopy, atomic and molecular physics, quantum and photoelectronics (including for recording information (compact discs), dyeing fabrics, as working substances of lasers based on dyes, etc).

In the last two decades, a number of fundamentally new discoveries have been made in atomic physics, in particular, obtaining a Bose condensate in pairs of Rydberg atoms of alkaline elements (by the way, the question of the shift and broadening of the spectral lines of atoms in such a gas is an extremely urgent mo-

dern task), the creation of fountains of cold atoms, the possibility of building Tl quantum measure, and so on, which is largely due to the unprecedented progress in the development of new experimental methods of research (magneto-optical traps, accelerators, sources of intense laser radiation, etc.). This stimulates the possibilities of studying the spectroscopic characteristics of atoms, including the parameters of spectral lines for atoms in the external gas of plasmas environments, increasingly with higher accuracy. Although modern atomic spectroscopy has a wide range of different quantum methods (in particular, Hartree-Fock self-consistent field (HF) and Dirac-Fock (DF) methods, methods of quantum defect, model potential, density functional (DF), various variants of perturbation theory (PT), including the Rayleigh-Schrödinger, Möller-Plesset PT, various versions of the exchange PT, and even new methods such as mega-DF, "Bertha" and so on) for calculating the electronic structure of atoms, interatomic potentials, various spectroscopic characteristics, etc., however, most

of them still have a number of fundamental shortcomings.

High precision data for collisional shifts and broadening the hyperfine structure lines of heavy elements (alkali, alkali-earth, lanthanides, actinides and others) in an atmosphere of the inert gases are of a great interest for modern quantum chemistry, atomic and molecular spectroscopy, astrophysics and metrology as well as for studying a role of weak interactions in atomic optics and heavy-elements chemistry [1-27]. As a rule, the cited spectral lines shift and broadening due to a collision of the emitting atoms with the buffer gas or plasmas atoms and ions are very sensitive to a kind of the interatomic interaction potential. Besides, calculation of the hyperfine structure line shift and broadening allows to check a quality of the wave functions and study a contribution of the relativistic and correlation effects to the energetic and spectral characteristics of the two-center (multi-center) atomic systems.

Modern representations about the characteristics of spectral lines of atomic systems, the most widespread variants of the theory of spectral lines of atoms and, in particular, the theory of shift and broadening of spectral lines of the hyperfine transitions for atoms (ions) in an atmosphere of buffer (inert) gases are presented in Refs. [1-5].

An analysis of modern quantum methods for calculating the characteristics of the spectroscopic characteristics of atoms and ions is presented, taking into account correlation, relativistic and radiation corrections to one degree or another is given in Refs. [3-6].
In this paper it has been developed a modified relativistic approach to describing the shift and broadening due to collisions of spectral lines of hyperfine structure for alkali atoms in an atmosphere of buffer (inert) gases. The approach is based on the generalized kinetic theory of spectral lines, exchange, relativistic PT with the Dirac-Hartree-Slater zeroth approximation and accouting for the complicated correlation effects by means of using the many-body polarization density-dependent functionals. The basic expressions for the collision shift and broadening hyperfine structure spectral lines are taken from the kinetic theory of spectral lines [1,9,10]. The

exchange perturbation theory (the modified version EL-HAV) has been used to calculate the corresponding potentials (see details in [2-8]).

The important feature of our scheme is correct taking into account the correlation (polarization) effects with using special effective functionals from [1,4-7,16-18]. The difference between our theoretical data and other calculation results can be explained by using different PT schemes and different approximations for calculating the wave functions. Some of the obtained results of calculating the interatomic potentials, local shifts, temperature dependent observed spectral hyperfine line shifts for the systems of the Rb, Cs-He are listed and compared with available theoretical and experimental data.

2. Fundamentals of the method

As the key features of the presented approach gave been described in Ref. [10-12], below we will concentrate on the original moments of our approach.
As usually, in order to compute a collision shift of the hyperfine structure spectral lines one should use the following expression, which is known in the kinetic theory of spectral lines shape (see Refs. [7-9]):

$$f_p = \frac{D}{p} = \frac{4\pi w_0}{kT} \int_0^\infty dw(R) \exp(-U(R)/kT) R^2 dR$$

(1)

Here T is a temperature, $U(R)$ is an effective potential of the a-b interatomic interaction, w_0 is a frequency of the hyperfine structure transition in an isolated active atom; $d\omega(R) = Dw(R)/w_0$ is a relative local shift of the hyperfine structure line.

The local shift is caused due to the disposition of the active atoms (say, the atoms of lead Pb and helium He) at the distance R. In order to calculate an effective potential of the interatomic interaction further we use the exchange PT formalism (the modified version EL-HAV) [1,8,9].

The relative local shift of the hyperfine structure line is defined as follows:

$$\delta\omega(R)=\frac{S_0}{1-S_0}+\Omega_1+\Omega_2-\frac{C_6}{R^6}\left(\frac{2}{\overline{E}_a}+\frac{1}{\overline{E}_a+\overline{E}_B}\right),(2a)$$

$$\overline{E}_{\alpha,b}=\left(I_{a,b}+E_{1a,b}\right)/2 \qquad (2b)$$

Here S_0 is the overlapping integral; C_6 is the van der Waals coefficient; I is the potential of ionization; $E_{1a,b}$ is the energy of excitation to the first (low-lying) level of the corresponding atom. The values Ω_1, Ω_2 in Eq. (2) are the first order non-exchange and exchange non-perturbation sums correspondingly [8-10]. These quantities can be determined by the following way:

$$\Omega_1=\frac{2}{N(1-S_0)\rho_0}\sum_k \cdot\frac{\langle \Phi_0'(1)|H_{HF}'|\Phi_k'(1)\rangle V_{k0}}{E_0-E_k}$$

$$\Omega_2=\frac{2}{N(1-S_0)\rho_0}\sum_k \cdot\frac{\langle \Phi_0'(1)|H_{HF}'|\Phi_k'(1)\rangle U_{k0}}{E_0-E_k}$$

$$\rho_0=<\Phi_0^1(1)|H_{HF}'|\Phi_0'(1)>/<\Phi_0^1(1)|\Phi_0'(1)>$$
(3)

where H_{HF}' is the operator of hyperfine interaction; N is the total number of electrons, which are taken into account in the calculation; E_k, $\Phi_k'(1)=F_{k_a}'(1)\phi_{k_b}(2\ldots N)$ are an energy and a non-symmetrized wave function of state $k=\{k_a,,k_b\}$ for the isolated atoms a and b.

The non-exchange matrix element of the Coulomb interatomic interaction is as:

$$V_{ko}=<\Phi_k'(1)\mid V(1)\mid \Phi_0'(1)>. \qquad (4)$$

Correspondingly the exchange matrix element is as follows:

$$U_{k0}=\sum_{i=2}^N \langle \Phi_k'(1)|V(i)|\Phi_0'(i)\rangle \qquad (5)$$

The operator $V(i)$ (for example, in a case of the system "a-b") is as follows:

$$V(i)=U_{SCF}(r_{a3})+U_{SCF}(r_{a4})-2U_{SCF}(R)+\frac{1}{r_{bi}}\cdot(6)$$

where $U_{SCF}(r)$ is the self-consistent field, created by the lead atomic core.

The van der Waals coefficient C_6 for the interatomic a-b interaction can be computed on the basis of the standard definition (see details. For example, in refs. [2,9-12,23]:

$$C_6(L,M)=C_{6,0}(L)-\frac{3M^2-L(L+1)}{(2L-1)(2L+3)}\cdot C_{6,2}(l) , \qquad (7)$$

Here $C_{6,0}(L)$ is the isotropic component of the interaction and $C_{6,2}(L)$ is the component corresponding to the $P_2(cos\ \theta)$ term in the expansion of the interaction in Legendre polynomials, where the angle specifies the orientation in the space-fixed frame. The dispersion coefficients $C_{6,0}(L)$ and $C_{6,2}(L)$ may be expressed in terms of the scalar and tensor polarizabilities $\alpha_0(L;iw)$ and $\alpha_2(L;iw)$ evaluated at imaginary frequencies [9]. Other details can be found in Refs. [8-21].

The key original moment of any computational scheme is connected with the method of calculation the electron wave functions.

As a rule, (see, for example, Ref. [8]), the non-relativistic Hartree-Fock or relativistic Dirac-Fock methods are used for calculating the corresponding wave functions [8-14]. Another variant is using the relativistic wave functions as the solutions of the Dirac equations with the corresponding density functional (the Dirac-Kohn-Sham theory) and effective potentials [7,14,15]. In our calculational scheme the relativistic optimized Dirac-Hartree-Slater scheme with basis formulas [10-12] is used.

3. Results and conclusions

In Tables 1,2 we present our theoretical results for the line shift f_p (1/Torr) in a case of the Rb-He and Cs-He pairs. The observed value (experiment) of the line shift (T=323K) and other theoretical results [6,10] for f_p are listed too. The theoretical results in Ref. [8] are obtained on the basis of calculation within the exchange PT with using the He wave functions in the approximation by Clementi et al (Theory[a] [8]) and wave functions in the Hartree-Fock approximation Theory[b] [8]). The

Dirac-Kohn-Sham scheme gas been used in Ref.[10].

Table 1. The observed $f \times$ (10^{-9} 1/Torr) shift for the diatomic system Rb-He: data of [8a] with using the He wave functions in the approximation by Clementi et al; (see text).

a-b	Rb-He	Rb-He	Rb-He	Rb-He
T, K	Experi-ment	Theory [10]	Theory[a] [6]	This work
323	105	101	75	102
423	-	89	64	91
523	-	80	56	82
623	-	73	50	75

The important feature of our scheme is correct taking into account the correlation (polarization) effects with using special effective functionals from [19,22]. The difference between our theoretical data and other calculation results can be explained by using different PT schemes and different approximations for calculating the wave functions. It is obvious that the using correct version of the exchange PT was well as the optimized basis's of wave functions and correct accounting for the exchange-correlation effects is principally necessary for an adequate description of the energetic and spectral properties of

Table 2. The observed $f \times$ (10^{-9} 1/Torr) shift for the diatomic system Cs-He: data of [8a] with using the He wave functions in the approximation by Clementi et al; [8b] -wave functions in the Hartree-Fock approximation (see text).

a-b	Cs-He	Cs-He	Cs-He	Cs-He	Cs-He
T, K	Experi-ment	Theory [a] [6]	Theory [b] [6]	Theory[a] [10]	This work
323	135	126	109	137	137
423	-	111	96	123	123
523	-	100	85	112	112
623	-	94	78	105	105

the alkali elements in an atmosphere of the heavy inert gases. It is represented a great interest a generalization of the presented approach on energy and radiation properties

and studying spectral lines characteristics for atomic and ionic systems in the corresponding plasmas environments.

References

1. Wilson S., *Handbook on Molecular Physics and Quantum Chemistry*. Wiley: N-Y., 2003.
2. Kondratenko P.A., Lopatkin Y.M., Sakun T.N., Sensitization processes in materials based on compounds containing a Xe-O bond. *Functional Materials*. **2008**. *15*(2), 192-197.
3. Kondratenko P.A., Lopatkin Y.M., Sakun T.N., Excited states in dye-based functional materials. *Functional Materials*. **2008**. *15*(3), 92-397.
4. Torrens I.M., *Interatomic potentials*. Acad. Press: N-Y., **1972**.
5. Freeman A.J., Frankel R.H., *Hyperfine interactions*.- N-Y.: Plenum, **1987.**
6. Khetselius, O.Yu. *Hyperfine structure of atomic spectra*. Astroprint: **2008**.
7. Glushkov, A.V. *Relativistic Quantum theory. Quantum mechanics of atomic systems*. Astroprint: Odessa, **2008**.
8. Batygin V. V., Sokolov I. M., Collisional shift and adiabatic broadening of line of the hyperfine transition in the ground state of thallium in an atmosphere of the buffer helium, krypton and xenon. *Opt. Spectr.*-**1983,** *55*, 30-38.
9. Khetselius O.Yu., Optimized perturbation theory to calculating the hyperfine line shift and broadening for heavy atoms in the buffer gas *In: Frontiers in Quantum Methods and Applications in Chemistry and Physics, Series: Progress in Theor. Chem. and Phys.,* Eds. M.Nascimento, J.Maruani, E.Brändas, G.Delgado-Barrio; Springer. **2015,** *29, 54-76.*
10. Lopatkin Yu.M., Mikhailenko V.I., Svinarenko A.A., Spectroscopy of the spectral lines broadening and shift for heavy elements in the buffer gas. *Photoelectronics.* **2013,** *22, 139-145.*
11. Malinovskaya S., Glushkov A., Khetselius O., Svinarenko A., Mischenko E., Florko T., Optimized perturbation theory scheme for calculating the interatomic potentials and hyperfine lines shift for heavy atoms

in the buffer inert gas. Int. J. Quant.Chem. **2009**.-*109*(14), 325-3329.

12. Svinarenko A.A., Mischenko E.V., Loboda A.V., Dubrovskaya Yu.V., Quantum measure of frequency and sensing the collisional shift of the ytterbium hyperfine lines in medium of helium gas. Sensor Electronics and Microsystem Techn. **2009**, *N1*, 25-29.

13. Florko T.A., Ambrosov S.V., Svinarenko A.A., Tkach T.B., Collisional shift of the heavy atoms hyperfine lines in an atmosphere of the inert gas. J. Phys.; Conf. Ser. **2012**, *397*, 012037

14. Glushkov, A.V. *Relativistic and Correlation Effects in Spectra of Atomic Systems*. Astroprint: **2006**.

15. Khetselius, O.Yu., *Quantum structure of electroweak interaction in heavy finite Fermi-systems.* Astroprint: Odessa, **2011**.

16. Ivanova, E., Glushkov, A. Theoretical investigation of spectra of multicharged ions of F-like and Ne-like isoelectronic sequences. J. Quant. Spectr. and Rad. Tr. **1986**, *36*(2), 127-145.

17. Ivanova, E.P., Ivanov, L.N., Glushkov, A., Kramida, A. High order corrections in the relativistic perturbation theory with the model zeroth approximation, Mg-Like and Ne-Like Ions. *Phys. Scripta* **1985**, *32,* 513-522.

18. Glushkov, A., Ivanov, L. Radiation decay of atomic states: atomic residue polarization and gauge noninvariant contributions. *Phys.Lett.A.* **1992,** *170,* 33

19. Khetselius, O.Yu. Relativistic perturbation theory calculation of the hyperfine structure parameters for some heavy-element isotopes. *Int. Journ. Quant. Chem.* **2009,** *109,* 3330-3335.

20. Khetselius, O.Yu. Relativistic calculation of the hyperfine structure parameters for heavy elements and laser detection of the heavy isotopes. *Phys.Scripta.* **2009,** *135,* 014023.

21. Svinarenko A., Nikola L., Prepelitsa G., Tkach T., Mischenko E., The Auger (autoionization) decay of excited states in spectra of multicharged ions: Relativistic theory. *Spectral Lines Shape*. **2010**. 16, 94-98

22. Jamieson M., Dalgarno A., Aymar M., Tharamel J., Study of exchange interactions in alkali molecular ion dimers with application to charge transfer in cold Cs. *J. Phys. B: At. Mol. Opt. Phys*. **2009,** 42, 095203.

23. Buchachenko A., Szczesniak M., Chalasinski G., Calculation of the Van der Waals coefficients for interaction of rare-earth metal atoms with helium atoms *J.Chem. Phys*. **2006**, 124, 114301.

24. Ehrlacher E., Huennekens J., Noble-gas broadening rates for barium transitions involving the metastable 6s5d ^{3}D$_j$ levels, *Phys. Rev. A*. **1992**, *46,* 2642-2648.

25. Kötteritzsch M., Gries W., Hese A., Foreign gas broadening and shift in the lead resonance line at lambda =283.3 nm. *J. Phys. B:At. Mol. Opt. Phys*. **1992**, *25,* 913-918.

26. Oks E., Dalimier E., Stamm R., Stehle C., Gonzalez M., Spectral Line Shapes in Plasmas and Gases, ed *Int. J. Spectr*. **2010**, *1,* 852581.

27. Griem R., *Spectral Line Broadening by Plasmas*. Academic Press: N-Y., **1974**.

PACS. 33.70.-w, 33.70.Jg

Lopatkin Yu.M., Sakun T.M.

RELATIVISTIC SPECTROSCOPY OF ATOMIC SYSTEMS: SPECTRAL LINES BROADENING AND SHIFT FOR HEAVY ELEMENTS IN THE BUFFER GAS AND PLASMAS ENVIRONMENT

Summary. It has been developed a modified relativistic approach to describing the shift and broadening due to collisions of spectral lines of hyperfine structure for alkali atoms in an atmosphere of buffer (inert) gases. The approach is based on the generalized kinetic theory of spectral lines, exchange, relativistic perturbation theory with the Dirac-Hartree-Slater zeroth

approximation and accounting for the complicated correlation effects by means of using the many-body polarization density-dependent functionals. The basic expressions for the collision shift and broadening hyperfine structure spectral lines are taken from the kinetic theory of spectral lines. The exchange perturbation theory (the modified version EL-HAV) has been used to calculate the corresponding potentials. The results of calculating the interatomic potentials, local shifts, temperature dependent spectral line shifts for the systems of the Rb, Cs-He are listed and compared with available theoretical and experimental data. The important feature of our scheme is correct taking into account the correlation (polarization) effects with using special effective functionals from. The difference between our theoretical data and other calculation results can be explained by using different perturbation theory versions and different approximations for calculating the wave functions basis's.

Key words: relativistic spectroscopy, spectral lines shift and broadening, atomic systems, relativistic theory, perturbation theory, gas and plasmas environments,

Лопаткін Ю.М., Сакун Т.М.

РЕЛЯТИВІСТСЬКА СПЕКТРОСКОПІЯ АТОМНИХ СИСТЕМ: РОЗШИРЕННЯ ТА ЗСУВ СПЕКТРАЛЬНИХ ЛІНІЙ ДЛЯ ВАЖКИХ ЕЛЕМЕНТІВ У БУФЕРНОМУ ГАЗОВОМУ ТА ПЛАЗМОВОМУ СЕРЕДОВИЩАХ

Резюме. Розроблено модифікований релятивістський підхід до опису зсуву та розширення за рахунок зіткнень спектральних ліній надтонкої структури для лужних атомів в атмосфері буферних (інертних) газів. Підхід базується на узагальненій кінетичній теорії спектральних ліній, обміну, релятивістській теорії збурень з нульовим наближенням Дірака-Хартрі-Слетера та врахуванням складних кореляційних ефектів за допомогою використання поляризаційних багаточастинкових залежних від густини функціоналів. Основні вирази для колізійного зсуву та розширення спектральних ліній надтонкої структури взяті з кінетичної теорії спектральних ліній. Для розрахунку відповідних потенціалів використано теорію обмінних збурень (модифікована версія EL-HAV). Наведено результати розрахунків локальних зсувів, температурно-залежних повних зсувів спектральних ліній для систем Rb, Cs-He та проведене порівняння з наявними теоретичними та експериментальними даними. Важливою особливістю нашої схеми є коректне урахування кореляційних (поляризаційних) ефектів із застосуванням спеціальних ефективних функціоналів густини. Різницю між нашими теоретичними даними та іншими результатами розрахунків можна пояснити використанням різних версій теорії збурень і різних наближень для розрахунку базису хвильових функцій.

Ключові слова: релятивістська спектроскопія, зміщення та розширення спектральних ліній, атомні системи, релятивістська теорія, теорія збурень, газове та плазмове середовища.

A.S. Sofronkov[1], A.V. Tjurin[2]

[1]Odessa State Environmental University, 15, Lvovskaya str., Odessa
[2]I.I. Mechnikov Odessa National University, 2, Dvoryanskaya str., Odessa
E-mail: sofronkovav@gmail.com

RELATIVISTIC AND CORRELATION EFFECTS IN AUGER SPECTROSCOPY OF ATOMS AND SOLIDS

It is presented an advanced, consistent theoretical scheme for determination of the energy and spectral characteristics of the Auger process (decay, transition) in atomic systems and solids with correct accounting for the relativistic and nuclear effects. As the basic approach to calculating the Auger spectra of solids there is used a consistent theoretical method, based on the S-matrix formalism by Gell-Mann and Low and relativistic many-body perturbation theory formalism. Universal relativistic Dirac-Hartree-Slater method is taken as a theoretical method for calculating the electronic wave functions and energies of the states and transitions. The advanced data on the Auger electron energy for some solids (Ge,Ag) with accounting for the relativistic and nuclear finite size effects are listed.

1. In the modern atomic, molecular physics, physics of solids and surfaces there are used different methods of spectroscopy of electromagnetic radiation and spectroscopy of charged particles in order to provide an analysis, diagnose and sensing the composition (analysis) of the energy and radiative properties of atomic, molecular systems, surface and near-surface layers of solids. Usually a classification of the main methods of spectroscopy used to analyze the above listed physical systems is based on the type of particles used to excite the spectrum and particles - carriers of information about the composition of the substance.

One of the most effective and spread methods to study the chemical composition of solid surfaces and near-surface layers [1-8] is the Auger electron spectroscopy. Analysis and sensing the Auger spectra in atomic, molecular systems and solids allow to get the important information a for the whole number of scientific and technological physical and chemical applications, including many topics of modern optics and spectroscopy, laser, astrophysics, ultra cold plasma diagnostics, forecasting properties of Rydberg substance, Bose-condensate of Rydberg atoms etc. One should underline the theoretical and practical interest for a such of applications and related physical disciplines, which include atomic, molecular, quantum optics and spectroscopy, quantum electro-

nics, l construction of kinetic models of new short-wave laser circuits, physics of laboratory, astrophysical plasma, quantum , sensor and photoelectronics etc.

Naturally, at the present time there are carried out relatively a great number of different theoretical models and schemes in order to calculate the corresponding energy and s[spectroscopic parameters of the Auger transitions, and, generally speaking, a total set of characteristics of the Auger spectra. Surely there are developed a group of effective experimental methodises in order to measure the Auger transitions characteristics (e.g. [1-12]).

It should be noted that there is a whole group of methods based on the use of data on photoionization cross sections and measurements of the dependence of the intensity of photoelectron lines on the kinetic energy of photoelectrons by varying the energy of the exciting X-ray radiation (for example, using synchrotron radiation) or by choosing an appropriate set of photoelectron lines (see, e.g., [1-5]).

The most popular in the theoretical Auger spectroscopy is so called two-step model, which is used most widely when calculating the Auger spectra (transitions, decay) characteristics [1-16]. The physical aspects of the cited model are quite reasonable. It is known that since the vacancy lifetime in an inner atomic shell is rather long (about 10^{-17} to 10^{-14}s), the

atomic system ionization and the Auger emission processes are considered to be two independent processes. Though the more correct dynamic theory of the Auger effect [3,7-9] is developed and the above mentioned processes are not believed to be independent from one another in this theory. The fact is taken into account that the relaxation processes due to Coulomb interaction between electrons and resulting in the electron distribution in the vacancy field have no time to be over prior to the transition. One should note that the consistent and quantitively correct Auger decay theory should take a definite number of the physically important complicated exchange-correlation effects into consideration. Above them one should separate such effects as exchange-polarization effects, an energy dependence of the vacancy mass operator, a continuum pressure, spreading of the initial state over a set of configurations etc. In a great number of papers it has been shown that in order to ger a current information about energy and spectral characteristics of the Auger process (decay, transition) it is necessary to provide a correct accounting for the relativistic, radiation and nuclear finite size effects contributions especially under consideration of the middle and heavy atomic and molecular systems, solids etc (eg.[10-14]).

The aim of the work is to provide a consistent theoretical scheme for determination of the energy and spectral characteristics of the Auger process (decay, transition) in atomic systems and solids with correct accounting for the relativistic, and   (relaxation) effects. As the basic approach to calculating the Auger spectra of solids we use an consistent theoretical method, based on the S-matrix formalism by Gell-Mann and Low and relativistic many-body perturbation theory formalism, presented in Refs. [11-14]. However, in contrast to the original version of the theoretical approach used [9-14], a simpler and more universal relativistic Dirac-Hartree-Slater method was taken as a theoretical method for calculating the electronic wave functions and energies of the hundred states. The numerical data on the Auger electron energy for some solids (Ge,Ag) with accounting for the relativistic and nuclear finite size effects are listed. Other details can be found in Refs. [9-16]

2. As the key moments of our method fpor accounting the relativistic and nuclear effects in Auger spectroscopy are shortly have been mentioned in Refs. [9,10], here we are limited only my the principally important model points. It should be recalled that when colliding with an atomic system, the primary electron e, which has energy sufficient to ionize one of the main levels of the atom, knocks out the electron ej from this level, transferring the atom A to an ionized, unstable state A^+ with a hole at the level which in the general case may correspond to some set of final states E_A.

Following to Ref. [9,11], one should determine the   uger transition probability and the Auger line intensity through the square of an electron interaction matrix element (the classical golden Fermi rule) having the form [11,13]:

$$V_{1234}^{\omega} = [(j_1)(j_2)(j_3)(j_4)]^{1/2} \sum_{\lambda\mu}(-1)^{\mu}\begin{pmatrix} j_1 j_3 & \lambda \\ m_1 - m_3 & \mu \end{pmatrix} \times \mathrm{Re}\, Q_{\lambda}(1234)$$

$$Q_{\lambda} = Q_{\lambda}^{\mathrm{Qul}} + Q_{\lambda}^{\mathrm{Br}}. \qquad (1)$$

The terms $Q_{\lambda}^{\mathrm{Qul}}$ and $Q_{\lambda}^{\mathrm{Br}}$ correspond to subdivision of the relativistic interelectron potential into Coulomb part $cos|\omega|r_{12}/r_{12}$ and Breit component $cos|\omega|r_{12}\alpha_1\alpha_2/r_{12}$. The real part of the electron interaction matrix element is determined using expansion in terms of the known Bessel functions:

$$\frac{cos|\omega|r_{12}}{r_{12}} = \frac{\pi}{2\sqrt{r_1 r_2}}\sum_{\lambda=0}(\lambda)J_{\lambda+\frac{1}{2}}(|\omega|r_{<})J_{-\lambda-\frac{1}{2}}(|\omega|r_{>})P_{\lambda}(\cos r_1 r_2)$$

(2)

where J is the 1$^{\mathrm{st}}$ order Bessel function, $(\lambda)=2\lambda+1$. The Coulomb part $Q_{\lambda}^{\mathrm{Qul}}$ is expressed in terms of radial integrals R_{λ} , angular coefficients S_{λ} [11-13]:

$$\mathrm{Re}\, Q_{\lambda}^{\mathrm{Qul}} = \frac{1}{Z}\mathrm{Re}\{R_l(1243)S_{\lambda}(1243) + R_{\lambda}(\tilde{1}243)S_{\lambda}(\tilde{1}24\tilde{3}) +$$

(3)

$$+ R_{\lambda}(1\tilde{2}4\tilde{3})S_{\lambda}(1\tilde{2}4\tilde{3}) + R_{\lambda}(\tilde{1}\tilde{2}4\tilde{3})S_{\lambda}(\tilde{1}\tilde{2}4\tilde{3})\}$$

As a result, the Auger decay probability is expressed in terms of $\mathrm{Re}\,Q_{\lambda}(1243)$ matrix elements:

$$\mathrm{Re}\,R_\lambda(1243) = \iint dr_1 r_1^2 r_2^2 f_1(r_1) f_3(r_1) f_2(r_2) f_4(r_2) Z_\lambda^{(1)}(r_<) Z_\lambda^{(1)}(r_>)$$

(4)

where f is the large component of radial part of single electron state Dirac function; function Z and angular coefficient are defined in refs. [7,8].

The other items in (3) include small components of the Dirac functions; the sign «~» means that in (3) the large radial component f_i is to be changed by the small g_i one and the moment l_i is to be changed by $\tilde{l}_i = l_i - 1$ for Dirac number æ$_i > 0$ and $l_i + 1$ for æ$_i < 0$. The Breit interaction is known to change considerably the Auger decay dynamics in some cases. The Breit part of Q is defined in [7]-[9]. The corresponding basis's of the relativistic wave functions are determine within the standard X_a method (e.g. [11,15,16]).

The calculation of radial integrals $\mathbf{Re}R_\lambda(1243)$ is reduced to the solution of a system of differential equations [11-13]:

$$y_1' = f_1 f_3 Z_\lambda^{(1)}(\alpha|\omega|r) r^{2+\lambda}$$

$$y_2' = f_2 f_4 Z_\lambda^{(1)}(\alpha|\omega|r) r^{2+\lambda}$$

$$y_3' = [y_1 f_2 f_4 + y_2 f_1 f_3] Z_\lambda^{(2)}(\alpha|\omega|r) r^{1-\lambda} \quad (5)$$

In addition,

$$y_3(\infty) = \mathbf{Re}R_\lambda(1243),$$

$$y_1(\infty) = X_\lambda(13). \quad (6)$$

In order to get the consistent relativistic expressions for the Auger widths and Auger electron transitions energies we use an consistent theoretical method, based on the S-matrix formalism by Gell-Mann and Low and relativistic many-body perturbation theory formalism, presented in Refs. [11-14].

The Auger width is obtained from the adiabatic Gell-Mann and Low formula for the energy shift [7]. In particular, the expression for the key contribution to the Auger level width with a vacancy $n_\alpha l_\alpha j_\alpha m_\alpha$ is given as follows [10-12]:

$$\sum_\lambda \frac{2}{(\lambda)(j_\alpha)} \sum_{\beta\gamma \le f} \sum_{k > f} Q_\lambda(\alpha k\,\gamma\beta) Q_\lambda(\beta\gamma\,k\alpha) \quad (7)$$

And further the corresponding "exchange diagrams" contribution is as:

$$\frac{2}{(j_\alpha)} \sum_{\lambda_1\lambda_2} \sum_{\beta\gamma \le f} \sum_{k > f} Q_{\lambda_1}(\alpha k\gamma\beta) Q_{\lambda_2}(\beta\gamma k\alpha) \begin{Bmatrix} j_\alpha & j_\gamma & \lambda_2 \\ j_k & j_\beta & \lambda_1 \end{Bmatrix}$$

(8)

The partial items of the $\sum_{\beta\gamma}\sum_k \square$ sum answer to contributions of $\alpha^{-1} \to (\beta\gamma)^{-1}K$ channels resulting in formation of two new vacancies $\beta\gamma$ and one free electron k: $\omega_k = \omega_\alpha + \omega_\beta - \omega_\alpha$. The final expressions for the width in the representation are listed in Refs. [9-13].

Regarding the accounting for the exchange-correlation corrections. The standard Slater potential and the modified correlation potential of the Gunnarson-Lundqvist type has been added into the Dirac-Hratree-Slater equations (see details, e.g., [10-15]).

The key element of novelty is the generation of optimized bases of relativistic Dirac-Hartree-Slater orbitals. To achieve this goal, one should use the formally accurate iterative approach, which is based on the procedure of minimizing the contribution to the imaginary part of the electronic energy shift due to the relativistic perturbation theory second order polarization diagrams associated with the exchange of longitudinal photons. The contribution of these diagrams depends on the calibration of the photon propagator. It is also important to correctly take into account exchange-correlation effects of "2" and higher PT orders, in particular, corrections for the polarization. The standard many-body polarization functional is usually used and added to the inter-electron interaction operator (see the details, for example, in refs. [10-16]). Very important point of the whole scheme is application of correct procedure for taking into account the states of the continuum within the Dirac-Slater-Sturm method (see details in Refs. [10,12]). The contribution of the lower order radiative corrections to the energy and spectral characteristics can be also taken into account with using the methodology [9-15], however,

one should wait for a quite little contribution into studied characteristics.

The formulas for the Auger decay probability include the radial integrals $R_\alpha(\alpha k\gamma\beta)$, where one of the functions describes electron in the continuum state. Following to Ref. [10], the energy of an electron formed due to a transition *jkl* is defined by the difference between energies of atom with a hole at *j* level and double-ionized atom at *kl* levels in final state:

$$E_A\left(\text{jkl}, L_J\right) = E_A^{+(j) - E_A^{2+(kl,L_J)}} \qquad (10)$$

To single out the above-mentioned correlation effects, the equation (12) can be presented as:

$$E_A(jkl, {}^{2S+1}L_J) = E(j) - E(k) - E(l) - \Delta(k,l; {}^{2S+1}L_J) \qquad (11)$$

where the item Δ takes into account the dynamic correlation effects (relaxation due to hole screening with electrons etc.)

Further, in order to take these effects into consideration, one should use the standard procedure, which is elaborated in an atomic spectroscopy (e.g.[2,3,11,15]).

For solid phase, the more precise form of equation (11) is given by the following equation [9]:

$$E^s{}_A(jkl, {}^{2S+1}L_J) = E_A(jkl, {}^{2S+1}L_J) + \Delta E^s + R_{rel} + e\Phi \qquad (12)$$

where ΔE^s is a correction for the binding energy change in the solid; R_{rel}, the same for out-of-atom relaxation; $e\Phi$ takes into account the standard work of output. The other topics can be, for example, found in refs. [9-16].

3. In table 1 we present our theoretical data (column "This") the data on the Auger electron energy for some solids (Ge, Ag) as well as the experimental data (column E), theoretical semi-empirical method data within the Larkins' equivalent core approximation [2,3] (column A), non-gauge-invariant relativistic Dirac-Fock method (colimn B), the gauge-invariant relativistic Dirac-Fock method (column C) [1,3,10].

Table 1. Experimental and theoretical data for Auger electron energy: E- experiment; A, semi-empirical method - [2]; B- [8]; C – [15]; D – [3], E- this work;

Solid	Auger line	E	Th: A	Th: B
Ge	$L_3M_{4,5}M_{4,5}\ {}^1G_4$	1146.2	1147.2	1146.6
Ag	$M_5N_{4,5}N_{4,5}\ {}^1G_4$	353.4	358.8	354.1
Solid	Auger line	E	Th: C	This
Ge	$L_3M_{4,5}M_{4,5}\ {}^1G_4$	1146.2	1146.2	1146.3
Ag	$M_5N_{4,5}N_{4,5}\ {}^1G_4$	353.4	353.4	353.6

The analysis of the presented data shows that, firstly, the computational accuracy of the classical Larkins' method is about a few eV as an average. The data, obtained within the relativistic perturbator theory methods ([10] and ours) are more correct. The corresponding improvement of the calculational accuracy is reached due to a considerable extent to more correct and consistent accounting for complex interelectron (vacancy) exchange-correlation effects as well as the relativistic and other solid state corrections. The data in the columns "C" and "This work" are more correct in comparison with data in the column B because of the more correct gauge-invariant procedure of generating the relativistic wave functions basis's. Besides, application of correct procedure for taking into account the states of the continuum within the Dirac-Slater-Sturm method (see details in Refs. [10,12] is also very important for adequate model. Naturally, accounting for the effects of the polarization interaction of quasiparticles (electrons and vacancies) and the screening on the basis of the using effective relativistic exchange-correlation functionals is important too. There is of a great interest an application of the method to studying the Auger processes in more heavy systems.

References

1. Aberg T., Hewat G. *Theory of Auger effect*. Springer-Verlag: Berlin, **1979.**
2. Amusia M. Ya. *Atomic photoeffect*. Acad.Press: N.-Y., **1988.**
3. Kulekshov V.F., Kukharenko Yu.A., Fridrikhov S.A. et al. *Spectroscopy and Electron Diffraction in Solid Surfaces Studies*. Nauka: M., 1985.

4. Sinanis, C., Aspromallis, G., Nicolaides, C. Electron correlation in Auger spectra of the Ne$^+$ K 2s2p^5(^{3,1}P^0)3p^{2}S satellites. J. Phys. B. At. Phys. **1995**, *28*, L423-428.

5. Armen, G.B., Larkins, F.P. Valence Auger and X-ray participator and spectator processes for neon and argon atoms. *J. Phys. B. At. Mol. Opt. Phys*. **1991**, *24*, 741-760.

6. Ignatenko, A.V., Svinarenko, A.A., Prepelitsa, G.P., Perelygina, T.B. Optical bi-stability effect for multi-photon absorption in atomic ensembles in a strong laser field. *Photoelectronics*. **2009**, *18*, 103-105.

7. Chernyakova, Y., Ignatenko, A., Vitavetskaya, L.A. Sensing the tokamak plasma parameters by means high resolution x-ray theoretical spectroscopy method: new scheme. *Sensor Electr. and Microsyst. Techn*. **2004**, *1*, 20-24.

8. Svinarenko, A., Khetselius, O., Buyadzhi, V., Florko, T., Zaichko, P., Ponomarenko E. Spectroscopy of Rydberg atoms in a Black-body radiation field: Relativistic theory of excitation and ionization. *J. Phys.: Conf. Ser*. **2014**, *548*, 012048

9. Prepelitsa G.P., Turin A.V., Chernyakova Yu.G., The features of emission spectra of the plasma in low inductive vacuum spark: Relativistic calculation with accounting for QED effects. *Phys. Aerodisper. Syst*. **2003,** *40*, 327-332.

10. Khetselius O.Yu., Nikola L.V., Turin A.V., Sukharev D.E., Sensing the finite size nuclear effect in calculation of the Auger spectra for atoms and solids. *Sensor Electr. and Microsyst. Techn*. **2007**, *N1*, 18-21.

11. Glushkov, A.V. *Relativistic Quantum theory. Quantum mechanics of atomic systems*. Astroprint: Odessa, **2008**

12. Ivanova, E.P., Ivanov, L.N., Glushkov, A., Kramida, A. High order corrections in the relativistic perturbation theory with the model zeroth approximation, Mg-Like and Ne-Like Ions. *Phys. Scripta* **1985**, *32,* 513-522.

13. Ivanov, L.N., Ivanova, E.P., Aglitsky, E. Modern trends in the spectroscopy of multicharged ions. *Phys. Rep.* **1988,** *166,* 315-390.

14. Glushkov, A.V., Ivanov, L.N. Radiation decay of atomic states: atomic residue polarization and gauge noninvariant contributions. *Phys. Lett. A* **1992,** *170,* 33-36

15. Khetselius, O.Yu. *Quantum structure of electroweak interaction in heavy finite Fermi-systems.* Astroprint: Odessa, **2011**.

16. Khetselius, O.Yu. Quantum Geometry: New approach to quantization of quasistationary states of Dirac equation for superheavy ion and calculating hyperfine structure parameters. *Proc. Int. Geometry Center*. **2012**, *5*(3-4), 39-45.

Sofronkov A.S., Tjurin A.V.

RELATIVISTIC AND CORRELATION EFFECTS IN AUGER SPECTROSCOPY OF ATOMS AND SOLIDS

Summary. It is presented an advanced, consistent theoretical scheme for determination of the energy and spectral characteristics of the Auger process (decay, transition) in atomic systems and solids with correct accounting for the relativistic and exchange-correlation (relaxation) nuclear effects. As the basic approach to calculating the Auger spectra of solids there is used a consistent theoretical method, based on the S-matrix formalism by Gell-Mann and Low and relativistic many-body perturbation theory formalism. Universal relativistic Dirac-Hartree-Slater method is taken as a theoretical method for calculating the electronic wave functions and energies of the states and transitions. The advanced data on the Auger electron energy for some solids (Ge,Ag) with accounting for the relativistic and nuclear finite size effects are listed.

Key words: atomic spectroscopy; Auger spectroscopy; relativistic theory; energy approach; atomic, plasmas, solids systems.

Софронков О.Н., Тюрін О.В.

РЕЛЯТИВІСТСЬКІ ТА КОРЕЛЯЦІЙНІ ЕФЕКТИ В ОЖЕ-СПЕКТРОСКОПІЇ АТОМІВ ТА ТВЕРДОГО ТІЛА

Резюме. Представлено вдосконалену послідовну теоретичну схему для визначення енергетичних і спектральних характеристик процесу Оже (розпаду, переходу) в атомних системах і твердих тілах з коректним врахуванням релятивістських і кореляційних (релаксаційних) ефектів. В якості основного підходу до розрахунку Оже-спектрів атомних систем, і далі твердих тіл використовується послідовний теоретичний метод, заснований на формалізмі S-матриці Гелл-Манна і Лоу та формалізмі релятивістської теорії збурень багатьох тіл. Універсальний релятивістський метод Дірака-Хартрі-Слетера береться як теоретичний метод розрахунку електронних хвильових функцій і енергій станів та переходів. Наведено передові дані про енергію оже-електронів для деяких твердих тіл (Ge,Ag) з урахуванням релятивістського та ядерного ефектів кінцевого розміру.

Ключові слова: атомна спектроскопія; Оже-спектроскопія; релятивістська теорія; енергетичний підхід; атомні системи, плазмове середовище, тверде тіло.

A.S. Kvasikova[1], I.M. Shpinareva[2], T.B. Tkach[3]

[1]State University of Intel. Technologies & Telecommunications, 1, Kuznechna str., Odessa
[2]I.I. Mechnikov Odessa National University, 2, Dvoryanskaya str., Odessa
[3]Odessa State Environmental University, 15, Lvovskaya str., Odessa
e-mail: tkachtb@gmail.com

OPTIMIZED QUANTUM DEFECT METHOD IN RELATIVISTIC THEORY OF SPECTRA OF LI-LIKE MULTICHARGED IONS

The relativistic theory of radiative transitions using the general relativistic quantum defect approximation (GDA) was also used to study the wavelengths and oscillator strengths for the $1s^2 2s$ ($^2S_{1/2}$) $\rightarrow 1s^2 3p$ ($^2P_{1/2}$) transitions in Li-like multicharged ions with a nuclear charge Z= 14-70. and. The obtained results were compared with available theoretical and experimental (summarized) data. An important point is related to the accurate accounting of the complex contributions of the exchange-correlation (polarization) effect and the use of an efficient single-quasi-particle representation based on the general relativistic approximation of the quantum defect, which significantly ensures a physically reasonable agreement between the theory and the experiment.

1. Introduction

In the last two decades, the sought-after interest grew even more, when the fundamentally important role of multi-electron Rydberg atoms (RA; i.e., atoms in highly excited states) and multi-charged ions, photon emission and absorption processes with their participation in a wide class of physical applications became apparent. We are talking, first of all, about the problems of astrospectroscopy, astrophysics (radiation processes in nebulae and fragments of Nadnova; according to the idea of Ginzburg et al., radiation transitions between the components of the fine, ultrafine structure of H-, Li-, Be-like ions, N, Fe provide diagnostics of the sought-after radiation), physics of the Sun and auroras (radiation of Ne, Ca, Fe ions, etc.), diagnostics of laboratory, astrophysical, thermonuclear plasma, topical problems of laser physics and quantum electronics, including creation of short-wavelength lasers (razers, grazers etc) [1-30].

There have been sufficiently many papers, devoted to calculations and compilation of energies and oscillator strengths for the Li-like ions and other alkali-like ions (see, for example, [1–14]). Particularly, Martin and Wiese have undertaken a critical evaluation and compilation of the spectral parameters for Li-like ions (Z=3-28) [1,2]. Khetselius [3] has studied the radiative transitions wavelengths and oscillator strengths for some Li-like multicharged ions within the relativistic many-body perturbation theory with the optimized Dirac-Kohn-Sham zeroth approximation and an effective taking the relativistic, exchange-correlation, nuclear, radiative effects into account. The method includes the generalized Glushkov-Ivanov-Ivanova procedure (relativistic energy approach) for generation of the optimal basis set of relativistic electron wave functions with fulfilment of the gauge invariance principle [17-22]. The results of the non-relativistic calculations of the energies and oscillator strengths of $1s2 2s_i 1s2 2p$ for Li-like systems up to $Z = 50$ are presented in Ref. [12]. The Hylleraas-type variational method and the $1/Z$ expansion method have been used. In ref. [13] there are listed the nonrelativistic dipole-length, -velocity, -acceleration oscillator strengths for 1s22s–1s22p transitions of LiI isoelectronic sequence calculated within a full core plus correlation method with using multiconfiguration interaction wave functions. Fully variational nonrelativistic Hartree-Fock wave functions were used by Bièmont in calculating 1s2n2L (n<8=s,p,d,f; 3<Z<22) Li-like

states [14]. In many papers the Dirac-Fock (DF) method, model potential, quantum defect approximation in the different realizations have been used for calculating the energies and oscillator strengths of the Li-like and similar ions (see Refs.[3-18]).

In our paper the relativistic theory of radiative transitions using the general relativistic quantum defect approximation (GDA) is used to study the wavelengths and oscillator strengths for $1s^2 2s(^2S_{1/2}) \rightarrow 1s^2 3p \,(^2P_{1/2})$ transitions in Li-like multicharged ions with a nuclear charge Z= 14-70. and. The model [15,16] has received the further development. The obtained results were compared with available theoretical and experimental (summarized) data. An important point is related to the effective accounting of the contributions of the exchange-correlation (polarization) effect and the use of an efficient 1-quasi-particle representation based on the general relativistic approximation of the quantum defect, which significantly ensures a physically reasonable agreement between the theory and the experiment.

2. The theoretical method

In atomic spectroscopy there is well known a nonrelativistic and relativistic quantum defect approximation (QDA). Usually, the most exact version of the QDA is provided by using the empirical data in order to determine the quantum defect values for different state. IN [15,16] it was presented ab initio optimized QDA scheme, satisfying a principle of minimization for the gauge dependent radiative contributions to Im δE_{ninv} for the certain class of the photon propagator calibration according to ideas of Refs. [19-22,25,26]. A relativistic quantum defect is usually defined as (see, for example, [15,16]:

$$\mu_\chi(E_n) = n - v_n + \gamma - |\chi|, \qquad (1)$$

where χ is he Dirac quantum number, and

$$\gamma = \sqrt{\chi^2 - (\alpha z)^2},$$
$$v_n = \frac{z\varepsilon}{\lambda},$$

$$\lambda = \sqrt{-E_n(1+\varepsilon)}, \varepsilon = 1 + \alpha^2 E_n. \qquad (2)$$

In the non-relativistic limit (i.e. the fine structure constant $\alpha \rightarrow 0$) expression (1) transfers to the well known non-relativistic expression for quantum defect:

$$\mu_{l^{NR}}(E_n) = n - n * n - \frac{z}{\sqrt{-2E_n}}, \qquad (3)$$

where n is the principal quantum number, $n*$ is an effective quantum number, E_n is an electron energy and z is a charge of a core (ion).

At present, there are detailed tables of QD values for states with different l for a number of one-quasiparticle atomic systems, in particular, neutral atoms of alkaline elements (see, e.g. [16] and refs therein). At the same time, it should be noted that for most ions of the iso-electronic series of alkali and other atoms and ions, detailed data, as a rule, are not available, since the standard method for determining the QD is a fitting from the experimental values of the energy levels, which for a huge number of multiply charged ions are currently generally, are missing. In the corresponding review of Section 1, we presented the usual Ritz-type variational formula for the series expansion for QD. Calculation of CD is carried out according to the standard formula of the form:

$$\mu_L(n) = a + b/(n-a)^2 + c/(n-a)^4 +$$
$$+ d/(n-a)^6 + e/(n-a)^8, \qquad (4)$$

where a, b, c, d, e are the Rydberg-Ritz coefficients. The corresponding orbitals of the relativistic QDA without the use of exchange-correlation potentials are determined by the analytical solution of the Dirac-type relativistic equation with a model Hamiltonian containing QD.

In our generalized QDA the "shell-external particle" interaction potential is improved by means of adding the model potentials of the following type:

$$V^{GMMP}(r) = V_C^D(r) + V_X^{SI}(r) + V_C[r \vee b] \quad .(5)$$

where V_C^D- QDA potential of atomic core, V_{XC}^{SI} is an exchange-correlation potential of the Kohn-Sham type and Gunnarsson-Lundqvist type. The datils regarding the last potentials

can be found in Refs. [15,16]. Further, the key element of our approach is the use of an iterative procedure for building an optimized one-electron representation for relativistic bi-spinors of the QDA model and, accordingly, a new ab initio scheme for determining the QD parameters, based on the fundamental principle of minimizing gauge-non-invariant contributions to the radiation widths of atomic levels ΔE_{ninv}, which is related with the exchange of longitudinal photons. Accordingly, the procedure for minimizing ΔE_{ninv} is further reduced to a chain of variations (in fact, we are talking about a system of equations of the Dirac-QDA type).

In the usual versions of the QD theory it is mandatory to have reliable experimental information in fact for the corresponding fitting of the CD. The expression for the normalized relativistic wave functions (Dirac spinors) of the discrete spectrum $E_n < 0$) for $r > r_0$ has the standard form is as:

$$\left.\begin{array}{c} G_{n\chi}(r) \\ F_{n\chi}(r) \end{array}\right\} = \pm \left[\frac{(1 \pm \varepsilon)(z - \lambda\chi)}{4zr\zeta(E_n)\Gamma(\nu_n + \gamma + 1)\Gamma(\nu_n - \gamma + 1)} \right]^{1/2}$$

$$\left\{ W_{\nu_n + 1/2, \gamma}(2\lambda r) \pm (\eta_n + \chi)W_{\nu_n - 1/2, \gamma}(2\lambda r) \right\},$$

(6a)

where

$$\zeta(E) = 1 + \frac{\lambda^3}{z} \frac{d\mu_\chi(E)}{dE}, \eta_n = \frac{z}{\lambda}. \quad (6b)$$

Here $W_{k, m}(x)$ is the Whittaker's type function, a $\gamma, \lambda, \upsilon_n, \varepsilon$ are determined on the basis of standard formulas.

For a continuous spectrum $(E \geq 0)$, the wave functions can be represented as a linear combination of two linearly independent relativistic Coulomb functions. The coefficients in this linear combination are determined so that at $r \to \infty$:

$$\left.\begin{array}{c} G_\chi(E,r) \\ F_\chi(E,r) \end{array}\right\} \approx \sqrt{\frac{\varepsilon \pm 1}{\pi p}} \begin{array}{c} \sin \\ \cos \end{array} [pr +$$

$$y \ln 2pr + \xi - arg\Gamma(\gamma + 1 + iy) - \frac{\pi\gamma}{2} + \delta_\chi(E)$$

(7a)

where

$$p = \sqrt{E(1 + \varepsilon)},$$
$$\varepsilon = 1 + \alpha^2 E,$$
$$y = \frac{z\varepsilon}{p},$$

$$\xi = \frac{1}{2}\arg\frac{\chi - i\frac{z}{p}}{\gamma - iy} \quad (7b)$$

Within an anergy approach [18-22] the probability of the E dipole transition is:

$$\Gamma_{\alpha_n} = \frac{1}{4\pi} \cdot V_{\alpha_n \alpha_n}^{|\omega_{\alpha_n}|} \quad (9)$$

where the matrix element is determined as follows:

$$V_{ijkl}^{|\omega|} = \iint dr_1 dr_2 \Psi_i^*(r_1)\Psi_j^*(r_2)\frac{\sin|\omega|r_{12}}{r_{12}}(1 - \alpha_1\alpha_2)\Psi_k^*(r_2)\Psi_l^*(r_1)$$

(10)

The corresponding oscillator strength: $gf = \lambda_g^2 \cdot \Gamma_{\alpha n}/6.67 \cdot 10^{15}$, where g is the degeneracy degree, λ is a wavelength in angstrems (Å). The relativistic QDA wave functions are substituted into matrix element (10). To increase an accuracy of computing oscillator strengths we add the two-quasiparticle polarization potential [19] into the radiation transition matrix element. All computing was performed with using the modified PC code "Superatom-ISAN" (version 93).

3. Results and conclusion

We applied the above described approach to calculating the energies and oscillator strengths of transitions in spectra of the Li-like ions with Z-13-70. Below we list the corresponding data for some chosen ions, namely S13+ Ca17+ Fe23+ Zn^{27+} Zr^{37+} Mo^{39+} Sn^{47+} Tm^{66+} Yb^{67+}. There are considered the radiative transitions from ground state to the low-excited and Rydberg states, particularly, $2s_{1/2}$ – $np_{1/2,3/2}$, $np_{1/2,3/2}$-$nd_{3/2,5/2}$ (n=2-12). To test the obtained results, we compare our calculation data on the oscillator strengths values for some Li-like ions with the known theoretical and compillated data [1,2,6-17,25].

As example, in table 1,2 we list our oscillator strengths values (ORMP and OQDA) for $2s_{1/2}$–$2p_{1/2,3/2}$ transitions in Li-like ions

$S^{13+}, Ca^{17+}, Fe^{23+}, Zn^{27+}, Zr^{37+}, Mo^{39+}, Sn^{47+}, Tm^{66+}, Yb^{67+}$.

Table 1. Oscillator strengths of the $2s_{1/2} - 2p_{1/2}$ transitions in Li-like ions

Ion	DF $2s_{1/2}$–$2p_{1/2}$	Our data $2s_{1/2}$–$2p_{1/2}$	Exp. $2s_{1/2}$–$2p_{1/2}$
S^{13+}	0.0299	0.0304	0.030
Ca^{17+}	0.0234	0.0239	0.024
Fe^{23+}	0.0177	0.0183	0.018
Zn^{27+}	0.0153	0.0159	–
Zr^{37+}	0.0114	0.0123	–
Mo^{39+}	–	0.0116	0.011
Sn^{47+}	0.0092	0.0099	–
Tm^{66+}	–	0.0078	–
Yb^{67+}	0.0067	0.0075	–

The DF calculation data by Zilitis [6] and the "best" compillated (experimental) data [1,2] for the some low-Z Li-like ions are listed in tables 1,2 for comparison too. It should be reminded that the experimental data on the oscillator strengths for many (especially, high-Z) Li-like ions are absent.

Table 2. Oscillator strengths of the $2s_{1/2} - 2p_{3/2}$ transitions in Li-like ions.

Ion	DF $2s_{1/2}$–$2p_{3/2}$	Exp. $2s_{1/2}$–$2p_{3/2}$	Our data $2s_{1/2}$–$2p_{3/2}$
S^{13+}	0.0643	0.064	0.0645
Ca^{17+}	0.0542	0.054	0.0546
Fe^{23+}	0.0482	0.048	0.0486
Zn^{27+}	0.0477	–	0.0480
Zr^{37+}	0.0543	–	0.0545
Mo^{39+}	–	0.056	0.0564
Sn^{47+}	0.0686	–	0.0689
Tm^{66+}	–	–	01146
Yb^{67+}	0.1170	–	0.1173

Let us note that an estimate of the gauge-non-invariant contributions (the difference between the oscillator strengths values calculated with using the transition operator in the form of "length" and "velocity") is about 2.5%. It means that the results are very closed within schemes with using the different photon propagator gauges.

In is worth to underline that the QDA

oscillator strengths data become more exact with the growth of the principal quantum number. The most optimal variant is consideration of essentially Rydberg atomic starts. At the same time the accuracy of the DF data may be decreased. The agreement between the Martin-Weiss data and our results for the transitions between low-lying terms is sufficiently good. An important point is related to the accurate accounting of the complex contributions of the exchange-correlation (polarization) effect and the use of an efficient single-quasi-particle representation based on the general relativistic approximation of the quantum defect, which significantly ensures a physically reasonable agreement between the theory and the experiment.

References

1. Seaton M.J., Quantum defect theory/ *Rep. Prog. Phys*. 1**983,** *46*, 167-258.
2. Martin G.A. and Wiese W. L., Tables of critically evaluated oscillator strengths for lithium isoelectronic sequenceю *Journ. of Phys. Chem. Ref. Data*. **1976**, *5,* 537-570.
3. Khetselius, O.Yu. Optimized relativistic many-body perturbation theory calculation of wavelengths and oscillator strengths for Li-like multicharged ions. Adv. Quant. Chem. **2019**, *78*, 223-251.
4. Khetselius, O.Yu. Relativistic perturbation theory calculation of the hyperfine structure parameters for some heavy-element isotopes. *Int. Journ. Quant.Chem.* **2009,** *109,* 3330-3335.
5. Khetselius, O.Yu. Relativistic calculation of the hyperfine structure parameters for heavy elements and laser detection of the heavy isotopes. *Phys.Scripta.* **2009,** *135,* 014023.
6. Zilitis V.A., Determination of the energies and oscillator strengths of Li-like ions// Opt. Spectr.-1983.-Vol.55.-P.215-218.
7. Froese Fischer C., Breit–Pauli energy levels, lifetimes, and transition probabilities for the beryllium-like to neon-like sequences//Atom.Dat.Nucl. Dat. Tabl. - 2004.-Vol.87.-P.1–184.
8. Barnett R., Johnson E., Lester W.Jr., Qu-

antum Monte Carlo determination of the lithium 2S-2P oscillator strength: Higher precision//Phys. Rev. A.-1995.-Vol.51.-P. 2049-2052.

9. Zong-Chao Yan and Drake G.W.F., Theoretical lithium 2S-2P and 2P-3D oscillator strengths, *Phys. Rev. A,* **1995,** *52,* R4316-4319.

10. Lianhua Qu, Zhiwen Wang and Baiwen Li, Theory of oscillator strength of the lithium isoelectronic sequence. *J. Phys. B: At. Mol. Opt. Phys.,* **1998,** *31,* 3601-3612.

11. Banglin, Deng.; Gang, Jiang; Chuanyu Zhang. Relativistic configuration-interaction calculations of electric dipole n = 2 − n = 3 transitions for medium-charge Li-like ions. *Atom. Dat. and Nucl. Dat. Tabl.* **2014,** *100,* 1337-1355.

12. Chen Chao, Wang Zhi-Wen, Oscillator strengths for 2s2–2p2P transitions of lithium isoelectronic sequence NaIX-CaXVIII, *Com. Theor. Phys.* **2005,** 4*3,* 305-312.

13. Hu Mu-Hong, Wang Zhi-Wen, Oscillator strengths for 2S–nP transitions of lithium isoelectronic sequence from Z = 11 to 20. Chinese Phys. B. **2009,** *18,* 2244-2258.

14. Bièmont E., Theoretical oscillator strengths in lithium isoelectronic sequence (3 <= Z <= 22). *Astr. and Astroph. Suppl.* **1977,** *27,* .489-494

15. Svinarenko A.A., Nikola L.V., Prepelitsa G.P., Tkach T., Mischenko E., The Auger (Autoionization) decay of excited states in spectra of multicharged ions: relativistic theory. *Spectral Lines Shape* (AIP). **2010,** 16, 94-98.

16. Tkach T.B., Optimized relativistic model potential method and quantum defect approximation in theory of radiative transitions in spectra of multicharged ions. *Photoelectronics.* **2012,** *21,* 22-27

17. Glushkov, A.V. *Relativistic Quantum theory. Quantum mechanics of atomic systems.* Astroprint: Odessa, **2008**

18. Ivanova, E.P., Ivanov, L.N., Glushkov, A., Kramida, A. High order corrections in the relativistic perturbation theory with the model zeroth approximation, Mg-Like and Ne-Like Ions. *Phys. Scripta* **1985,** *32,* 513-522.

19. Ivanova, E., Glushkov, A. Theoretical investigation of spectra of multicharged ions of F-like and Ne-like isoelectronic sequences. J. Quant. Spectr. and Rad. Tr. **1986,** *36*(2), 127-145.

20. Glushkov, A.V.; Ivanov, L.N. Radiation decay of atomic states: atomic residue polarization and gauge noninvariant contributions. *Phys. Lett. A* **1992,** *170,* 33-36.

21. Glushkov A.V.; Ivanov, L.N. DC strong-field Stark effect: consistent quantum-mechanical approach. *J. Phys. B: At. Mol. Opt. Phys.* **1993,** *26,* L379-386.

22. Glushkov, A.V. Advanced Relativistic Energy Approach to Radiative Decay Processes in Multielectron Atoms and Multicharged Ions. *In: Nishikawa, K., Maruani, J., Brandas, E., Delgado-Barrio, G., Piecuch, P. (Eds) Quantum Systems in Chemistry and Physics: Progress in Methods and Applications, Ser.: Progress in Theor.l Chem.and Phys.,* Springer: Dordrecht, **2012**; Vol. *26,* pp 231–252.

23. Khetselius, O.Yu. *Quantum structure of electroweak interaction in heavy finite Fermi-systems.* Astroprint: Odessa, **2011**

24. Khetselius, O.Yu. Atomic parity non-conservation effect in heavy atoms and observing P and PT violation using NMR shift in a laser beam: To precise theory. *J. Phys.: Conf. Ser.* **2009,** *194,* 022009

25. Khetselius, O.Yu. Quantum Geometry: New approach to quantization of quasistationary states of Dirac equation for superheavy ion and calculating hyperfine structure parameters. *Proc. Int. Geometry Center.* **2012,** *5(*3-4), 39-45.

26. Svinarenko, A., Khetselius, O., Buyadzhi, V., Florko, T., Zaichko,P., Ponomarenko, E. Spectroscopy of Rydberg atoms in a Black-body radiation field: Relativistic theory of excitation and ionization. *J. Phys.: Conf. Ser.* **2014,** *548,* 012048.

27. Khetselius, O.Yu., Lopatkin, Yu.M., Dubrovskaya, Yu.V, Svinarenko, A.A. Sensing hyperfine-structure, electroweak interaction and parity non-conservation effect in heavy atoms and nuclei: New nuc-

lear-QED approach. *Sensor Electr. and Microsyst. Techn*. **2010**, *7*(2), 11-19.

28. Glushkov A.V., Malinovskaya S.V., Loboda A.V., Shpinareva I.M., Gurnitskaya E.P., Korchevsky D.A., Diagnostics of the collisionally pumped plasma and search of the optimal plasma parameters of x-ray lasing: Calculation of electron-collision strengths and rate coefficients for Ne-like plasma. *J.Phys. C Ser*. **2005**, *11*, 188-198.

29. Ignatenko, A.V., Svinarenko, A.A., Prepelitsa, G.P., Perelygina, T.B. Optical bi-stability effect for multi-photon absorption in atomic ensembles in a strong laser field. *Photoelectronics*. **2009**, *18*, 103-105.

30. Shpinareva I.M., Photoionization and stark effect of hydrogen molecule and Wannier-Mott beexcitons in an electric field. *Photoelectronics*. **2004**, *13*, 30-33.

Kvasikova A.S., Shpinareva I.M., Tkach T.B.

OPTIMIZED QUANTUM DEFECT METHOD IN RELATIVISTIC THEORY OF SPECTRA OF LI-LIKE MULTICHARGED IONS

Summary. The relativistic theory of radiative transitions using the general relativistic quantum defect approximation (GDA) was also used to study the wavelengths and oscillator strengths for the $1s^22s$ ($^2S_{1/2}$) $\rightarrow$ $1s^23p$ ($^2P_{1/2}$) transitions in Li-like multicharged ions with a nuclear charge $Z= 14-70$. and. The obtained results were compared with available theoretical and experimental (summarized) data. An important point is related to the accurate accounting of the complex contributions of the exchange-correlation (polarization) effect and the use of an efficient single-quasi-particle representation based on the general relativistic approximation of the quantum defect, which significantly ensures a physically reasonable agreement between the theory and the experiment.

Key words: relativistic theory, quantum defect method, radiative transitions, lithium-like ions

Квасикова А.С., Шпінарева І.М., Ткач Т.Б.

ОПТИМІЗОВАНИЙ МЕТОД КВАНТОВОГО ДЕФЕКТУ В РЕЛЯТИВІСТСЬКІЙ ТЕОРІЇ СПЕКТРІВ ЛІТІЙ-ПОДІБНИХ БАГАТОЗАРЯДНИХ ІОНІВ

Резюме. Релятивістська теорія радіаційних переходів з використанням узагальненого релятивістського наближення квантового дефекту (GDA) використана і з для дослідження довжин хвиль та сил осциляторів для переходів $1s^22s$ ($^2S_{1/2}$) $\rightarrow$ $1s^23p$ ($^2P_{1/2}$) та інших у Li-подібних багатозарядних іонах із зарядом ядра $Z=14-70$. Проведено порівняння отриманих результатів з наявними теоретичними та експериментальними (зведеними) даними. Важливий момент розробленої моделі пов'язаний з додатковим ефективним урахуванням обмінно-кореляційного (поляризаційного) ефекту та використанням ефективного одноквазічастинкового представлення на основі узагальненого релятивістського наближення квантового дефекту, що суттєво забезпечує фізично розумну узгодженість між теорією та експериментом.

Ключові слова: релятивістська теорія, метод квантового дефекта, радіаційні переходи, літій-подібні іони

PACS 33.20.-t

A.V. Ignatenko[1], V.F. Mansarliysky[1], P.A. Zaichko[2], T.M. Sakun[3]

[1]Odessa State Environmental University, 15, Lvovskaya str., Odessa
[2]Odessa National Maritime Academy, 4, Didrikhson str., Odessa
[3]National Aviation University, 1, Liubomyra Huzara ave., Kiev
E-mail: ignatenkoav13@gmail.com

DENSITY FUNCTIONAL AND GREEN'S FUNCTIONS METHOD TO COMPUTING SPECTRAL PARAMETERS OF DIATOMIC MOLECULES

It is presented a new effective method of calculating the energy and spectral parameters of diatomic molecules based on the hybrid theory of the quasi-particle density functional and the theory of Green's functions. As an illustration, the data of the calculation of the vertical ionization potentials and the coupling constants (vibrational structure) of the photoelectron spectra of a number of diatomic molecules, in particular, N_2, are received. It is presented a detailed comparison of the received results with the data of standard theories of the Hartree-Fock type, the multi-configuration electron propagator method, and the extended theory based on Koopmans' theorem using multi-configurational self-consistent field wave functions with different sets of basis functions. Iit is shown that the consistent, maximally precise consideration of exchange-correlation effects and reorganization effects within the framework of the combined theory leads to a rather significant improvement in the agreement of theoretical and experimental data both in terms of ionization potentials and photoelectron spectra in general..

1. Introduction

Currently, the optics and spectroscopy of ordinary molecular, as well as combined and hybrid photon-atom-molecular systems, and, as a part of it, photoelectron spectroscopy (PES), belong to one of the directions of modern optics and spectroscopy, which are intensively developing, which, firstly, is associated with the use of fundamentally new methods and technologies in relevant experimental research, in particular, based on new powerful sources of laser radiation, and secondly, with the sharply increasing theoretical and applied value of relevant data regarding energy and spectral properties of ordinary molecular (diatomic and polyatomic molecules), as well as combined and hybrid photon-atom-molecular systems, that is, molecules in the field of intense electromagnetic radiation for numerous physical and other applications and applications [1-28]. Modern molecular optics and spectroscopy has in its theoretical and computational arsenal a rather huge number of diverse theoretical approaches to the calculation of energy and spectroscopic characteristics of molecules (ionization and excitation potentials, spectra of excited states, potential energy curves, spectroscopic molecular steels, dipole moments, parameters of the vibrational and rotational structure of the spectra, etc.). Among them, such well-known powerful and consistent approaches as self-consistent field methods of the Hartree-Fock-Rothaan (HFR), Hartree-Fock-Slater (HFS), X ✔ -method, in multi- and even mega-configurational versions should be especially noted and highlighted, the density functional method (DFT) in numerous implementations, the Green's function method (GF), coupled-cluster theories (CCT), the valence bond method (RCI-VB) with configuration interaction and various versions formalism of perturbation theory (RT), etc.

In this paper we present new effective method of calculating the energy and spectral parameters of diatomic molecules based on the hybrid theory of the quasi-particle density functional and the theory of Green's functions [1,9-11]. As an illustration, the data of the computing vertical ionization potentials and

179

the coupling constants (vibrational structure) of the photoelectron spectra of a number of diatomic molecules, in particular, N$_2$, are given, and a detailed comparison of some available data. The approach is based on the Green's function method (Cederbaum-Domske and Khetselius versions) [2-4] and Fermi-liquid DFT formalism [5-8].

2. Combined Green's functions and Fermi-liquid quasiparticle density functional theory

As the key moments of the combined method have been presented in Refs. [1,9-11], here we concern only such a points, which are important for computing vertical ionization potentials and the coupling constants (vibrational structure) of the photoelectron spectra of diatomic molecules. According to [1,2, 9] the molecular Hamiltonian van be written in the following form as follows:

$$H = H_E + H_N + H_{EN}^{(1)} + H_{EN}^{(2)}, \qquad (1)$$

$$H_E = \sum_i \epsilon_i(R_0) a_i^t a_i + \frac{1}{2} \sum V_{ijkl}(R_0) a_i^t a_j^t a_l a_k -$$
$$- \sum_{i,j} \sum_{k \in f} [V_{ikjk}(R_0) - V_{ikkj}(R_0)] a_i^t a_j \qquad (2)$$

$$H_N = \hbar \sum_{s=1}^M \omega_s \left(b_s^t b_s + \frac{1}{2} \right),$$

$$H_{EN}^{(1)} = 2^{-1/2} \sum_{s=1}^M \left(\frac{\partial \epsilon_i}{\partial Q_s} \right)_0 (b_s + b_s^t)[a_i^t a_i - n_i] +$$

$$+ \frac{1}{4} \sum_i \sum_{s'=1}^M \left(\frac{\partial^2 \epsilon_i}{\partial Q_s \partial Q_{s'}} \right)_0 (b_s + b_s^t)(b_{s'} + b_{s'}^t)[a_i^t a_i - n_i], \qquad (3)$$

$$H_{EN}^{(2)} = 2^{-3/2} \sum_{s=1}^M \sum \left(\frac{\partial V_{ijkl}}{\partial Q_s} \right)_0 (b_s + b_s^t)[\delta v_1 a_i^t a_j^t a_k$$
$$+ \delta v_2 a_l a_k a_i^t a_j^t + 2\delta v_3 a_j^t a_k a_l a_i^t] +$$

$$+ \frac{1}{8} \sum \sum_{s,s'=1}^M \left(\frac{\partial^2 V_{ijkl}}{\partial Q_s \partial Q_{s''}} \right)_0 (b_s + b_s^t)(b_{s'} + b_{s'}^t) \cdot$$
$$[\delta v_1 a_i^t a_j^t a_k + \delta v_2 a_l a_k a_i^t a_j^t + 2\delta v_3 a_j^t a_k a_l a_i^t] \qquad (4)$$

with $n_i = 1$ (0), $i \in f$ ($i \notin f$), $\delta \sigma_f = 1$ (0), $(ijkl) \in \sigma_f$, where the index set v_1 means that at least φ_k and φ_l or φ_i and φ_j are unoccupied, v_2 that at most one of the orbitals is unoccupied, and v_3 that φ_k and φ_j or φ_l and φ_j are unoccupied; $\in_i(R)$ are the one-particle HF energies and f denotes the set of orbitals occupied in the HF ground state; R_0 is the equilibrium geometry on the HF level); the ω_s are the HF frequencies; b_s, b_s^t are destruction and creation operators for vibrational quanta, Q_s are dimensionless normal coordinates are as follows:

The usual way is to define the HF-single-particle component H_0 of the Hamiltonian (4) is as in Refs. [1,2]. Correspondingly in the one-particle picture the density of occupied states is given by

$$N_k^0(\epsilon) = \frac{1}{2\pi\hbar} \int_{-\infty}^\infty dt \, e^{i\hbar^{-1}(\epsilon - c_k)t} \langle 0| \, e^{\pm i\hbar^{-1}\widetilde{H}_{0'}} |0\rangle, \qquad (5)$$

$$\widetilde{H}_0 = \sum_{s=1}^M \hbar \omega_s b_s^t b_s + \sum_{s=1}^M g_s^k (b_s + b_s^t) + \qquad (6)$$
$$+ \sum_{s,s'=1}^M \gamma_{ss'}^k (b_s + b_s^t)(b_{s'} + b_{s'}^t)$$

$$g_s^i = \pm \frac{1}{\sqrt{2}} \left(\frac{\partial \epsilon_i}{\partial Q_s} \right)_0, \qquad \gamma_{ss'}^i = \pm \frac{1}{4} \left(\frac{\partial^2 \epsilon_i}{\partial Q_s \partial Q_{s'}} \right)_0. \qquad (7)$$

To get function $N_k(\epsilon)$ one calculates the GF $G_{kk'}(\epsilon)$ (see details in Refs. [1,2,9]:

$$G_{kk'}(\epsilon) = -i\hbar^{-1} \int_{-\infty}^\infty dt \, e^{i\hbar^{-1}\epsilon t} \langle \psi_0| \, T\{ a_k(t) a_k^t(0) \} |\psi_0\rangle \qquad (8)$$

Choosing the unperturbed H_0 to be $H_0 = \sum \epsilon_i a_i^t a_i + H_N$ one could define GF as

$$G_{kk'}^{OB}(t) = \pm \delta_{kk'} i \exp[-in^{-1}(\varepsilon_k \mp \Delta\varepsilon)t] \cdot$$
$$\cdot \sum_n |\langle \hat{n}_k | U_k | 0 \rangle|^2 \exp(\pm in_k \cdot \hat{\omega}_k t) \qquad , (9)$$

The direct method for calculation of $N_k(\in)$ as the imaginary part of the GF includes a definition of the vertical I.P. (V.I.P.s) of the reference molecule and then of $N_k(\in)$.

The zeros of the functions:

$$D_k(\in) = \in - \left[\in^{\mathrm{op}} + \Sigma(\in)\right]_k, \qquad (10)$$

where $\left(\in^{\mathrm{op}} + \Sigma\right)_k$ denotes the k-th eigenvalue of the diagonal matrix of the one-particle energies added to matrix of the self-energy part, are the negative V. I. P. 's for a given geometry. One can write [1,5,9]:

$$(V.I.P.)_k = -(\in_k + F_k)',$$
$$F_k = \Sigma_{\mathrm{kk}}\left(-(V.I.P.)_k\right) \approx \frac{1}{1 - \partial\Sigma_{\mathrm{kk}}(\in_k)/\partial_\in}\Sigma_{\mathrm{kk}}(\in_k)$$

$$(11)$$

Expanding the ionic energy E_k^{N-1} about the equilibrium geometry of the reference molecule in a power series of the normal coordinates leads to a set of linear equations for the unknown normal coordinate shifts δQ_S, and new coupling constants:

$$g_1 = \pm\left(1/\sqrt{2}\right)\left[\partial\left(\in_k + F_k\right)/\partial Q_l\right]_0 \qquad (12)$$

$$\gamma_{ll'} = \pm\left(\frac{1}{4}\right)\left[\partial^2\left(\in_k + F_k\right)/\partial Q_l/\partial Q_{l'}\right]_0$$

The coupling constants $g_l, \gamma_{ll'}$ are calculated by the well-known perturbation expansion of the self-energy part. One could write:

$$\sum_{kk}^{(2)}(\in) = \sum_{\substack{i,j \\ s\notin F}}\frac{\left(V_{ksij} - V_{ksji}\right)V_{ksij}}{\in + \in_s - \in_i - \in_j} + \sum_{\substack{i,j \\ s\notin F}}\frac{\left(V_{ksij} - V_{ksji}\right)V_{ksij}}{\in + \in_s - \in_i - \in_j}$$

$$(13)$$

and the coupling constant g_l, are as [1,3]:

$$g_l \approx \pm\frac{1}{\sqrt{2}}\frac{\partial\in_k}{\partial Q_l}\frac{1 + q_k(\partial/\partial\in)\sum_{kk}\left[-(V.I.P.)_k\right]}{1 - (\partial/\partial\in)\sum_{kk}\left[-(V.I.P.)_k\right]}$$

$$(14)$$

The pole strength of the corresponding GF:

$$\rho_k = \left\{1 - \frac{\partial}{\partial\in}\sum_{kk}\left[-(V.I.P.)_k\right]\right\}^{-1}; 1 \geq \rho_k \geq 0,$$

$$g_l \approx g_l^0\left[\rho_k + q_k(\rho_k - 1)\right],$$

$$g_l^0 = \pm 2^{-1/2}\partial\in_k/\partial Q_l \qquad (15)$$

It is important to underline that computing the latter parameters by the standard methods requires serious resources. But there is more effective and quite precise approach to this problem. It is connected with using quasiparticle Fermi-liquid theory of the DFT in versions [1,5-7,9]. Especially this approach is effective in computing he vertical I.P. (V.I.P.s), phoelectron spectra (the coupling constants of vibrational structure). The master equations can be obtained on the basis of variational principle, if one starts from a Lagrangian of a molecule L_q [5,7]. It should be defined as a functional of quasiparticle densities:

$$v_0(r) = \sum_\lambda n_\lambda |\Phi_\lambda(r)|^2, \qquad (16)$$

$$v_1(r) = \sum_\lambda n_\lambda |\nabla\Phi_\lambda(r)|^2, \qquad (17)$$

$$v_2(r) = \sum_\lambda n_\lambda[\Phi_\lambda^*\Phi_\lambda - \Phi_\lambda^*\Phi_\lambda]. \qquad (18)$$

The densities v_0 and v_1 are similar to the HF electron density and kinetical energy density correspondingly; the density v_2 has no an analog in the HF or DFT theory and appears as result of account for the energy dependence of the mass operator Σ. A Lagrangian L_q can be written as a sum of a free Lagrangian and Lagrangian of interaction: $L_q = L_q^0 + L_q^{int}$, where the interaction Lagrangian is defined in the form, which is characteristic for a standard DFT (as a sum of the Coulomb and exchange-correlation terms), but, it takes into account for a mass operator energy dependence of Σ:

$$L_q^{int} = L_K - \frac{1}{2}\sum_{i,k=0}^{2}\int\beta_{ik}F(r_1,r_2)v_i(r_1)v_k(r_2)dr_1dr_2$$

$$(19)$$

where F is an effective exchange-correlation interaction potential. The constants β_{ik} are defined in Refs. [1,5,6]. The constant β_{02} can be calculated by analytical way, but it is very useful to keep in mind its connection with a spectroscopic factor F_{sp} [5-7]:

$$F_{sp} = \left\{1 - \frac{\partial}{\partial\in}\sum_{kk}\left[-(V.I.P.)_k\right]\right\}$$

$$(20)$$

The multiplier $[1-\Sigma_2]$ is easily calculated if the Gunnarsson-Lundqvist-like correlation potential is used as V_{XC} and Σ_2 is determined as fol-

lows:

$$\sum(r) = 0,254\rho(r)[0,328\rho^{-2/3}(r) + \qquad (21)$$
$$+0,204\rho^{-2/3}(r)/\{1+18,376\rho^{1/3}(r)\}]$$

The new element is linked with using the DFT correlation Gunnarsson-Lundqvist as well as the Lee-Yang-Parrr functionals etc. (c.g.[12-16]). For all calculations it has been used the PC code Supermolecule (version 93).

4. Results and conclusions

As an illustration, Table 1 shows the experimental values of VIP (a), single-particle HF energies (b), the value of VIP calculated on the basis of the Koopmans theorem (KT) plus the reorganization correction (EKT; c), VIP calculated by the usual and extended GF method (d,f,g), our data within the combined GF-DFT theory (h). For comparison, the data of the multi-configuration electron propagator (MCEP) method, an extended theory using Koopmans' theorem (EKT) are also given (the extended EKT theory uses multi-configurational self-consistent wave functions with different sets of electron orbital basis functions (from res. [1-3,7,8,13,14]).

Table 1. Theoretical and experimental VIPs (eV) for the nitrogen molecule: experiment (a), HF single-particle energies (b), VIP values based on Koopmans' theorem (KT) plus reorganization correction (EKT; c), VIP calculated by the conventional and extended method GF (d,f,g), data from the multi-configuration electron propagator (MCEP;e) method, our data from the combined GF-DFT theory (h).

Orbital	Exp (a)	KT $-\in_k^b$ (b)	EKT $-\in_k^b$ (c)	GF $-\in_k^b$ (d)
$3\sigma_g$	15.6	17.24	16.37; 16.13 16.84; 15.66	15.31
$1\pi_u$	16.98	16.73	16.73	16.80
$2\sigma_u$	18.78	21.13	21.13	19.01
Orbital	MCEP $-\in_k^b$ (e)	GF+ Reorg (f)	GF-All (g)	Our Data (h)
$3\sigma_g$	15.52	16.0	15.50	15.58
$1\pi_u$	17.24	15.7	16.83	16.97
$2\sigma_u$	18.56	19.9	18.59	18.77

In table 2. given data for the bond constants g (in eV) for the N_2 molecule in different approximations: g^0 – the value of the constant g in the HF approximation without taking into account corrections for correlation and reorganization; g^R is the value of the constant g, taking into account only the correction for the effect of reorganization; $g^{R+C(a)}$ and $g^{R+C(b)}$ - are values of the constant g, taking into account corrections for correlation and reorganization, obtained within the framework of the Sederbaum-Domsky DFT method (a) and our QP-DFT (b).

Table 2 Bond constant g (in eV) in different approximations for the N_2 molecule (see text)

Orbital	g^0	g^R
$3\sigma_g$	-0.095	-0.074
$1\pi_u$	-0.344	-0.334
$2\sigma_u$	+0.268	+0.267
Orbital	$g^{R+C\,(a)}$	$g^{R+C\,(b)}$
$3\sigma_g$	-0.0965	-0.0964
$1\pi_u$	-0.337	-0.3302
$2\sigma_u$	+0.177	+0.1635

The results listed in the tables show slightly better agreement between data of the presented approach and experiment than the results of calculations in other versions of the DV method.

It is obvious that a carrying out more perfect than the existing methods to computing spectral molecular characteristics of molecular systems should include more careful accounting for correlation effects,. Developed one-quasiparticle representation used here can be taken as the zeroth approximation in one of the sophisticated versions of the many-body PT such as , for example, the Möller-Plesset PT etc.

References

1. Glushkov, A.V., Ignatenko, A., Tsudik, A., Mykhailov, A.L., Quasiparticle Fermi-Liquid Density Functional Approach to Atomic and Diatomic Systems. Spectroscopic factors *In: Glushkov A.V., Khetselius O.Y., Maruani J., Brändas E. (Eds)*

Advances in Methods and Applications of Quantum Systems in Chemistry, Physics, and Biology, Ser.: *Progress in Theoretical Chem. and Phys.*, Cham: Springer. **2021**, *33*, 133-150.

2. Köppel, H., Domcke, W., Cederbaum, L., Green's function method in quantum chemistry. *Adv. Chem. Phys*. **1984**, *57*, 59-132

3. Cederbaum, L., Domcke, W., On vibrational structure of photoelectron spectra by the Green's functions method. *J.Chem. Phys*. **1984**, *60*, 2878-2896.

4. Khetselius, O.Yu. *Quantum structure of electroweak interaction in heavy finite Fermi-systems*. Astroprint: Odessa, **2011**.

5. Glushkov, A. An universal quasiparticle energy functional in a density functional theory for relativistic atom. *Opt. and Spectr*. **1989**, *66*(1), 31-36.

6. Glushkov, A.V. New approach to theoretical definition of ionization potentials for molecules on the basis of Green's function method. *J. Phys. Chem*. **1992**, 66, 2671-2677.

7. Glushkov, A.V. *Relativistic Quantum theory. Quantum mechanics of atomic systems*. Astroprint: Odessa, **2008**.

8. Glushkov, A.V. *Relativistic and correlation effects in spectra of atomic systems*. Astroprint: Odessa, **2006**.

9. Ignatenko A.V., Svinarenko A.A., Mansarliysky V.F., Sakun T.N., Optimized quasiparticle density functional and Green's functions method to computing bond energies of diatomic molecules Photoelectronics. **2020**. *29,* 86-93.

10. Ignatenko, A.V. and Lavrenko, A.P., Spectroscopic factors of diatomic molecules: optimized green's functions and density functional method. Photoelectronics. **2019**. Vol.28. P.83-89.

11. Ignatenko, A., Glushkov, A., Lepikh, Y., Kvasikova A, Photoelectron spectroscopy of diatomic molecules: optimized Green's functions and density functional approach**.** *Photoelectr*. **2018**,*27*,44-51.

12. Ponomarenko, E.L., Kuznetsova, A.A., Dubrovskaya, Yu.V., Bakunina, E.V. Energy and spectroscopic parameters of diatomics within generalized equation of motion method. *Photoelectronics*. **2016**, *25*, 114-118.

13. Morrison R.C., Liu, G., Extended Koopmans' Theorem: Approximate Ionization Energies from MCSCF Wave Functions. *J. Comput. Chem*. **1992**, *13*, 1004-1010.

14. Lagowscki, J., Vosko, S. Analysis of local and gradient-correction correlation energy functionals using electron removal energies. *J. Phys.B: At. Mol. Opt. Phys*. **1988**, *21*(1), 203-208.

15. Guo, Y., Whitehead, M. Effect of the correlation correction on the ionization potential and electron affinity in atoms. *Phys.Rev.A*. **1989**, *39*(1), 28-34.

16. Khetselius, O.Yu., Lopatkin Yu.M., Dubrovskaya, Yu.V, Svinarenko A.A. Sensing hyperfine-structure, electroweak interaction and parity non-conservation effect in heavy atoms and nuclei: New nuclear-QED approach. *Sensor Electr. And Microsyst. Techn*. **2010,** 7(2), 11-19.

17. Florko, T., Ambrosov, S., Svinarenko A., Tkach, T. Collisional shift of the heavy atoms hyperfine lines in an atmosphere of the inert gas. *J. Phys: Conf. Ser*. **2012**, *397*(1), 012037.

18. Glushkov, A.V., Ivanov, L.N. Radiation decay of atomic states: atomic residue polarization and gauge noninvariant contributions. *Phys. Lett. A* **1992**, *170,* 33-36.

19. Ivanova, E.P., Ivanov, L.N., Glushkov, A., Kramida, A. High order corrections in the relativistic perturbation theory with the model zeroth approximation, Mg-Like and Ne-Like Ions. *Phys. Scripta* **1985**, *32,* 513-522.

20. Khetselius, O. Yu. *Hyperfine structure of atomic spectra*; Astroprint: Odessa, **2008**.

21. Khetselius, O. Relativistic perturbation theory calculation of the hyperfine structure parameters for some heavy-element isotopes. *Int. J. Quant. Chem.* **2009,** *109,* 3330–3335.

22. Khetselius, O. Relativistic calculation of the hyperfine structure parameters for heavy elements and laser detection of the heavy isotopes. *Phys. Scr.* **2009,** *135,* 014023.

23. Svinarenko A.A., Mischenko E., Loboda A., Dubrovskaya Yu. Quantum measure of frequency and sensing the collisional shift of the ytterbium hyperfine lines in medium of helium gas. *Sensor Electr. and Mi-*

crosyst. Techn. **2009**, 1, 25-29.

24. Ivanova, E., Glushkov, A. Theoretical investigation of spectra of multicharged ions of F-like and Ne-like isoelectronic sequences. J. Quant. Spectr. and Rad. Tr. **1986**, *36*(2), 127-145.

25. Khetselius O., Florko T., Svinarenko A., Tkach T. Radiative and collisional spectroscopy of hyperfine lines of the Li-like heavy ions and Tl atom in an atmosphere of inert gas. *Phys.Scripta*. **2013**, *T153*, 014037.

26. Khetselius, O.Yu. Hyperfine structure of radium. *Photoelectron*. **2005**, *14*, 83-85

27. Khetselius O.Yu., Quantum Geometry: New approach to quantization of the quasistationary states of Dirac equation for super heavy ion and calculating hyper fine structure parameters. *Proc. Int. Geometry Center*. **2012**, *5*(3-4), 39-45.

28. Khetselius, O., Glushkov, A., Dubrovskaya, Yu., Chernyakova, Yu., Ignatenko, A., Serga, I., Vitavetskaya, L. Relativistic quantum chemistry and spectroscopy of exotic atomic systems with accounting for strong interaction effects. In: *Wang YA, Thachuk M, Krems R, Maruani J* (eds) *Concepts, Methods and Applications of Quantum Systems in Chemistry and Physics*. Springer, Cham, **2018**; Vol. 31, pp. 71-91.

PACS 33.20.-t

Ignatenko A.V., Mansarliysky V.F., Zaichko P.A., Sakun T.M.

DENSITY FUNCTIONAL AND GREEN'S FUNCTIONS METHOD TO COMPUTING SPECTRAL PARAMETERS OF DIATOMIC MOLECULES

Summary. A new effective method of calculating the energy and spectral parameters of diatomic molecules based on the hybrid theory of the quasi-particle density functional and the theory of Green's functions is described. As an illustration, the data of the calculation of the vertical ionization potentials of the coupling constants (vibrational structure) of the photoelectron spectra of a number of diatomic molecules, in particular, N_2, are given. It is presented a detailed comparison of the received data with the data of standard theories of the Hartree-Fock type, the multi-configuration electron propagator method, and the extended theory based on Koopmans' theorem using multi-configurational self-consistent field wave functions with different sets of basis functions. It is shown that the consistent, maximally precise consideration of exchange-correlation effects and reorganization effects within the framework of the combined theory leads to a rather significant improvement in the agreement of theoretical and experimental data both in terms of ionization potentials and photoelectron spectra in general.

Keywords: optimized one-quasiparticle approximation, Green's function, density functional, diatomic molecules, spectral characteristics

PACS 33.20.-t

Ігнатенко Г.В., Мансарлійський В.Ф. , Заїчко П.А., Сакун Т.М.

МЕТОД ФУНКЦІОНАЛУ ГУСТИНИ ТА ФУНКЦІЙ ГРІНА ДЛЯ ОБЧИСЛЕННЯ СПЕКТРАЛЬНИХ ПАРАМЕТРІВ ДВОХАТОМНИХ МОЛЕКУЛ

Резюме. Викладено новий ефективний метод обчислення енергетичних та спектральних параметрів двоатомних молекул, що базується на гібридній теорії квазічастинкового функціонала густини і теорії функцій Гріна. Як ілюстрація наведені дані обчислення вертикальних потенціалів іонізації і констант зв'язку (коливальної структури) фотоелектронних спектрів ряду двохатомних молекул, зокрема, N_2. Проведено докладне

порівняння деяких отриманих даних з даними стандартних теорій типу Хартрі-Фока, методу багатоконфігураційного електронного пропагатору, розширеною теорією на основі теореми Koopmans' з використанням багатоконфігураційних самоузгоджених хвильових функцій з різними наборами базисних функцій. Показано, що послідовне максимально коректне врахування обмінно-кореляційних ефектів, ефектів реорганізації в рамках комбінованої теорії призводить до досить істотного поліпшення згоди теоретичних та експериментальних даних як по потенціалам іонізації, так й фотоелектронним спектрам взагалі.

Інформація для авторів
наукового збірника «Photoelectronics»

У збірнику "Photoelectronics" друкуються статті, що містять відомості про наукові дослідження і технічні розробки в напрямках:

* **фізика напівпровідників;**
* **гетеро- і низькорозмірні структури;**
* **фізика мікроелектронних приладів;**
* **лінійна і нелінійна оптика твердого тіла;**
* **оптоелектроніка та оптоелектронні прилади;**
* **квантова електроніка;**
* **сенсорика.**

Збірник "Photoelectronics видається англійською мовою.
Рукопис подається автором у двох примірниках англійською мовою.

Електронна копія статті повинна відповідати наступним вимогам:
1. Для тексту дозволяються формати: – MS Word (rtf, doc).
2. Рисунки приймаються у форматах – EPS. TIFF. BMP, PCX, JPG. GIF, CDR. WMF, MS Word I MS Giaf, Micro Calc Origin (opj).

На першій сторінці рукопису наводяться:
1. Коди PAC і УДК. Допускається використання декількох шифрів, що розділяються комами.
2. Прізвища і ініціали авторів.
3. Установа, повна поштова адреса, номер телефону, номер факсу, адреси електронної пошти для кожного з авторів.
4. Назва статті.
5. Реферат обсягом до 200 слів англійською мовою.

Текст друкувати шрифтом Times New Roman 12 пунктів через два інтервали, формат сторінок — А4, в дві колонки. *Назва* статті друкується прописними літерами 16 пунктів, заголовки підрозділів – напів жирним шрифтом.

Рівняння необхідно друкувати в редакторі формул MS Equation Editor. Необхідно давати визначення величин, що з'являються в тексті вперше.

Посилання на літературу наводяться у рукопису в квадратних дужках послідовно, у порядку їхньої появи в тексті статті. Перелік посилань наводити після тексту з відповідною нумерацією.

Підписи до рисунків і таблиць друкуються в тексті рукопису в порядку появи відповідної ілюстрації під нею.

Резюме обсягом до 200 слів друкується англійською, російською і українською мовами (для авторів з України) наводиться в кінці рукопису після переліку посилань. Перед текстом резюме відповідною мовою вказуються УДК, прізвища та ініціали всіх авторів, назва статті, після резюме надаються ключові слова.

Рукописи надсилаються за адресою:
Відп. секр. Куталовій М. І., вул. Пастера, 42. ОНУ, м. Одеса, 65082 E-mail: photoelectronics@onu.edu.ua , тел. 0482-726-63-56.

Збірники "Photoelectronics" знаходяться на сайті: http://photoelectronics.onu.edu.ua

**Информация для авторов
научного сборника «Photoelectronics»**

В сборнике "Photoelectronics " печатаются статьи, которые содержат сведения о научных исследованиях и технических разработках в направлениях:

* физика полупроводников;
* гетеро- и низкоразмерные структуры;
* физика микроэлектронных приборов;
* линейная и нелинейная оптика твердого тела;
* оптоэлектроника и оптоэлектронные приборы;
* квантовая электроника;
* сенсорика

Сборник"Photoelectronics издаётся на английском языке.
Рукопись подается автором в двух экземплярах на английском языке.

Электронная копия статьи должна отвечать следующим требованиям:
1. Для текста допустимы следующие форматы - MS Word (rtf, doc).
2. Рисунки принимаются в форматах – EPS. TIFF. BMP, PCX, JPG. GIF, CDR. WMF, MS Word И MS Giaf, Micro Calc Origin (opj).

На первой странице рукописи приводятся:
1. Коды РАС и УДК. Допускается использование нескольких шифров, которые разделяются запятой.
2. Фамилии и инициалы авторов.
3. Учреждение, полный почтовый адрес, номер телефона, номер факса, адреса электронной почты авторов.
4. Название статьи.
5. Реферат объемом до 200 слов на английском языке.
Текст должен печататься шрифтом Times New Roman 12 пунктов на бумаге формата А4.
Название статьи печатаются прописными буквами и отмечаются полужирным шрифтом 16 пунктов, а заголовки подразделов - полужирным шрифтом.
Уравнения необходимо печатать в редакторе формул MS Equation Editor. Необходимо давать определение величин, которые появляются в тексте впервые.
Ссылки на литературу нумеруются в квадратных скобках последовательно, в порядке их появления в тексте статьи. Перечень ссылок приводится после текста статьи с соответствующей нумерацией.
Подписи к рисункам и таблицам печатаются в тексте рукописи в порядке появления иллюстраций после них.
Резюме объемом до 200 слов печатается на английском, русском языках и на украинском (для авторов из Украины). Перед текстом резюме соответствующим языком указываются УДК, фамилии и инициалы всех авторов, название статьи.

Рукописи принимаются по адресу: Отв. секр. Куталовой М. И., ул. Пастера. 42. ОНУ, г. Одесса, 65082, E-mail: photoelectronics@onu.edu.ua , тел. 0482 - 726 6356 .

Статьи сб."Photoelectronics " находятся на сайте: http://photoelectronics.onu.edu.ua

Information for contributors
of «Photoelectronics» articles

"Photoelectronics" Articles publishes the papers which contain information about scientific research and technical designs in the following areas:

- **Physics of semiconductors;**
- **Hetero- and low-dimensional structures;**
- **Physics of microelectronic devices;**
- **Linear and non-linear optics of solids;**
- **Optoelectronics and optoelectronic devices;**
- **Quantum electronics;**
- **Sensorics.**

«Photoelectronics» Articles is published in English.
Authors send two copies of papers in English.

Electronic copy of a material can be sent by e-mail to the Editorial Board and should meet the following requirements:
1. The following formats are applicable for texts – MS Word (rtf, doc).
2. Figures should be made in formats – EPS, TIFF, BMP, PCX, JPG, GIF, WMF, MS Word I MS Giaf, Micro Calc Origin (opj).

The title page should contain:
1. Codes of PACS
2. Surnames and initials of authors
3. Name of institution full postal address, number of telephone and fax, electronic address
4. TITLE OF THE PAPER
5. An *abstract* of paper should be not more than 200 words before a text of summary a title of paper, surnames and initials of authors should be placed.
The text should be printed in Times New Roman, 12 points, in two columns on an A4 page.
Equations are printed in MS Equation Editor.
References should should be numbered in square brackets consecutively throughout the text. The list of references is given after the text of the article.
Only high-quality *illustrations* will be taken for publication. Legends and symbols should be printed inside. All figures should be numbered in the sequence of their record in text.
Figure and table captions are printed in the text of the manuscript in the order in which illustrations appear after them.
A summary of up to 200 words is printed in English, Ukrainian (for authors from Ukraine), Russian, is to be given at the end of the manuscript after the list of references. UDC, surnames and initials of all authors, the title of the article are indicated before the text of the abstract in the appropriate language.
For additional information please contact the Editorial Board

The papers should be sent to the address:
Kutalova M.I., Odessa I. I. Mechnikov National University, 42 Pastera str, 65026 Odessa, Ukraine, e-mail: wadz@mail.ru, tel. +38-0482-7266356
Information is on the site: http://www.photoelectronics.onu.edu.ua

"Photoelectronics" Articles is defined by the decision of the Highest Certifying Commission as the specialized edition for physical-mathematical and technical sciences and published and printed at the expense of budget items of Odessa I.I. Mechnikov National University.